

POLITECNICO DI TORINO

Master of Science in Mechatronic Engineering

Department of Control and Computer Engineering



**Politecnico
di Torino**

Master Thesis

Design and implementation of Compliant Control Strategies for a Series Elastic Actuated upper limb exoskeleton for neurorehabilitation

Supervisor:

Prof. CHIABERGE Marcello

Candidate:

SALATINO Laura 279873

Co-supervisors:

Eng. PhD BUCCELLI Stefano

Eng. PhD TESSARI Federico

Eng. BUCCHIERI Anna

October 2021

” sì sì ce la faccio, ma se non ce la faccio, non mi scoraggio”.

A mamma ed a papà.

LIST OF FIGURES.....	7
LIST OF TABLES.....	13
LIST OF EQUATIONS	16
ABBREVIATIONS	18
ABSTRACT	19
CHAPTER 1: STATE OF THE ART.....	20
1.1. Stroke and Poststroke Neurorehabilitation and Therapy	21
1.1.1. Post stroke rehabilitations.....	22
1.2. Upper Limb Robotic Exoskeletons.....	24
1.2.1. Assistive Robots	24
1.2.2. Classification of upper-limb exoskeleton robots	25
1.2.2.1. Software and Control Strategies Classification.....	28
1.2.3. Possible Challenges in Upper-Limb Exoskeleton Development	31
1.2.4. Commercially Available Upper Limb Exoskeletons	31
1.3. Series Elastic Actuator	36
1.3.1. Advantages and disadvantages of SEAs.....	36
1.3.2. Classification of SEA	37
1.3.3. Brushless DC Motor	40
1.3.4. Gearbox: Harmonic Drive	42
1.3.5. Sensors: Encoder	43
CHAPTER 2: THEORETICAL BACKGROUND.....	44
2.1. Robotics	45
2.1.1. Task Space and Joint Space	45
2.1.2. Denavit-Hartenberg convention	46
2.1.3. Direct Kinematics	47
2.1.4. Inverse Kinematics	47
2.1.4.1. Geometric Jacobian.....	48
2.1.5. Direct Dynamics.....	49
2.1.6. Inverse Dynamics	49
2.2. Control Strategies	50

2.2.1. Joint and Task Space Control	50
2.2.2. PID	51
2.2.2.1. Proportional Term	51
2.2.2.2. Integral Term.....	52
2.2.2.3. Derivative Term	52
2.2.3. Position control.....	52
2.2.4. Torque control	53
2.2.5. Impedance/Admittance control.....	53
2.2.5.1. Admittance control.....	54
2.2.5.2. Impedance Control	56
2.2.5.3. Comparison between Admittance and Impedance control: pros and cons of dual control strategies..	58
2.2.6. Transparency Control	59
CHAPTER 3: MATERIALS AND METHODS.....	60
3.1. Software	61
3.1.1. MATLAB and Simulink.....	61
3.1.1.1. Simscape Library in Simulink.....	61
3.1.1.2. Multibody.....	61
3.1.2. App Designer.....	61
3.1.3. Creo Parametric.....	61
3.1.3.1. Simscape Multibody Link Creo Plug-In	62
3.2. Real Time target machine	62
3.2.1. Simulink Real Time.....	62
3.2.2. Speedgoat	62
3.3. Metrics and parameters for validation	63
3.3.1. Root-mean square error (RMSE).....	63
3.3.2. Standard Deviation (SD)	64
3.3.3. Fast Fourier Transform (FFT)	64
3.3.4. Rise Time, Settling Time, and Overshoot.....	64
3.4. Mechatronic components of Series Elastic Actuator	65
3.4.1. SEA with EC-90 motor:	65
3.4.2. SEA with EC-45 motor:	65
3.4.3. EC: Brushless DC Motor.....	66
3.4.4. Servo controllers: ESCON and EPOS	67
3.4.5. Harmonic drive.....	69
3.4.6. Compliant element.....	69
3.4.7. Encoders	71
3.4.7.1. Wrap/Unwrap method.....	72

3.5. Experimental Setup for Real Time simulation	73
3.5.1. Actuators under test: system components.....	73
3.5.1.1. EC90 motor SPT2P compliant element.....	73
3.5.1.2. EC90 motor STA compliant element.....	73
3.5.1.3. EC45 motor SPT1P compliant element.....	74
3.5.2. SEA characterization	74
3.5.2.1. Infinite inertial load.....	75
3.5.2.2. Finite inertial load	76
3.5.3. 1 Degree of Freedom	77
3.5.4. 2 Degrees of Freedom	78
3.5.4.1. Denavit-Hartenberg configuration of 2 DoF system	79
3.5.4.2. Jacobian matrix of 2 DoF system.....	80
3.6. Simulink models for Real Time simulation on Speedgoat.....	81
3.6.1. Seafloat_ESCON Simulink model	81
3.6.2. Seafloat_EPOS Simulink model.....	82
3.7. Characterization of Series Elastic Actuator (SEA).....	83
3.7.1. Simulink modelling for real time SEA testing: Speedgoat.....	83
3.7.2. SEA modelling on Simulink-Simscape	84
3.7.2.1. Behaviour analysis of the SEA model.....	87
3.7.2.2. Simulink model for infinite inertial load simulation	87
3.7.2.3. Simulink model for finite inertial load simulation	88
3.8. Control Strategy of 1 Degree of Freedom	90
3.8.1. Position control.....	90
3.8.1.1. Simulink model.....	90
3.8.1.2. Graphical User Interface (GUI).....	91
3.8.1.3. PID tuning.....	91
3.9. Control Strategies of 2 Degrees of Freedom	92
3.9.1. Admittance control: Joint Space.....	92
3.9.1.1. Elastic system.....	94
3.9.1.2. Viscoelastic system	94
3.9.1.3. Noise filtering of input signal.....	95
3.9.1.4. Graphical User Interface (GUI).....	95
3.9.2. Impedance control: Task Space.....	95
3.9.2.1. Viscous system.....	97
3.9.2.2. Elastic system.....	97
3.9.2.3. Viscoelastic system	98
3.9.2.4. Transparency	98

CHAPTER 4: RESULTS AND DISCUSSION.....	99
4.1. Characterization of Series Elastic Actuator (SEA).....	100
4.1.1. Functioning of the implemented SEA Simulink model.....	100
4.1.2. Frequency Analysis of real time collected data: infinite inertial load	102
4.1.2.1. Torsional stiffness evaluation of the compliant element for different EC45 SPT1P SEAs (FSJ45A joints)	107
4.1.2.2. Torque and displacement comparison between Speedgoat and Simulink data	109
4.1.3. Speedgoat and Simulink data comparison: finite inertial load	110
4.2. Control Strategy for 1 Degree of Freedom (DoF)	111
4.2.1. Position control.....	111
4.2.1.1. Fixed Input Trajectory and PID Evaluation	112
4.2.1.2. Variable Input Trajectory PID Evaluation and fixed PID coefficient	114
4.2.1.3. PID final optimal parameters tuned for position control.....	117
4.3. Control Strategies for 2 Degrees of Freedom	118
4.3.1. Admittance control: Joint Space.....	118
4.3.1.1. Purely elastic admittance filter.....	118
4.3.1.2. Viscoelastic system	121
4.3.2. Impedance control: Task Space.....	123
4.3.2.1. Purely elastic system	123
4.3.2.2. Purely viscous system	126
4.3.2.3. Viscoelastic system	129
4.3.2.4. Transparency	133
4.3.2.5. Viscous, Elastic, Viscoelastic and Transparent impedance system.....	135
CHAPTER 5: CONCLUSION	137
BIBLIOGRAPHY	140

List of figures

Figure 1: post-stroke temporal phases.....	23
Figure 2: Different types of orthoses. (a) end-effector based assistive robot, (b) exoskeletons assistive robot. From [1].....	25
Figure 3: Different control strategies: based on the task to be completed, the assistive control strategy provide a control aligned with the task to be performed while the resistive control strategy gives an orthogonal one. The corrective control method helps the patient to finish the task if he/she is not able to accomplish it. Reference to [2].....	29
Figure 4: Float Competitors, commercially available exoskeletons. (a): ALEx, (b): ArmeoPower, (c): HARMONY	32
Figure 5: General representation of a Series Elastic Actuator (SEA)	36
Figure 6: (a) general configuration of FSEA, (b) linear SEA, (c) free body of an FSEA. Reference to [28].	38
Figure 7: (a) motor- reaction force sensing type of RFSEA configuration, (b) gear-reaction force sensing type of RFSEA configuration, (c) possible configuration of SEA (MARIONET), (d) free-body on RFSEA. Reference to [28].....	38
Figure 8: (a) internal transmitted force of gear sensing type configuration of TFSEA, (b) external transmitted force of gear sensing type configuration of TFSEA, (c) differential elastic actuator (DEA), (d) free-body configuration on TFSEA Reference to [28]......	39
Figure 9: (a) Brushless DC Motor, (b.1) trapezoidal back-EMF, (b.2) sinusoidal back-EMF. Reference to [47].	40
Figure 10: Harmonic Drive components and different views: (a) 3D view, (b) 2D view. Reference to [53].	42
Figure 11: from task (red) to joint(blue) space by using Kinematics and Dynamics. J: Jacobian matrix, HTM: homogeneous transformation matrix from Denavit-Hartenberg convention.....	46
Figure 12: DH parameters	46
Figure 13: PID control scheme.....	51
Figure 14: Position control scheme	52
Figure 15: Torque control scheme.....	53
Figure 16: Admittance control scheme	54
Figure 17: Task Space Admittance control scheme	55
Figure 18: Joint Space Admittance control scheme	55
Figure 19: Impedance control scheme.....	56
Figure 20: Task Space Impedance control scheme	57
Figure 21: Joint Space Impedance control scheme	58
Figure 22: From Desktop to Real-Time Simulation and Testing, Reference to [91].	62

Figure 23: Supported Real-Time Testing Configurations. Reference to [91].	63
Figure 24: Step response in time: rise time, settling time and overshoot analysis. Reference to [95].	64
Figure 25: Operating range curve. (a) from EC 90 datasheet, red zone: continuous operation, white zone: short term operation, black curve: assigned power rating; (b) assigned power rating obtained with MATLAB plot of data from WebPlotDigitizer tool.	66
Figure 26: Operating range curve. (a) from EC 45 datasheet, red zone: continuous operation, white zone: short term operation, black curve: assigned power rating; (b) assigned power rating obtained with MATLAB plot of data from WebPlotDigitizer tool.	67
Figure 27: Harmonic Drive, CSD-17-2A-100,	69
Figure 28: Custom made compliant element, (a) SPT1P: spiral geometry, titanium material with 1 pin for connection, (b), STA: star geometry, steel material, (c) SPT2P: spiral geometry, titanium material with 2 pins for connection	69
Figure 29: AksIM-2 Off-Axis Rotary Absolute Magnetic Encoder, reference to [103]	71
Figure 30: From angular to linear domain, wrap/unwrap operation.	72
Figure 31: SEA configuration: EC90 motor with SPT2P compliant element, focus on each SEA component disassembled, BLDC motor, Harmoni Drive, Encoders, and compliant element	73
Figure 32: SEA configuration: EC90 motor with STA compliant element, focus on each SEA component disassembled, BLDC motor, Harmoni Drive, Encoders, and compliant element	73
Figure 33: SEA configuration: EC45 motor with SPT1P compliant element, focus on each SEA component disassembled, BLDC motor, Harmoni Drive, mirrored Encoders, and compliant element	74
Figure 34: Infinite inertial load test bench. The test bench is blocked, so it is not free to move. This configuration simulates an infinite inertial load. The main components are a SEA, bellow, and industrial torsionmeter.	75
Figure 35: Finite and known inertial load, test bench free to move. The main components are a SEA, bellow, and industrial torsionmeter.	76
Figure 36: CAD with CREO of single degree of freedom test bench	77
Figure 37: (a) CAD with CREO of double degrees of freedom test bench and (b) real test bench, scapular joint	78
Figure 38: Mechanical stops of 2DoF system. (a) absolute range of motion (ROM) of 60° for motor 1, (b) absolute ROM of 60° for motor 2	79
Figure 39: Denavit-Hartenberg configuration of 2DoF system. d_i =distance between x_{n-1} and x_n along z_{n-1} ; a =distance between O_n and O_{n-1} along x_n .	79
Figure 40: Seafloat_ESCON Simulink model block scheme	81
Figure 41: Seafloat_EPOS Simulink model scheme	82
Figure 42: Simulink model (Seafloat_ESCON) of SEA characterization in Real Time.	83
Figure 43: (a) efficiency as function of temperature. Focus on a constant temperature of 25° to analyse the efficiency as function of speed. (b) efficiency dependence of angular velocity a constant temperature.	85

Figure 44: (a) normalized KV factors curve of efficiency of Harmonic Drive and efficiency with respect to torque, (b) efficiency dependence from torque applied	86
Figure 45: Antagonist input of SEA, motor validation scheme of Simulink model	87
Figure 46: Simulink model scheme of SEA characterization with block model, infinite inertia load. Offline model.....	87
Figure 47: (a) Simulink model scheme of SEA characterization with load. Offline model and Multibody figure, (b) multibody block on Simulink.....	88
Figure 48: Simulink model for 1 degree of freedom position control. (b) focus on position control scheme	90
Figure 49: Seafloat_EPOS Simulink scheme for admittance control.....	92
Figure 50: Admittance Control in Joint space.....	93
Figure 51: Desired Pose of the end-effector in Task space (a) and respective joint's position in Joint space after inverse kinematics computation (b)	93
Figure 52: Fast Fourier Transform of input torque signal T1 and T2 are input torque of the admittance filter for each joint.....	95
Figure 53: Task space impedance control, Seafloat_EPOS model	96
Figure 54: Impedance control scheme in task space	97
Figure 55: Free Run system: the motor speed increases until the maximum reachable angular speed since there is no load.	100
Figure 56: Balanced system is a blocked system with null speed and motion. The combination of the torque exerted by the motor and the resisting torque brings the velocity of the motor to drop to a null value	100
Figure 57: motor driving torque can overcome the resisting torque, the motor can drag the load during its motion, thus the resulting motor speed is positive.	101
Figure 58: motor driving torque cannot overcome the resisting torque, the motor cannot drag the load during its motion, thus the resulting motor speed is negative	101
Figure 59: Input current chirp signal used for frequency analysis of SEAs. The signal is a logarithmic bidirectional chirp with a maximum frequency of 20 Hz. From spectrogram analysis of the chirp signal (a) it's possible to notice the different frequencies of the chirp signal (in yellow), with a focus on the maximum target frequency.....	102
Figure 60: Magnitude Bode Diagram of transfer function between the input current and the relative measured encoders displacement of three actuators. The graph shows the respective resonance peaks at resonant frequencies: the resonant frequency allow to evaluate which is the optimal working conditions for each compliant element.....	103
Figure 61: Magnitude Bode Diagram of torque and displacement, compared in the same plot. Thanks to the direct parallelism it is possible to notice the relative linear relationship given by the torsional stiffnesses K.....	104

Figure 62: Spectrogram plot of torque used to analyse the optimal working frequencies of the torque. It can be notice that the intensity of the torque is optimal at the resonant frequency while it decreases at the increasing of the frequency.	104
Figure 63: Linear model to map the error between expected and measured torque data.	105
Figure 64: Probability distribution of the residulas errors that affect the torque measurements.....	105
Figure 65: Hysteresis analysis of three different actuators.	107
Figure 66: Torsional stiffness comparison between four actuators made up with same components: EC45, harmonic drive, custom mae compliant element with same geometry and same material (SPT1P).....	108
Figure 67: Torque and displacement comparison between Simulink and Speedgoat results for an infinite inertial load Simulink and test bench setup.	109
Figure 68: Current, speed, displacement, and torque comparison between Simulink and Speedgoat results for a finite inertial load Simulink and test bench setup.	110
Figure 69: Absolute error of current, speed, displacement and torque comparison between Simulink and Speedgoat data for EC45 motor SPT1P compliant element.....	110
Figure 70: Absolute error of current, speed, displacement and torque comparison between Simulink and Speedgoat data for EC90 motor STA compliant element	111
Figure 71: Absolute error of current, speed, displacement and torque comparison between Simulink and Speedgoat data for EC90 motor SPT2P compliant element.....	111
Figure 72: Analysis of the desired trajectory variation: sine wave with constant amplitude $A = 30^\circ$ and period $T = 10s$ as the proportional parameter P varies. (a) entire signal, (b) focus on a peak to see the differences	112
Figure 73: Analysis of the desired trajectory variation: sine wave with constant amplitude $A = 30^\circ$ and period $T = 10s$ as the integrative parameter I varies. (a) entire signal, (b) focus on a peak to see the differences	113
Figure 74: Analysis of the desired trajectory variation: sine wave with constant amplitude $A = 30^\circ$ and period $T = 10s$ as the derivative parameter D varies. (a) entire signal, (b) focus on a peak to see the differences	114
Figure 75: Analysis of the desired low frequency trajectory variation: sine wave with constant amplitude $A = 30^\circ$ and period $T = 8s$ as the proportional parameter $I = 0.2$ or $I = 0.3$ varies. (a) entire signal, (b) focus on a peak to see the differences	115
Figure 76: Analysis of the variation of the desired trajectory at high frequency: sine wave with constant amplitude $A = 30^\circ$ and period $T = 2s$ as the proportional parameter $I = 0.2$ or $I = 0.3$ varies. (a) entire signal, (b) focus on a peak to see the differences	115
Figure 77: Reference position: 30° step with the optimal PID values found.	116
Figure 78: Reference position: 20° ramp with the optimal PID values found.	117
Figure 79: Elasticc admittance experimental comparison between different combination of elastic coefficients	118

Figure 80: Admittance Control in Joint space	119
Figure 81: Pure elastic admittance filter analysis for each joint with a torsional stiffness of the spring constant and equal to $K=1000$ Nm/rad. Admittance filter behaviour, output dynamic position with respect to an external torque perturbation as input.	120
Figure 82: Intensity with which the virtual dynamics of the system is modified by varying the external torque exerted in a purely elastic system with strong spring constant.	120
Figure 83: Viscoelastic admittance experimental comparison between different combination of viscous and elastic coefficients	121
Figure 84: Viscoelastic admittance filter analysis for each joint with a loose spring constant $K=70$ Nm/rad, $\beta=30$ Nm/rad/s. Admittance filter behaviour, output dynamic position with respect to an external torque perturbation as input.	122
Figure 85: Intensity with which the virtual dynamics of the system is modified by varying the external torque exerted in a viscoelastic system.	122
Figure 86: Coefficient of the elastic stiffness of the filter in impedance: measured value	123
Figure 87: Impedance control scheme in task space	124
Figure 88: Input/output relationship of the impedance elastic filter. Focus on the perturbed pose and the obtained force.	125
Figure 89: Pose and generalized forces in the cartesian space. Behaviour of a pure elastic impedance transfer function	126
Figure 90: Force analysis with respect to pose and speed. Focus on the action of the elastic filter on position, but not on speed.	126
Figure 91: Viscous friction coefficients of a purely viscous system. Slope with respect to a force / speed graph.	127
Figure 92: Input/output relationship of the impedance viscous filter. Focus on the perturbed pose, then the produced speed and the obtained force.	128
Figure 93: pose and generalized forces in the cartesian space. Behaviour of a pure viscous impedance transfer function	129
Figure 94: Force analysis with respect to pose and speed. Focus on the action of the viscous filter on speed, but not on pose	129
Figure 95: Linear stiffness coefficients of a viscoelastic system. Slope with respect to a force / pose graph.	130
Figure 96: Viscous friction coefficients of a viscoelastic system. Slope with respect to a force / speed graph.	130
Figure 97: Input/output relationship of the impedance viscoelastic filter. Focus on the perturbed pose, then the produced speed and the obtained force.	131
Figure 98: Pose and generalized forces in the cartesian space. Behaviour of a viscoelastic impedance transfer function	132

Figure 99: Force analysis with respect to pose and speed. Focus on the action of the viscoelastic filter on both pose and speed.....	132
Figure 100: Force analysis in modulus and direction: transparent system.....	133
Figure 101: Residual impedance of the system.....	134
Figure 102: Comparison between viscous, elastic, and viscoelastic impedance control in task space ...	135
Figure 103: Comparison between viscous, elastic, viscoelastic and transparent system. Reference to relationship between pose and generalized force	136
Figure 104: Comparison between viscous, elastic, viscoelastic and transparent system. Reference to relationship between speed and generalized force	136

List of tables

Table 1: post-stroke disabilities and difficulties, inspired by [7]	22
Table 2: Assistive robots' classification.....	24
Table 3: Application field classification of upper-limb exoskeleton	26
Table 4: Mechanical classification of upper-limb exoskeleton	26
Table 5: Control strategies classification of upper-limb exoskeleton	28
Table 6: Float comparison with competitors	36
Table 7: Pros and cons of utilization of SEA	37
Table 8: Main differences between BLDC and PSMS motors.....	41
Table 9: Different switching methods	41
Table 10: admittance/impedance comparison	59
Table 11: EC 90 datasheet, reference to [96].	66
Table 12: EC 45 datsheet, reference to [97].	67
Table 13: comparison between ESCON and EPOS	68
Table 14: EPOS working modes, reference to [100, 101].....	68
Table 15: Harmonic Drive datasheet, reference to [102]	69
Table 16: Qualitative evaluation of the main technical features. Analysis on the geometry of the compliant element	70
Table 17: SEA characterization EC 90 motor SPT2P compliant element	73
Table 18: SEA characterization EC 90 motor STA compliant element	74
Table 19 : SEA characterization EC45 motor SPT1P compliant element	74
Table 20: Test Bench for Series Elastic Actuator (SEA) characterization: infinite inertial load	75
Table 21: Test Bench for Series Elastic Actuator (SEA) characterization: finite inertial load	76
Table 22: 1 degrees of freedom test bench configuration2 Degrees of Freedom	77
Table 23: 2 degrees of freedom test bench configuration	78
Table 24: geometric parameters of 2 DoF system.....	79
Table 25: Denavit Hartenberg table of parameters.....	79
Table 26: datasheet of EC 90 flat BLDC motor. Data taken from datasheet are then reported into Simplified PMSM Drive Simulink-Simscape block	85
Table 27: datasheet of EC 45 flat BLDC motor. Data taken from datasheet are then reported into Simplified PMSM Drive Simulink-Simscape block	85
Table 28: datasheet of Harmonic Drive CSD-17-2A-100. Data taken from datasheet are then reported Harmonic Drive Simulink-Simscape..... block	85
Table 29: Torsional stiffness of custom-made compliant element. Data taken from datasheet are then reported into Rotational Spring Simulink-Simscape block	86

Table 30: Inputs of the Simulink model to test the correct behaviour of the motor's model	87
Table 31: Simulink-Multibody properties. Those features are inserted into Simulink-Multibody block .	89
Table 32: Resonance frequencies of the analysed compliant element. Value taken from the Magnitude Bode Diagram.	103
Table 33: Linear regression model EC45 motor with SPT1P compliant element. Focus on the torsional stiffness of the compliant element under test.	106
Table 34: Linear regression model E90 motor with STA compliant element. Focus on the torsional stiffness of the compliant element under test.	106
Table 35: Linear regression model EC90 motor with SPT2P compliant element. Focus on the torsional stiffness of the compliant element under tes.	106
Table 36: Linear regression model EC45 motor with SPT1P (FSJ45A01) compliant element. Focus on the torsional stiffness of the compliant element under test.	108
Table 37: Linear regression model EC45 motor with SPT1P (FSJ45A02) compliant element. Focus on the torsional stiffness of the compliant element under test.	108
Table 38: Linear regression model EC45 motor with SPT1P (FSJ45A03) compliant element. Focus on the torsional stiffness of the compliant element under test.	109
Table 39: Linear regression model EC45 motor with SPT1P (FSJ45A04) compliant element. Focus on the torsional stiffness of the compliant element under test.	109
Table 40: Summary and comparative table of the analysis of the data obtained during the tuning of the proportional term P, keeping constant the values of the integrative coefficient I and derivative D. Reference trajectory: sine wave with constant amplitude $A = 30^\circ$ and period $T = 10s$	112
Table 41: Summary and comparative table of the analysis of the data obtained during the tuning of the integrative term I keeping constant the values of the proportional coefficient P and derivative D. Reference trajectory: sine wave with constant amplitude $A = 30^\circ$ and period $T = 10s$	113
Table 42: Summary and comparative table of the analysis of the data obtained during the tuning of the derivative term D keeping constant the values of the proportional coefficient P and integrative I. Reference trajectory: sine wave with constant amplitude $A = 3$	114
Table 43: Summary and comparative table of the data analysed and collected with the definitive parameters of the PID. Specific analysis of the integrative term $I = 0.2$	115
Table 44: Summary and comparative table of the data analysed and collected with the definitive parameters of the PID. Specific analysis of the integrative term $I = 0.3$	116
Table 45: Summary and comparative table of the data analysed and collected for a step trajectory with the definitive parameters of the PID.	116
<i>Table 46: Summary and comparative table of the data analysed and collected for a ramp trajectory with the definitive parameters of the PID.</i>	<i>117</i>
Table 47: Optimal PID parameters for closed-loop position control	117
Table 48: Relationship between PID parameters	117

Table 49: Torsional stiffnesses of the virtual dynamic spring imposed by the admittance filter. Absolute percentage error between imposed (desired) values and experimentally obtained values.118

Table 50: Desired and measured elastic stiffness coefficients. Relative absolute error is reported.123

Table 51: desired and measured viscous friction coefficients. Relative absolute error is reported.....127

Table 52: Residual impedance of the system: viscous component134

List of equations

Equation 1: dynamic equation of motion.	28
Equation 2: Hooke's equation	37
Equation 3: Motor torque with respect to input motor current.....	37
Equation 4: Back electromotive force. N: the number of winding turns per phase, l: the length of the rotor, r: the internal radius of the rotor, B: the rotor magnetic field density, ω : the motor's angular velocity. ...	40
Equation 5: Transmission ratio of Harmonic Drive	42
Equation 6: pose representation with respect position (p_e) and orientation (ϕ_e)	45
Equation 7: generalized coordinates of a n-DoF manipulator	45
Equation 8: direct kinematics equation with respect to the pose).....	45
Equation 9: Denavit-Hartenberg matrix. $c(\theta_i, a_i) = \cos\theta_i, a_i$, and $s\theta_i, a_i = \sin\theta_i, a_i$	47
Equation 10: Homogeneous Transformation matrix. R: rotation matrix, t: translation vector.....	47
Equation 11: Direct kinematic function expressed by HTM. q: joint variables' vector; n, s, a: unit vectors of a frame attached to RFe, p: position vector of the origin with respect to Rfb	47
Equation 12: J_p (3xn) Jacobian matrix relating joint velocities and end-effector linear velocities.	48
Equation 13: J_o (3xn) Jacobian matrix relating joint velocities and end-effector angular velocities.....	48
Equation 14: Geometric Jacobian.....	48
Equation 15: Computation of the Geometric Jacobian. $z_i - 1$ is given by the third column of the rotation matrix $R_i - 10$, p_e is given by the first three elements of the fourth column of the transformation matrix T_{e0} . $p_i - 1$ is given by the first three elements of the fourth column of the transformation matrix $T_i - 10$	48
Equation 16: Direct Dynamics equation	49
Equation 17: Inverse Kinematics relationship.....	49
Equation 18: Inverse Dynamics relationship.....	49
Equation 19: Dynamics equations.....	49
Equation 20: proportional integrative derivative control law. K_p, K_i, K_d coefficient. e: tracking error	51
Equation 21: proportional control law.....	51
Equation 22: integrative control law	52
Equation 23: derivative control law	52
Equation 24: Admittance transfer function	56
Equation 25: Impedance transfer function	58
Equation 26: Root-mean square error	63
Equation 27: settling time	65
Equation 28: overshoot.....	65
Equation 29: Abbreviations for DH convention.....	80

Equation 30: homogeneous transformation matrix from reference frame (RF) i and $i-1$. (a) from RF1 to RF0, (b) from RF2 to RF1.....	80
Equation 31: Homogeneous transformation matrix of the overall 2DoF system from RF2 to RF0	80
Equation 32: Geometric Jacobian for a generic two revolute joints.....	80
Equation 33: Coefficients for the geometric Jacobian, $c_i = \cos\theta_i$ and $s_i = \sin\theta_i$	80
Equation 34: Geometric Jacobian for 2 degrees of freedom system	80
Equation 35: Analytic Jacobian for 2 degrees of freedom system	80
Equation 36: Torque estimated from different displacements of encoder and torsional stiffness of SEA's compliant element	81
Equation 37: Torque estimated from different displacements of encoder and torsional stiffness of SEA's compliant element	82
Equation 38: PID formulation block. P, I,D,N: external coefficient to be tuned	91
Equation 39: Focus on purely elastic K admittance transfer function.....	94
Equation 40: Admittance filter transfer function for a pure elastic system.....	94
Equation 41: Hooke's law, rotational domain	94
Equation 42: Focus on viscoelastic admittance transfer function	94
Equation 43: Viscoelastic admittance filter.....	94
Equation 44: Discrete time LPF filter transfer function; K: filter gain, T: filter time constant, T_s : filter sample time	95
Equation 45: Low pass filter anti-noise.....	95
Equation 46: Motor rated torque. K_T : torque constant [mNm/A], i : current [A].....	96
Equation 47: Viscous impedance filter	97
Equation 48:Elastic impedance filter	97
Equation 49:Viscoelastic impedance filter.....	98
Equation 50: Pure elastic admittance filter with loose spring constant, $K=1000$ Nm/rad.....	119
Equation 51: Pure elastic admittance filter with loose spring constant, $K=70$ Nm/rad, $\beta=30$ Nm/rad/s.	121
Equation 52:Transfer function of pure elastic impedance filter	124
Equation 53: Transfer function of pure viscous impedance filter	127
Equation 54: Impedance transfer function for a viscoelastic filter.....	131

Abbreviations

AAN: Assisted-As-Needed

ADL: Activities of Daily Living

Back EMF: Back Electromotive Force

BLDC: Brushless DC Motor

Ci: $\cos(\theta_i)$

CSP: Cyclic Synchronous Position Mode

CST: Cyclic Synchronous Torque Mode

DOF: Degrees of Freedom

EC: Electronically Commutated

EEG: Electroencephalography

EMG: Electromyography

FFT: Fast Fourier Transform

FOC: Field-Oriented Control

FSEA: Force Sensitive Series Elastic Actuator

F/T: Force/Torque

GUI: Graphical User Interface

HD: Harmonic Drive

HIL: Hardware in the Loop

ICR: Instant Centre of Rotation

PID: Proportional-Integrative-Derivative

PMSM: Permanent Magnet Synchronous Motor

RCP: Rapid Control Prototyping

RFSEA: Reaction Sensitive Series Elastic Actuator

RMSE: Root-Mean Square Error

SD: Standard Deviation

SEA: Series Elastic Actuator

Si: $\sin(\theta_i)$.

SPT1P: Spiral Geometry, Titanium Material With 1 Pin for Connection

SPT2P: Spiral Geometry, Titanium Material With 2 Pins for Connection

STA: Star Geometry, Steel Material

TFSEA: Series Elastic Actuator Sensitive to Transmitted Force

TIA: Transient Ischemic Attack

VIA: Variable Impedance Actuator

WHO: World Health Organization

Abstract

Stroke is a cerebrovascular disease that occurs when there is a blockage or haemorrhage that reduces the blood supply to the brain; consequently, the brain does not receive sufficient oxygen and nutrients, leading to the death of brain cells. Stroke is the second leading cause of death in the world and in Italy. Stroke's survivors usually are left with impairments and motor problems, which make daily living activities difficult.

Rehabilitation plays a fundamental role in the patient's motor recovery: the need for repetitive and precise assistive movements makes robotics an ideal application in rehabilitation. Technology-supported training is emerging as a solution to support physiotherapists by providing high-intensity, repetitive and activity-specific treatments, to improve the recovery process and facilitate restoration of upper limb function.

Upper limb exoskeletons are mechatronic and anthropomorphic systems designed to interact with the patient. Series Elastic Actuators (SEAs) are actuator systems suitable for interacting with the environment: the compliant element is used to measure and control the torque interaction between motor and load. One of the main features of the exoskeleton is transparency, i.e., the possibility of creating a torque control that is quite accurate to create a safe environment for the patient. In this regard, SEAs are a good solution to implement a compliant control.

The purpose of this thesis is to design and implement different compliant control strategies for a multi-joint system that make human-machine interaction user-friendly by modifying the virtual dynamic of the system. To work on the multi degrees of freedom (DOF) system it was necessary to characterize and validate the operation of the Series Elastic Actuators. Thanks to the aid of a real time machine, Speedgoat, different types of SEAs were tested in real time to validate frequency behaviour and study the main characteristics of the joint. After validating the SEA mechatronics, this thesis has been focused on compliant control design. To obtain such control, first it was implemented a single DOF position control based on a PID controller properly tuned to satisfy different input profiles (steps, ramps, and sine waves at different frequencies).

Secondly, the author worked on compliant control strategies that allow the implementation of partially assistive modalities of the upper limb exoskeleton. Since rehabilitation robots interact with the human body, it is necessary to consider the manipulator and the patient as a single coupled mechanical system. To reach the desired, appropriate, and safe dynamic interaction between man and robot, the following compliant control techniques were investigated: impedance control (force loop) and its dual, admittance control (position loop). The two techniques were implemented on a multi-joint system with two DOF, the admittance was developed in the joint space, while the impedance was developed in the task space. The results show how, thanks to the compliance and correct tuning of the impedance/admittance filter parameters, it is possible to interact with the end-effector by modifying the virtual dynamics of the system.

Chapter 1: State of the Art

This chapter analyses the state of the art regarding upper limb exoskeletons. The main characteristics of the exoskeletons are analysed, and a classification is provided. A focus on the state of the art of the Series Elastic Actuators (SEA) is done.

1.1. Stroke and Poststroke Neurorehabilitation and Therapy

The World Health Organization (WHO) definition of stroke is: “*Rapidly developing clinical signs of focal (or global) disturbance of cerebral function, with symptoms lasting 24 hours or longer or leading to death, with no apparent cause other than of vascular origin*” [3].

Stroke is a cerebrovascular disease that occurs when there is a blockage or haemorrhage that reduces the blood supply to the brain; consequently, the brain does not receive sufficient oxygen and nutrients, leading to the death of brain cells. Due to the severity of the event, stroke is the second leading cause of death worldwide and the leading cause of acquired disability in adults. Also in Italy, stroke is the second leading cause of death, and, after ischemic heart diseases, it is responsible for 9-10% of all deaths and is the leading cause of disability. 20-30% of people affected by stroke die within one month of the event and 40-50% within the first year. Only 25% of stroke survivors recover completely, 75% survive with some form of disability, and of these halves have a deficit so severe that they lose self-sufficiency [4, 5]. Survivors of a stroke usually are left with impairments, mainly motor disabilities, leading to potentially life-changing event that can have lasting physical and emotional effects such as paralysis, loss of physical strength on one side of the body (hemiparesis), and memory problems that make activities of daily living (ADL) difficult. [1, 6]

There are three main types of strokes:

- *Ischemic stroke*: This is the most common type of stroke, making up 87% of all cases. A blood clot prevents blood and oxygen from reaching an area of the brain.
- *Haemorrhagic stroke*: it occurs when a blood vessel ruptures. These are usually the result of aneurysms or arteriovenous malformations (AVMs).
- *Transient Ischemic Attack (TIA) or Ministroke*: Occurs when a specific blood is temporally inadequate ,but then resumes after a short period of time so symptoms resolve without treatment.

The types and severities of disabilities that follow a stroke depend on which area of the brain is damaged. In Table 1, inspired by [7], the main consequences of a cerebral stroke are explained, and the major neurorehabilitation activities are proposed. The fields highlighted in blue are the ones of greatest interest for this thesis: robotic neurorehabilitation aims to overcome and resolve motor dysfunctions.

Consequences of cerebral stroke	Rehabilitation objectives and activities
Paralysis of half the body or face (hemiparesis)	Improve mobility
	Learn movements to compensate for paralysis
	Learn to perform exercises with aids
Difficulty walking	Improve the ability to walk
	Learn to use walkers or a wheelchair
Speech disturbances (aphasia, dysarthria, dysphonia)	Improve the ability to speak and understand
	Learn other communication techniques
Disorders of swallowing	Treat swallowing disorders so that the patient can return to eating and drinking
	Adopt means that improve the swallowing disorder and food intake
Sensitivity disturbances, such as the perception of temperature or the sense of touch	Improve perception
	Learn to manage sensitivity disorders
Visual disturbances, for example diplopia (seeing double) or visual field disturbances (hemianopia)	Improve visual perception
	Learning how to manage vision disorders through exercise
Disturbances in perception, such as recognizing faces	Improve perception
	Learning how to manage situations of everyday life through exercise
Apraxia (inability to perform or perform gestures correctly, in the absence of paralysis)	Step by step relearn activities of everyday life
	Learn to manage disorders due to apraxia
Emotional changes	Treat mental illness
	Activate psychological counselling
Memory disturbances	Exercises for memory
	Learn to manage memory disorders

Table 1: post-stroke disabilities and difficulties, inspired by [7]

1.1.1. Post stroke rehabilitations

Rehabilitation is essential for the recovery of post-stroke patients. It is defined as "*A set of interventions aimed at optimizing functioning and reducing disability in individuals with health conditions interacting with their environment*"[8]. Rehabilitation is a process in which a person with disabilities is brought to reach the best possible level of autonomy on a physical, functional, social, intellectual, and relational level, with the least restriction of his operational choices, even within the limits of his impairment.

Neurological rehabilitation or neurorehabilitation is the branch of rehabilitation medicine that deals with the recovery of deficits and disabilities caused by neurological diseases. Therapy is known to be most effective when performed right after the stroke episode, but it is not always available [9]. There are three phases following the stroke, depending on the amount of time that has passed since the episode elapsed, as shown in Figure 1.

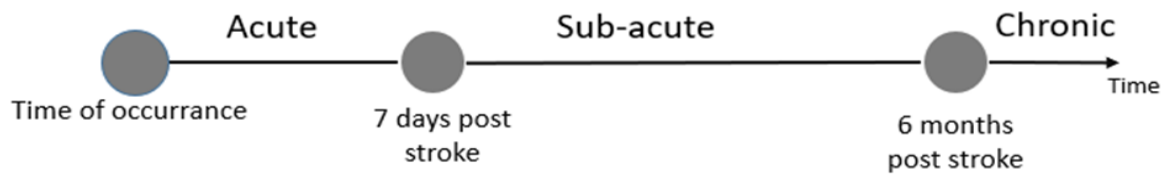


Figure 1: post-stroke temporal phases

Depending on the time elapsed since the stroke, specific rehabilitation techniques are applied (chapter 1.2.2.1), in particular:

- acute phase: passive mode (*Passive assistive mode control strategy is preferred*)
- sub-acute phase: hybrid mode (*Triggered passive assistive mode control strategy is preferred*)
- chronic phase: active mode (*Assisted-as-needed and Corrective mode control strategy are preferred*)

The positive outcome of physical rehabilitation, in the case of neurological disorders, strongly depends on: stroke phase at which the therapy is applied, duration, intensity and orientation to the training task as well as on the patient's health, attention and effort conditions [10]. Physiotherapy, for stroke survivors after completing acute stroke rehabilitation, has shown continued improvement, suggesting that recovery may continue for many years after the stroke [1, 8, 11-13]. The most important element in neurorehabilitation is a repetitive, well-targeted, specific, and personalized practice, to exercise those skills impaired due to the stroke, such as weakness, lack of coordination, walking problems, loss of sensitivity, problems with the grip of the hand, loss of vision or difficulty speaking or understanding [14]. Successful stroke recovery often involves specific therapies, neurorehabilitation, and support systems, including:

- Speech therapy: with regards to oral production or understanding issues.
- Physical therapy: to support movement and coordination relearning process.

Traditional **physical therapy** involves professionals, such as physiotherapists, who work with the affected individual to perform repetitive movements and exercises. However, this process can be laborious, costly, and psychologically demanding. An individual's ability to move is required to perform basic ADLs. Movement disorders drastically reduce a patient's quality of life; Disorders, of the upper limbs specifically, in particular limit the independence of the affected subjects [15]. The need for repetitive and precise assistive movements makes robotics an ideal application in this area [16]. Robotic therapy can be considered a valid alternative because of the possibility to provide intensive training, ranging from passive to active rehabilitation and it increases the number of repetitions a therapist might impose, as well as the engagement of the patient in terms of motivation by employing innovative technologies (e.g., Virtual Reality), ranging from passive to active rehabilitation. The goal of the rehabilitation training is not only to maximize the number of repetition but to optimize the patient's attention and effort as well [17]. Compared to conventional therapy, robotic assisted rehabilitation is more effective in improving the

recovery of motor function of the upper limbs, especially in patients suffering from chronic stroke [11]. For this reason, technology-supported training is emerging as a solution to support physiotherapists by providing high-intensity, repetitive and activity-specific treatments, to improve the recovery process and facilitate restoration of upper limb function and to relieve pressure on the healthcare system [11].

1.2. Upper Limb Robotic Exoskeletons

Upper limb exoskeletons are mechatronic systems designed to interact with the user for the purpose of amplifying power, assisting, or replacing motor function. Since these devices mechanically interact with the musculoskeletal structure of the human upper limb, they are usually anthropomorphic in nature. [18] The upper limb exoskeletons are designed to work in parallel with the human upper limb and are attached to the human arm in multiple places: it is therefore necessary for a robot to adapt to different arm lengths [18]. An ideal system for rehabilitation and care should tend to be an extension of the affected limb. The two main applications of robotic systems in this research field are rehabilitation and motorized assistance or tremor suppression to perform ADLs [16]. A robotic exoskeleton is an intelligent human-machine system that combines human intelligence and machine power. In robotics, an exoskeleton is a wearable device that consists of a structural mechanism with actuators and sensors whose connections and joints correspond to those of the human body. The robotic exoskeleton transmits the torques to the human joints from the actuators through its links [19]. The first application of the active exoskeleton robot was to provide external energy to a soldier so that he could carry more weight than his strength [20]. The aim of an exoskeleton is to replicate the kinematics and dynamics of the human musculoskeletal structure and thus support the movement of the limb.

1.2.1. Assistive Robots

ASSISTIVE ROBOTS	ORTHOSIS	EXOSKELETON	UPPER - LIMB	
			LOWER - LIMB	
			OTHERS	
		DEVICE ALIGN END-EFFECTR	UPPER - LIMB	
			LOWER - LIMB	
			OTHERS	UNILATERAL
	BILATERAL			
	MULTI-ROBOT			
	PROSTHESIS	UPPER - LIMB		
		LOWER - LIMB		
OTHERS				

Table 2: Assistive robots' classification

Robotic devices for the upper limb are classified into two classes: prostheses and orthoses, as shown in Table 2. The prosthesis is an artificial replacement that can be worn in place of a missing body part. The orthosis is an orthopaedic apparatus that is used to support and correct a person's disabilities or to improve

the functionality of the moving parts of the body [21]. End-effector-based devices contact the patient's limb only in its most distal part which is attached to the patient's upper extremity (i.e. the end effector) while the upper extremity segments create a mechanical chain: in this way the movements of the end effector also indirectly modify the position of other segments of the patient's body [15].

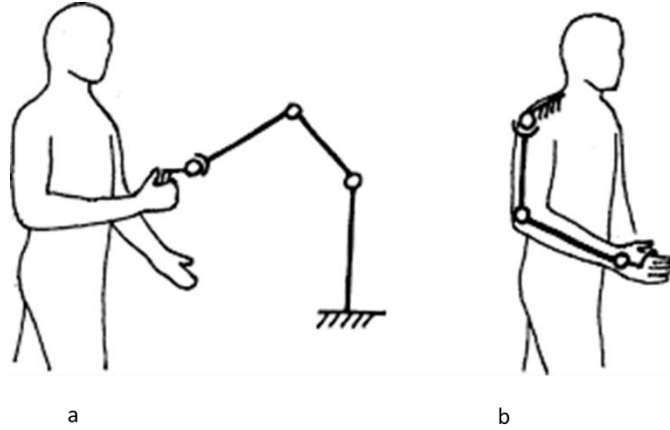


Figure 2: Different types of orthoses. (a) end-effector based assistive robot, (b) exoskeletons assistive robot. From [1]

The joints of the end-effector robots do not correspond to those of the human limb [11]. The mechatronic structure of these robots is simple, as is their control strategy, but the movements allowed are limited to 3 rotations and 3 translations [15] and it is not possible to control the torque on specific joints of the upper limbs [1]. On the other hand, exoskeleton is a device with a mechanical structure that reflects the skeletal structure of the limb: the articular axes of the robot correspond to the articular axes of the human upper limb. This design allows independent, simultaneous, and precise control of movements in certain joints of the limbs. Since the position of the centre of rotation of many joints in the human body, especially the shoulder complex, can change significantly during movement, special mechanisms are needed to ensure patient safety [15]. Exoskeletons offer a wider range of motion (up to 7 degrees of freedom) than end effector robots [11].

1.2.2. Classification of upper-limb exoskeleton robots

The design specifics of an upper limb exoskeleton depend on its application and the segment of the applied limb. The complex nature of human upper limb anatomy makes it hard to design an exoskeleton to assist upper limb movements. Since an upper limb exoskeleton robot interacts directly with the human user, safety is paramount [22, 23]. Upper limb exoskeletons can be classified by considering the characteristics of their mechanical designs and/or software systems (control methods) [2, 18-20, 23, 24]. The main classifications are shown in Table 4, Table 5 and Table 3. Upper limb exoskeletons are classified according to the domain of application, as shown in Table 3. In this thesis we worked on the control of Float EVO, an exoskeleton whose domain of application is to provide assistance to the post-stroke patient.

APPLICATION DOMAIN CLASSIFICATION	ASSISTANCE
	SERVICES
	MEDICINE

	MILITARY
	MANUFACTURING

Table 3: Application field classification of upper-limb exoskeleton

MECHANICAL CLASSIFICATION	ACTUATION	ELECTRIC ACTUATION
		PNEUMATIC ACTUATION
		HYDRAULIC ACTUATION
	APPLIED LIMB SEGMENT	SHOULDER
		ELBOW
		WRIST
		HAND
	POWER TRANSMISSION	GEAR DRIVES
		CABLE DRIVEN
		LINKAGES
	MECHANIC CONFORMATION	SOFT-BODIED EXOSKELETON
		RIGID-BODIED EXOSKELETON
	DEGREES OF FREEDOM	ACTIVE
		PASSIVE
		SINGLE JOINT
MULTI-JOINT		
LINK CONFIGURATION	SERIAL	
	PARALLEL	
	HYBRID	

Table 4: Mechanical classification of upper-limb exoskeleton

The mechanical classification is based on the type of actuators used in the exoskeleton robot such as electric, pneumatic, hydraulic, or other types of actuators that include hybrid methods; Electric actuators provide high control accuracy and fast response, key features for optimal control of an exoskeleton [25]. There are some drawbacks to using an electric actuator like an high cost, a low power / mass ratio, which leads to the achievement of a trade-off between power and portability of the exoskeleton and the high intrinsic impedance in the actuator which makes the whole orthosis very rigid; the low compliance / high rigidity of the system make it unsafe, especially in the event of unforeseen events [16]. The inclusion of a flexible component in the arrangement with the actuator can alleviate the high impedance of electric motors: Series elastic actuators (SEA) are developed for this purpose. SEAs reduce inertia in the user interface to provide precise and stable force control, thereby improving subject safety [18]. However, this principle is not always true as the elastic energy stored in the spring can be released suddenly [18]. The disadvantage of applying with an elastic element is the lower functional bandwidth [18]. However, the rehabilitation field does not usually require high bandwidths [15].

The pneumatic actuators are powered by compressed air. A pneumatic type of actuator is lighter and allows for the maintenance of a high output torque, [1] have a lower impedance, are low maintenance and can be stopped under a load without compromising patient safety [18]. The biggest drawback is their limited precision and accuracy.

Hydraulic actuators are powered by hydraulic pressure. They can produce more torque than electric and pneumatic actuators [18]. Similar to pneumatic actuators, control is less precise than electric motors, and incompressible liquid from a pump could contaminate the entire system and safety could be compromised [1].

On the other hand, the classification based on the applied limb segment, allows to classify the upper-limb exoskeleton robots as hand exoskeleton robot, forearm exoskeleton robot, full upper-limb exoskeleton robot or combined segment exoskeleton robot.

The classification can be based on the power transmission method such as gear drive, cable drive, linkage mechanism, and other methods. The cable-driven transmission method allows for a lightweight design of the exoskeleton as all the cushions can be placed on the back or end of the exoskeleton itself.

A huge classification rises when talk about soft or rigid exoskeletons. Soft robotics is the specific subfield of robotics that deals with building robots from highly yielding materials, like those found in living organisms. Soft robotics adapts to the surrounding environment. Unlike robots built with rigid materials, soft robots allow for greater flexibility and adaptability for performing tasks, as well as greater safety when working with humans [16].

Soft orthotic systems are lighter, less extended, and have less inertia than their rigid counterparts. The soft exoskeletons conform and bend with the joints of the user's body. An inherent advantage of soft-body insoles is the low profile and ease of concealment. On the other hand, these systems don't have a rigid outer frame. Soft body systems essentially depend on the user's skeletal system to provide the rigid frame. This makes power transmission complicated and challenging. The entire power transfer occurs through the user's body and therefore the amount of force / torque that can be applied is limited compared to rigid body systems. In contrast, rigid exoskeletons are robust and provide rigid mechanical support of the body. The rigid body design also allows forces / torques to be transmitted without the user's limb undergoing any load, but a main con is that the rigid frame exoskeletons tend to be heavy, requiring to be paired with high torque actuators, and subsequently end up needing larger power sources. The size, weight, and inertia of these systems could prevent individuals from achieving basic ADL[16].

Then, the upper-limb exoskeleton robots can be classified according to the number of active joints or based on the linkage configuration, the upper-limb exoskeleton robots can be classified as serial, parallel or hybrid, or, additionally, they can be divided in accordance with the intended application such as rehabilitation robots, assistive robots, human amplifiers, haptic interfaces, or other uses;

To properly guide the exoskeleton's movement the system normally needs sensing methods as input signals. It is possible to use both external sensor (position or force/torque) or also use the bio-signals (EEG, EMG) as input. The position defines the spatial configuration of the exoskeleton. Through the position it is possible to study the kinematics and dynamics of the exoskeleton: it is therefore necessary to detect the position through sensors, such as the use of encoders (chapter 3.4.7). On the other hand, to be able to estimate the forces and torques involved at the joints, force / torque sensors are needed. Sometimes redundant force / torque sensors are mounted on the system to introduce additional safety levels [25]. An

input signal, which can also be used as a trigger of the system [2], is normally measured in a non-invasive way through skin electrodes placed on the skin surface of the injured arm. Detection of upcoming motor activities can help the exoskeleton decide which joints to move. If the signal is well filtered and analysed, this surface EMG approach could be very useful for controlling the movement of the exoskeleton since theoretically no force interaction is required between the human arm and the exoskeleton [25]. As with the detection of the EMG signal, the EEG signal can also be detected using a non-invasive electrode system.[26]

1.2.2.1. Software and Control Strategies Classification

SOFTWARE CLASSIFICATION (CONTROL METHODS)	ASSISTIVE	PASSIVE CONTROL	PASSIVE TRAJECTORY TRACKING
		PARTIALLY ASSISTIVE CONTROL	PASSIVE MIRRORING
			IMPEDANCE CONTROL
	CORRECTIVE	TUNNELING	ADMITTANCE CONTROL
	RESISTIVE	-	

Table 5: Control strategies classification of upper-limb exoskeleton

An important classification that is worth analysing carefully is the one based on the types of control strategies that are implemented, as reported in Table 5. In dynamic modelling, the limb is treated as a mechanical system with rigid links joined together with rotating joints. This model predicts the torques produced by inertial, gravitational, Coriolis and centrifugal effects: the forces due to gravitational effects are much larger than centrifugal, Coriolis and inertial loads [27]. The general form of the equation of motion is: [28].

$$\tau = M(\theta)\ddot{\theta} + V(\theta, \dot{\theta}) + G(\theta)$$

Equation 1: dynamic equation of motion.

τ : joint torque vector; $M(\theta)$: inertia matrix; $V(\theta, \dot{\theta})$: Coriolis and centrifugal vector; $G(\theta)$: gravity vector.

A control strategy is a planned set of controls. The different types of control strategies allow to manoeuvre the device in different ways: according to the type of target patient and according to the post-stroke phase in which the same is found, different control strategies are adopted. The control requirements and control objectives of an exoskeleton are different from those of industrial robots as the human operator is not only the commander of the control system, but also a component of the control system [24]. To control an upper-limb exoskeleton, the system must transmit the detected signals via a controller to the actuators. There are three main control strategies for an upper-limb exoskeleton: assistance, correction, resistance.

- Assistive Mode
- Correction mode
- Resistive mode

The rehabilitation process is not focused on a single strategy and a clear division between the control strategies cannot be defined. Indeed control methods focus on a combination of these strategies and, in

particular, control strategies used by commercially available upper limb exoskeletons are a combination of assistive (along the longitudinal direction with respect to the task) and corrective (along the orthogonal

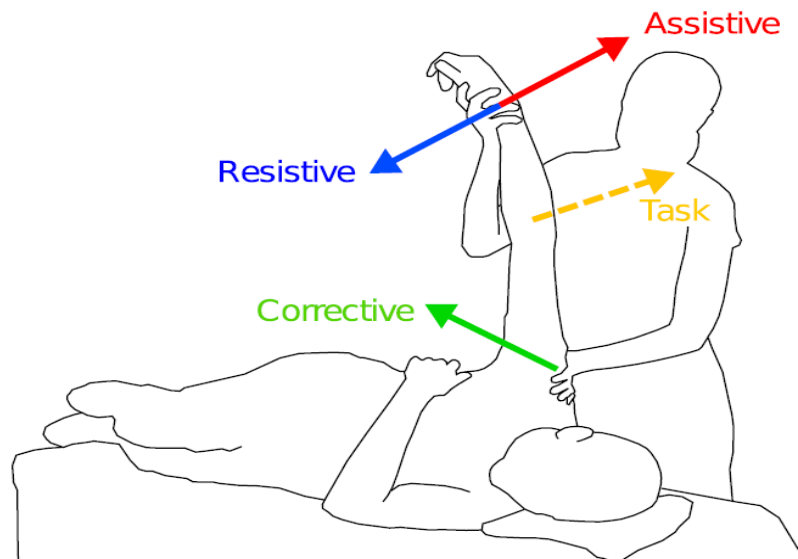


Figure 3: Different control strategies: based on the task to be completed, the assistive control strategy provide a control aligned with the task to be performed while the resistive control strategy gives an orthogonal one. The corrective control method helps the patient to finish the task if he/she is not able to accomplish it. Reference to [2]

direction with respect to the task) ones [2, 18], as shown in Figure 3 (figure taken from [2]). The effect of training can be extensible by increasing the active participation of patients offering only the necessary robotic assistance (Assisted-As-Needed, AAN) [29]. AAN strategies require control and modulation of the physical human-robot interaction [14]. This translates into the modification of the virtual dynamics of the system so that the behaviour of the robot can vary from very rigid to very compliant. The control strategies that can be adopted for AAN are, for example, impedance control and admittance control, further discussed in chapter 2.2.5.

The *Assistive Mode Control Strategy* implies that the robot is supporting the weight of the injured limb and providing the forces to complete the task [30]. If the patient is not making any effort, the completion of the activity can still be performed depending on the level of assistance provided by the robot. The assistance, therefore, helps the patient to complete the task [18]. In the case of an assistive strategy, the exoskeleton assists the patient by providing support in the direction of the task to be completed [2]. The assistive mode can either be passive and partially assistive modality which differentiate for level of participation of the patient. A reference trajectory represents a suggested path through which the controlled variable should converge on the set point. A possible way to control an exoskeleton is to control its movement rigidly and with a passive control along a certain reference trajectory with the help of the position feedback control: the close-loop feedback control is to be tuned attenuating in such a way that, if there are unexpected muscle contractions by the patient (e.g. Spasms), the patient is not injured [18]. In *Passive Trajectory Tracking* of control, the patient is completely passive inside the exoskeleton and is fully assisted by the robot to complete the required task. This modality is particularly practicable in the acute phase of the post-stroke as the limb does not respond [2]. Passive trajectory tracking can be achieved with the help of many different techniques [18]. A possible passive assistive strategy consists in rigidly

controlling the movement along a desired trajectory and, thanks to a feedback control, correcting the movement with high corrective gains [2]. The most commonly used passive control consists in the use of the Proportional Integral Derivative feedback control (PID), which allows to adjust both the position of the end-effector and the force of interaction between the user and the machine, along a predetermined reference [2]. In addition, the passive mirroring control category can be used for exoskeletons intended to simultaneously support both human arms (e.g., Harmony SHR, chapter 1.2.4). Control is based on passive synchronous miming of the sound limb and is based on a master-slave configuration in which the healthy limb represents the master and the injured limb the slave [18]. Passive movements to stimulate neuroplasticity were found to be inadequate and limited at best as the user does not participate in the execution of the task [31]. As the neurorehabilitation stage and the post-stroke temporal stage progress, it is necessary that movement control be shared between the patient and the robot [18], for those reasons it is necessary to introduce a compliant control strategies that allow human-robot interaction: this type of control is *Partially Assistive Control* , also called '*Assisted-As-Needed*' since the action of the exoskeleton occurs only when necessary. This allows for greater freedom of movement of the patient's arm and implies that the limb is not completely numb. This modality is therefore used in the subacute and chronic phases of the post-stroke. Partial assistance is based on increasing the compliance of the exoskeleton, or on the modification of corrective gains [2]. The two main examples of assistive-as-necessary control are impedance and admittance control. These types of controls allow to change the virtual dynamics of the system making the robot more compliant (chapter2.2.5). The Impedance is a control strategy in which the motion of the limb is measured and the robot provides the corresponding force feedback [15], while the admittance is control strategy in which the force exerted by the user is measured, and the device generates the corresponding displacement [15].

Corrective control mode provides that robot only acts when the patient makes wrong movements, forcing the injured limb to perform the actual movement that should have been performed by the patient [18]; the exoskeleton corrects the patient's erroneous movements, when present, providing support in an orthogonal direction to the task to be performed [2]. This control method is used when the user is participatory but does not perform the movement correctly. If the user does not participate, this technique will no longer support the user [18]. In the corrective mode the robot acts only when the patient does not perform the movement correctly, forcing the limb to recover a desired coordination. In this case the exoskeleton provides corrective force in a direction orthogonal to the desired movement: if the patient fails to complete the assigned task, the corrective mode does not help to complete the action - which occurs in the assisted mode. An example of a corrective approach is tunnelling [2]. Tunnelling consists in creating virtual channels for the end-effector or the joints of the exoskeleton in which the subject moves: once they have exited the channels, the input control returns them to the channel as if a spring impedance were connected from the limb to the focal point of the virtual canal [18]. In tunnelling, assistance is clearly decoupled from correction [2]. A support force towards the canal is generally included to prevent the subject from stalling during movement [18]. Tunnelling control can be seen as impedance control with a focused zone

of no action, i.e., the supporting power range can be considered as an auxiliary term and the spring damper-like power towards the channel focal point as a term remedy [32].

Applying the *Resistive mode*, the robot limits movement by increasing the complexity of the task for the patient. Resistive controls can be used in exoskeletons for tremor suppression for exercise. [18]; the exoskeleton opposes the task to be completed [2]. No control has been developed yet: It is not usually implemented for post-stroke rehabilitation because post-stroke patients are too weak.

1.2.3. Possible Challenges in Upper-Limb Exoskeleton Development

The main difficulties in the design and development of exosuits are:

- Kinematic compatibility
- Singularities of mechanical system
- Workspace limitations
- Discomfort and misalignment

The design of the exoskeleton should be kinematically compatible with the variable anthropomorphic parameters of the end user. The mechanism of the exoskeleton, which supports the shoulder and wrist joint, must be kinematically a spherical joint [33]. The kinematic structure of the exoskeleton is described and optimized to allow natural ways of interacting with the user and avoiding singular configurations within the workspace [18]. Wearable exoskeletons are not able to provide a wide range of motion in comparison to the human upper limb. The human upper limb has a natural singularity and does not create problems in moving the limb from the singular position. Unlike the human upper limb, actuators in the exoskeleton require infinite torque to move from a single position [30]. The mechanical singularity hinders the manipulation of the exoskeleton. Singularity is defined when two joints of an exoskeleton are aligned with each other and consequently, the exoskeleton loses a degree of freedom and needs an infinite torque. This problem can be solved with two approaches. One is to include possible situations in the exoskeleton control strategy [34]. The other approach is to incorporate possibilities into the exoskeleton design by applying mechanical constraints [18]. In the upper limb exoskeleton, singularity occurs especially when the axis for internal / external rotation of the shoulder and the axis for pronation / supination of the forearm are aligned with each other [30]. The instant centre of rotation ICR at the elbow and shoulder joints generally changes with the joint. During the movement, misalignments of the articular axes between man and robot can also occur: the misalignment of the joint can lead to interaction forces and high torques at the connection points, therefore a high pressure that causes discomfort for the user [24].

1.2.4. Commercially Available Upper Limb Exoskeletons

To date, technological development has led to the creation of several upper limb exoskeletons, three of which are currently on the market: ALEx [35-37], ArmeoPower [38, 39] and HARMONY [40-42]. The technical specifications are shown in table (Table 6) and compared with the previous exoskeleton designed by IIT-Rehab Technologies (Float), and the one currently under development (FloatEvo).

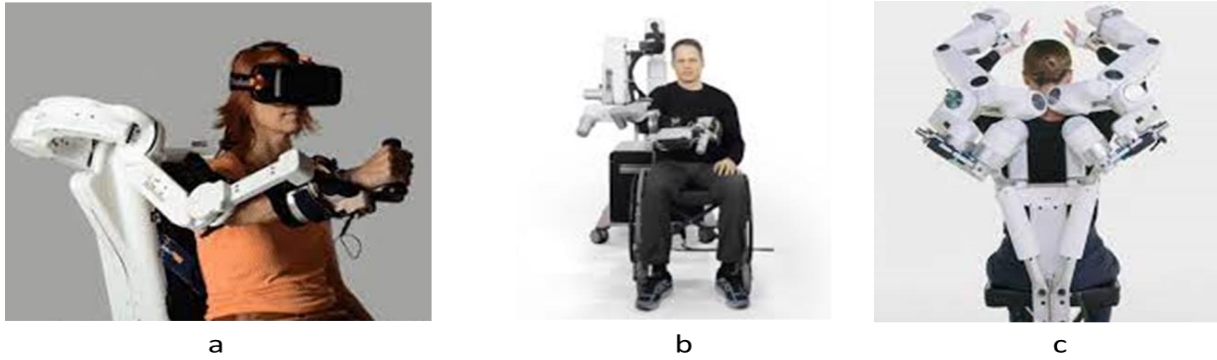


Figure 4: Float Competitors, commercially available exoskeletons. (a): ALEX, (b): ArmeoPower, (c): HARMONY

	Float	FloatEVO	ALEX	ArmeoPower	HARMONY
INTENDED USE	Rehabilitation after shoulder joint injuries.	Neurological rehabilitation.	Neurological, stroke: upper limb neuromotor rehabilitation.	Neurological	Neurological
	Musculoskeletal rehabilitation.	Musculoskeletal rehabilitation.	Orthopaedic: shoulder rehabilitation.	Orthopaedic	Musculoskeletal rehabilitation.
				Perform upper limb extremity therapy rehabilitative exercises.	Upper-limb prosthetic or transplant rehabilitation
ANTHROPOMETRIC REQUIREMENTS	Height range: 160÷185 cm			Maximum weight: 135 kg	
	Maximum weight: 95 kg				
TARGET PATIENTS	Patients affected by neurological, orthopaedic, musculoskeletal disorders and disfunctions.	Patients affected by neurological, orthopaedic, musculoskeletal disorders and disfunctions.	Patients affected by neurological, orthopaedic, musculoskeletal disorders and disfunctions.	Patients with central nervous or peripheral neurogenic, spinal, muscular or bone-related disorder.	Patients affected by neurological injury, neuromuscular disease/disorder, musculoskeletal disease.
	Post-traumatic or post-surgical injuries patients.				
WEARABILITY	Three fabric interface braces:	Three fabric interface braces:	Two fabric interface braces:	Two fabric interface braces:	Two fabric interface braces:
	arm/forearm/corset	arm/forearm/corset	arm/forearm. Hand handles.	arm/forearm. Hand braces.	arm/forearm. Hand handles.
INVOLVED JOINTS	Shoulder	Shoulder	Shoulder	Shoulder	Shoulder
	Elbow	Elbow	Elbow	Elbow	Elbow
		Wrist	Wrist	Wrist	Wrist
				Hand (MANOVO SPRING)	
	Link 1			Height adjustment	

COMPONENT SIZES	From sagittal plane to shoulder centre: 157.55 ÷ 202.8 mm		The exoskeleton can be adapted to different anthropometric measures.	Range 400mm	Autosizing adjustment
	Link 2			Forearm lengths	
	From coronal plane to shoulder centre: 74.9 ÷ 129.9 mm			Elbow to handgrip 310÷420mm	
	Link 3			Upper arm lengths	
	From the shoulder centre to elbow centre: 250.05 ÷ 300.05 mm			Shoulder to elbow 250÷340mm	
USERS	Patient	Patient	Patient	Patient	Patient
	Therapist	Therapist	Therapist	Therapist	Therapist
RATIONAL USE	The therapist is opportunely trained and know how to adapt and personalize the functioning of the exoskeleton according to the patient's clinical condition.	The therapist is opportunely trained and know how to adapt and personalize the functioning of the exoskeleton according to the patient's clinical condition.	The therapist is opportunely trained and know how to adapt and personalize the functioning of the exoskeleton according to the patient's clinical condition.	The therapist is opportunely trained and know how to adapt and personalize the functioning of the exoskeleton according to the patient's clinical condition.	The therapist is opportunely trained and know how to adapt and personalize the functioning of the exoskeleton according to the patient's clinical condition.
NUMBER OF ARMS	1	1 (tipper)	2	1	2
EXOSKELETON WEIGHT	Overall: 230 kg		Overall: 16.4 kg	Overall: 205 kg	Excluding the frame 31.20 Kg
	Only robotic arm: 13 kg		Robotic arm: 4.5 kg		
MAXIMUM JOINT VELOCITY	45 deg/s		500 deg/s		
TORQUE			Max. continuous joint torque 40 Nm		Continuous joint torque 34.4 Nm at shoulder
					13 Nm at elbow
			Max. peak torque 80 Nm		1.25 Nm at wrist
LIFE EXPECTATION					
OPERATING TEMPERATURE AND HUMIDITY	18° - 30° C			10°- 35° C	
	40 - 60 %			30% -75 % relative air humidity	
CONDITIONS OF USE	Indoor premises dedicated	Indoor premises dedicated for			

	for therapy, dry and flat surfaces.	therapy, dry and flat surfaces.	therapy, dry and flat surfaces.	therapy, dry and flat surfaces.	therapy, dry and flat surfaces.
ACTUATED JOINTS	Shoulder flexion-extension	Shoulder flexion-extension	Shoulder flexion-extension	Shoulder flexion-extension	Shoulder flexion-extension
	Shoulder abd-adduction	Shoulder abd-adduction	Shoulder abd-adduction	Horizontal shoulder flexion-extension	Shoulder abd-adduction
	Horizontal shoulder flexion-extension	Horizontal shoulder flexion-extension	Shoulder intra-extra rotation	Shoulder intra-extra rotation	Shoulder intra-extra rotation
	Shoulder intra-extra rotation	Shoulder intra-extra rotation	Elbow flexion-extension	Elbow flexion-extension	Elbow flexion-extension
		Elbow flexion-extension		Forearm pronation-supination	Forearm pronation-supination
				Wrist flexion-extension.	Wrist flexion-extension.
				Actuated hand ManovoPower (optional).	
PASSIVE JOINTS	Elbow flexion-extension	Forearm pronation-supination	Forearm rotation-supination	Sensorized hand grip	
			Wrist flexion-extension		
RANGE OF MOTION	SHOULDER		SHOULDER	SHOULDER	SHOULDER (ROM)
	Horizontal abduction from 0° to 100°		Abduction/adduction from 0° to 110°	Flexion/extension from 40° to 120°.	Abduction 118° (170)
	Abduction from 15° to 110°		Rotation from -40° to 60°	Horizontal abduction from -169° to 50°.	Adduction 60°
	Flexion: from 30° to 90		Flexion/extension from 10° to 155°	Internal/external rotation from 0° to 90°.	Forward flexion 160°
	From 55° intra rotation to -55° extra rotation		ELBOW	ELBOW	Extension 45°
			Flexion/extension from 0° to 160°	Flexion/extension from 0° to 100°	External rotation 79° (62)
			FOREARM	WRIST	Internal rotation 80° (48)
			Pronation/supination from -90° to 90°	Flexion/extension from -60° to 60°	Elbow flexion 150° (145)
			WRIST	FOREARM	Pro/supination 172°
			Flexion/extension from -50° to 50°	Pronation/supination from -60° to 60°	
IMPLEMENTED ADL	Reaching.		Self-care, dressing and eating needs.	Reach and grasp, explore and manipulate objects.	Drink from a glass. Reach and grasp, explore and manipulate objects.
	Exploring surrounding.				
MOVEMENT CONTROL	A user interface (display) is		A user interface (display) is used to set the desired	A user interface (display) is used to set the desired:	

	used to set the desired operating mode and the control parameters.		operating mode and the control parameters.	Exercise workspace Difficulty level of the exercise	
FEEDBACK FOR THE USER	No feedback is provided.		Visual feedback on monitor or through virtual reality.	Assessment tools for patient's performance. Information is shown on a display.	
TYPE OF MOBILIZATION	Passive		Passive	Passive	Passive
	Active-assistive		Active-assistive	Active-assistive	Active-assistive
				Assist-as-needed	Assist-as-needed
WEIGHT/FRICTION COMPENSATION MECHANISM	Friction compensation		Friction compensation	Friction compensation	Friction compensation
			Weight compensation	Weight compensation	Weight compensation
OPERATING MODE	Kinematic: passive mobilization of the limb according to elementary movement of the shoulder with the recording of the trajectory (position control).		Passive: the robot moves the arm by replay a pre-recorded trajectory.	Active operation: patient's hand is borne by the robotic arm but not operated by it. All the motion activity is performed by the patient.	Pre-programmed exercises.
	Transparency: patient/therapist free active mobilization of the limb, the trajectory is recorded.				Torque control: transparent, assistive, resistive, corrective, support.
	Replay trajectory: passive mobilization of the shoulder by following the trajectories defined with kinematic or transparency mode (position control).		Assist-as-needed: Alex detects patient's small intention of movement and provides a variable level of assistance according to patient's needs.	Partial activation: patient's hand is borne by the robotic arm and is assisted by it in performing the movement, the therapist sets the degree of assistance. Arm support that adapts to patient's capabilities.	
				Passive operation: the movement is performed by the robot alone.	Assist-as-needed.
DISJOINT CONTROL	It is possible to perform elementary movement separately.		It is possible to set the control only on one limb while the other is still or mirrored. It is possible to		Bilateral sync therapy: set the control only on one limb while the other is still or mirrored.

			perform movement for the single joints.		
SHOULDER KINEMATIC MODEL	The shoulder mechanism is composed by five electric joints that can replicate all shoulder complex movements (both scapulohumeral and scapulothoracic joints)	RPY spheric joint.	The shoulder mechanism is composed by three rotational joints to compose a spheric joint with the centre inside the human shoulder.		RPY spheric joint.
	Spheric Euler joint.				

Table 6: Float comparison with competitors

1.3. Series Elastic Actuator

In general, actuators are built to be as rigid as possible to increase bandwidth. Unlike rigid actuators, a Series Elastic Actuator (SEA), contains an elastic element in series with the mechanical energy source [43]. The Series Elastic Actuator (SEA) is a type of variable impedance actuator (VIA) [28]. SEAs are used to introduce compliance into robotic exoskeletons. The use of SEA has shown good results in terms of human-robot interaction by improving the safety and energy efficiency of the mechanism compared to rigid actuators [44]. SEA is an actuator system suitable for interacting with the environment: compliant element is used to measure and control the interaction between motor and load [45]. The mechanical properties of the compliant element must be carefully designed: the bandwidth of the actuator should be validated through standardized experiments. Chapter 3.4 shows how we proceeded to characterize the SEA used in *Float EVO*.

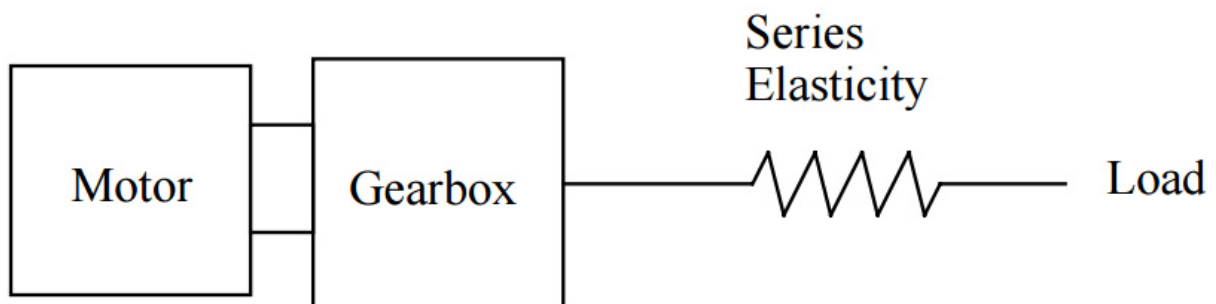


Figure 5: General representation of a Series Elastic Actuator (SEA)

1.3.1. Advantages and disadvantages of SEAs

PROS	CONS
Decoupled Actuator Inertia and Less Reflected Inertia	Limited Stiffness

Reduction of Friction Effects	Limited Bandwidth
Inherent Safety and Impact Resistance	
Energy Storage	Extra Mechanical Element
Higher Shock Tolerance	
More Accurate and Stable Force Control	High Power Requirements
Easy To Achieve Stable Force Control.	

Table 7: Pros and cons of utilization of SEA

In a Series Elastic Actuator, the load is coupled to the transmission by means of a compliant element such as, for example, a spring. Relative applied torque produces a spring displacement. The spring element decouples the inertia of the motor from the exoskeleton [29]. The SEA allows the force control loop to be treated as a position control, since the length of the spring can be considered proportional to the force delivered: greater compliance in the force control ring allows for greater control gains [46]. The conventional actuation provides that the gears transmit force / torque to the load in a proportional way to the torque of the motor which is proportional (for electrical motors) to the supplied current (Equation 3). The torque transmitted to the final load by an SEA should be proportional to the deformation of the spring (Equation 2), which is a key component of a SEA: the SEA transforms the motor current-dependent torque generation problem to the spring deformation decision problem [45].

$$\tau = k(\theta - \theta_0)$$

Equation 2: Hooke's equation

$$\tau^{motor} = kT * i$$

Equation 3: Motor torque with respect to input motor current

Linear Series Elastic Actuators (SEAs) are proposed to achieve accurate force control at the exoskeleton-limb interface: the total number of force sensors and actuators needed is minimized using the adaptive mechanism and SEAs [45]. For an exoskeleton to interact safely with a human limb, it is important to measure and control the interaction force: by controlling the deformation of a series-connected elastic element, a SEA can provide accurate force control, back-driveability, and adjustable impedance without the use of additional force sensors [34].

1.3.2. Classification of SEA

Three criteria are proposed to assess the ability of SEAs to meet these requirements.

- Sensitivity to forces: SEA should respond sensitively to external forces.
- Compliance: For safety, it is necessary to react in a manner consistent with external force.
- Transmissibility: the efficiency of torque transmission must be high [28].

In general, the force / torque is generated by a power source (a motor) and is transmitted to the load through a transmission (a reducer) as it is amplified. The transmission usually does not provide back-driveability, which causes non-transparency in the rigid actuator system; the torque generated by the power supplies can be transmitted to the load with high efficiency, while the force from the load cannot be transmitted to the generator. A compliant component is incorporated in the SEAs to accurately measure / control the load side interaction force and to achieve high fidelity force control. The position of the spring, however, can be different leading to various SEA configurations. SEA is classified into three types based on the relative position of the spring with respect to the gear:

- Force Sensitive Series Elastic Actuator (FSEA) which positions the spring after the drive gear,
- Reaction Sensitive Series Elastic Actuator (RFSEA) that locates the spring before the drive gear
- Series Elastic Actuator sensitive to Transmitted Force (TFSEA) where the spring is inside the transmission gear.

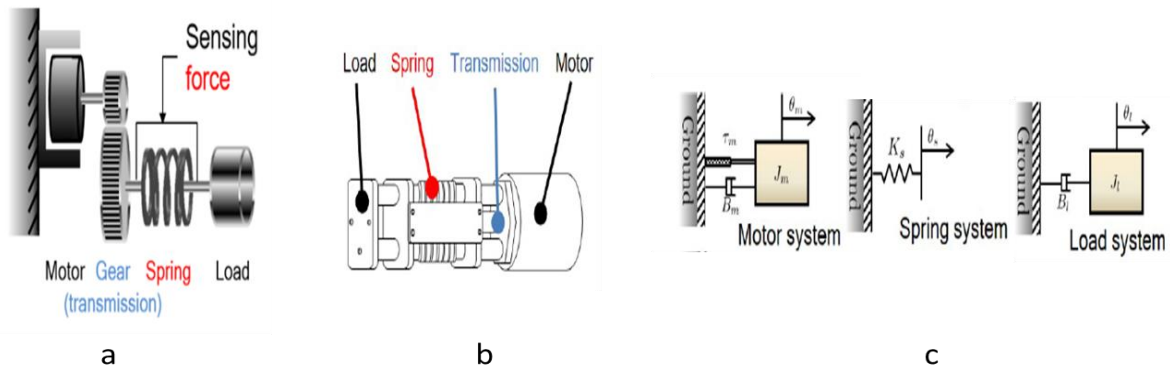


Figure 6: (a) general configuration of FSEA, (b) linear SEA, (c) free body of an FSEA. Reference to [28].

For this thesis, The Force Sensitive Series Elastic Actuator (FSEA) model will be specifically analysed. FSEA combines a motor, a reducer, and a spring coupled with a load as reported in Figure 6, taken from [28]. This system allows to quantify the force generated by the actuator to the load by directly measuring the displacement of the spring. Particularly, the spring deformation is usually measured using encoders both at the motor and load sides. (Chapter 3.4.7) Then the torque can be calculated by multiplying the deformation of the spring and the stiffness coefficient. (Equation 2).

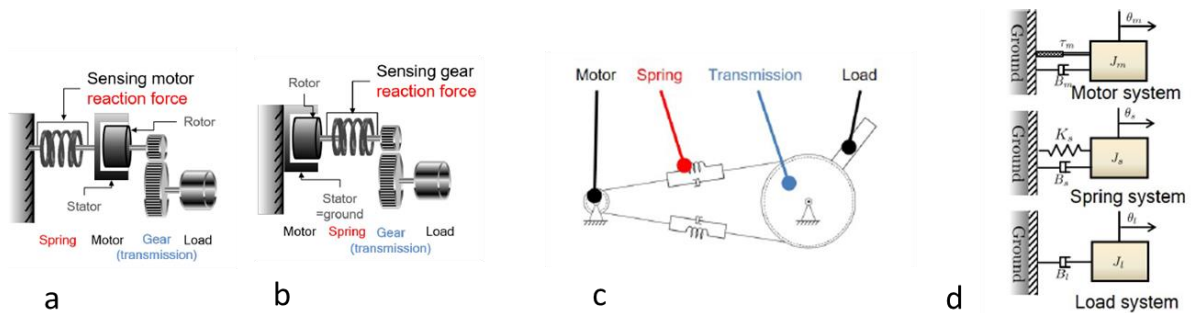


Figure 7: (a) motor- reaction force sensing type of RFSEA configuration, (b) gear-reaction force sensing type of RFSEA configuration, (c) possible configuration of SEA (MARIONET), (d) free-body on RFSEA. Reference to [28].

In Reaction Sensitive Series Elastic Actuator (RFSEA) the spring can be interposed between the mass and the stator of the motor. The motor generates relative torques between the stator and rotor that are amplified at the transmission stage and transferred directly to the load, as shown in Figure 7 taken from [28]. In this case, the spring deflection measures the direct torque of the motor and the reduced external torque.

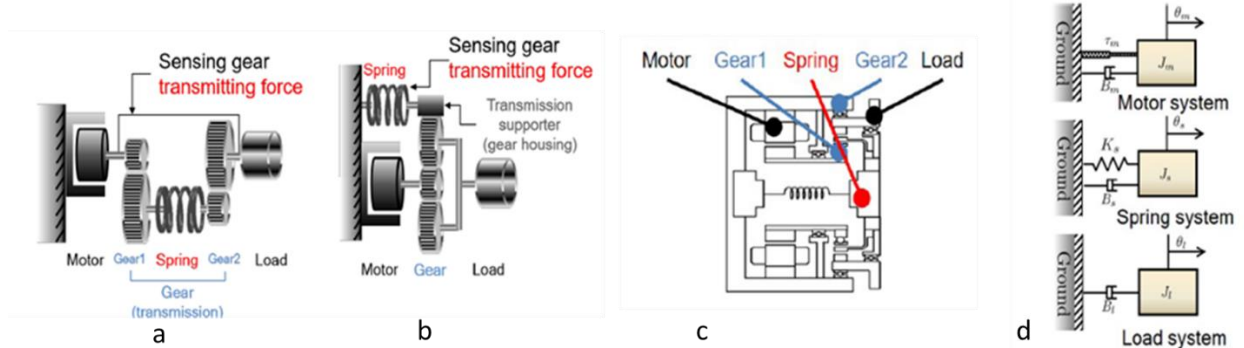


Figure 8: (a) internal transmitted force of gear sensing type configuration of TFSEA, (b) external transmitted force of gear sensing type configuration of TFSEA, (c) differential elastic actuator (DEA), (d) free-body configuration on TFSEA Reference to [28].

In the Transmitted Force-Sensing Series Elastic Actuator (TFSEA) the spring is placed between the drive gears, so it can measure the drive torque inside the gears. Particularly, a differential gear is used as a planetary gear and a Harmonic Drive as a compliant component. In this configuration the motor torque is transmitted to the load via the differential gear, as reported in Figure 8, taken from [28]. The spring is attached to the gear housing, which is connected to the differential gear, so that the torque that the gear transmits can be measured at the level of the spring by employing position sensors [28].

In the following paragraphs is reported the theoretical background of each element constituting the SEA, starting from the Brushless DC motor then the Gearbox, the Compliant element and finally the employed sensors.

1.3.3. Brushless DC Motor

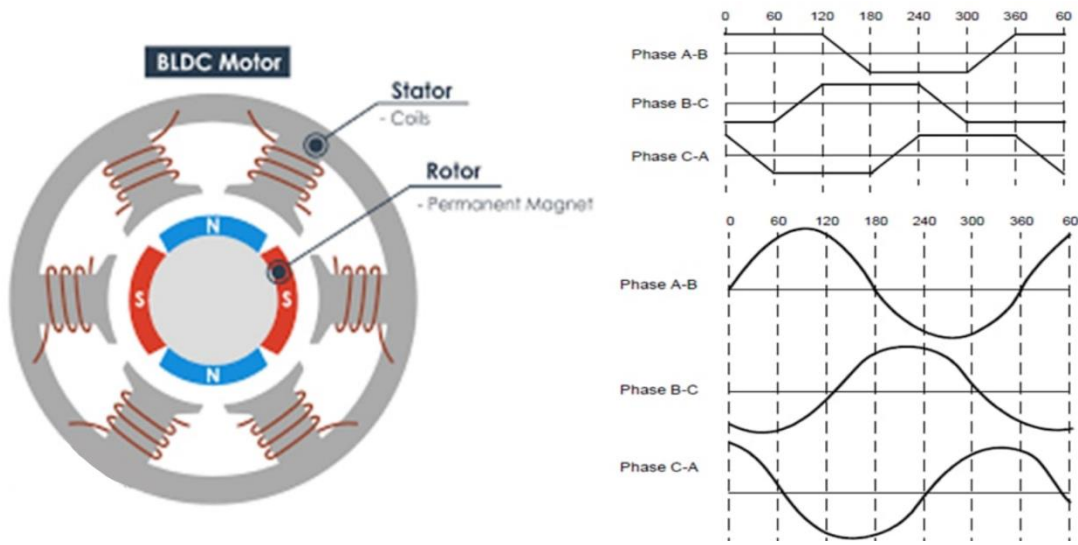


Figure 9: (a) Brushless DC Motor, (b.1) trapezoidal back-EMF, (b.2) sinusoidal back-EMF. Reference to [47].

A brushless DC motor (BLDC) converts electrical energy into rotational motion that is generated through the attraction and repulsion of the magnetic poles of the permanent electromagnets. A BLDC requires a complex controller to convert DC power into three-phase voltages using electronically controlled switching. In a BLDC there are the rotor (permanent magnet) and the stator (coil windings): by applying direct current to the coil, the coil is excited and becomes an electromagnet. An interaction force is therefore created between the permanent magnet of the rotor and the electromagnet. Since motors act as a generator when they are rotating, a back-EMF voltage is induced in the stators which opposes the motor drive voltage [47]. Permanent magnets on the rotor of the BLDC motor provide a constant rotor magnetic field and make possible a motor with high efficiency, high volume of torque and low moment of inertia [48, 49]. As a BLDC rotates, each winding generates a voltage known as the Back Electromotive Force (back EMF). The back EMF opposes the voltage supplied to the windings according to Lenz's law. Back EMF mainly depends on three factors:

- Angular velocity of the rotor
- Magnetic field generated by the rotor magnets
- The number of turns in the stator windings

$$\text{back EMF} = (E) \propto NlrB\omega$$

Equation 4: Back electromotive force. N : the number of winding turns per phase, l : the length of the rotor, r : the internal radius of the rotor, B : the rotor magnetic field density, ω : the motor's angular velocity.

BLDC motors are a type of synchronous motor: the magnetic field generated by the stator and the magnetic field generated by the rotor rotate at the same frequency. Each switching sequence has one of the windings energized at positive power (the current enters the winding), the second winding is negative (the current exits the winding) and the third is in a non-voltage condition. The torque is produced due to the interaction between the magnetic field generated by the stator coils and the permanent magnets [50], [51]. There are two types of permanent magnet brushless DC motors, which depend on their back-EMF waveforms. The

BLDC motor has the trapezoidal (six phase) back-EMF (electromotive force) waveform. The one with sinusoidal back-EMF is called PMSM (Permanent Magnet Synchronous Motor) [45].

The main differences between a PSMS and BLDC are shown in the following table:

	BLDC	PMSM
Winding Distribution	Trapezoidal	Sinusoidal
Energized Phase	Two Phases	Three Phases
Back-Emf Waveform	Trapezoidal	Sinusoidal
Torque Strength	Strong	Weak

Table 8: Main differences between BLDC and PSMS motors

The stator is the fixed part of the motor. Most BLDC motors have three stator windings connected in a star [51]. There are two types of stators winding variants:

- Trapezoidal motors
- Sinusoidal motors

This differentiation is done based on the interconnection of the coils in the stator windings to provide the different types of back electromotive force (EMF).

The rotor is the rotating part of the engine. The rotor is made of permanent magnet and the number of pairs of poles with alternating North (N) and South (S) poles can vary. The magnetic material for making the rotor is chosen according to the required density of the magnetic field. The commutation of a BLDC motor is electronically controlled: to rotate the BLDC motor, the stator windings must be energized in sequence. The sensors that are used for detecting the stator position are usually Hall effect sensors. Knowing the position of the rotor, it is possible to understand which winding will be energized.

Switching methods widely used for the BLDC motor are:

- Trapezoidal (or six-phase)
- Sinusoidal
- Field-oriented control (foc)

The main difference between those three different switching methods, are shown in the Table 9, inspired by [52]:

COMMUTATION METHODS	SPEED CONTROL	TORQUE CONTROL		REQUIRED FEEDBACK DEVICES	ALGORITHM COMPLEXITY
		Low Speed	High Speed		
TRAPEZOIDAL	Excellent	Torque Ripple	Efficient	Hall Sensors	Low
SINUSOIDAL	Excellent	Excellent	Inefficient	Encoder	Medium
FOC	Excellent	Excellent	Excellent	Current Sensor, Encoders	High

Table 9: Different switching methods

1.3.4. Gearbox: Harmonic Drive

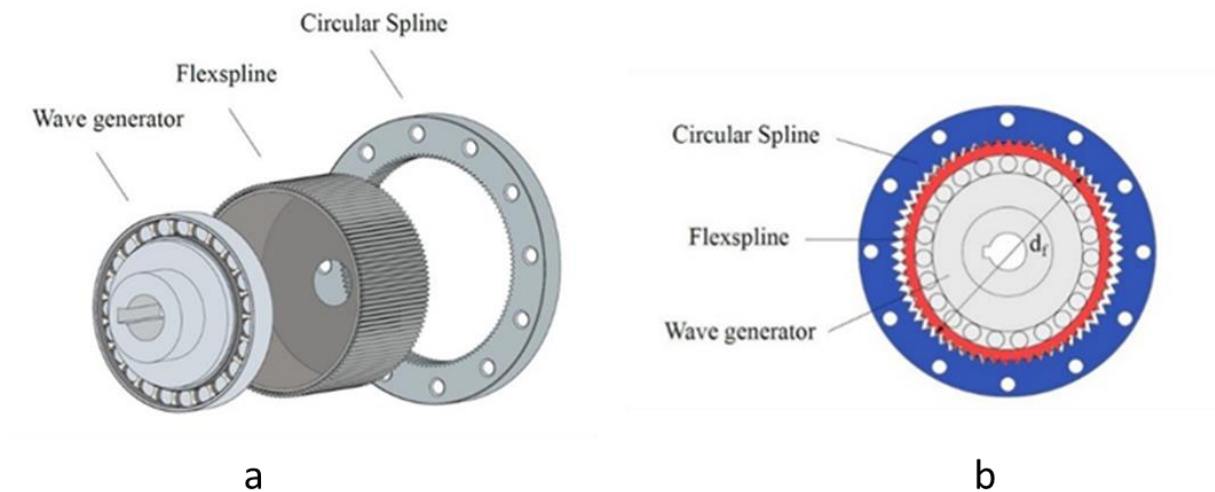


Figure 10: Harmonic Drive components and different views: (a) 3D view, (b) 2D view. Reference to [53].

A gearbox is a contained gear train, or a mechanical unit or component consisting of a series of integrated gears within a housing. A gearbox alters torque and speed between a driving device like a motor and a load. The Harmonic Drive is a mechanical speed-changing device which consists of:

- Circular Spline (CS): external ring, circle.
- Flex Spline (FS): internal ring, ellipsoid.
- Wave generator (WG).

The FS has fewer teeth and consequently a smaller effective diameter than the CS. The wave generator is a link with two rollers that rotates inside the FS. The Harmonic Drive reverses the orientation between input and output and introduces a reduction ratio of the input speed to the output speed which depends on the difference in the number of teeth in the circular spline and in the flex spline.

$$\text{Ratio } i = \frac{\text{input speed}}{\text{output speed}} = \frac{\text{FS teeth}}{\text{CS teeth} - \text{FS teeth}}$$

Equation 5: Transmission ratio of Harmonic Drive

the main characteristics to be evaluated in a gear box are:

- Maximum input speed
- Repeatable maximum output torque
- Transmission ratio
- Torque-to-weight ratios for both nominal and acceleration torque

Due to their greater ability to reduce overall weight, and since electric motors tend to perform better at high operating speeds [54].

1.3.5. Sensors: Encoder

Digital angular position transducers are devices in which the angular position is quantized, i.e., the angle of rotation of the movable shaft ($0 + 360^\circ$) is divided into a discrete number of parts: to each part is associated a digital signal. The encoder is a sensing device that provides feedback by converting the detected motion into an electrical signal: then, the electrical signal can be read by a control device in a control-loop. The read signal sent by the encoder can be used to determine position, speed and/or direction and can be the input to a control system. Encoders might be based on different type of technologies such as mechanical, magnetic, resistive, and optical.

Encoders may produce:

- Incremental signal: it specifies that the position has changed.
- Absolute signal: it provides both the indication that the position has changed and an indication of the absolute position of the encoder.

There are mainly two types of angular transducers with digital output: the incremental encoder and the absolute one. The incremental encoder is a rotary sensor that generates one or two sinusoidal or square pulse trains characterized by a certain number of pulses for each revolution of the shaft (resolution of the encoder). On the other hand, an absolute encoder outputs a combination of logic levels (0 and 1) as many bits as the output signal. The mobile part of the device consists of a disk that can rotate around an axis keyed on the machine whose angular rotation is to be detected. The disk is divided into a number of sectors equal to $2n$ being n the number of bits of the exit signal [52].

Chapter 2: Theoretical Background

In this chapter the main theoretical concepts used for the study and development of this experimental thesis are shown. Fundamental aspects of signal analysis, the key concepts of modern robotics and the main structures of control theory will be analysed.

2.1. Robotics

The main notions of robotics are reported in the following chapters.

2.1.1. Task Space and Joint Space

During this thesis, there has been a lot of talk about Task Space and Joint Space. It is necessary to define the concept of Task / Joint space in the robotic field and understand how this is reflected in the control theory. Task space is defined by the position and orientation of the end-effector of a robot. Usually, the tasks are defined in terms of motion and pose of the end-effectors of robotic manipulator, while the Joint Space refers to the subspace in which single joints are defined through generalized coordinates. To describe kinematics and pose of end-effectors in the space, at least 6 variables are required (orientation and position). The vector pose x_e defines the geometric position and orientation of the end-effector in space. The position p_e can be defined by a minimum number of coordinates, the orientation ϕ_e can be defined by a minimum representation (e.g., Euler angles). This representation of position and orientation allows the description of an end-effector task.

$$x_e = \begin{bmatrix} p_e \\ \phi_e \end{bmatrix}$$

Equation 6: pose representation with respect position (p_e) and orientation (ϕ_e)

The pose x_e is defined in the space where the task is specified: this space is called the operational (or task) space while the joint space denotes the space in which the vectors of each joint variables are defined.

$$q_e = \begin{bmatrix} q_1 \\ \vdots \\ q_n \end{bmatrix}$$

Equation 7: generalized coordinates of a n-DoF manipulator

Considering the dependency of position and orientation from the joint variables, the direct kinematics equation can be written as:

$$x_e = K(q)$$

Equation 8: direct kinematics equation with respect to the pose

The vector function $K(\cdot)$ — nonlinear in general — allows computation of the operational space variables from the knowledge of the joint space variables.[55, 56] Workspace is the region described by the origin of the end effector frame when all the manipulator joints execute all possible motions, and it is an index of robot performance. The workspace is a specification of the reachable end-effector configuration, and it is not related to a particular task. The set of positions that can be reached with all possible set of positions and orientations of the end-effector, is called dexterous workspace.

- Reachable workspace: the region that the origin of the end-effector frame can reach with at least one orientation.
- Dexterous workspace: region that the origin of the end-effector frame can describe while attaining different orientations. Its workspace is a subspace of the reachable workspace.

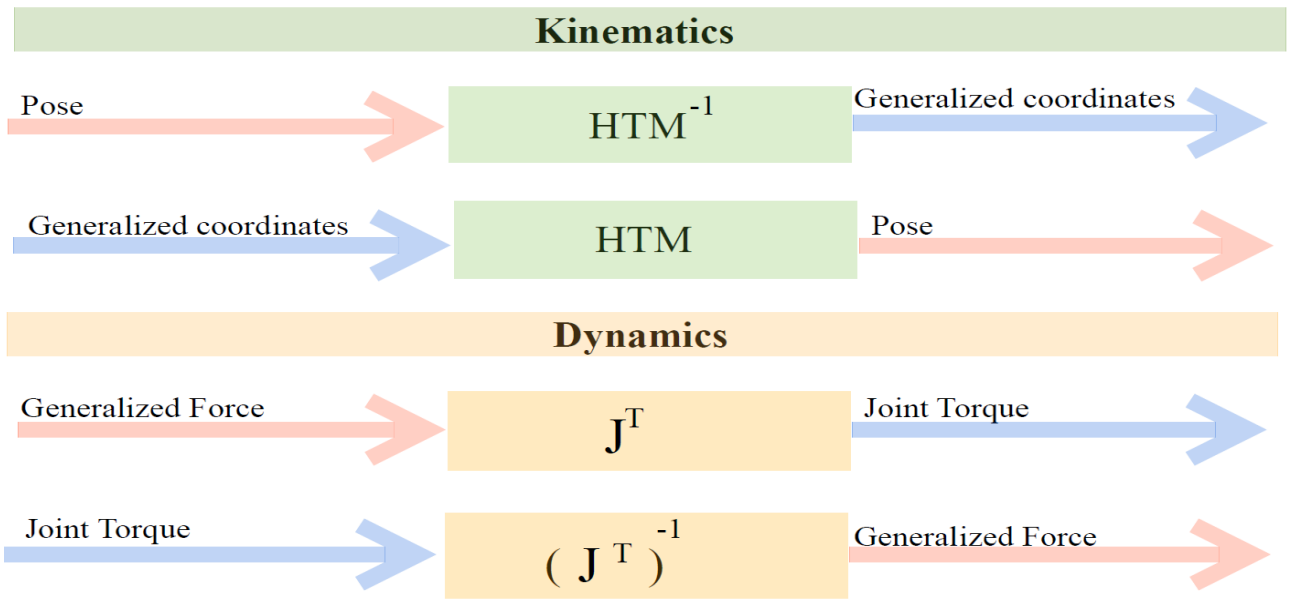


Figure 11: from task (red) to joint(blue) space by using Kinematics and Dynamics. J : Jacobian matrix, HTM : homogeneous transformation matrix from Denavit-Hartenberg convention

2.1.2. Denavit-Hartenberg convention

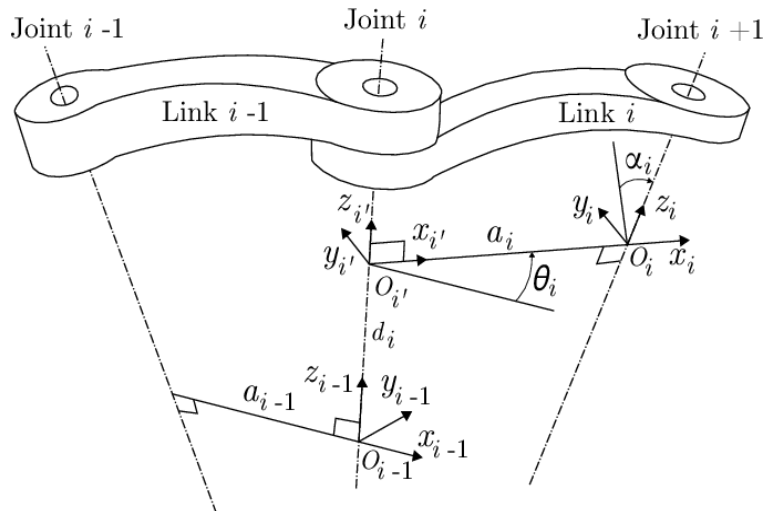


Figure 12: DH parameters

The Denavit-Hartenberg (DH) convention is a systematic method for calculating the direct kinematics equation for an open chain manipulator. The choice of link frame i takes place according to the following rules: choose the axis z_i along the axis of the joint j_{i+1} and then identify the origin O_i as the intersection of the z_i axis with the normal common to the z_{i-1} and z_i axes; Then choose x_i along the normal common to the axes z_{i-1} and z_i with direction from j_i to j_{i+1} and finally choose the y_i axis to complete right-handed frame.

The DH does not give a unique definition in the following cases, whose determination is arbitrary:

- for reference frame (RF) 0, only the direction of the z_0 axis is specified, while for the last RF $_n$, z_n is not uniquely defined, but x_n must be orthogonal to the z_{n-1} axis;
- when two consecutive axes are parallel, the normal common between them it is not uniquely defined, while when two consecutive axes intersect, the direction of x_i is arbitrary;

- when Joint j_i is prismatic, the direction of z_{i-1} is arbitrary.

The non-univocity of the system can be exploited to simplify the DH: the axes of two consecutive RFs can be parallel. After defining the axes, the position and orientation (poses) of the RF_i with respect to RF_{i-1} are completely specified as they depend on known parameters: a_i , which is the distance between O_i and O_{i-1} ; d_i represents coordinate of O_i along z_{i-1} , while α_i is the angle between axes z_{i-1} and z_i about axis x_i to be taken positive when rotation is made counter-clockwise and the last parameter is ϑ_i , the angle between axes x_{i-1} and x_i about axis z_{i-1} to be taken positive when rotation is made counter-clockwise. a_i and α_i are always constant and depend only on the connection geometry between consecutive joints established by Link i . The resulting coordinate transformation is:

$$A_i^{i'}(q_i) = \begin{bmatrix} c\theta_i & -s\theta_i c\alpha_i & s\theta_i s\alpha_i & a_i c\vartheta_i \\ s\theta_i & c\theta_i c\alpha_i & -c\theta_i s\alpha_i & a_i s\vartheta_i \\ 0 & s\alpha_i & c\alpha_i & d_i \\ 0 & 0 & 0 & 1 \end{bmatrix}$$

Equation 9: Denavit-Hartenberg matrix. $c(\theta_i, \alpha_i) = \cos(\theta_i, \alpha_i)$, and $s(\theta_i, \alpha_i) = \sin(\theta_i, \alpha_i)$.

2.1.3. Direct Kinematics

The equation of direct kinematics relates the variables of the joint space with the variables of the task space. The purpose of direct kinematics is to calculate the end-effector pose as a function of the joint variables. The pose of a body with respect to a reference frame is described by the position vector of the origin and the unit vectors of a frame attached to the body. Let's define two reference frames: a base reference frame RF_b and the end-effect reference frame RF_e . With respect to the RF_b , the direct kinematics function can be expressed by the homogeneous transformation matrix. A homogeneous transformation matrix (HTM) is a 4x4 roto-translation matrix.

$$T_e^b \stackrel{\text{def}}{=} \begin{bmatrix} R_e^b & t_e^b \\ \mathbf{0}^T & 1 \end{bmatrix}$$

Equation 10: Homogeneous Transformation matrix. R : rotation matrix, t : translation vector

$$T_e^b(q) = \begin{bmatrix} n_e^b(q) & s_e^b(q) & a_e^b(q) & p_e^b(q) \\ 0 & 0 & 0 & 1 \end{bmatrix}$$

Equation 11: Direct kinematic function expressed by HTM. q : joint variables' vector; n, s, a : unit vectors of a frame attached to RF_e , p : position vector of the origin with respect to RF_b

To calculate and solve the direct kinematics problem, the Denavit-Hartenberg convention can be used.

2.1.4. Inverse Kinematics

The problem of inverse kinematics consists in determining the joint variables corresponding to a given position and orientation of the end-effector. The problem of inverse kinematics is fundamental as it allows to define the motions in the joints space such that there is a predefined motion of the end-effector. Solving the equation of inverse kinematics is difficult as:

- The equations to be solved are generally non-linear;

- There may be multiple solutions. The problem of multiple solutions depends both on the number of degrees of freedom of the manipulator and on the number of non-null Denavit-Hartenberg convention parameters; in general, the greater the number of non-null parameters, the greater the number of feasible solutions.
- there can be infinite solutions in case of singularity or redundancy of the manipulator.
- Some solutions may not be mechanically admissible as they do not belong to the dexterous workspace.

The main tool used for solving the inverse kinematics problem is the Jacobian operator which allows the determination of singular configurations, the analysis of redundancy and to define the relationship between force and torques applied to the actuator.

2.1.4.1. Geometric Jacobian

The Jacobian operator relates the joints velocities (linear and angular) with the end-effector velocities by defining a differential kinematics relationship. If the Jacobian relates all possible velocities acting on the manipulator, then it is called Geometric Jacobian and it is a 6xn matrix. Let's analyse separately the linear and the angular velocities.

$$\dot{p}_e = Jp(q) * \dot{q}$$

Equation 12: Jp (3xn) Jacobian matrix relating joint velocities and end-effector linear velocities.

$$\omega_e = Jo(q) * \dot{q}$$

Equation 13: Jo (3xn) Jacobian matrix relating joint velocities and end-effector angular velocities.

$$\begin{bmatrix} \dot{p}_e \\ \omega_e \end{bmatrix} = \begin{bmatrix} Jp \\ Jo \end{bmatrix} \dot{q}$$

Equation 14: Geometric Jacobian

On the other hand, also for the computation of the Jacobian matrix is better to proceed separately between linear and angular velocities in fact, the overall geometric Jacobian is given by:

$$\begin{bmatrix} Jp \\ Jo \end{bmatrix} = \begin{bmatrix} [z_i - 1] \\ 0 \\ [z_i - 1 \times (p_e - p_{i-1})] \\ z_i - 1 \end{bmatrix}$$

Equation 15: Computation of the Geometric Jacobian. $z_i - 1$ is given by the third column of the rotation matrix R_{i-1}^0 , p_e is given by the first three elements of the fourth column of the transformation matrix T_e^0 . p_{i-1} is given by the first three elements of the fourth column of the transformation matrix T_{i-1}^0 .

The Jacobian matrix depends on the frame in which the end-effector velocity is expressed. If the end-effector pose is specified in terms of a minimal number of parameters in the operational space as in Equation 6, it is possible to compute the Jacobian via differentiation of the direct kinematics function with respect to the joint variables, by using the Analytical Jacobian.

2.1.5. Direct Dynamics

The goal of statics is to determine the relationship between the generalized forces applied to the end-effector and the generalized forces applied to the joints - forces for prismatic joints, torques for revolute joints - with the manipulator at an equilibrium configuration. On the other hand, Dynamics studies the relations between the task space forces/torques and the joint forces/torques in non-static equilibrium. The dynamic equations of the robot can be obtained adopting the Lagrange approach. The direct dynamics problem consists in the computation of the joint accelerations, velocities, and positions from the knowledge of the initial conditions and the external forces applied $J^T F_e$.

$$F_e = (J^T)^{-1} \tau_i$$

Equation 16: Direct Dynamics equation

2.1.6. Inverse Dynamics

The inverse dynamics problem consists in the computation of the command torques that must be applied by the joint actuators to obtain a desired dynamic behaviour by given accelerations, velocities, and positions. This solution is useful for the trajectory planning problems and for the implementation of control algorithms [57]. For non-redundant manipulators, the inverse mapping is given by (inverse kinematics relationship)

$$\dot{q} = J^{-1} \dot{x}$$

Equation 17: Inverse Kinematics relationship

Near singular configurations, J loses rank, such that its inverse becomes numerically unstable. The respective mapping for end-effector forces and torques to joint space does not suffer from these instabilities

$$\tau_i = J^T F_e$$

Equation 18: Inverse Dynamics relationship

To make use of forward dynamics simulations, robotic manipulators can be modelled as a system of articulated, rigid bodies. The equations of motion describe the relationship between generalized loads τ in the joints, external loads f , acting on the end-effector and motion in generalized coordinates q , as shown in

Equation

19

$$\tau_i + J^T F_e = H(q)\ddot{q} + C(q, \dot{q}) + G(q)$$

Equation 19: Dynamics equations

2.2. Control Strategies

This chapter analyses the main control techniques that are implemented for the control of an exoskeleton.

2.2.1. Joint and Task Space Control

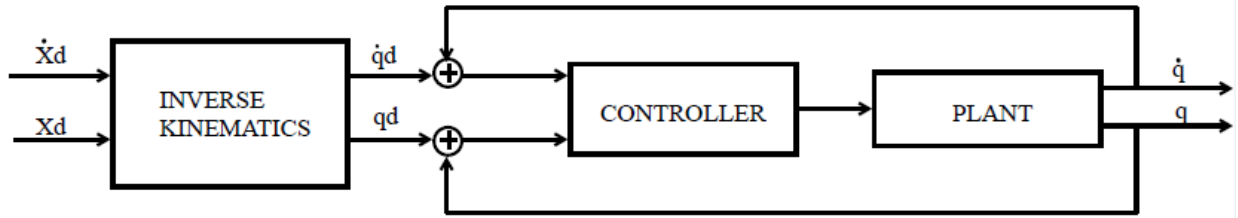


Figure 18: Joint Space Control scheme

In task space control it is allowed to control motor plasticity while joint space strategies control the strength, position, impedance or admittance factors of the control of task space strategies[15]. Robots are programmed and controlled to perform specific tasks defined in the task space. In joint space-based control, tasks are first mapped into joint space using inverse kinematic techniques and then the controller is designed in force / torque space based on joint space information. The robot is controlled to trace the trajectory in the joint space. [55]

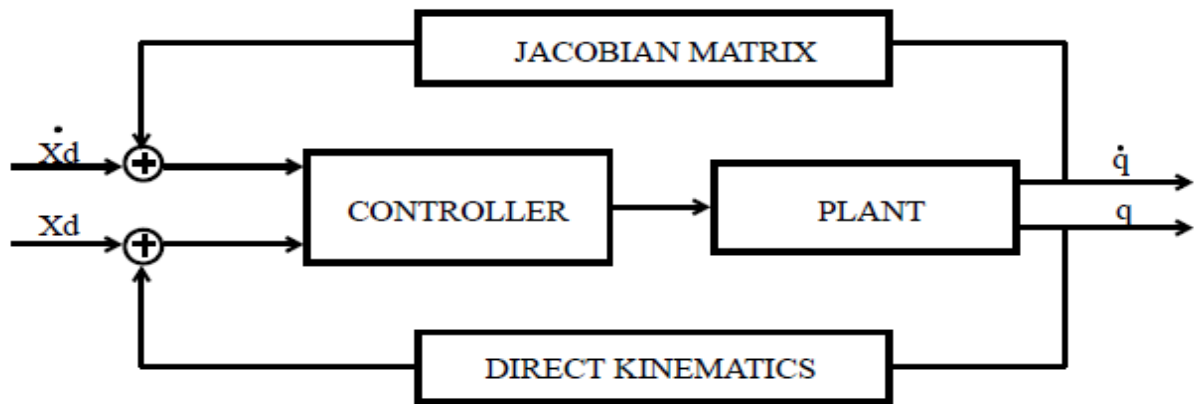


Figure 19: Task Space Control scheme

The task space control is first designed in the end-effector space and then transformed into the couple space. Since no inverse kinematics is performed, the robots can be adequately controlled even in the event of a kinematic singularity.[58]

2.2.2. PID

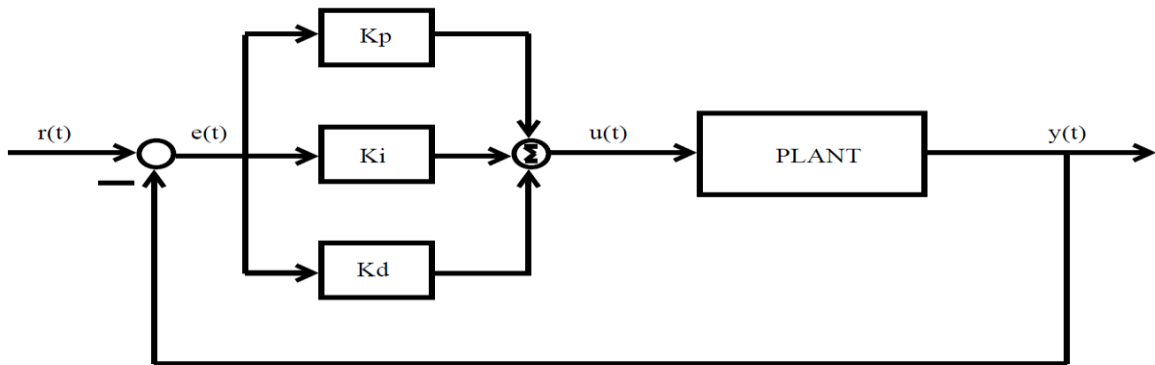


Figure 13: PID control scheme

A Proportional-Integrative-Derivative (PID) control is a closed-loop control technique that applies a continuous correction, in proportional, integrative, and derivative terms, to the tracking error that must be minimized. The PID operates on the error signal by producing a control signal. Starting from the information available from sensors, the desired actuator output is calculated by considering the proportional, integral, and derived responses and adding these three components to calculate the output. The PID modifies the dynamics of a closed loop system through the tuning of the parameters K_p , K_i , K_d . [59-69]. It is not necessary for a PID controller to carry out the proportional, integrative and / or derivative action at the same time: it is in fact possible to design a PID controller that has some parameters null (e.g., P, PI, PD).

- The proportional term ensures the stability of the system.
- The integral term allows to reach the steady state value.
- The derivative term induces a damping.

$$u(t) = K_p e(t) + K_i \int e(t)dt + K_d \frac{de(t)}{dt}$$

Equation 20: proportional integrative derivative control law. K_p , K_i , K_d coefficient. e : tracking error

2.2.2.1. Proportional Term

$$u(t) = K_p e(t) + K_i \int e(t)dt + K_d \frac{de(t)}{dt}$$

Equation 21: proportional control law

The proportional term produces an output value proportional to the error value and considers the present values.

- High gain can cause system instability;
- A small gain may not minimize the error and therefore the control action does not correctly manage the disturbances in the system.

2.2.2.2. Integral Term

$$u(t) = K_p e(t) + K_i \int e(t)dt + K_d \frac{de(t)}{dt}$$

Equation 22: integrative control law

The contribution of the integral term is proportional to both the magnitude of the error and the duration of the error and considers the past values. In fact, the integral term is the sum of the instantaneous error over time and provides the accumulated offset that would have had to be corrected earlier. The accumulated error is then multiplied by the integral gain (K_i) and added to the controller output. The integral term speeds up the achievement of the desired value and eliminates the residual steady-state error that occurs with a pure proportional controller. The ramp rate (integral time constant) must be greater than the process time constant to avoid oscillations.

2.2.2.3. Derivative Term

$$u(t) = K_p e(t) + K_i \int e(t)dt + K_d \frac{de(t)}{dt}$$

Equation 23: derivative control law

The derived term predicts the behaviour of the system. Therefore, it does not consider the error, but the variation of the error, trying to bring the latter to zero and improving the settling time and the stability of the system. The purpose of the derivative term is to reduce overshoot.

2.2.3. Position control

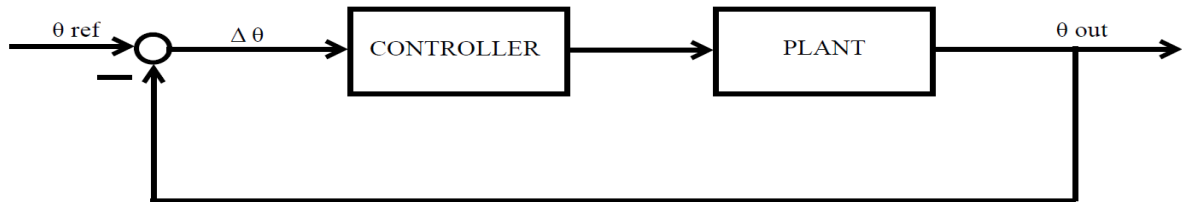


Figure 14: Position control scheme

The position control controls the position to be reached at any instant of time. Position/velocity control is often used in passive motion like predefined trajectory following and it aims to achieve a desired joint position/velocity in order to track a trajectory [1, 25]. The position can be defined both in the joint space and in the task space. In the first case, the positions that each single joint must occupy in space at a defined moment of time are defined. In the case of a multi degrees of freedom manipulator, each joint will have its own internal control in place. In the second case, the position that the end-effector must reach in space at a precise instant in time is defined. In the case of position control, the forces / torques acting either at the single joint or at the end-effector, are not taken into consideration.

2.2.4. Torque control

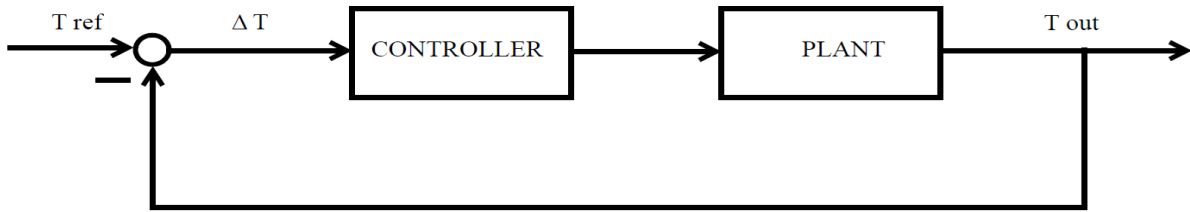


Figure 15: Torque control scheme

Torque control controls the force / torque exerted in a predefined instant of time, no matter where in space this is acting. Force/torque control aims to aid or even further augment the user's capability, a controller may estimate how much force/torque is needed and send the command to the actuators [1, 25]. Torque can be defined both in the joint space and in the task space. In the first case, the torques that each single joint must exercise are defined. In the case of a multi degrees of freedom manipulator, each joint will have its own internal torque control. In the second case, the torque that the end-effector must exert in space at a precise instant of time is defined. In the case of torque control, the position, either of the single joint or of the end-effector, is not taken into consideration. The force control produces high forces from small displacement: small position error can result in a large force error.

2.2.5. Impedance/Admittance control

Rehabilitation robots interact with the human body: for this reason, it is necessary to consider the manipulator and the patient as a single coupled mechanical system [70, 71]. A single position control is not sufficient to guarantee an appropriate and safe dynamic interaction between man and robot. The real-time adaptability between the robotic exoskeleton and the contact forces is needed to improve the interaction between two bodies [18]. Many exoskeleton controllers rely on more flexible impedance control, or its dual admittance control, with reduced corrective gains, instead of using rigid (high corrective gain) position feedback controllers. This choice is made to exhibit mechanical properties like human ones. These controllers allow to implement a good compromise between the tracking capabilities and compliance of the robotic arm [2]. The stiffness adjustment allows the user to feel if the exoskeleton is difficult or easy to move, sensing resistance. In most robots for upper limb rehabilitation, control methods are implemented on an impedance or admittance filter [25]. Impedance is a model-based force/torque controller with position feedback, while its dual, admittance control, is a position controller with force feedback.[72] In the impedance control approach, the movement of the limb is measured, and the robot provides the corresponding force feedback, while in the admittance control approach, the force exerted by the user is measured and the device generates the corresponding displacement [2, 15]. In impedance control the force is controlled where the position is given to the closed loop controller as feedback. Impedance control is used to modulate the dynamic behaviour of the system by accepting flow as an input and producing effort [73, 74]. The admittance control modulates the force accepting the effort as input and producing the flow. If force / torque sensors are equipped on the human-machine interface, the user's

movement produces a force-interacting force that directly translates into the movement of the exoskeleton [25].

2.2.5.1. Admittance control

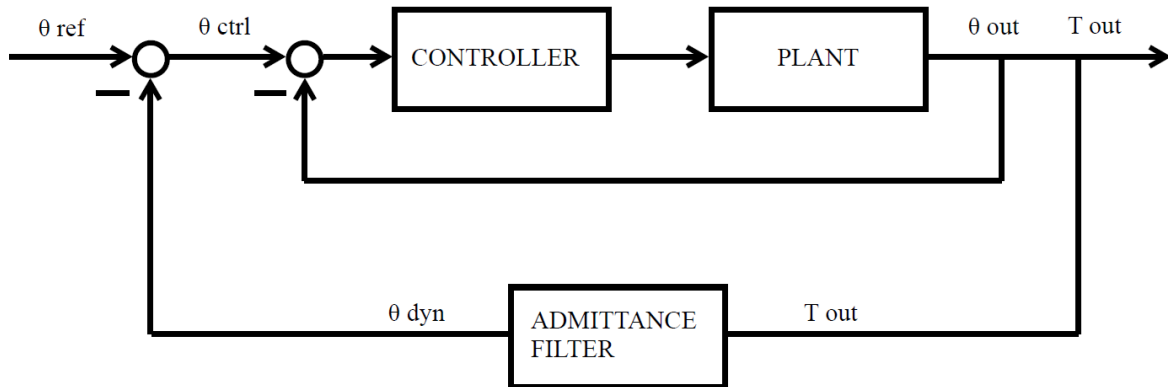


Figure 16: Admittance control scheme

The admittance control is a closed loop position control. Admittance controller accepts effort (e.g., force/torque signals) as inputs and yield flow (e.g., desired position commands) to actuators. The admittance control imposes a filter (admittance filter) that allows to modify the virtual dynamics of the robot, making it more compliant. When designing a control in pure position control, it is not possible in any way to modify the trajectory that leads the robot to reach that precise position. By applying an admittance filter, instead, it is possible to deviate the predefined trajectory of the robot, while always referring to a precise position to be reached. In this case, it is possible to interact with the robot itself, thus modifying the dynamics of the system. [69, 75-78]. In the field of robotic neurorehabilitation, a filter in admittance allows to manage the exoskeleton, thus creating a safer environment for the user. For example, let's consider the case in which, during the therapy, a patient wearing an exoskeleton makes a movement that causes pain: if the robot was in pure position control, the physiotherapist or the engineer who follows the patient, is unable to intervene with the robot, since the final position to be reached is fixed and pre-established. If, on the other hand, the exoskeleton was controlled in admittance, the robot becomes manoeuvrable and therefore the predetermined trajectory can be modified. The same concept and consideration are valid for the dual configuration, the impedance control (2.2.5.2). Even admittance control, as well as position control, can be implemented in both the task space, as shown in Figure 17 and the joint space, as shown in Figure 18 or even both.

Task Space Admittance control

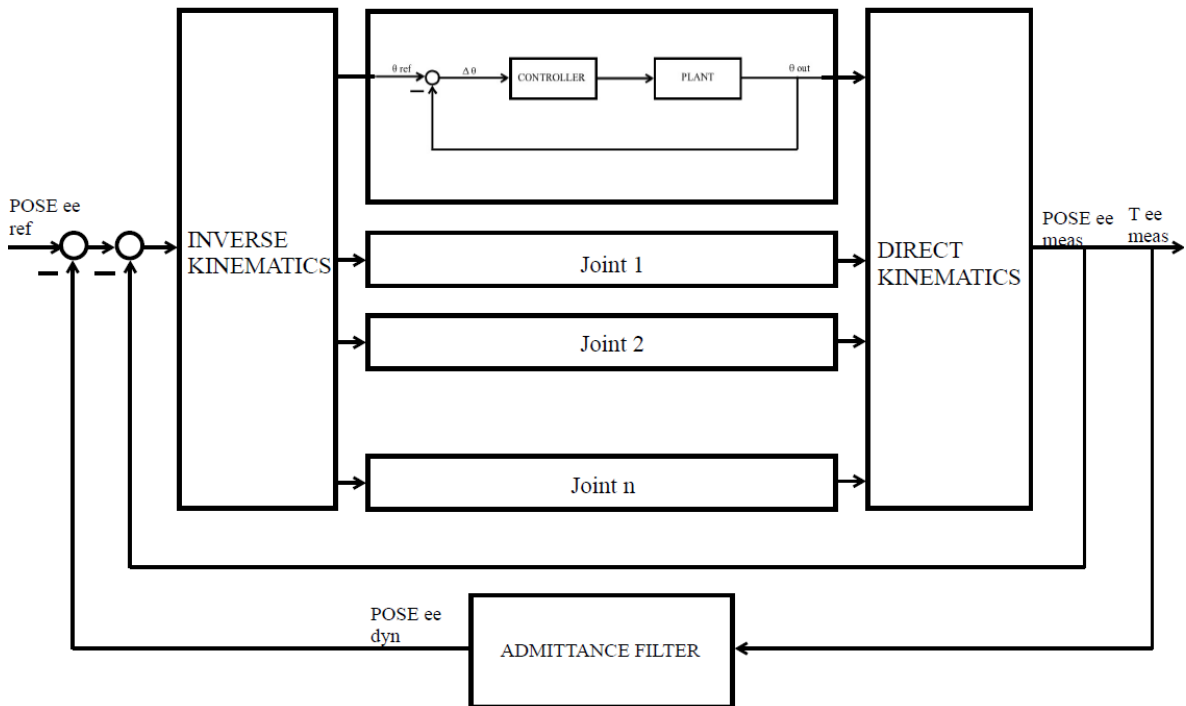


Figure 17: Task Space Admittance control scheme

Joint Space Admittance control

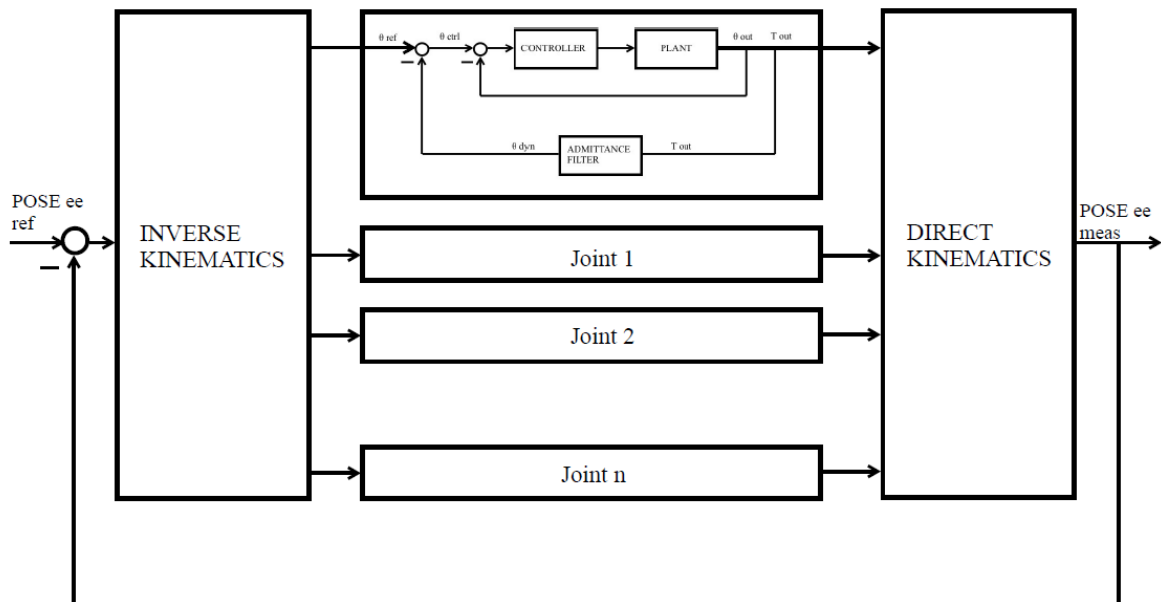


Figure 18: Joint Space Admittance control scheme

Equations



A dynamic system can be modelled as a mass spring damper system whose equations are:

linear: $m\ddot{x} + \beta\dot{x} + k(x - x_0) = F$

rotational: $J\ddot{\theta} + \beta\dot{\theta} + k(\theta - \theta_0) = T$

Take the rotational equation into analysis and pass to the Laplace domain:

$$J\theta s^2 + \beta\theta s + k\theta = T + k\theta_0$$

$$\theta(Js^2 + \beta s + k) = T + k\theta_0$$

The transfer function (TF) is defined as the ratio between the output and the input quantity. In an admittance filter, the input consists of a torque, the output from the position, so, the TF of the admittance filter in the Laplacian domain:

$$\frac{\theta}{T + k\theta_0} = \frac{1}{Js^2 + \beta s + k}$$

Equation 24: Admittance transfer function

This transfer function is a proper one, therefore it can be directly implemented in the control scheme.

2.2.5.2. Impedance Control

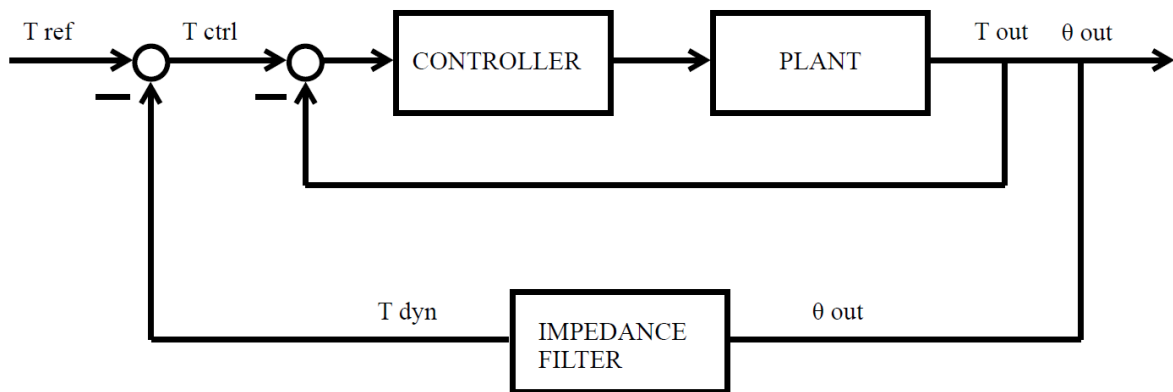


Figure 19: Impedance control scheme

Impedance control is a torque closed loop control. Impedance control is used to modulate the system's dynamic behaviour [70, 71]. It accepts flow (e.g., position/velocity) as inputs and yield effort (e.g., force/torque) [25]. The impedance control imposes a filter (impedance filter) that modifies the virtual dynamics of the system making the robot more compliant. In this case, it is therefore possible to modify the torque imposed, both at the single joint and at the end effector, by varying its intensity. Thanks to the impedance control, when the input reference torque is zero, the transparency control is obtained, that is a control that allows not to feel the load and the physical-mechanical weight of the exoskeleton itself.[70, 71, 76, 79-86]. Impedance control implies that the actuators should be high-precision force sources [29].

Mass and inertia of the exoskeleton should be minimized. Even impedance control, as well as torque control, can be implemented in both the task space, as shown in Figure 20 and the joint space, as shown in Figure 21 or even both.

Task Space Impedance control

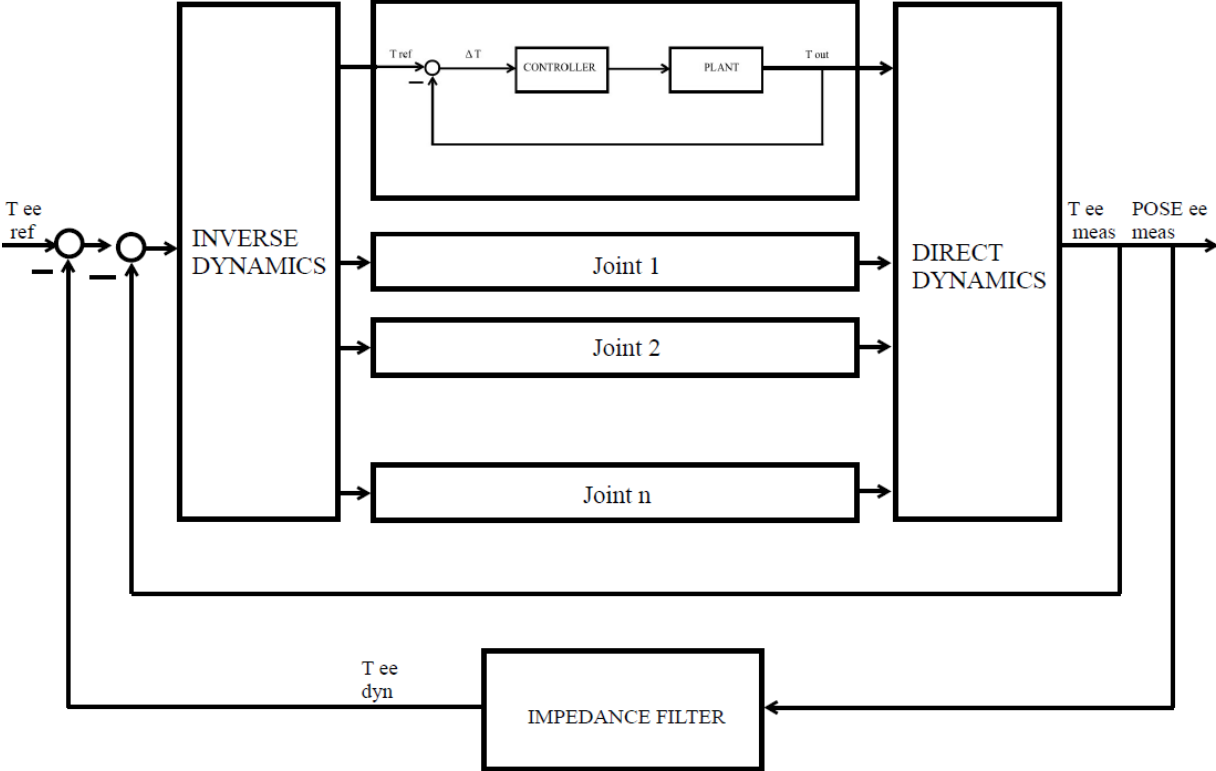


Figure 20: Task Space Impedance control scheme

Joint Space Impedance control

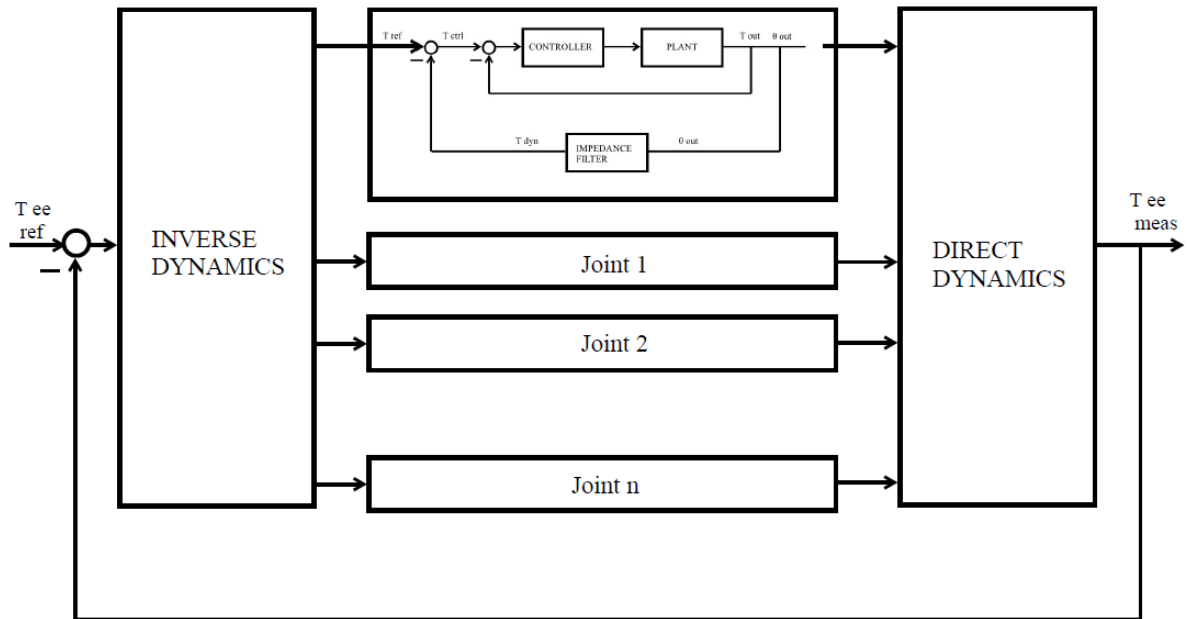


Figure 21: Joint Space Impedance control scheme

Equations



Recalling the equations described for the admittance filter in chapter 2.2.5.1 (equations), take the rotational equation into analysis and pass to the Laplace domain:

$$J\theta s^2 + \beta\theta s + k\theta = T + k\theta_0$$

$$\theta(Js^2 + \beta s + k) = T + k\theta_0$$

The transfer function (TF) is defined as the ratio between the output and the input quantity. In an impedance filter, the input consists of a position, the output is a torque, so, the TF of the impedance filter in the Laplacian domain:

$$\frac{T + k\theta_0}{\theta} = Js^2 + \beta s + k$$

Equation 25: Impedance transfer function

This transfer function is a unproper one, therefore it cannot be directly implemented in the control scheme.

2.2.5.3. Comparison between Admittance and Impedance control: pros and cons of dual control strategies

The advantages and disadvantages of impedance and admittance control systems are complementary. In general, impedance-controlled robots have stable interaction but poor accuracy in free space due to friction. This low accuracy can be improved by using inner torque sensors, as SEA, and low friction

couplings. Admittance control compensates for the mass and friction of the device and provides greater accuracy in non-contact tasks but can be unstable during dynamic interactions [15]. This problem is eliminated by using series elastic actuators (SEA). Devices that use admittance control also require high gear ratios (eg harmonic drives) for precise motion control [76, 77]. Impedance control is efficient for lightweight rear-guided exoskeletons (often driven by cable devices). In these systems, problems arise when it is necessary to compensate for gravity and friction.[2]. For exoskeletons lacking rear guidance, admittance control may be more appropriate, because the forces at the interfaces with the human limb must be measured to move the robot, thus considering its inertia and dynamic effects [87] . The limitation of impedance control is that the system becomes unstable if the mechanical impedance is high and requires natural dynamics [81].The main advantage of using the admittance controller is that it does not require model feedforward to compensate for natural dynamics, rather it depends on the high PID gains of the joint position. However, this type of controller maintains its stability as long as it does not have a high impedance [30]. The main pros and cons of the two dual control strategies are shown in Table 10.

Admittance		Impedance	
Closed-loop control of motion		Closed-loop control of force	
Pro	Cons	Pro	Cons
No need for natural dynamic compensation	Constrained motion	Stable at low impedances	Free motion
	Inverse kinematic is required: deal with singularities		Gravity/frictions compensation is needed for good force replication
	Instability for high admittance (low impedance)		Inverse dynamic needed to deal with position derivatives

Table 10: admittance/impedance comparison

2.2.6. Transparency Control

One of the main features of the exoskeleton is transparency, i.e., the possibility of creating a torque control that is quite accurate to create a safe environment for the patient. In this regard, SEAs are a good solution to implement a complaint control. Transparency is a performance indexes that quantifies an exoskeleton ability to precisely produce a programmed assistance to the subject [2]. Transparency measures the ability of the robot not to apply any resistance to freedom of movement, it allows the patient not to perceive the actual weight of the exoskeleton. Transparency is an index of the mechanical properties of the structure, of its actuation, and of the performance of the dedicated low-level control feedforward compensation of gravity and friction[88]. A lack of transparency can generate unwanted resistance during the movement of the upper limb of subjects from which excessive muscular efforts can arise to complete even simple movements[89, 90]. The level of transparency directly affects the physical behaviour of the robot and possibly disrupts the robot's strategy rehabilitation control

Chapter 3: Materials and Methods

This section analyses both the " materials ", that is what software or hardware has been used for the design of the controls, and the " methods ", that is the way in which the design took place. In particular, the description of the software environments used and the hardware with which it was possible to implement the codes developed for the control part are presented. Descriptions of the components used are also given, together with the description of the different SEAs joints used. Subsequently, the specific descriptions of the test benches used for the purposes of the tests are reported: the setups of the test benches with one degree of freedom and two degrees of freedom are described in detail.

3.1. Software

Recent technological advances have enabled the development of viable exoskeletal robots. The modelling software allowed the exoskeletons to be tested in simulations before they were manufactured, enabling rapid prototype development. Biomechanical modelling allows the exoskeleton to mimic the dynamics of the human limb [28]. In this chapter, the main software and environment used for the development of this thesis are shown and briefly described.

3.1.1. MATLAB and Simulink

MATLAB is a numerical programming and computing platform of MathWorks company. Simulink is a software simulation environment, belonging MathWorks company, in which systems can be designed and simulated with the aid of block diagrams. Simulink allows to develop a model-based design of a software. Thanks to Simulink it is possible to design an offline system, based on a simulation time, and then deploy on a real time target machine, like Speedgoat, to see its behaviour in Real Time.

3.1.1.1. Simscape Library in Simulink

Simscape is a Simulink toolbox that allows to model and simulate multidomain physical systems. With Simscape it is possible to create models of physical systems within the Simulink environment. Simscape allows to develop control systems and test system-level performance. To be able to implement models in other simulation environments, such as for hardware-in-the-loop (HIL) systems, Simscape supports C code generation.

3.1.1.2. Multibody

Simscape Multibody provides a multibody simulation environment for 3D mechanical systems, using blocks representing bodies, joints, constraints, force elements and sensors. Simscape Multibody formulates and solves the equations of motion for the complete mechanical system. CAD geometries, including masses, inertias, joints, constraints, and 3D geometries can be imported into the model.

3.1.2. App Designer

App Designer is a MATLAB (MathWorks Company) tool that allows you to create your own graphical user interface (GUI). During this thesis, several graphical interfaces have been designed. In particular, the use of the GUI makes the choice of some parameters, corresponding Simulink models, more intuitive and user-friendly, especially when these models are deployed on Speedgoat for real time simulation.

3.1.3. Creo Parametric

Creo is a 3D CAD design software that allows to design the entire product. In this thesis, all the test benches are being previously recreated in Creo environment and then used both for testing purposes, by using multibody, and for study the correct geometries of the system.

3.1.3.1. Simscape Multibody Link Creo Plug-In

To transfer the CAD models developed in the CREO environment, the specific plug-in was used in the Multibody-Simscape environment. Through this plug-in, the spatial configurations, reference systems, and mechanical and physical properties of bodies, which are defined in Creo, also remain unchanged in the Simulink environment.

3.2. Real Time target machine

This sub-chapter shows the tools and hardware that allow the deployment of offline codes in real time to be able to characterize the behaviour of a system, previously analysed in simulation, even in a real test bench.

3.2.1. Simulink Real Time

Simulink Real-Time allows to create real-time applications from Simulink models and run them on Speedgoat target hardware connected to the physical system. It is designed for real-time test and simulation activities, including Rapid Control Prototyping (RCP) and Hardware-In-the-Loop (HIL) simulation.

3.2.2. Speedgoat

Speedgoat is hardware target where it is possible to run real-time applications created from Simulink models. Using the Speedgoat Simulink driver blocks in the model, it is possible to automatically generate the application in real time, then download and run it on the target machine. The typical configuration of the direct connection between Speedgoat and the Host PC is the one shown Figure 22.

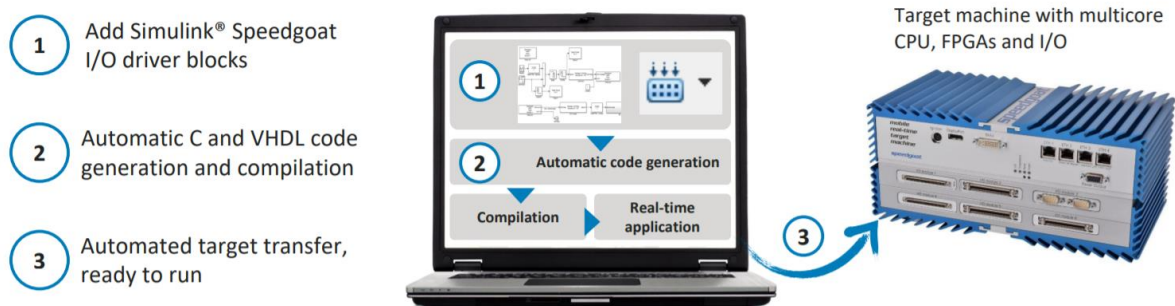


Figure 22: From Desktop to Real-Time Simulation and Testing, Reference to [91].

MATLAB 2019b was used. To test Simulink designs on hardware, you can use the Model-Based Design Workflow, as shown in Figure 23.

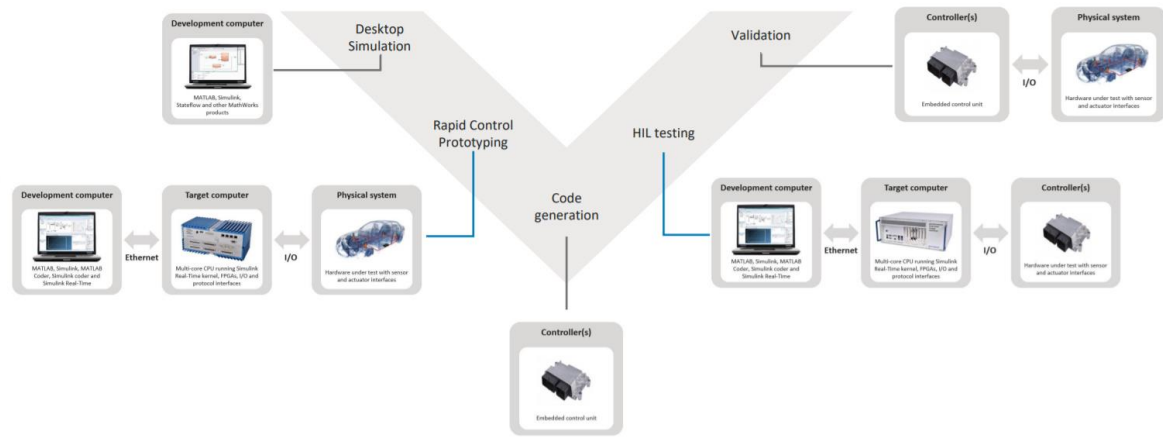


Figure 23: Supported Real-Time Testing Configurations. Reference to [91].

The Performance real-time target machine is used for The Performance real-time target machine is used for rapid control prototyping or plant simulation with hardware-in-the-loop (HIL). This target machine is designed specifically for Simulink Real-Time in close collaboration with MathWorks

3.3. Metrics and parameters for validation

A widely used quantitative measure for evaluating system performance is bandwidth [27]. Systems with a higher bandwidth are controllable with higher frequency command signals. Bandwidth is a measure of the effectiveness of trade-offs between weight and stiffness. To maintain performance, the lowest natural frequency of the robot exoskeleton should be higher than the human-generated highest frequency command signal [24]. In this chapter, a briefly description of parameters, used for analysis purposes, and metrics, used for validation purpose, is explained.

3.3.1. Root-mean square error (RMSE)

Root-mean square error is a statistical quantity that is a measure of accuracy. The RMSE is the square root of the mean squared error (MSE): mean of the squares of the errors, which is the mean squared difference between the estimated $\hat{\theta}$ values and the actual value θ . The RMSE allows to quantify the difference between an estimated and an observed value. The root-mean square error is always a non-negative value: the more RMSE tends to zero, the greater the perfect fit of the predicted data with those observed [92]. Consider wanting to calculate RMSE of a signal of N samples, with N0 the number of initial samples neglected as belonging to a transient time for reaching steady state; given an estimated $\hat{\theta}$ and an observed value θ , the RMSE is:

$$RMSE = \sqrt{\frac{\sum_{i=N_0}^N (\hat{\theta} - \theta)^2}{N - N_0}}$$

Equation 26: Root-mean square error

3.3.2. Standard Deviation (SD)

The standard deviation (SD) σ is a statistical measure that evaluates the amount of variation or dispersion of a set of values. The expected value is the average value of a set of values: the lower the standard deviation, the more the values tend towards the expected value. Given a data set or probability distribution, the standard deviation is the square root of the variance: the latter is a measure of dispersion, that is, a measure of how well a set of numbers is distributed with respect to their mean value.[93]

3.3.3. Fast Fourier Transform (FFT)

A fast Fourier transform (FFT) is an algorithm that calculates the discrete Fourier transform (DFT) of a sequence by converting the signal from its original domain (e.g. time) to the frequency domain, defining the power of the signal. [94].

3.3.4. Rise Time, Settling Time, and Overshoot

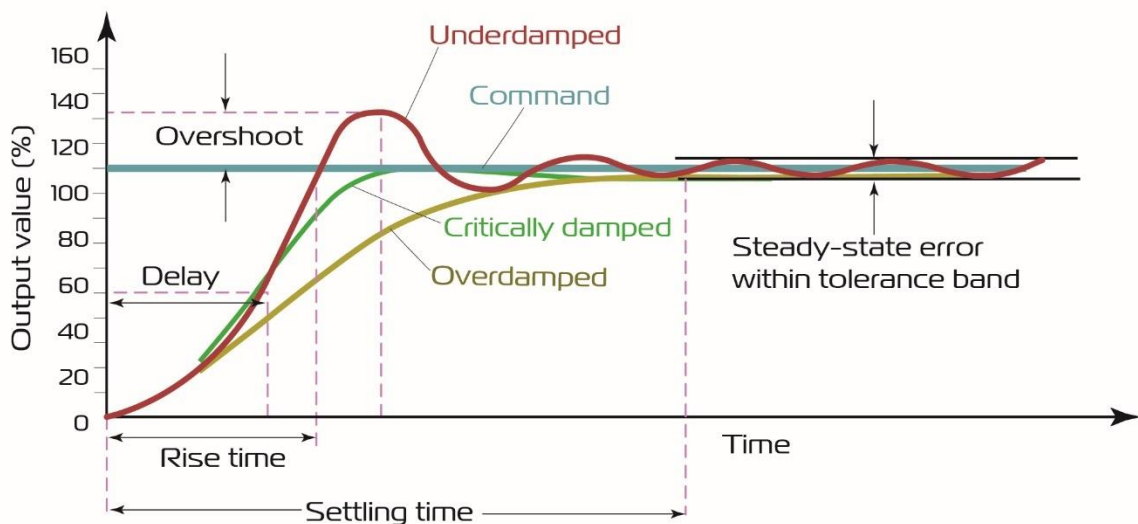


Figure 24: Step response in time: rise time, settling time and overshoot analysis. Reference to [95].

The rise time t_r is the time required for the response to rise from 0% to 100% of its steady state value. Depending on the type of system being analysed, the rise time is defined with different percentages. Consider a second order systems:

- underdamped: 0%-100%
- critically damped: 5%-95%
- overdamped: 10%-100

The settling time $\pm \alpha * 100 \%$, $t_{s,\alpha}$ is the amount of time required for the step response to reach and stay within a range about $\pm \alpha * 100 \%$ of the steady-state value. Typical values of α are: $\alpha=0.01$, $\alpha=0.02$, $\alpha=0.05$. Given a system having damping factor equal to ξ , natural frequency ω_0 and tolerance α , then, the settling time of the system will be:

$$ts_{\alpha\%} = -\frac{\ln(\alpha)}{\xi \omega_0}$$

Equation 27: settling time

The overshoot \hat{s} of a signal is defined as the excess of the signal over its target. The overshoot is the maximum amount by which the response exceeds the steady state value and is therefore the amplitude of the first peak. The overshoot is often written as a percentage of the steady-state value. In control theory, overshoot refers to an output that exceeds its final steady state value: it is the maximum peak value of the response curve measured by the desired system response.

Given an input step to a second order ξ damping system:

$$\hat{s} = 100 * e^{\left(\frac{-\xi * \pi}{\sqrt{1-\xi^2}}\right)}$$

Equation 28: overshoot

3.4. Mechatronic components of Series Elastic Actuator

During this experimental thesis, several series elastic actuators (SEA) have been tested. SEAs were tested with different motors (EC 90 flat Ø90 mm, brushless, 90 Watt and EC 45 flat Ø43.5 mm, brushless, 80 Watt), different servo-controllers (ESCON 70/10 and EPOS4) and with different springs depending on the joints. The compliant element (spring) was designed and built custom-made. The several SEAs developed for the Float EVO upper-limb exoskeleton are different each other, depending on the type of motor used and the type of custom-made compliant element. Two different motors were tested, and three different springs were analysed. The spring, sometimes, was mounted in different configuration.

3.4.1. SEA with EC-90 motor:

The SEA consists of a current/torque-controlled BLDC motor (EC 90 flat Ø90 mm, brushless, 90 Watt) with a servo driver (ESCON 70/10 or EPOS4), a harmonic gear (Harmonic Drive, CSD-17-2A-100) a torsional spring (custom-made), and two encoders (AksIM-2 off-axis rotary absolute encoder 18-bit resolution). The custom-made compliant elements which have been tested are:

- STA: star-shaped spring made of steel.
- SPT2P: spiral shaped spring made of steel with 2 pins.

3.4.2. SEA with EC-45 motor:

The SEA consists of a current/torque-controlled BLDC motor (EC 45 flat Ø43.5 mm, brushless, 80 Watt) with a servo driver (ESCON 70/10 OR EPOS4), a harmonic gear (Harmonic Drive, CSD-17-2A-100) a torsional spring (custom-made), and two encoders (AksIM-2 off-axis rotary absolute encoder 19-bit resolution). The custom-made compliant element which has been tested is:

- SPT1P: spiral shaped spring made of steel with 1 pin.

3.4.3. EC: Brushless DC Motor

The EC motor is a brushless, electronically commutated permanent magnet DC motor (BLDC) (chapter: 0) with Hall sensors.

EC 90 flat Ø90 mm, brushless, 90 Watt

The EC 90 motor used in the SEA configuration is 24 V nominal voltage with 2590 rpm nominal speed and maximum continuous torque is 444 mNm. The maximum percentage of efficiency is 84%. The main characteristics of EC 90 are shown in the Table 11.

EC 90 flat Ø90 mm, brushless, 90 Watt	
nominal voltage	24 V
nominal speed	2590 rpm
nominal torque (maximum continuous torque)	444 mNm
maximum efficiency	84%
terminal resistance phase to phase	0.343 Ω
mechanical time constant	21.1 ms
rotor inertia	3060 gcm ²

Table 11: EC 90 datasheet, reference to [96].

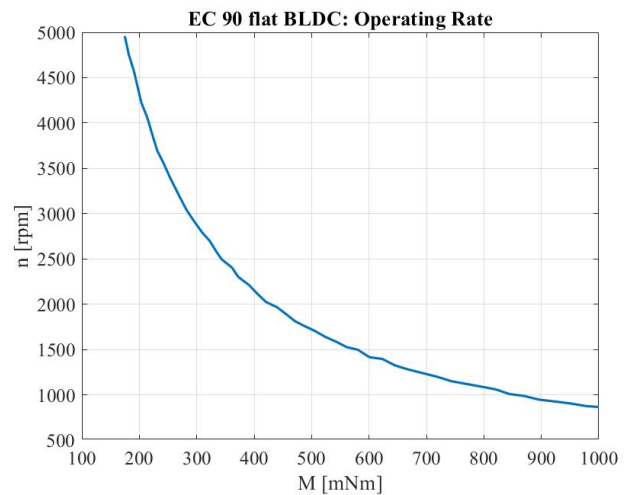
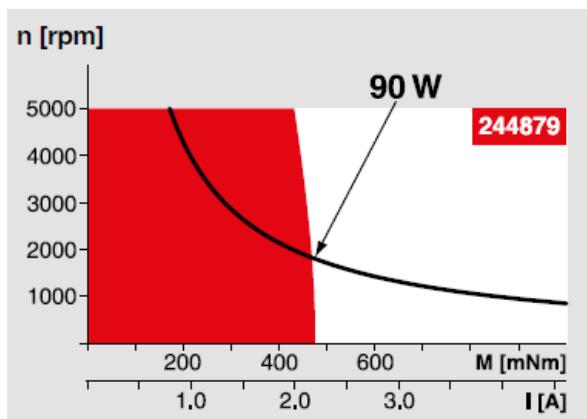


Figure 25: Operating range curve. (a) from EC 90 datasheet, red zone: continuous operation, white zone: short term operation, black curve: assigned power rating; (b) assigned power rating obtained with MATLAB plot of data from WebPlotDigitizer tool

To evaluate the relationship between the torque and speed, the operating range plot has been considered. From datasheet the curve is given. By using WebPlotDigitizer online tool, the curve has been selected so the assigned power rating (point-to-point correspondence between torque and speed) has been found. The data obtained, have been plot on MATLAB.

EC 45 flat Ø43.5 mm, brushless, 80 Watt

The EC 45 motor used in the SEA configuration is 24 V nominal voltage with 4560 rpm nominal speed and maximum continuous torque is 167 mNm. The maximum percentage of efficiency is 84.9 %. The main characteristics of EC 45 are shown in the Table 12.

EC 45 flat Ø43.5 mm, brushless, 80 Watt	
nominal voltage	24 V
nominal speed	4560 rpm

nominal torque (maximum continuous torque)	167 mNm
maximum efficiency	84.9 %
terminal resistance phase to phase	0.573 Ω
mechanical time constant	6.350 ms
rotor inertia	181 gm ²

Table 12: EC 45 datasheet, reference to [97].

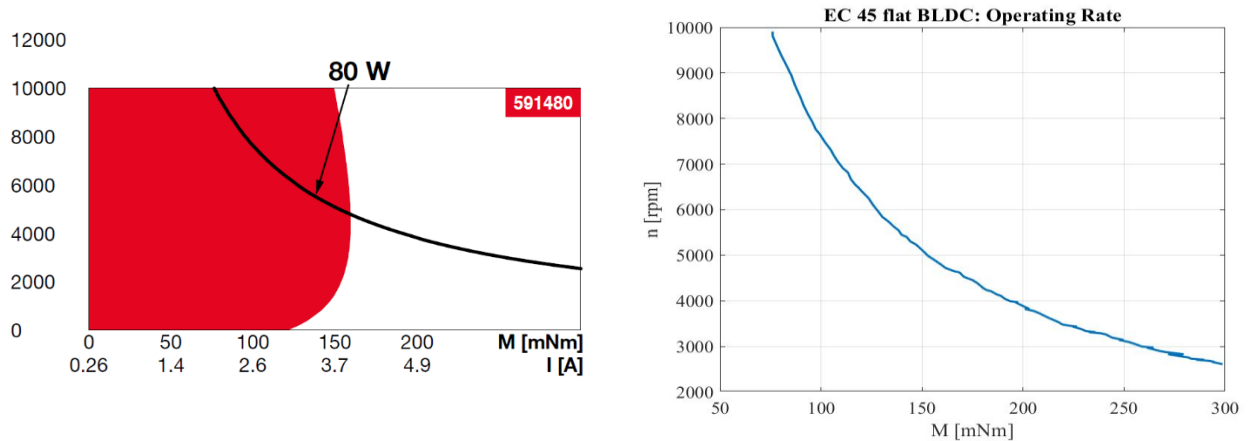


Figure 26: Operating range curve. (a) from EC 45 datasheet, red zone: continuous operation, white zone: short term operation, black curve: assigned power rating; (b) assigned power rating obtained with MATLAB plot of data from WebPlotDigitizer tool

To evaluate the relationship between the torque and speed, the operating range plot has been considered. From datasheet the curve is given. By using WebPlotDigitizer online tool, the curve has been selected so the assigned power rating (point-to-point correspondence between torque and speed) has been found. The data obtained, have been plot on MATLAB.

3.4.4. Servo controllers: ESCON and EPOS

Maxon motor control's ESCON 70/10 is a small-sized, powerful 4-quadrant PWM servo controller for the highly efficient control of permanent magnet-activated brushless EC motors up to approximately 700 Watts, as reported in datasheets [98, 99].

Maxon motor control's EPOS4 50/5 is a small-sized, fully digital, smart positioning control unit. Its high-power density allows flexible use for brushless EC (BLDC) motors up to approximately 250 Watts. The EPOS4 is specially designed to be commanded and controlled as a slave node in a CANopen network. Those servo controllers can work with various feedback options, such as Hall sensors, incremental or absolute encoders. The main difference between ESCON and EPOS servo controllers is that ESCON is a velocity and torque controller only while EPOS can control also position. The other differences between ESCON and EPOS are shown in the Table 13.

ESCON	EPOS
Velocity and current/torque control only.	Position, Velocity, and Current-/Torque control.
Maxon's "ESCON Studio" software	Maxon's "EPOS Studio" software
Commanding by analog or digital I/O signals.	Sinusoidal / FOC motor communication in case of brushless motors with an encoder.
Different predefined functions can be linked to I/O signal states: e.g. A/D communication	Different bus interfaces: e.g., CANopen

No data exchange or commanding by USB interface possible.	Master controller mandatory to command the EPOS4 by bus.
USB can just be accessed for initial commissioning, parameter tuning, parameter up-/download, controller monitoring, or data recording with Maxon's "ESCON Studio" software	Motion control slave based on CANopen device profile for drives and motion control
No software libraries or protocol specification available.	Commanding by analog input just possible for velocity and current control.
No documentation of internal control structures and control algorithms available	Position control can just be commanded by bus commands by a master
	Comprehensive documentation about the EPOS4's object dictionary and control structures / algorithms.
	Software libraries for Windows and Linux systems

Table 13: comparison between ESCON and EPOS

The EPOS servo controller can be set to different operating modes, according to the type of self-tuning control it is wanted to be implemented. The main modes are collected in the Table 14. In this thesis two typologies have been studied and implemented, based on the CANopen communication protocol: CSP and CST mode.

Homing Mode (HMM)	The axis references to an absolute position using the selected homing method.
Profile Position Mode (PPM)	The axis moves to an absolute or relative position using a motion profile.
Profile Velocity Mode (PVM)	Motor shaft rotates with a certain speed with velocity profile.
Cyclic Synchronous Position Mode (CSP)	The axis moves to an absolute or relative position.
Cyclic Synchronous Velocity Mode (CSV)	The axis moves with the commanded velocity.
Cyclic Synchronous Torque Mode (CST)	Applies a certain torque (that is: torque = current x torque constant) to the motor winding

Table 14: EPOS working modes, reference to [100, 101]

3.4.5. Harmonic drive

The used gear box is a Harmonic Drive, CSD-17-2A-100, which size is 17 cm and reduction ratio are 100. The main characteristics of the harmonic drive are shown in the Table 15.



Figure 27: Harmonic Drive, CSD-17-2A-100,

CSD-17-2A-100	
Ratio	100
Size	17 Cm
Repeatable Peak Torque T_R	37 Nm
Average Torque T_A	27 Nm
Rated Torque T_N	16 Nm
Maximum Input Speed	10000 Rpm (Oil) 7300 rpm (Grease)
Average Input Speed	6500 rpm (Oil) 3500 rpm (Grease)
Moment Of Inertia	0.054×10^{-4} Kgm ²
Weight	0.1 Kg

Table 15: Harmonic Drive datasheet, reference to [102]

The efficiency of the Harmonic Drive is not constant, but it depends on the torque factor V and on the type of the gear used.

3.4.6. Compliant element

The compliant elements of the SEA (springs) were made custom-made from a team of mechanical engineers of the Rehab - IIT laboratory.

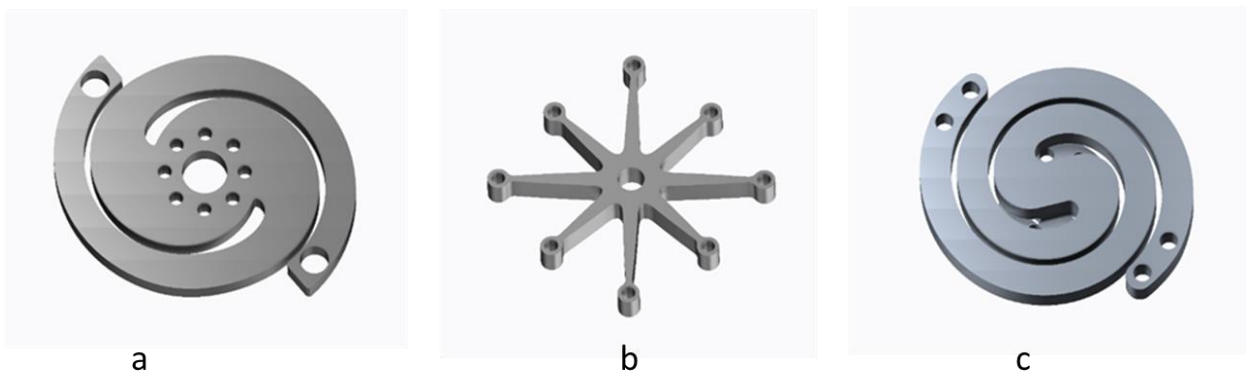


Figure 28: Custom made compliant element, (a) SPT1P: spiral geometry, titanium material with 1 pin for connection, (b), STA: star geometry, steel material, (c) SPT2P: spiral geometry, titanium material with 2 pins for connection

The springs custom made analysed are:

- SPT1P (SP → spiral T → titanium 1P → pin)
- STA (ST → star A → steel (A from Italian 'acciaio'))
- SPT2P (SP → spiral T → titanium 2P → 2 pins)

From the study of the state of the art on the compliant element for Series Elastic Actuators intended for the realization of an actuated upper limb exoskeleton, emerged that the average torque needed for the main groups of joints are:

- scapular joint: 50Nm – 60 Nm
- spherical joint: 32 Nm – 35 Nm

The choice of the optimal elastic element is made by considering some technical features of the torque with respect to the displacement:

- linearity
- low hysteresis
- absence of dead band

In general terms, however, the performance of a torsional elastic element, that must be inserted in a specific space, can be maximized by trying to obtain high values in the maximum torque to which it can be subjected. It is unknown which stiffness of the elastic element is optimal for the best compromise between stiffness of the structure and sensitivity of the measurement. A greater deformation with the same torque, in fact, creating a greater phase shift between the two encoders allows a higher measurement resolution; however, a less rigid structure may be more difficult to control. The application in the SEA certainly requires a high-performance element, for this reason the materials that correctly behaves under elastic strain have been chosen. The materials generally used for high performance springs have a high resilience and are, as in our tests, alloy steels (A) and titanium alloys (T). These materials also have high fatigue limits. Once the material has been chosen and the objectives of maximum torque and maximum deformation have been defined, the geometry of the spring is constructed. It will vary slightly depending on the material chosen or the different Young's modulus and the yield and fatigue stress that can be tolerated. The geometries of the compliant elements have been drawn starting from the evaluation of some qualitative features reported in Table 16.

	Reachable stiffness	Maximum deformation or maximum rotation	Axial encumbrance	Uniform distribution of tensions	Compatibility with available space	Scalability
Star geometry (STA)	High	Low	Low	High	Low	Medium
Spiral geometry (SPT)	Low	High	Medium	Low	High	High

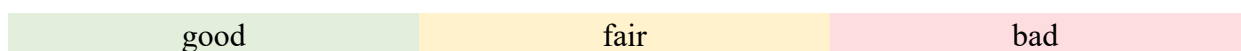


Table 16: Qualitative evaluation of the main technical features. Analysis on the geometry of the compliant element

The main geometry features are related on the type of assembly into the system designed:

- axial compactness
- easy to assembly
- fatigue resistance (low stress concentration, good surface finish, suitable material)
- low weight
- cheap
- scalable

To define which configuration was the best one and to understand if there were some critical experimental aspects that have not been considered in the theoretical evaluation, some tests have been performed. What emerged was that the spiral geometry is the optimal one since with the same torque withstood, it can guarantee greater deformations and because it occupies less volume. By frequency analysis, it emerged that the hysteresis of this type of configuration was lower than the one with star geometry, as reported in chapter 0. On the other hand, spiral geometry is more expansive to reproduce because of it is difficult to design and reproduce. An additional point of interest is the introduction of the bearings: they were inserted in the hypothesis that they could have positive effects on hysteresis. In the type of shape chosen, in fact, the only points where, in theory, a sliding of the elastic element with respect to the support occurs, are the external fixings. The sliding causes friction losses and therefore hysteresis in the element loading and unloading cycle. Thanks to the bearings, this loss of energy can be minimized.

3.4.7. Encoders



Figure 29: AksIM-2 Off-Axis Rotary Absolute Magnetic Encoder, reference to [103]

AksIM-2 is a non-contact, high performance off-axis absolute rotary encoder designed for integration into applications with limited space. The AksIM-2 encoder system consists of an axially magnetised ring and a redhead. A typical application is a robot arm joint with a cable feed through the ring, or a precision gearbox where the ring is mounted on the main transmission shaft: the two encoders Upstream and downstream of the compliant element.

3.4.7.1. Wrap/Unwrap method

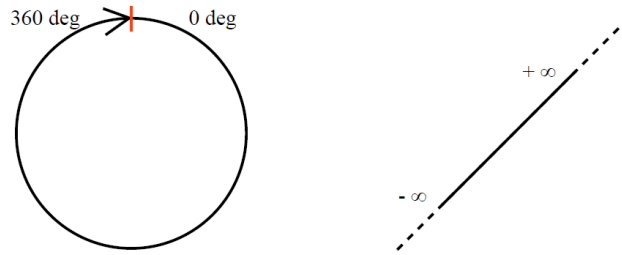


Figure 30: From angular to linear domain, wrap/unwrap operation

Phases unwrap or unwrap is a process used to reconstruct a signal's original phase. Unwrap algorithms add appropriate multiples of 2π to each phase input to restore original phase values. The data read by the encoders are expressed in ticks' units of measurement. To be able to transform the data into more useful units of measurement (e.g., degrees or radians), an unwrap operation is performed. The unwrap allows to linearize the circular domain of the angles. In fact, the angles, expressed both in radians and in degrees, belong to a domain $[0^\circ-360^\circ$ or $0-2\pi]$. Consider the angles in degrees: in angular domain, a difference, minimal, which implies the passage from 360° to 361° as a difference from 360° to 1° , causing an erroneous difference of 359 degrees. Thanks to the unwrap operation, the angular domain is linearized to be able to work in the range $[-\infty, +\infty]$ so that, using the same example, a difference from 360° to 361° is considered as a single degree difference.

3.5. Experimental Setup for Real Time simulation

This section focuses on the explanation of the mechatronic components used and on the setup of the various test benches tested.

3.5.1. Actuators under test: system components

This section analyses the characteristics of the Series elastic actuators that have been tested.

3.5.1.1. EC90 motor SPT2P compliant element



Figure 31: SEA configuration: EC90 motor with SPT2P compliant element, focus on each SEA component disassembled, BLDC motor, Harmoni Drive, Encoders, and compliant element

The configuration of this joint has the SEA which is made up of the elements shown Table 17. The elements that make up the SEA mechanically can be viewed in Figure 31. The compliant element is a titanium spring of spiral geometries. The peculiarity of this SEA is the presence of the AksIM-2 off-axis rotary absolute encoder 18-bit resolution which are placed parallel and in the same direction. This provides that the displacement of the spring is read as the actual difference between the upstream position and downstream position of the compliant element as shown in Equation 2.

SEA CHARACTERIZATION		
SEA CONFIGURATION	MOTOR	EC 90
	GEAR BOX	HARMONIC DRIVE CSD-17-2A-100
	SPRING	SPT2P
ENCODERS	2 ABSOLUTE ENCODER – AKSIM 18 bit	

Table 17: SEA characterization EC 90 motor SPT2P compliant element

3.5.1.2. EC90 motor STA compliant element

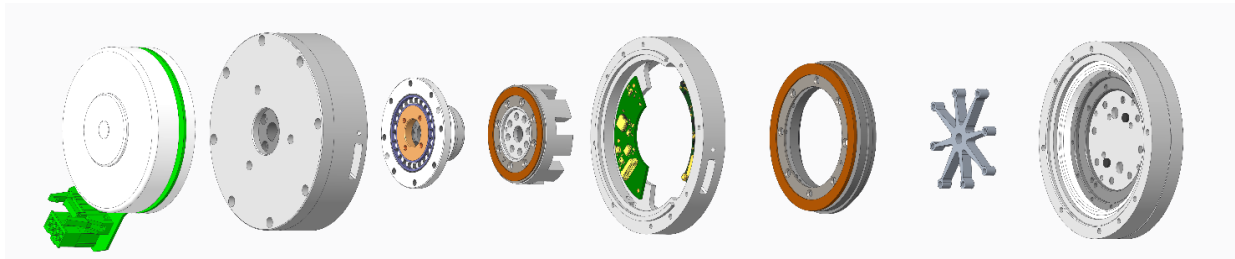


Figure 32: SEA configuration: EC90 motor with STA compliant element, focus on each SEA component disassembled, BLDC motor, Harmoni Drive, Encoders, and compliant element

The configuration of this joint has SEA which consists of the elements shown in Table 18. The elements that make up the SEA mechanically can be viewed in Figure 32 . The compliant element is a star geometry steel spring. Also, in this joint, the peculiarity of is the presence of the AksIM-2 off-axis rotary absolute

encoder 18-bit resolution which are placed parallel and in the same direction. This provides that the displacement of the spring is read as the actual difference between the upstream position and downstream position of the compliant element as shown in Equation 2.

SEA CHARACTERIZATION		
SEA CONFIGURATION	MOTOR	EC 90
	GEAR BOX	HARMONIC DRIVE CSD-17-2A-100
	SPRING	STA
ENCODERS	2 ABSOLUTE ENCODER – AKSIM 18 bit	

Table 18: SEA characterization EC 90 motor STA compliant element

3.5.1.3. EC45 motor SPT1P compliant element



Figure 33: SEA configuration: EC45 motor with SPT1P compliant element, focus on each SEA component disassembled, BLDC motor, Harmoni Drive, mirrored Encoders, and compliant element

The configuration of this joint has an SEA which consists of the elements shown Table 19. The elements that make up the SEA mechanically can be viewed in Figure 33. The compliant element is a titanium spring of spiral geometries. The characteristic of this SEA lies in the presence of the 19-bit resolution AksIM-2 off-axis rotary absolute encoders which are mirrored and in opposite direction, as well as having a higher resolution than the encoders used in the joints with EC90 motor. This foresees that the displacement of the spring is read as the algebraic sum between the upstream position and downstream position of the compliant element as shown in Equation 2.

SEA CHARACTERIZATION		
SEA CONFIGURATION	MOTOR	EC 45
	GEAR BOX	HARMONIC DRIVE CSD-17-2A-100
	SPRING	SPT1P
ENCODERS	2 ABSOLUTE ENCODER – AKSIM: 18 bit and 20 bit	

Table 19 : SEA characterization EC45 motor SPT1P compliant element

3.5.2. SEA characterization

For the characterization of the Series Elastic Actuators, the SEA was analysed in two different configurations: the first test bench requires the SEA to be subjected to a infinite inertial load, in fact the joint was blocked to the wall, in the second case, the joint has been subjected to a known load and therefore free to move.

3.5.2.1. Infinite inertial load

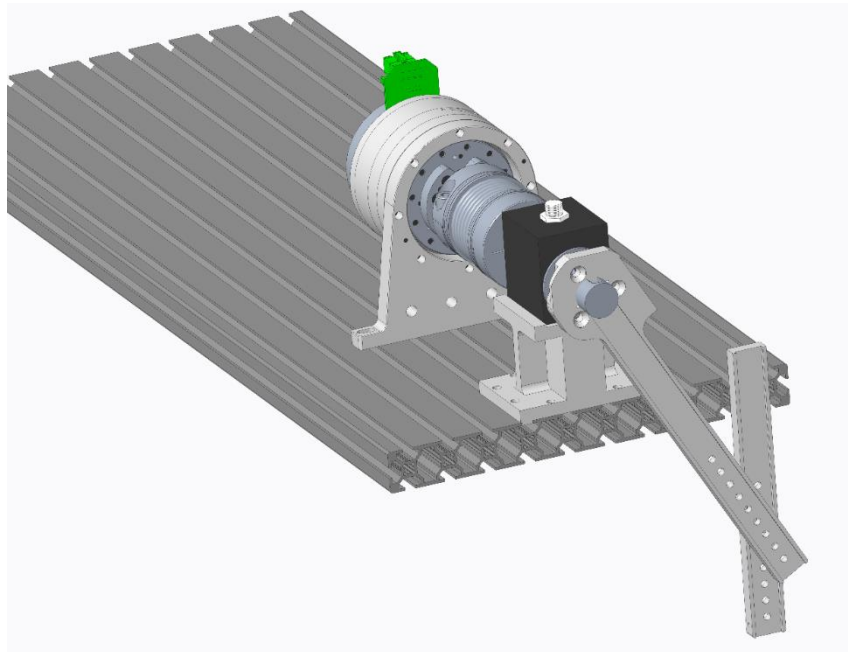


Figure 34: Infinite inertial load test bench. The test bench is blocked, so it is not free to move. This configuration simulates an infinite inertial load. The main components are a SEA, bellow, and industrial torsionmeter.

The test bench for the characterization of the SEA subjected to an infinite inertia load, consists of the SEA, whose characteristics have been described in chapter 3.4, an ESCON servo controller (chapter 3.4.4), an industrial torsionmeter and a real time target machine, Speedgoat (chapter 3.2.2). The setup details are described in Table 20. To verify and validate that the SEA behaves as a reliable torque sensor, an industrial torsionmeter was used. In this case it will be possible to test that the torque calculated by Hooke's Law (Equation 2) and the one read by the torsionmeter at the slow axis of the SEA joint, are equal. The main feature of the following setup Figure 34 is to exert an infinite inertia load since the system is locked to the wall. This configuration made it possible to analyse the frequency behaviour of the SEA (see chapter 4.1 for the results). The setup is then used to provide input to the SEA, thanks to the deployment of the Simulink Seafloat_ESCON model on Speedgoat (chapter 3.6.1) and, thanks to the encoders, the SEA itself and the torsionmeter, data are saved on the Speedgoat, from which the data are then retrieved to be analysed and studied offline with the Simulink-Simscape model (chapter 3.7.2).

SEA CHARACTERIZATION		
SEA CONFIGURATION	MOTOR	EC 90 or EC 45
	GEAR BOX	HARMONIC DRIVE CSD-17-2A-100
	SPRING	SPT2P / STA or SPT1P
SERVO CONTROLLER	ESCON	
TORSIOMETER		
ENCODERS	2 ABSOLUTE ENCODER - AKSIM	

Table 20: Test Bench for Series Elastic Actuator (SEA) characterization: infinite inertial load

3.5.2.2. Finite inertial load

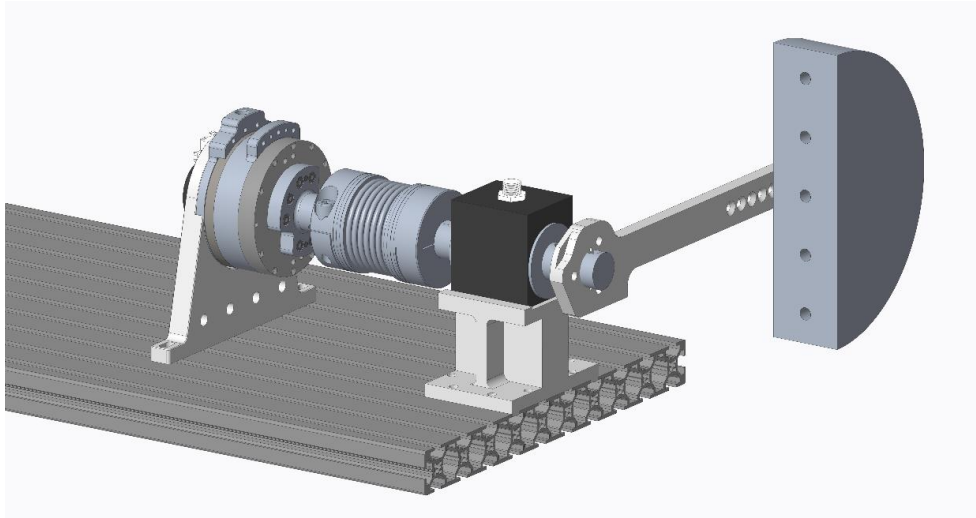


Figure 35: Finite and known inertial load, test bench free to move. The main components are a SEA, bellow, and industrial torsionmeter.

The setup under analysis is mechanically identical to that described in the previous paragraph 3.5.2.1, with the only difference that the load exerted is no longer infinite, but there is a mass, as shown in Figure 35 that creates a resistant torque caused by the force of gravity when the system is in motion. The joint is therefore free to move. The setup details are described in Table 21. Also in this configuration, the system is driven by the inputs chosen by the Simulink model (Seafloat_ESCON), which is deployed on the Speedgoat real time target machine and then the data is analysed to validate the operation of the model. Also in this case, to verify and validate that the SEA behaves as a reliable torque sensor, an industrial torsionmeter was used. In this case it will be possible to test that the torque calculated using Hooke's Law and that read by the torque meter at the slow axis of the SEA joint, are equal.

SEA CHARACTERIZATION		
SEA CONFIGURATION	MOTOR	EC 90 or EC 45
	GEAR BOX	HARMONIC DRIVE CSD-17-2A-100
	SPRING	SPT2P / STA or SPT1P
SERVO CONTROLLER	ESCON	
TORSIOMETER		
ENCODERS	2 ABSOLUTE ENCODER - AKSIM	
LOAD	MASS	3 kg
	LENGHT	0.6 m

Table 21: Test Bench for Series Elastic Actuator (SEA) characterization: finite inertial load

3.5.3. 1 Degree of Freedom

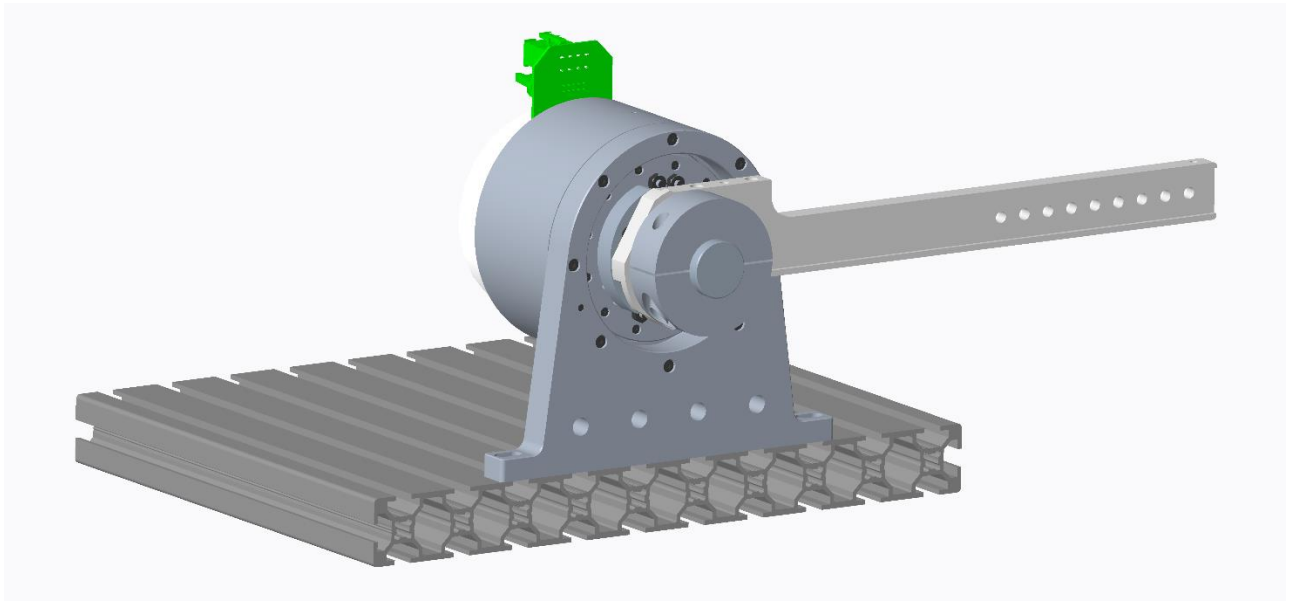


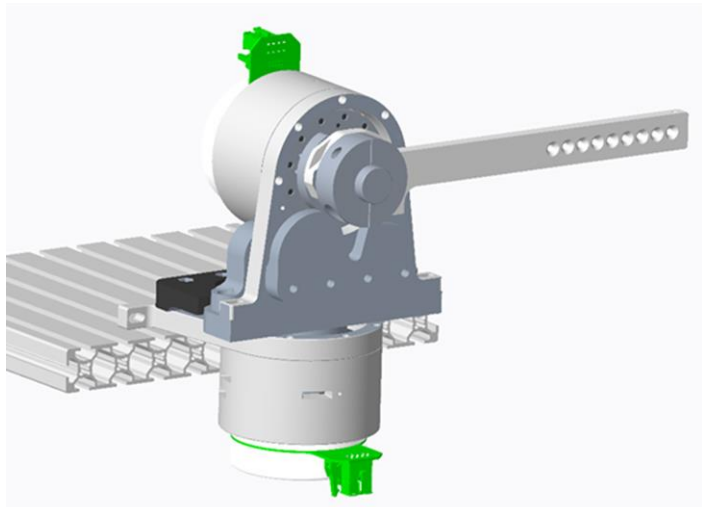
Figure 36: CAD with CREO of single degree of freedom test bench

The test bench used for the design of the position control of a single degree of freedom system, at (1 DoF), consists of a SEA (EC 90 motor, Harmonic Drive, custom made STA spring), two Aksim absolute encoders and an ESCON servo controller. The system is free to move, it has not any kind of mechanical stops.

1 DoF POSITION CONTROL SETUP			
SEA CONFIGURATION	MOTOR	EC 90	
	GEAR BOX	HARMONIC DRIVE CSD-17-2A-100	
	SPRING	STA	
Torsional stiffness K Nm/rad		1072,6	
SERVO CONTROLLER	ESCON		
ENCODERS	2 ABSOLUTE ENCODER - AKSIM		

Table 22: 1 degrees of freedom test bench configuration 2 Degrees of Freedom

3.5.4. 2 Degrees of Freedom



a



b

Figure 37: (a) CAD with CREO of double degrees of freedom test bench and (b) real test bench, scapular joint

The test bench used for the design of the admittance control of a system with several degrees of freedom (2 DoF), consists of a two SEA (EC 90 motor, Harmonic Drive, custom made spring STA and SPT2P) with their respective absolute encoders (Aksim) and with two EPOS servo controllers. The choice of the EPOS instead of the ESCON as servo controller, lies in the fact that the admittance control must rely on a stable position control and the EPOS, automatically, does the autotune of the PID parameters for the position control.

2 DoF ADMITTANCE CONTROL SETUP				
MOTOR 1	SEA CONFIGURATION	MOTOR	EC 90	
		GEAR BOX	HARMONIC DRIVE CSD-17-2A-100	
		SPRING	STA	
	Torsional stiffness K Nm/rad		1072,6	
	SERVO CONTROLLER	EPOS		
ENCODERS	2 ABSOLUTE ENCODER - AKSIM			
MOTOR 2	SEA CONFIGURATION	MOTOR	EC 90	
		GEAR BOX	HARMONIC DRIVE CSD-17-2A-100	
		SPRING	SPT2P	
	Torsional stiffness K Nm/rad		384,88	
	SERVO CONTROLLER	EPOS		
ENCODERS	2 ABSOLUTE ENCODER - AKSIM			

Table 23: 2 degrees of freedom test bench configuration

The system is not free to move, but it has some mechanical stops as shown in Figure 38.

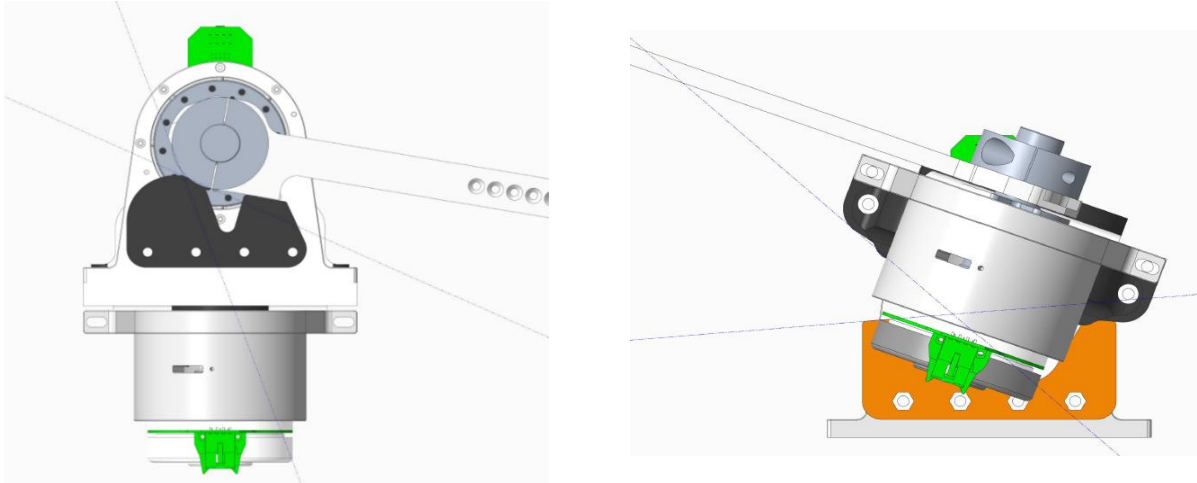


Figure 38: Mechanical stops of 2DoF system. (a) absolute range of motion (ROM) of 60° for motor 1, (b) absolute ROM of 60° for motor 2

3.5.4.1. Denavit-Hartenberg configuration of 2 DoF system

To work in the Cartesian space defined by the two degrees of freedom manipulator, it is necessary to define its spatial configuration. To do this, the Denavit-Hartenberg convention was used for direct kinematics analysis (chapter 2.1.2).

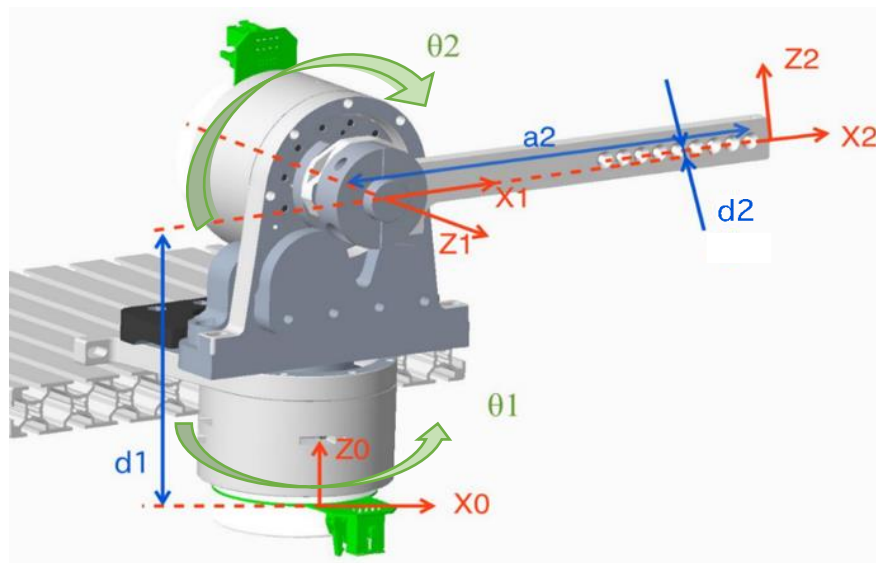


Figure 39: Denavit-Hartenberg configuration of 2DoF system. d_i =distance between x_{n-1} and x_n along z_{n-1} ; a =distance between O_n and O_{n-1} along x_n

Using the geometric parameters of the system, whose measurements have been experimentally calculated thanks to the aid of the CAD model developed on CREO and whose values are reported in Table 24, the table of the Denavit-Hartenberg parameters has been defined, as reported in Table 25 .

a2	d1	d2
0.270 m	0.21074 m	0.04864 m

Table 24: geometric parameters of 2 DoF system

link	a	α	d	θ
1	0	90	d1	θ_1
2	a2	-90	-d2	θ_2

Table 25: Denavit Hartenberg table of parameters

The corresponding homogeneous transformation matrix are (equation 42), considering that:

$$ci = \cos(\theta_i) \text{ and } si = \sin(\theta_i).$$

Equation 29: Abbreviations for DH convention

$$A_1^0 = \begin{bmatrix} c1 & 0 & s1 & 0 \\ s1 & 0 & -c1 & 0 \\ 0 & 1 & 0 & d1 \\ 0 & 0 & 0 & 1 \end{bmatrix} \quad A_2^1 = \begin{bmatrix} c2 & 0 & -s2 & a2c2 \\ s2 & 0 & c2 & a2s2 \\ 0 & -1 & 0 & -d2 \\ 0 & 0 & 0 & 1 \end{bmatrix}$$

Equation 30: homogeneous transformation matrix from reference frame (RF) i and $i-1$. (a) from RF1 to RF0, (b) from RF2 to RF1.

$$A_0^2 = A_1^0 A_2^1 = \begin{bmatrix} c1c2 & -s1 & -c1s2 & a2c1c2 - d2s1 \\ s1c2 & c1 & -s1s2 & a2s1c2 + d2c1 \\ s2 & 0 & c2 & a2s2 + d1 \\ 0 & 0 & 0 & 1 \end{bmatrix}$$

Equation 31: Homogeneous transformation matrix of the overall 2DoF system from RF2 to RF0

3.5.4.2. Jacobian matrix of 2 DoF system

To perform some transformation between joint and task space, the Jacobian matrix has been computed. Starting from the configuration described in the Denavit – Hartenberg convention, to compute the Jacobian matrix, some elements have been computed. Let's firstly define that the system is made up two revolute joints. As explained in the chapter 2.1.4.1, the geometric Jacobian is therefore computed.

$$J = \begin{bmatrix} z_0 \wedge (p_2 - p_0) & z_1 \wedge (p_2 - p_1) \\ z_0 & z_1 \end{bmatrix}$$

Equation 32: Geometric Jacobian for a generic two revolute joints

$$p_0 = \begin{bmatrix} 0 \\ 0 \\ 0 \end{bmatrix} \quad p_1 = \begin{bmatrix} 0 \\ 0 \\ d1 \end{bmatrix} \quad p_2 = \begin{bmatrix} a2c1c2 - d2s1 \\ a2s1c2 + d2c1 \\ a2s2 + d1 \end{bmatrix} \quad z_0 = \begin{bmatrix} 0 \\ 0 \\ 1 \end{bmatrix} \quad z_1 = \begin{bmatrix} s1 \\ -c1 \\ 0 \end{bmatrix}$$

Equation 33: Coefficients for the geometric Jacobian, $ci = \cos(\theta_i)$ and $si = \sin(\theta_i)$

$$J = \begin{bmatrix} -a2s1c2 - d2c1 & -a2c1s2 \\ a2c1c2 - d2s1 & -a2s1s2 \\ 0 & a2c2 \\ 0 & s1 \\ 0 & -c1 \\ 1 & 0 \end{bmatrix}$$

Equation 34: Geometric Jacobian for 2 degrees of freedom system

The first three rows of the Geometric Jacobian represents the Analytic Jacobian, the one used in this thesis for the computation of the inverse dynamics.

$$J_A = \begin{bmatrix} -a2s1c2 - d2c1 & -a2c1s2 \\ a2c1c2 - d2s1 & -a2s1s2 \\ 0 & a2c2 \end{bmatrix}$$

Equation 35: Analytic Jacobian for 2 degrees of freedom system

3.6. Simulink models for Real Time simulation on Speedgoat

This chapter is dedicated to the explanation of the Simulink models used for the online analysis of the functioning of the various test benches. The Simulink models are then deployed on Speedgoat.

3.6.1. Seafloat_ESCON Simulink model

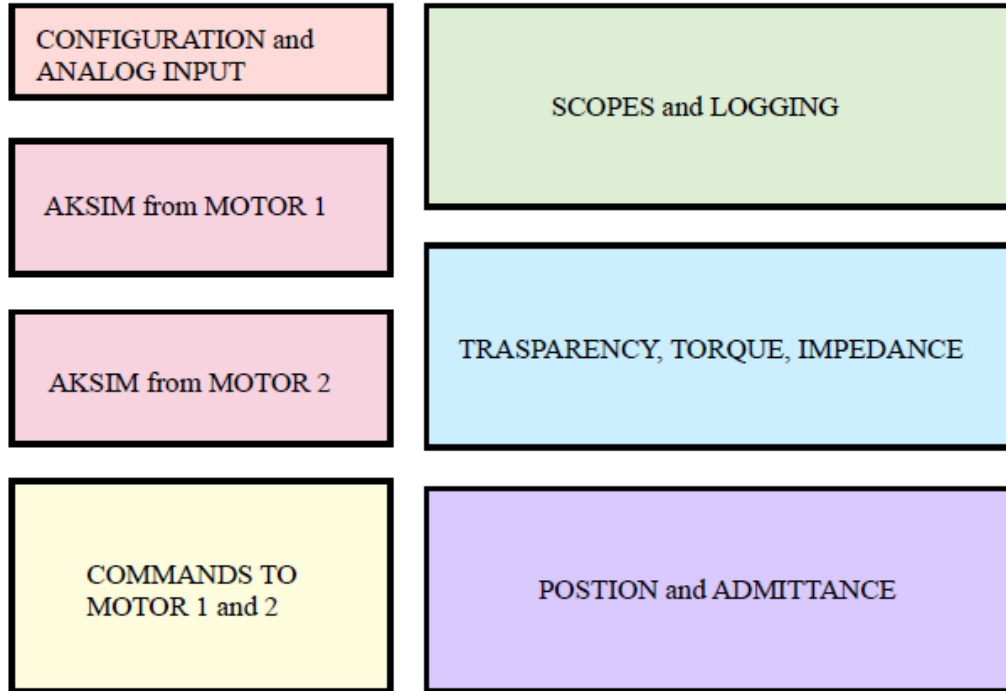


Figure 40: Seafloat_ESCON Simulink model block scheme

For the design of the position control of the one degree of freedom system and for the SEA characterization, a Simulink model was used, which we will call Seafloat_ESCON, formed by several blocks, as shown in Figure 40. The model used includes the design of two motors (with related encoders), but for single degree of freedom analysis, only motor 2 was considered. The main blocks of the Seafloat_ESCON model are:

- Configuration and analog input: this block represents the communication block with the Real Time Speedgoat simulator.
- Two blocks relating to the AKSIM encoders in which the wrap / unwrap operation is also performed for the correct reading of the angles. Thanks to this block we obtain the estimated couples deriving from:

$$\tau^{SEA} = K * \Delta\theta^{Aksim}$$

Equation 36: Torque estimated from different displacements of encoder and torsional stiffness of SEA's compliant element

- Commands to motor 1 and 2: in this block the reference current that must enter the motor to obtain the desired behaviour as output is chosen. It refers to an ESCON servo controller that provides torque / speed control.
- Transparency, Torque, Impedance: this subsystem analyses two control methods of the single degree of freedom, the torque (transparency is obtained when the input torque is zero) and the impedance.
- Position and admittance: in this subsystem the controls in position and admittance are analysed and implemented.

3.6.2. Seafloat_EPOS Simulink model

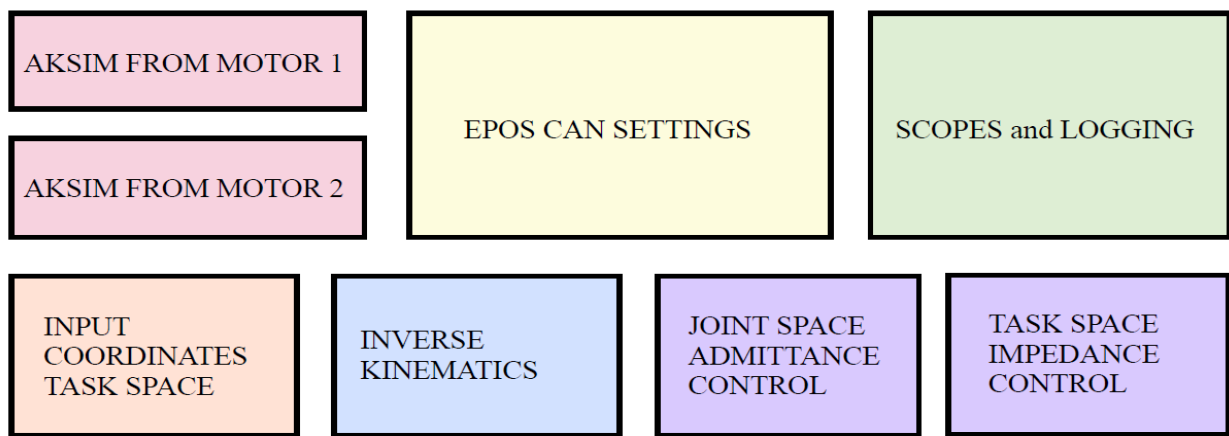


Figure 41: Seafloat_EPOS Simulink model scheme

To design the two degrees of freedom admittance and impedance control, the Simulink Seafloat_EPOS model was developed. The model consists of several blocks, as shown in Figure 41.

- Epos Can Settings: this block allowsto establish the connection with the EPOS servo controllers which use the CANopen communication protocol.
- Blocks of the Aksim: in these blocks the connection between model, Speedgoat and encoder is established. The wrap / unwrap operation is performed for the correct reading of the angles. Thanks to this block we obtain the estimated couples deriving from:

$$\tau^{SEA} = K * \Delta\theta^{Aksim}$$

Equation 37: Torque estimated from different displacements of encoder and torsional stiffness of SEA's compliant element

- Input coordinated task space: in this block the coordinates at which the end-effector must be located are defined, then the trajectory of the two degrees of freedom system in the task space is defined.
- Inverse kinematics block is necessary to pass from the task space to the joint space and then derive the positions at which each joint must be for the end effector to follow the predefined trajectory.

- Admittance control block describes the elastic or viscoelastic system, in which the admittance filter is applied to modify the virtual dynamics of the system. Admittance control is implemented in the joint space.
- Impedance control block describes the elastic, viscous or viscoelastic system, in which the impedance filter is applied to modify the virtual dynamics of the system. Impedance control is implemented in the task space.

3.7. Characterization of Series Elastic Actuator (SEA)

This chapter describes and explains the Simulink models that are used for the analysis and characterization of Series Elastic Actuators.

3.7.1. Simulink modelling for real time SEA testing: Speedgoat

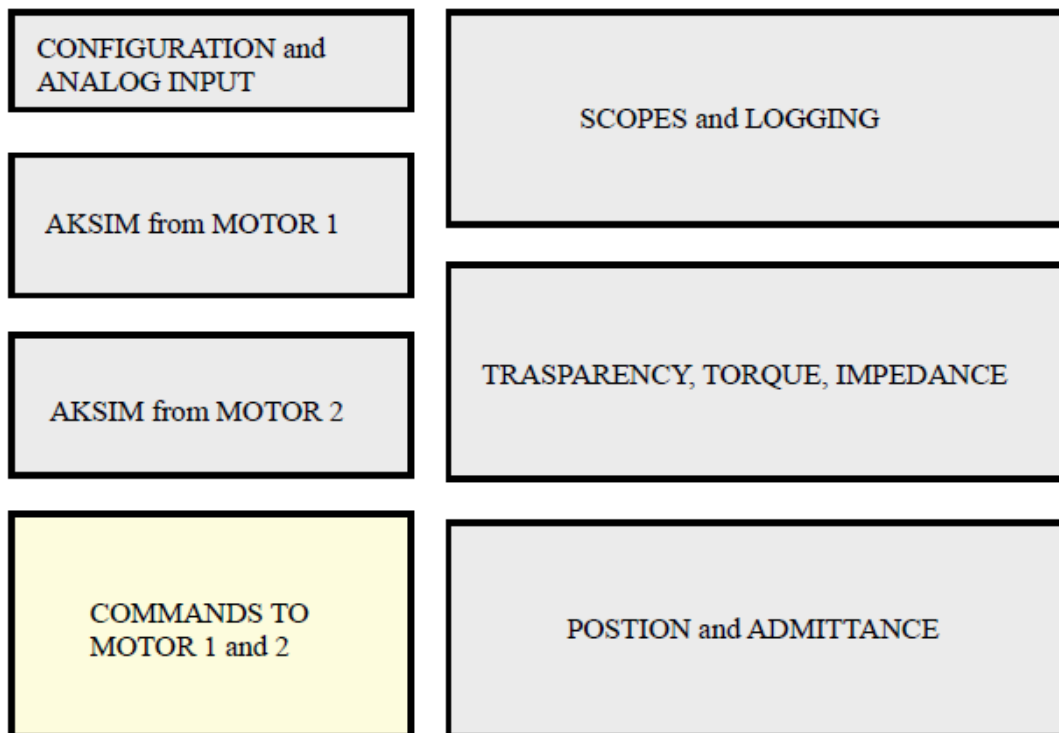


Figure 42: Simulink model (Seafloat_ESCON) of SEA characterization in Real Time.

The model is used to drive ESCON servo controllers, which in turn drive and operate the motor, via deployment on Speedgoat. Once the system is put in motion, thanks to the encoder and torsionmeter, data are collected and saved by the Speedgoat itself. The Simulink model has its own Graphical User Interface (GUI) that allows to define the desired current inputs and the correct torsional constant of the compliant element of the SEA joint, as well as the resolution of the encoders used (18-19-20 bit). Two current inputs are provided: a chirp current signal, and a ramp current signal (step + slew rate). The chirp is used to perform frequency analyses with the test bench configuration with infinite inertial load. A chirp signal is a constant amplitude signal in which the frequency varies in linear or logarithmic way over time: the used chirp signal was a logarithmic bidirectional chirp. This type of signal allows to analyse, with a single type

of input, the behaviour of the system at different frequencies. The ramp current inputs are given by the combination of a step, whose amplitude is variable, and a slew rate in series, to make the step's behaviour smoother, which would instead imply an immediate change of trend. The amplitudes of the steps can be varied to verify the operation of the motor with a setup with a known finite load. The current signals supplied are all limited in amplitude up to a maximum of continuous 4 A by a saturation block, for a safety reasons. As explained in chapter 3.4.7.1, to have accurate and realistic measurements of the data collected by the Aksim, the wrap / unwrap operation is necessary. Thanks to the real time machine Speedgoat, it is possible to save the data collected by the torsionmeter, save the current inputs provided and the positions of the encoders, and then analyse the data obtained.

3.7.2. SEA modelling on Simulink-Simscape

The SEA consists of three elements: motor, harmonic drive, and compliant element (chapter 1.3). To analyse the behaviour of the SEA, it was initially necessary to recreate an offline model, in a simulation environment. The purpose of offline modelling lies in the fact that, having a correctly functioning offline model, in the future it will be possible to refer only to the model for the characterization of any SEA, by only modifying the parameters of the various components. We therefore want to recreate a standard model that allows the validation of any SEA. The model in the Simulink-Simscape environment was created based on the information given by the component datasheets (chapter 3.4). The recreated model is standard: the parameters of the mechanical components, obtained from a datasheet, can be changed from a MATLAB script connected to the Simulink model. Thanks to the SEA offline model, it was possible to test different configurations of the actuator, two different types of BLDC motors EC45 and EC90 and different types of custom-made springs were tested. The harmonic drive used did not change, specifically a CSD-17-2A-100 Harmonic Drive was used. The model is tested with real data taken from online simulations made with the real time target machine Speedgoat. Having an offline model that works correctly allows not to waste time and validate the operation of your SEA joint directly with a run of the MATLAB model. The Table 26 shows the main characteristics of the SEA used, which are characterized and analysed in frequency. From the datasheet of the EC 45 and EC 90 motors, thanks to the use of the *WebPlotDigitizer* tool, it was possible to obtain the Continuous operation maximum torque envelope and the Corresponding rotational speeds: these parameters were then inserted in the respective block of the Simscape motor.

EC 90 flat BLDC			
Motor and driver overall efficiency	Speed at which efficiency is measured	Torque at which efficiency is measured	Constant voltage
84%	2590 rpm	444 mN*m	24 V
Torque control time constant	Supply series resistance	Rotor inertia	Torque constant
21.1 ms	0.343 Ω	3060 g*cm ²	70.5 mNm/A
slow axis inertia		fast axis inertia	
619.2 kg*mm ²		3.46 kg*mm ²	

Table 26: datasheet of EC 90 flat BLDC motor. Data taken from datasheet are then reported into Simplified PMSM Drive Simulink-Simscape block

EC 45 flat BLDC			
Motor and driver overall efficiency	Speed at which efficiency is measured	Torque at which efficiency is measured	Constant voltage
84.9 %	4560 rpm	167 mN*m	24 V
Torque control time constant	Supply series resistance	Rotor inertia	Torque constant
6.35 ms	0.573 Ω	181 g*cm ²	40.4 mNm/A
slow axis inertia		fast axis inertia	
1001 kg*mm ²		1.48 kg*mm ²	

Table 27: datasheet of EC 45 flat BLDC motor. Data taken from datasheet are then reported into Simplified PMSM Drive Simulink-Simscape block

For the modelling of the Harmonic Drive, reference was made to the values taken from the datasheet. To model efficiency, the following procedure was followed. Starting from the graph that shows the dependence of the efficiency as the working temperature varies and the motor speed, knowing that the working temperature is about constant $T = 25^\circ \text{C}$ has been obtained a graph showing the variation in efficiency as the motor speed varies (Figure 43).

Harmonic Drive CSD-17-2A-100		
Number of teeth on elliptical gear	Number of teeth on circular gear	Reduction Ratio
100	101	100
Input shaft torque at no load	Nominal output torque	Efficiency at nominal output torque
0.0140 [Nm]	15.997 [Nm]	0.77

Table 28: datasheet of Harmonic Drive CSD-17-2A-100. Data taken from datasheet are then reported Harmonic Drive Simulink-Simscape block

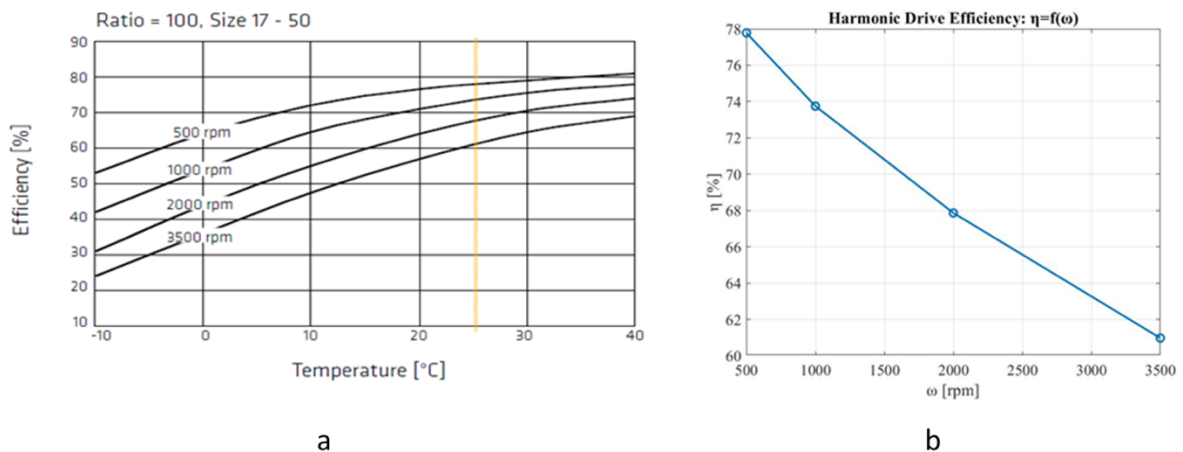


Figure 43: (a) efficiency as function of temperature. Focus on a constant temperature of 25° to analyse the efficiency as function of speed. (b) efficiency dependence of angular velocity at constant temperature.

In parallel, starting from the normalized graph of the datasheet (WebPlotDigitizer and then imported into MATLAB) which shows the relationship between the K factor - the ratio between the point efficiency and the nominal efficiency - and the V factor - the ratio between applied torque and nominal torque. A normalized graph has been obtained which shows the variation of point efficiency as the applied torque varies (Figure 44).

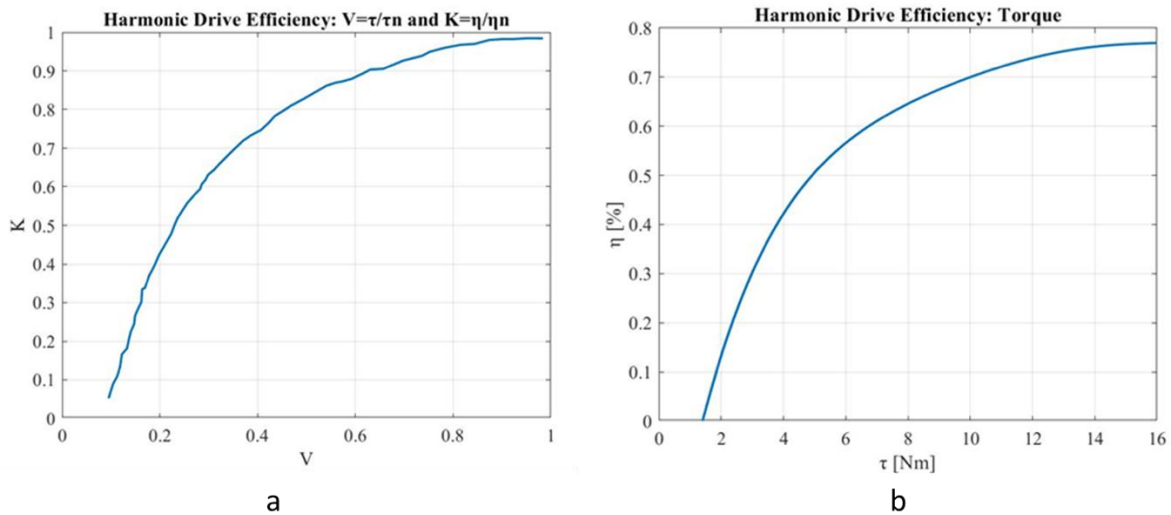


Figure 44: (a) normalized KV factors curve of efficiency of Harmonic Drive and efficiency with respect to torque, (b) efficiency dependence from torque applied

From the analysis of the graphic use obtained, it was possible to obtain the following information necessary for modelling the harmonic drive in the Simulink Simscape environment:

- Input shaft torque at no load: torque calculated when the harmonic efficiency is minimal
- Nominal output torque: torque calculated when the efficiency of the harmonic drive is maximum
- Efficiency at nominal output torque: maximum efficiency at nominal torque

The reported graphs in Figure 44.b show the dependency of the harmonic drive efficiency from the angular speed and from the torque.

The modelling of the compliant element is based on the data obtained experimentally from the analysis of the custom-made springs made in chapter 0. Table 29 shows the analysed torsional stiffness.

Torsional Stiffness		
STA	SPT2P	SPT1P
1073 Nm/rad	385 Nm/rad	988 Nm/rad

Table 29: Torsional stiffness of custom-made compliant element. Data taken from datasheet are then reported into Rotational Spring Simulink-Simscape block

The goal of the SEA model in Simulink is twofold: the first is to validate that the SEA works exactly as a reliable torque sensor, the second is to create an offline model that allows to universally test any SEA without having to do any necessary tests in Real Time. As regards the first objective, the SEA is modelled with the addition of torque sensors, which provide estimates comparable to those of the industrial torsionmeter in real time; in addition, a rotational motion sensor that allows to detect the displacement of the spring is used to obtain the ideal estimated torque in simulation. It is clear that, considering the disturbances present in a real simulation environment, the torque measured by the torsionmeter and the one read by the ideal torque sensor are effectively comparable, as is Hooke's law applied with the real measurements of the Aksim and the one obtained ideally with the ideal rotational motion sensor are about the same except for no-idealities.

3.7.2.1. Behaviour analysis of the SEA model

To validate the correct functioning of the motor model, a Simulink model was made that allows to analyse the behaviour of the actuator in different load situations.

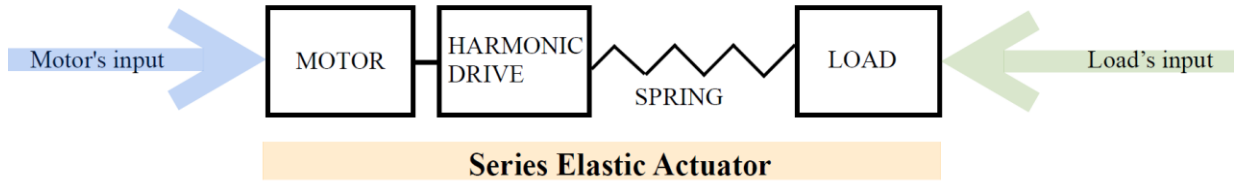


Figure 45: Antagonist input of SEA, motor validation scheme of Simulink model

The system consists of two antagonist inputs, as shown in Figure 45: the motor provides a constant torque at the input of the compliant element, while the torque exerted by the load, in the output of the spring, is variable to analyse the corresponding motor response.

The motor is analysed in the following configurations:

- No load applied: the motor is free to move
- The torque supplied to the motor input is exactly balanced by the torque generated by the load
- The torque supplied to the motor is greater than that generated by the load
- The torque generated by the load is greater than that supplied by the motor.

The torques supplied to the motor and the load are shown in Table 30. The torques exerted by the load are amplified by the harmonic drive reduction factor which, as reported in chapter 3.4.5, has a reduction factor of 100.

	Free run system	Balanced system	Motor drags load	Load drags motor
Motor torque [Nm]	0.25	0.25	0.25	0.25
Load torque [Nm]	0	25	15	35

Table 30: Inputs of the Simulink model to test the correct behaviour of the motor's model

3.7.2.2. Simulink model for infinite inertial load simulation

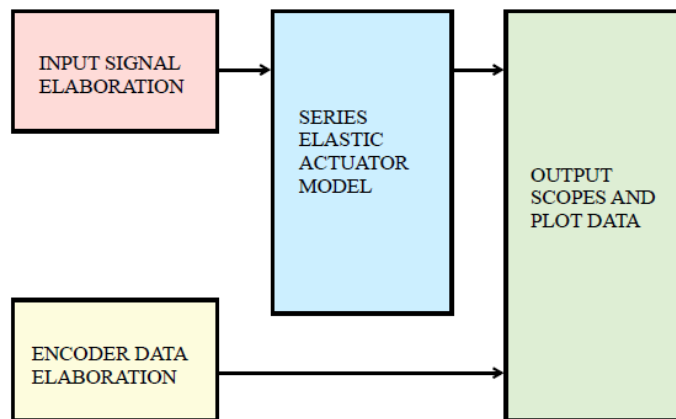


Figure 46: Simulink model scheme of SEA characterization with block model, infinite inertia load. Offline model

This model reproduces the situation of the test bench setup described in chapter 3.5.2.1. The model therefore allows to simulate the behaviour of the SEA when the latter is blocked to the wall, therefore it

has an infinite inertial load: a current is supplied to the motor which drives the compliant element. The model consists of several blocks:

- Input signal processing: in this block the same current signal (chirp) that was supplied to the test bench for real time simulations on Speedgoat is supplied.
- Series elastic actuator model: this block reproduces the SEA model as described in chapter 3.4. Through the MATLAB script connected to the Simulink model it is possible to change the values concerning the motor, the spring, and the harmonic drive, depending on the joint being analysed. To reproduce the infinite inertial load condition, in the Simulink Simscape model a mechanical rotational reference (Simulink-Simscape library, chapter 3.1.1.1) is used at the output of the elastic element. Sensors are added to the block modelling the SEA which allow to obtain simulated data relating to spring displacement, motor rotational speed and motor torque. This data are then plotted into the plot block.
- Encoder data elaboration: in this block it is possible to get the data, related to the position of the Aksim, which are saved by Speedgoat during the real time simulation. In this subsystem the unwrap operation is performed.
- Output scope and plot data: this block allows to view the signal responses and to verify that the simulation data behave like those obtained through the real time simulation on a test bench

3.7.2.3. Simulink model for finite inertial load simulation

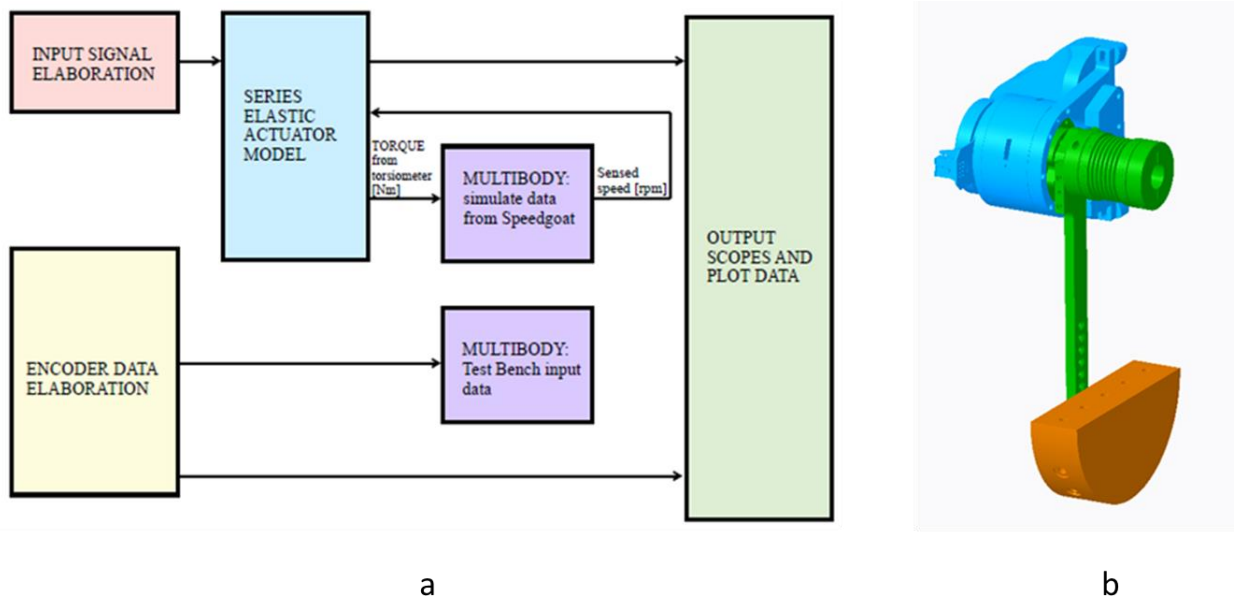


Figure 47: (a) Simulink model scheme of SEA characterization with load. Offline model and Multibody figure, (b) multibody block on Simulink

This Simulink model has been designed to recreate the situation where the SEA is subjected to a finite inertial load, so is free to move. Reference is made to chapter 3.5.2.2. The model consists of several subsystems:

- Input signal processing: in this block the same current signal (ramp signal) that was supplied to the test bench for real time simulations on Speedgoat is supplied.
- Series elastic actuator model: this block reproduces the SEA model. Through the MATLAB script connected to the Simulink model it is possible to change the values concerning the motor, the spring, and the harmonic drive, depending on the joint being analysed.
- Multibody: to reproduce the inertial and load conditions reproduced on the test bench it was necessary to import the CAD model of the test bench into MATLAB through the Creo plugin (chapter 3.1.3.1). In the multibody model the mechanical properties of each component have been set, such as mass, centre of mass and main moments of inertia (see Table 31). The multibody model receives as input the torques read by the industrial torsionmeter: the movement of the multibody allows the sensing of a speed that would be produced with that given input torque. The estimated speed is then used as a disturbance input to the SEA model to simulate real working conditions and consider the external disturbances that interfere with the real test bench system. The second multibody block receives in input the pairs that are generated by the SEA as a torque sensor, with Hooke's law. The multibody system is shown in Figure 47.b.
- Encoder data elaboration: in this block it is possible to get the data, related to the position of the Aksim, which are saved by Speedgoat during the real time simulation. In this subsystem the unwrap operation is performed.
- Output scope and plot data: this block allows to view the signal responses and to verify that the simulation data behave like those obtained through the real time simulation on a test bench.

MULTIBODY COMPONENTS								
MASS								
FIRST ELEMENT			SECOND ELEMENT			LOAD		
3,35 Kg			1,36 Kg			6,5 Kg		
CENTER OF GRAVITY WITH RESPECT TO FISSO COORDINATE FRAME								
FIRST ELEMENT			SECOND ELEMENT			LOAD		
Xg	Yg	Zg	Xg	Yg	Zg	Xg	Yg	Zg
3,4e+01 mm	-4,0e-01 mm	-5,3+01 mm	1,1e+02 mm	-1,4e+01 mm	4,9e-02 mm	1,3e+02 mm	-2,7e+02 mm	-6,9e-02 mm
PRINCIPAL MOMENTS OF INERTIA								
FIRST ELEMENT			SECOND ELEMENT			LOAD		
Ix	Iy	Iz	Ix	Iy	Iz	Ix	Iy	Iz
6,9e+03 kg*mm ²	1,5e+0 kg*mm ²	1,5e+04 kg*mm ²	2,1e+03 kg*mm ²	3,9e+03 kg*mm ²	5,3e+03 kg*mm ²	4,9 e+03 kg*mm ²	1,6e+04 kg*mm ²	1,8e+04 kg*mm ²

Table 31: Simulink-Multibody properties. Those features are inserted into Simulink-Multibody block

3.8. Control Strategy of 1 Degree of Freedom

The following paragraphs explain the design and implementations of the position control on a single degree of freedom system.

3.8.1. Position control

Referring to the chapter 2.2.3 which shows the block diagram of a control in place, the design of this control method is now explained. The objective of a position control in closed loop system is that the error, between the desired position and the output position, is minimal: in this way the system output will be almost equal to the input provided.

3.8.1.1. Simulink model

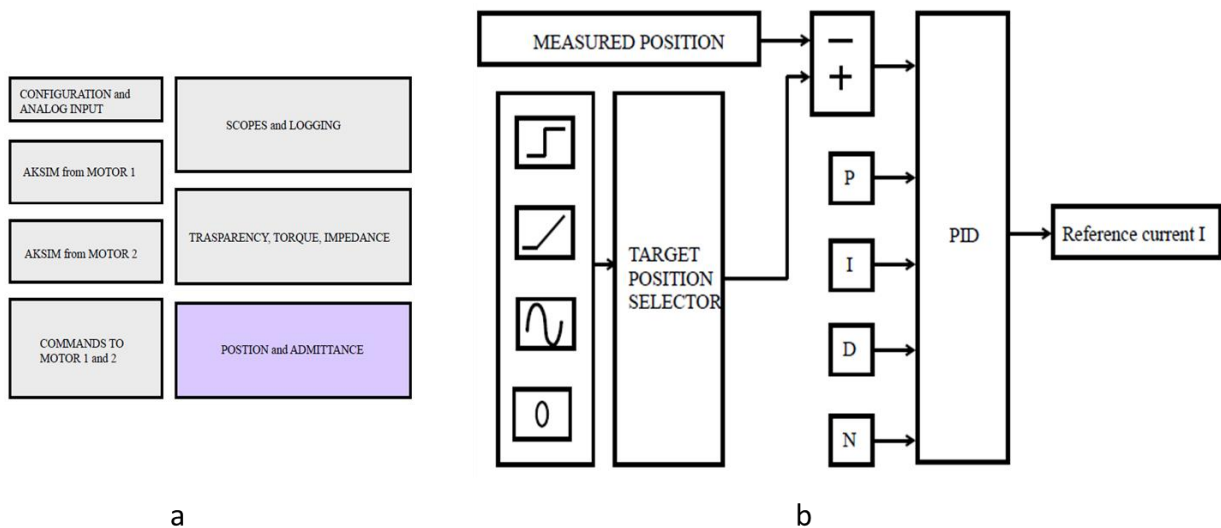


Figure 48: Simulink model for 1 degree of freedom position control. (b) focus on position control scheme

The Simulink model used is the Seafloat_ESCON. Now focus the attention on the subsystem that controls position and admittance, focusing on position control.

The subsystem is schematized in Figure 48 b. In this subsystem it is possible to identify:

- Double input:
 - A target position that can be chosen between a step, a ramp, or a sine wave. These inputs are selectable from the Graphical User Interface (GUI).
 - A measured position which is the output coming from the position detected by the encoders.
- Feedback branch that allowsto estimate the error between the desired input and the one read by the encoders (therefore the one measured).
- A PID control block whose PIDN parameters can be chosen from the GUI, to be able to do the tuning in Real Time of the parameters and then find the optimal ones.

- Output: PID output current which will be the input to be able to move the single joint, then select the current necessary to drive the motor. According to motor datasheet (chapter 3.4.1), a saturation limit to $\pm 7A$ has been set.

3.8.1.2. Graphical User Interface (GUI)

A graphical user interface (GUI) has been developed to make Simulink user-model communication more intuitive. The GUI presented is divided into multiple sub-tabs. Once the model has been deployed on target, after having performed the load of the model, it is possible to proceed with the Torque Reset to have an accurate measurement of the torque without any noise caused by previous measurements. The GUI developed for position control provides the possibility to modify the PID parameters (P, I, D) in Real Time and to choose which reference position should be desired for the control feedback in position. It is possible to choose between a step input, a ramp, or a sinusoid, then it is possible to select the amplitude of the chosen signal and, in the case of the sinusoid, also its frequency.

3.8.1.3. PID tuning

To obtain the correct behaviour of the position control, it is necessary to select the correct parameters: we proceeded with the tuning of the PID parameters. As explained in chapter 2.2.2 the PID is a type of proportional-integrative-derivative closed-loop control. The PID used is a parallel (not ideal), discrete PID (z-domain, required sampling time T_s). The low pass filtering with pulsation pole N on the derivative term has the function of preventing the production of excessive numerical noise due to the derivation operation.

$$PID = P + I \cdot T_s \frac{1}{z - 1} + D \frac{N}{1 + N \cdot T_s \frac{1}{z - 1}}$$

Equation 38: PID formulation block. P, I, D, N: external coefficient to be tuned

During the experimentation of the position control, before proceeding with the experimental method to search for the optimal values of the PID, we proceeded with the additional implementation of an autotune block. Autotune has been implemented in two ways: both open loop autotune and closed loop autotune. Unfortunately, blocking in Real Time does not give the desired results because:

- The response has a high overshoot, which is not acceptable in a control designed for an upper-limb exoskeleton in the medical field
- The response tends to be unstable, highly oscillating due to incorrect PID values.

Through experimentation and a specific debug of the MATLAB block, it was understood that the main problem is since, if the initial values set for the PID are not sufficiently like the optimal ones, the system tends to diverge. Having obtained unwanted results with the autotune method, I proceeded through manual tuning of the PID parameters. The tuning took place first, by choosing a predefined trajectory to follow (a sinusoid with fixed amplitude and frequencies - for the results see chapter 4.2.1) and varying the parameters one at a time: obtained a satisfactory coefficient, this remained fixed, allowing the next one to

vary up to obtain, in the first instance, the optimal values of the PID parameters. To then verify that these parameters were correct, different position profiles were tested.

3.9. Control Strategies of 2 Degrees of Freedom

The following paragraphs explain the design and implementations of the compliant control strategies on a 2 degrees of freedom system.

3.9.1. Admittance control: Joint Space

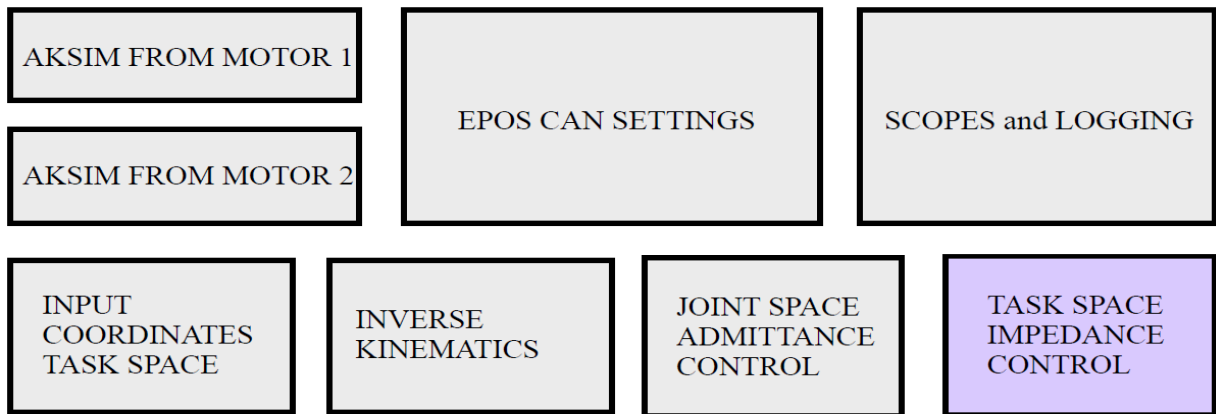


Figure 49: Seafloat_EPOS Simulink scheme for admittance control

For the design and development of the admittance control, the Seafloat_EPOS model was used. The admittance filter is applied on a closed loop position control, therefore, to have an accurate and reliable measurement of the position control, EPOS servo controllers have been chosen. EPOS was used in Cyclic Synchronous Position (CPS) mode (see Table 14). The single joint receives in input a desired position θ^{ik} . When the system is perturbed from the outside with a τ^{aksim} torque, we deviate from the desired reference position by a quantity θ^{dyn} . The tracking error that enters the EPOS servo controller control is $\theta^{ctrl} = \theta^{ik} - \theta^{dyn}$: this last quantity governs and drives the EPOS configured in CPS mode. With Cyclic Synchronous Position Mode, the trajectory generator is in the control device and it provides a target position to the drive device in cyclic synchronous manner, thus the drive performing position control and torque control. The target position represents the position that the drive is supposed to move using the motion control parameters (such as velocity, acceleration, and deceleration). CSP mode works in such a way that when the difference between θ^{ik} and θ^{dyn} is nonzero, then the motor increments its position by a θ^{ctrl} amount. The θ^{ctrl} is then transformed into increments so that the magnitude can be compared with the position read by the EPOS internal encoder (pos_actual), expressed in increments. The EPOS encoder is placed at the fast axis of the system, therefore before the reduction of 100 introduced by the harmonic drive takes place. The configuration and explanation of θ^{ik} , θ^{dyn} and θ^{ctrl} is explained in Figure 50. Since in the CSP working mode the EPOS requires increments at the input, it is necessary to translate the reference system defined by the DH convention in chapter 3.5.4.1, to an experimental reference system based on the test bench.

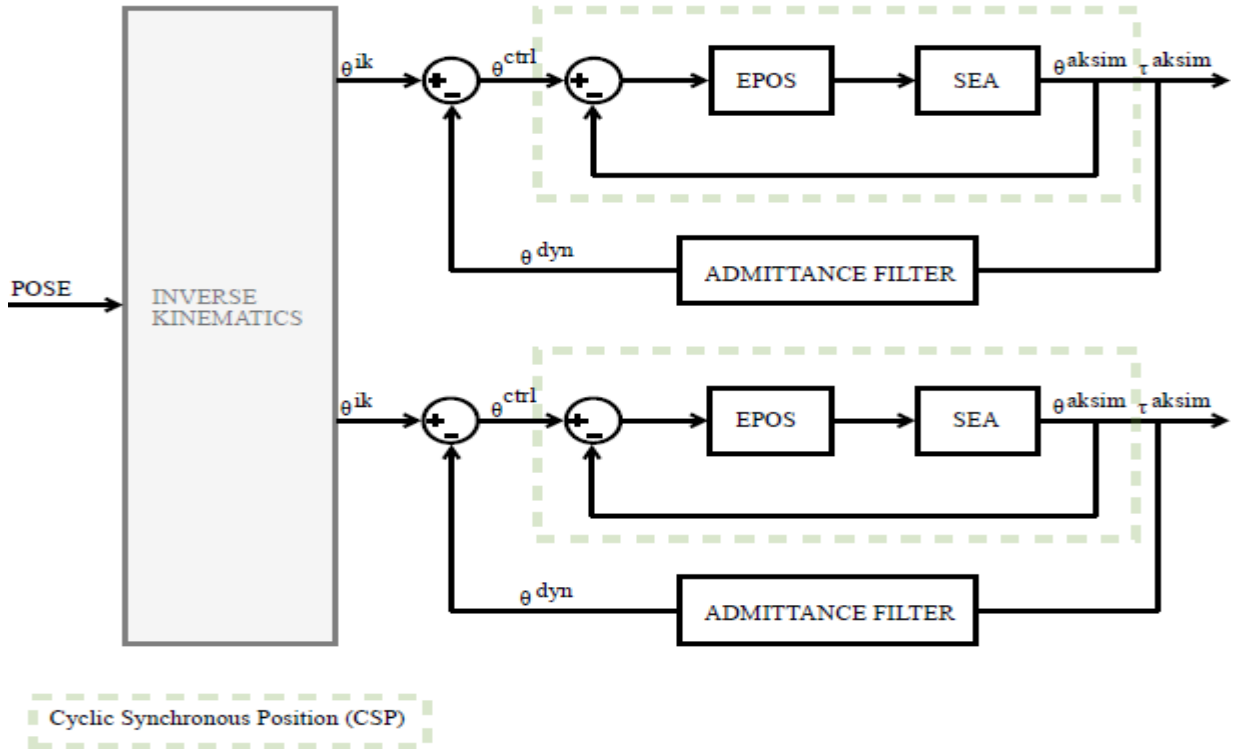


Figure 50: Admittance Control in Joint space

It was necessary to make the two reference systems coincide by bringing the DH system to that of the 0-centered EPOS. Different implementations of the admittance filter are explained, one purely elastic and the other one is viscoelastic. The results obtained are shown in chapter 4.3.1 . The input position trajectory defined in the task space, shown in Figure 51, has been chosen so that it falls within the cloud-point of the dexterous workspace. Thanks to the inverse kinematics block, which allows to pass from task space to joint space, the reference trajectories shown in Figure 51.b, are obtained, one for each joint. Based on those specific trajectories, admittance control can be implemented. The limited dexterous workspace imposes a further mechanical limit. Since the admittance filter allows user to deviate from the predefined trajectory, the safety limit placed at the filter output ensure the user not be able to impose a deviation greater than the mechanical limits of the system itself.

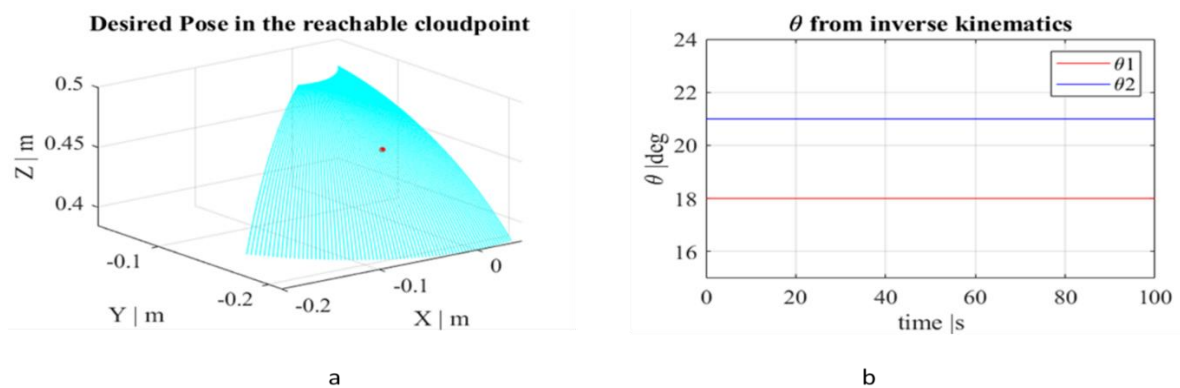


Figure 51: Desired Pose of the end-effector in Task space (a) and respective joint's position in Joint space after inverse kinematics computation (b)

3.9.1.1. Elastic system

Each dynamic system behaves like that of a mass-spring-damper system. This section analyses the behaviour of a purely elastic system (spring). The purely elastic admittance filter modifies the virtual dynamics by acting only on the position.

$$\frac{\theta}{T + k\theta_0} = \frac{1}{Js^2 + \beta s + k}$$

Equation 39: Focus on purely elastic K admittance transfer function

Through the tuning of parameter K, it is possible to obtain a control which is more compliant, and which therefore can deviate from the predefined position trajectory, making the human-robot interaction more user-friendly and safer, but that always returns to the position of desired reference, thanks to the behaviour of the spring. In the Simulink Seafloat_EPOS model, a purely elastic control has been implemented for the manoeuvrability of a two-degree-of-freedom system in the Joint space. The block diagram in Figure 50 represents the admittance control acting on each joint. Each single joint has its own parameter tuning. Within the 'Admittance Filter' block, the following transfer function has been implemented.

$$\frac{\theta}{T} = \frac{1}{k}$$

Equation 40: Admittance filter transfer function for a pure elastic system

3.9.1.2. Viscoelastic system

Each dynamic system behaves like that of a mass-spring-damper system. This section analyses the behaviour of a viscoelastic system (damper and spring). By the intrinsic nature of the spring, referring to Hooke's law, the system tries to return to its equilibrium position to have zero elastic potential energy. This return force is essential for the system to always follow the desired trajectory as a reference trajectory.

$$\tau = K \cdot (\theta - \theta_0)$$

Equation 41: Hooke's law, rotational domain

The viscoelastic admittance filter modifies the virtual dynamics by acting both on the speed and on position.

$$\frac{\theta}{T + k\theta_0} = \frac{1}{Js^2 + \beta s + k}$$

Equation 42: Focus on viscoelastic admittance transfer function

Through the tuning of parameters β and K, it is possible to obtain a control which is more compliant, and which therefore can deviate from the predefined position trajectory, making the human-robot interaction more user-friendly and safer. In the Simulink Seafloat_EPOS model, a viscoelastic control has been implemented for the manoeuvrability of a two-degree-of-freedom system in the Joint space. Within the 'Admittance Filter' block, the following transfer function has been implemented.

$$\frac{\theta}{T + k\theta_0} = \frac{1}{\beta s + k}$$

Equation 43: Viscoelastic admittance filter

3.9.1.3. Noise filtering of input signal

Since a torque entering the filter causes a change in position, it is necessary to separate those that are voluntarily applied from those that are noise or unwanted peaks. Regarding the analysis of the input signal to the admittance filter, it is necessary a low pass filter for the removal of noise. The implemented discrete low pass filter has the general transfer function:

$$H(z) = K \frac{\left(\frac{T_s}{T}\right)z^{-1}}{1 + \left(\frac{T_s}{T} - 1\right)z^{-1}}$$

Equation 44: Discrete time LPF filter transfer function; K : filter gain, T : filter time constant, T_s : filter sample time

Thanks to the analysis of the Fast Fourier Transform (FFT) of the input torques T_1 and T_2 , it is possible to note that the noise has a frequency of about 1 Hz.

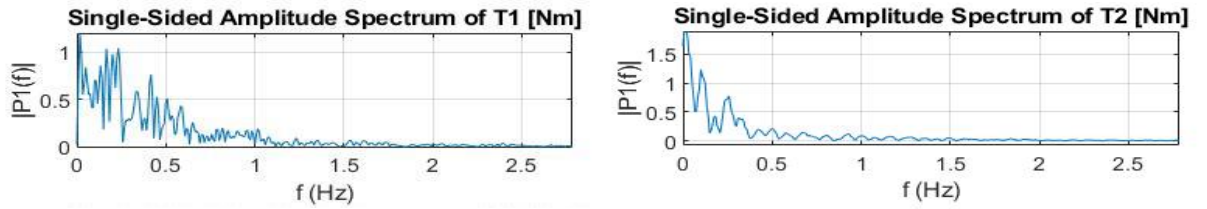


Figure 52: Fast Fourier Transform of input torque signal T_1 and T_2 are input torque of the admittance filter for each joint.

To filter the signal correctly, we choose a frequency of the low pass filter pole that is at least a decade before the noise frequency. Then is obtain the equation of the noise-reject low pass filter.

$$H(z) = \frac{1}{0.1s + 1}$$

Equation 45: Low pass filter anti-noise

3.9.1.4. Graphical User Interface (GUI)

As in the case of the Seafloat_ESCON model, an entire graphical user interface has also been created for the Seafloat_EPOS model. In this case, through the GUI it is possible to choose the working mode of EPOS servo controller (see Table 14). Then it is possible to select which kind of filter apply: if elastic or viscoelastic. After selecting the desired filter, from GUI it is possible varying the parameters of the viscous system, (K or β and K), to obtain the desired dynamics directly in Real Time and therefore to analyse the different behaviours of the system as the parameters vary. The analysis on the behaviour of the viscous and viscoelastic system are shown in chapter 4.3.1.

3.9.2. Impedance control: Task Space

The impedance control in the task space has been implemented on Speedgoat thanks to the deployment of the Seafloat_EPOS model in Figure 53. The impedance control has been developed and implemented in such a way as to apply the filter directly on the end effector, i.e., in the task space. The control scheme on which the filter is applied is formed by an external closed loop control of position and an internal, i.e., in the joint space, closed loop control in torque. It is also a model-based control of force acting directly in the task space as the forces in the Cartesian space are estimated with the help of the inverse of the Jacobian

matrix transpose, but not measured. One of the future developments is to make this model a closed loop external control of force instead of position, using a force / torque (F /T) sensor, such as the ATI. Thanks to the internal torque control system on the single joints, except for external forces, such as the torque exerted by the force of gravity and dependent on the precise position of the system, it is possible to rely on the force estimated in the Cartesian space.

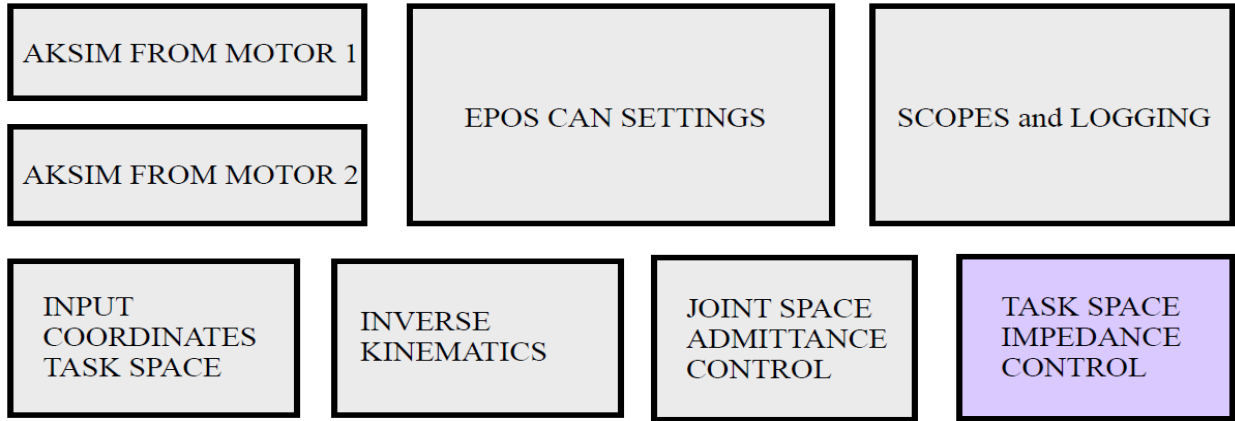


Figure 53: Task space impedance control, Seafloat_EPOS model

The control in the task space is done starting from a position in the desired in Cartesian space: three generalized coordinates X Y and Z are provided in input so that they belong to the cloud point representing the reachable workspace, as shown in the Figure 51.a : the same trajectory given for the admittance control is given in order to make the two different control strategies comparable. Thanks to the impedance filter, which can be elastic, viscous, or viscoelastic, a generalized force is obtained at the end effector. This is modelled by the inverse dynamics: the transposition of the Jacobian matrix (Equation 34) allows to obtain the torques that must be applied to the single joints. Once the torque has been obtained at the joints, it is passed into the workspace of the joints. each single joint is driven by the servo controller which works in Cyclic Synchronous Torque (CST) mode. The torque generated by the Jacobian transpose becomes the reference for the closed loop control and, the difference between the input torque and the one read by the SEA used as a torque sensor τ^{aksim} , acts as the system tracking error and drives the motor. A PID was inserted before the signal was input into the EPOS servo controller. the PID used consists only of a proportional term P. The EPOS works in CST mode. With Cyclic Synchronous Torque Mode, the trajectory generator is in the control device, and it provides a target torque to the drive device in cyclic synchronous manner, thus the drive performing torque control. The target input torque is given in thousands of Motors rated torque which is given by the Equation 46.

$$\tau^{motor} = K_T * i$$

Equation 46: Motor rated torque. K_T : torque constant [mNm/A], i : current [A]

The torque generated by the EPOS is then compared with that produced by the SEA to generate the control feedback. The torque generated by the SEA τ^{aksim} is used as a reference to perform the direct dynamic and obtain the model based generalized estimated force. On the other hand, as regards the positions of each joint read by the Aksim downstream of the compliant element of the SEA, these enter a subsystem

in which the pose of the end effector is calculated through direct kinematics as explained in the Equation 31. This measured pose comes-in as control feedback. Refer to the control scheme schematized in Figure 54.

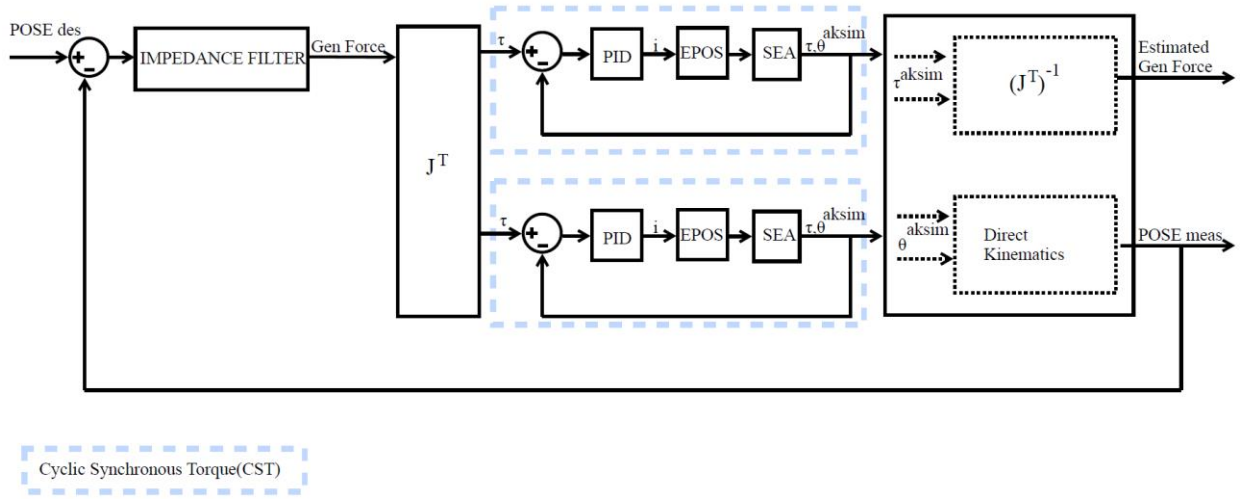


Figure 54: Impedance control scheme in task space

3.9.2.1. Viscous system

Being able to represent each dynamic system as a mass-spring and damper system, it is possible to recreate a system that would allow to analyse the behaviour of a damper. In a purely viscous system, the transfer function, described in Equation 47, requires that the virtual dynamics be modified by acting on the speed at which the system is in motion.

$$\frac{T + k\theta_0}{\theta} = Js^2 + \beta s + k$$

Equation 47: Viscous impedance filter

In a purely viscous system, a reference position is not established. When acting from the outside by applying a force that modifies the position of the end effector in the Cartesian space, the system will attenuate the speed of a β coefficient but will not tend to its own reference position: the new pose in the Cartesian space will be equal to the one in which the end effector was brought after applying an external force.

3.9.2.2. Elastic system

Being able to represent each dynamic system as a mass-spring and damper system, it is possible to recreate a system that would allow us to analyse the behaviour of a spring. In a purely elastic system, the transfer function, described in Equation 48, provides that the virtual dynamics is modified by acting on the position at which the system is, with respect to a known reference position.

$$\frac{T + k\theta_0}{\theta} = Js^2 + \beta s + k$$

Equation 48: Elastic impedance filter

To modify the position of the end effector around an established reference position in the Cartesian space, the elastic element of the filter was studied. Due to the intrinsic property of the spring, this tends to zero its potential energy, bringing itself to its equilibrium position θ_0 .

3.9.2.3. Viscoelastic system

Being able to represent each dynamic system as a mass-spring and damper system, we wanted to recreate a system that would allow us to analyse the behaviour of a spring-damper system.

$$\frac{T + k\theta_0}{\theta} = Js^2 + \beta s + k$$

Equation 49: Viscoelastic impedance filter

The optimal system is a spring-damper system. In this configuration it is, in fact, possible to modulate the speed of the system and avoid excessive oscillations, using the viscous component, and to tend to the defined target pose, thanks to the elastic component.

3.9.2.4. Transparency

To be able to evaluate the transparency of the system, a pure control with zero torque in the joint space has been implemented: in fact, by setting the filter values in null impedance, a torque control in the joint space is obtained. In this way it is possible to evaluate the intensity of the resistance provided by the mechanical characteristics of the exoskeleton.

Chapter 4: Results and Discussion

This chapter reports the results obtained with relative discussion. Thanks to the graphs shown, it is possible to understand the behaviour of the implemented control strategies.

4.1. Characterization of Series Elastic Actuator (SEA)

The first section of this chapter is entirely dedicated to the analysis of the results obtained from the characterization of the actuated joints SEAs.

4.1.1. Functioning of the implemented SEA Simulink model

The main results of the correct functioning of the implemented motor model in the Simulink-Simscape environment, are summarized below. The functioning of the motor under analysis is based on the relationship between driving torque (motor) and resisting torque (load).

Free run system: in this configuration the motor is free to move as it does not find a resistance torque, as shown in Figure 55.

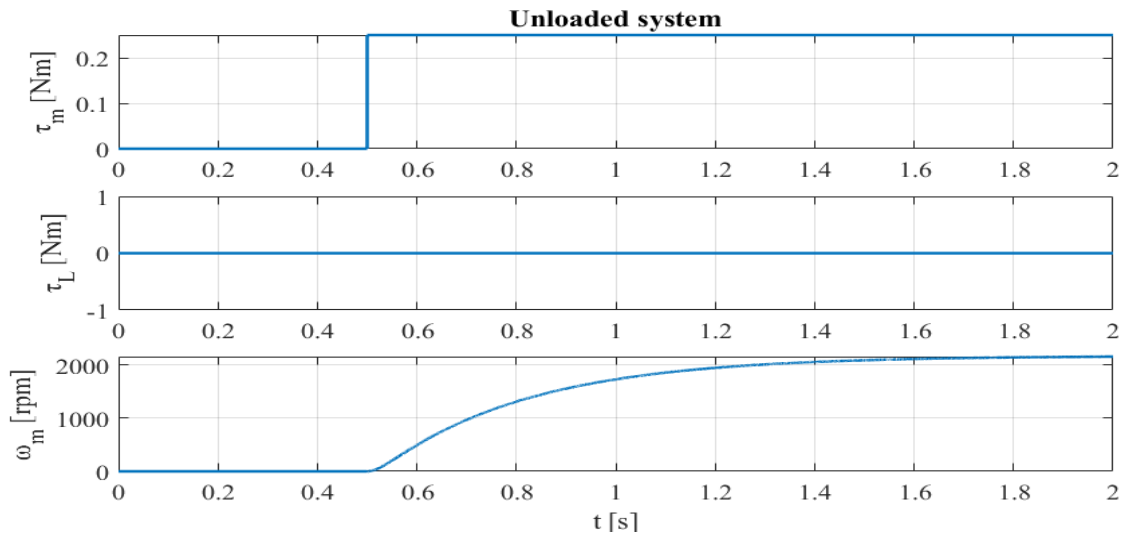


Figure 55: Free Run system: the motor speed increases until the maximum reachable angular speed since there is no load.

Balanced system: the system is blocked, in this case there is no movement, speed is zero, as shown in Figure 56.

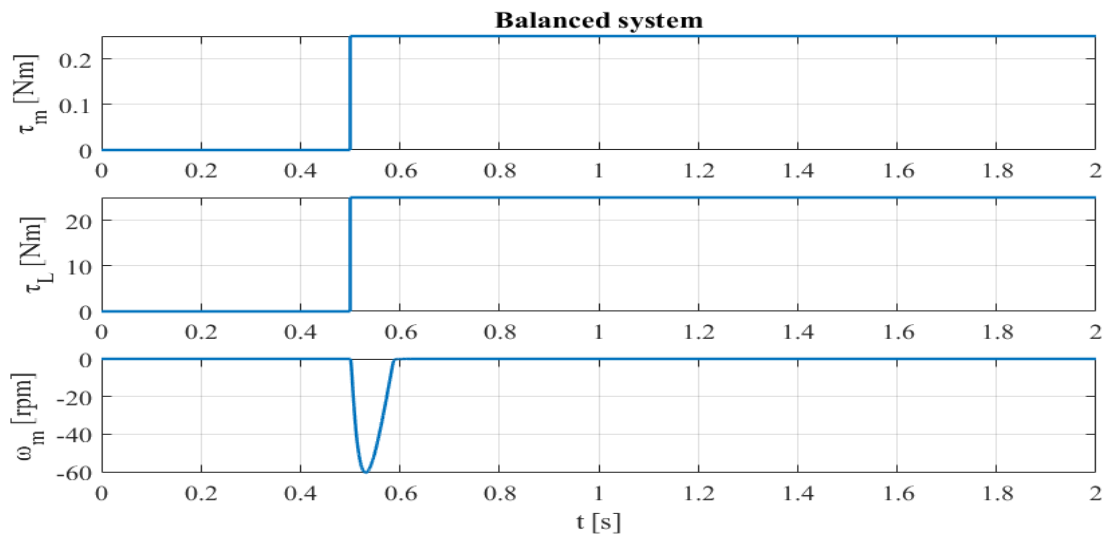


Figure 56: Balanced system is a blocked system with null speed and motion. The combination of the torque exerted by the motor and the resisting torque brings the velocity of the motor to drop to a null value

Motor drags load: in this case the motor is overcoming the torque produced by the load: the driving torque overtake the resisting torque. The speed of the motor is positive and therefore the motor itself allows the movement of the load, as shown in Figure 57.

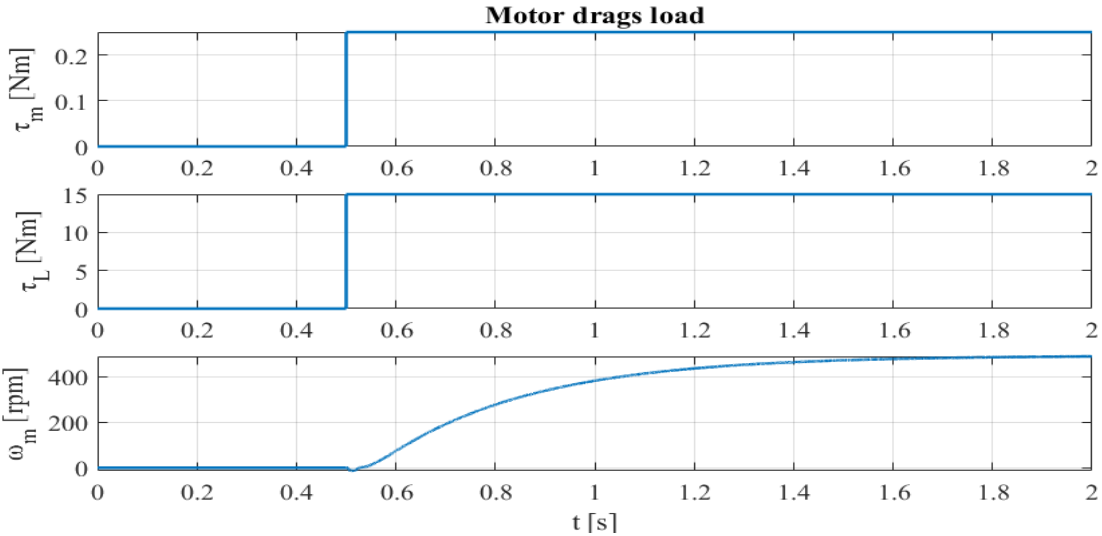


Figure 57: motor driving torque can overcome the resisting torque, the motor can drag the load during its motion, thus the resulting motor speed is positive.

Load drags motor: in this configuration the torque supplied by the compliant element overcomes the torque produce by the motor, so the load drags the motor. In this case the resisting torque overtakes the driving torque, and the motor speed is negative, since it is the load torque that drives the motor, as shown in Figure 58.

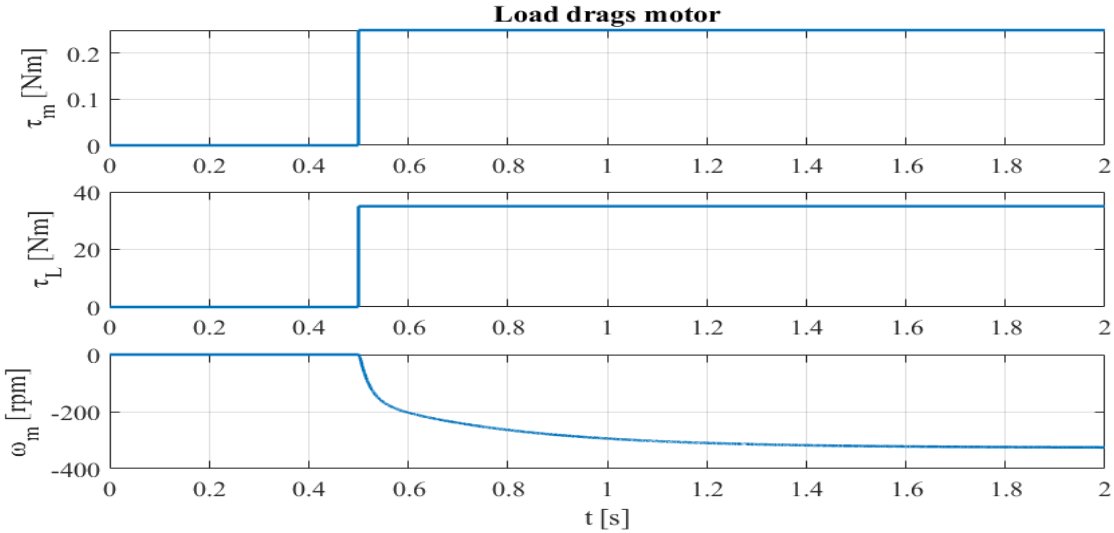


Figure 58: motor driving torque cannot overcome the resisting torque, the motor cannot drag the load during its motion, thus the resulting motor speed is negative

4.1.2. Frequency Analysis of real time collected data: infinite inertial load

The input signal used to perform the frequency analysis of the compliant element of the Series Elastic Actuator (SEA), is a current chirp. A chirp is a signal having constant amplitude and varying frequencies: this signal is useful because it is possible to test different frequencies with a single input. The chirp is based on the Swept cosine which generates a swept-frequency cosine with a linear instantaneous output frequency that may differ from the one specified by the frequency and time parameters. The desired input chirp has a logarithmic frequency sweep and has bidirectional sweep mode. Bidirectional sweep mode is based on the mirroring of the first half of the signal, at each double of sample time. The input chirp signal used for the frequency analysis is shown in Figure 59.a: from the analysis of the spectrum of the chirp signal, it is possible to notice that the target frequency is $f=20\text{Hz}$, as shown in Figure 59.

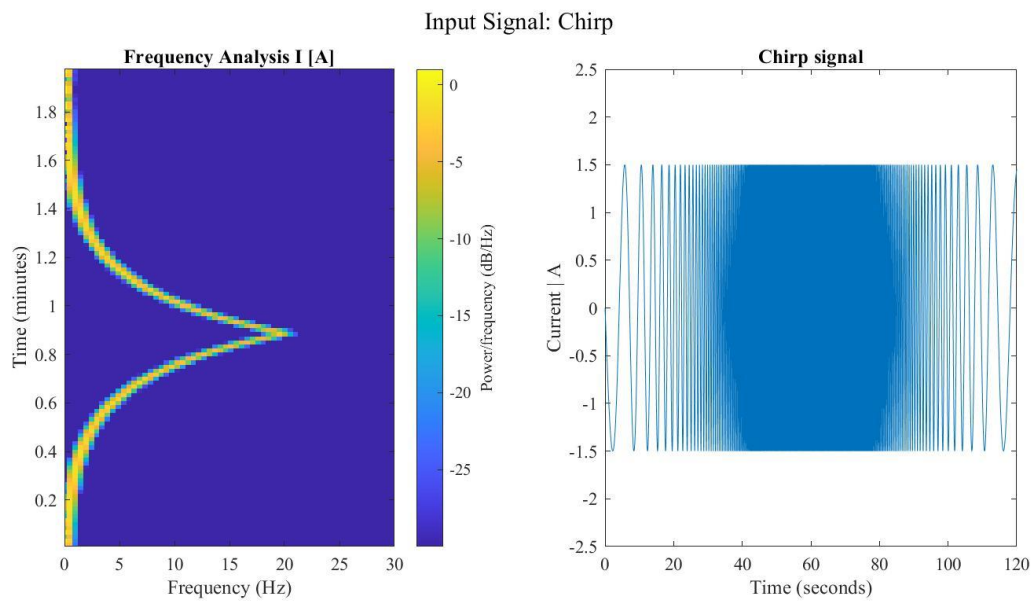


Figure 59: Input current chirp signal used for frequency analysis of SEAs. The signal is a logarithmic bidirectional chirp with a maximum frequency of 20 Hz. From spectrogram analysis of the chirp signal (a) it's possible to notice the different frequencies of the chirp signal (in yellow), with a focus on the maximum target frequency.

To evaluate the optimal frequency at which the compliant element can work, Bode Diagrams have been studied. The implemented transfer function is given from the modulation of $\Delta\theta$ over the input current I . The optimal work frequencies are given by resonance one, for each system, as it is shown in Figure 60. Making a comparison between the two joints having the EC 90 motor, the resonance peak decreases as the torsional stiffness of the compliant element decreases. The frequencies at which the resonant peaks are elapsed are reported in Table 32.

$$H = \frac{\Delta\theta(s)}{I(s)} \text{ transfer function}$$

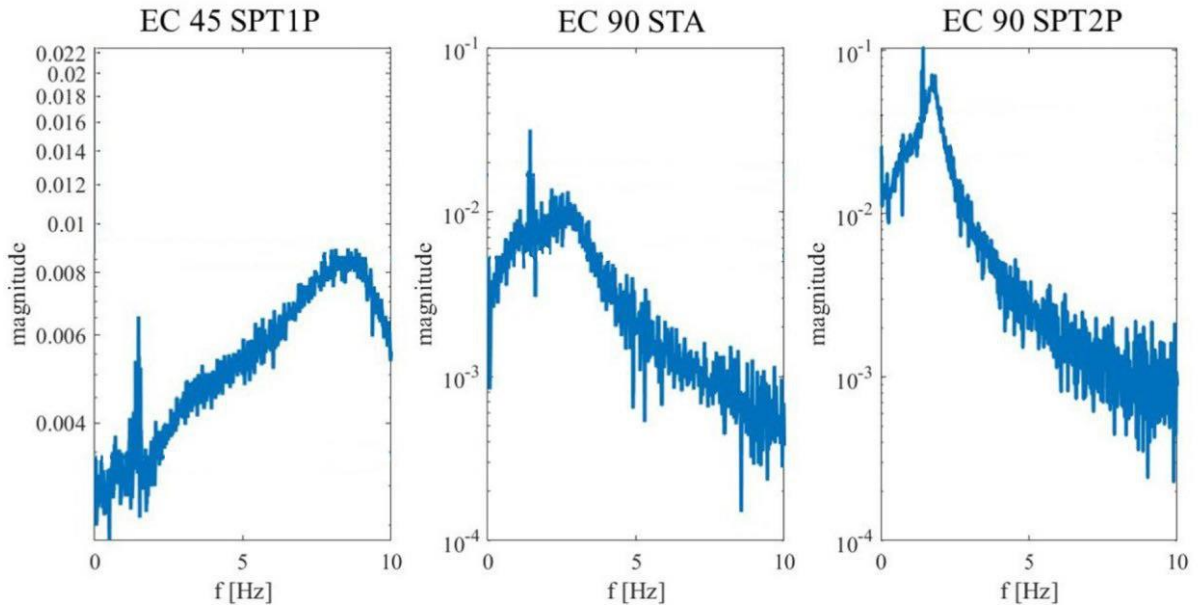


Figure 60: Magnitude Bode Diagram of transfer function between the input current and the relative measured encoders displacement of three actuators. The graph shows the respective resonance peaks at resonant frequencies: the resonant frequency allow to evaluate which is the optimal working conditions for each compliant element.

Resonance Frequencies		
EC 45 SPT1P	EC 90 STA	EC 90 SPT2P
7,93 Hz	2,53 Hz	1,64 Hz

Table 32: Resonance frequencies of the analysed compliant element. Value taken from the Magnitude Bode Diagram.

Proceeding with the frequency analysis of the compliant element, it is possible to notice that, by plotting the Magnitude Bode Diagram of the displacement data provided by the AskIm encoder $\Delta\theta$ and the one of the torque read from the torsionmeter τ , the two measurements are related by the multiplication of a constant, which is the torsional stiffness of the compliant element under test, as shown in Figure 61. This evaluation satisfies the Hooke's equation (Equation 2).

Frequency Analysis $\Delta\theta$ [rad] and τ [Nm]

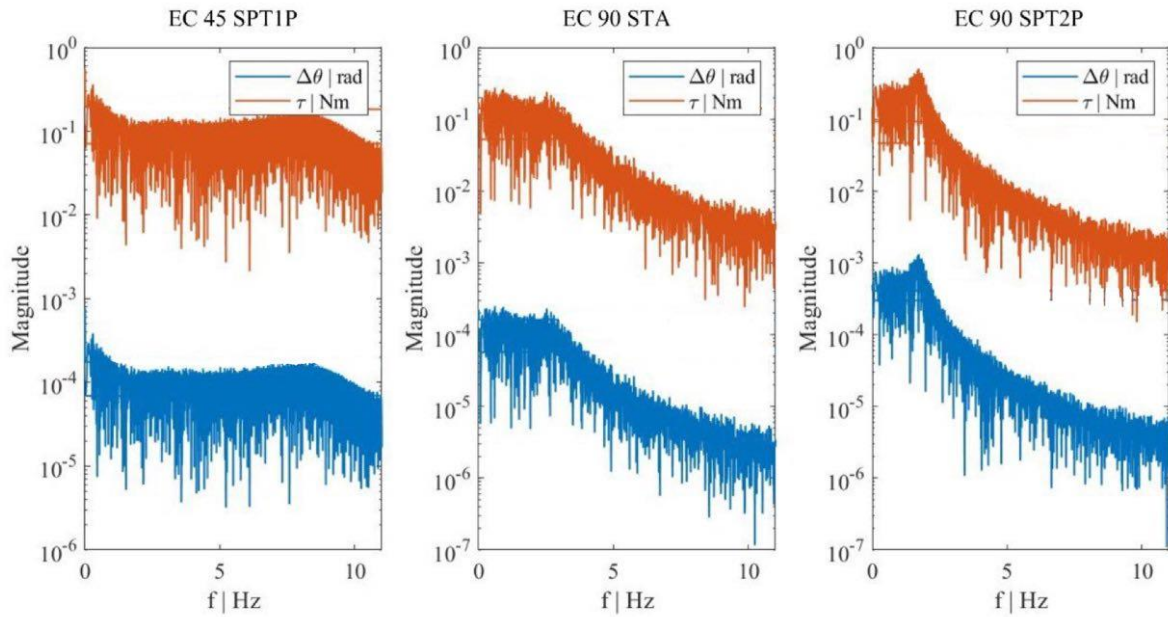


Figure 61: Magnitude Bode Diagram of torque and displacement, compared in the same plot. Thanks to the direct parallelism it is possible to notice the relative linear relationship given by the torsional stiffnesses K .

The frequency analysis of the torque has been made by considering the overall time of simulation (2 minutes). In this way, it is possible to notice that by increasing the frequency, the intensity of the respective expressed torque decrease. In fact, as depicted in Figure 62, the maximum torque is expressed at the resonance frequency.

Frequency Analysis τ [Nm]

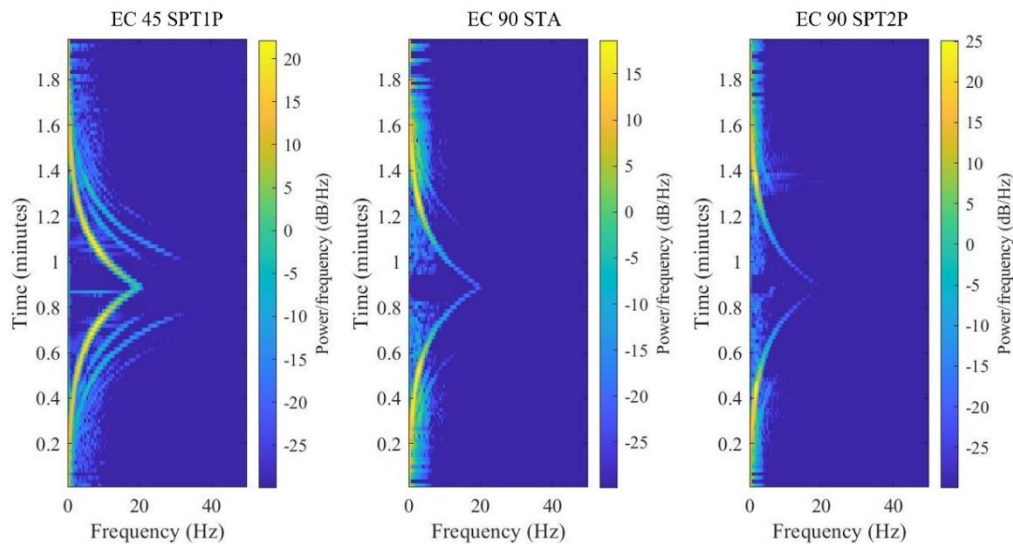


Figure 62: Spectrogram plot of torque used to analyse the optimal working frequencies of the torque. It can be notice that the intensity of the torque is optimal at the resonant frequency while it decreases at the increasing of the frequency.

The aim of the computation of the linear model of the torque is to define the accuracy of the SEA as a torque sensor. The linear model consists of the definition of a regression line; then, the residuals are defined as the difference between experimental data and the regression line (ideal ones). From the

computation of the residuals, it can be defined the error of which the torque is affected. The linear model plots are shown in Figure 63 and probability of the occurrence of the error is shown Figure 64. Furthermore, by analysing the data reported in Table 33, Table 34, Table 35 , the torsional stiffness of the compliant element of the SEA under test can be found. In particular, the torsional stiffnesses of the compliant elements are:

- $K_{spt1p}=961,47 \frac{Nm}{rad}$
- $K_{sta}=1072,6 \frac{Nm}{rad}$
- $K_{spt2p}=384,88 \frac{Nm}{rad}$

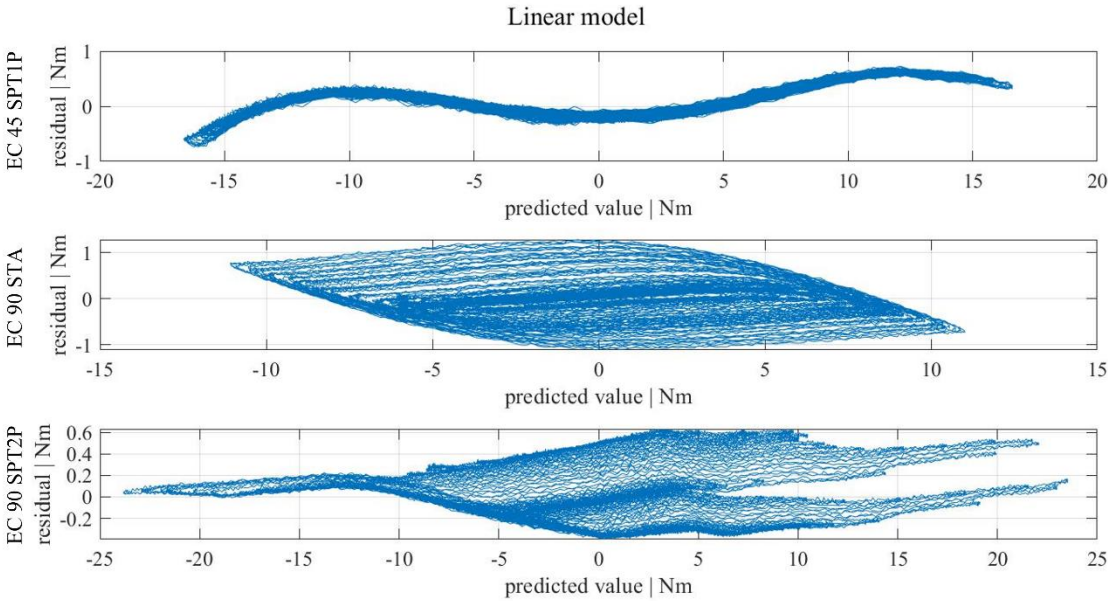


Figure 63: Linear model to map the error between expected and measured torque data.

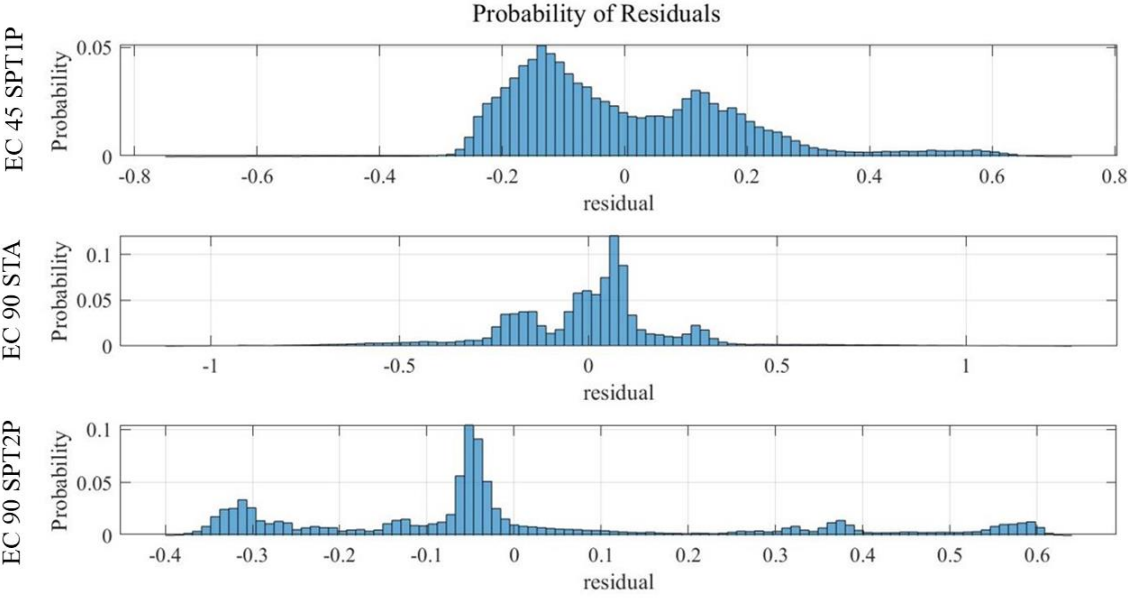


Figure 64: Probability distribution of the residulas errors that affect the torque measurements

EC45 SPT1P Linear regression model: $T \sim 1+\Delta\theta$ Encoder					
Estimated coefficients					
		Estimate	SE	tStat	pValue
	Intercept	0,18318	0,0005368	341,25	0
	$\Delta\theta$ Encoder	-961,47	0,094135	-10214	0
Observations and errors data					
Number of observations	Error degrees of freedom	RMSE	R-Squared	Adjusted R-Squared	F-statistics vs. constant model
120000	119998	0,184	0,999	0,999	104000000

Table 33: Linear regression model EC45 motor with SPT1P compliant element. Focus on the torsional stiffness of the compliant element under test.

EC90 STA Linear regression model: $T \sim 1+\Delta\theta$ Encoder					
Estimated coefficients					
		Estimate	SE	tStat	pValue
	Intercept	-0,064286	0,00070213	-91,559	0
	$\Delta\theta$ Encoder	-1072,6	0,19636	-5462,2	0
Observations and errors data					
Number of observations	Error degrees of freedom	RMSE	R-Squared	Adjusted R-Squared	F-statistics vs. constant model
120000	119998	0,243	0,996	0,996	29800000

Table 34: Linear regression model E90 motor with STA compliant element. Focus on the torsional stiffness of the compliant element under test.

EC90 SPT2P Linear regression model: $T \sim 1+\Delta\theta$ Encoder					
Estimated coefficients					
		Estimate	SE	tStat	pValue
	Intercept	0,049504	0,00075675	65,417	0
	$\Delta\theta$ Encoder	-384,88	0,054574	-7052,4	0
Observations and errors data					
Number of observations	Error degrees of freedom	RMSE	R-Squared	Adjusted R-Squared	F-statistics vs. constant model
120000	119998	0,262	0,998	0,998	49700000

Table 35: Linear regression model EC90 motor with SPT2P compliant element. Focus on the torsional stiffness of the compliant element under test.

If a sensor is suffering from hysteresis, for one same input value the output may vary depending on whether the input is increasing or decreasing at the time of measurement. Hysteresis corresponds to the maximum difference between the two outward and return paths of the output of a sensor during the calibration cycle. It is expressed as a percentage of the full scale (% f.s.). Thanks to frequency analysis, hysteresis of three actuators under test has been discussed. The hysteresis is defined as a loss of energy due to the frictions of the mechanical components and it is a cause of a delay on the desired torque transmission: more pins are presents in the assembly, then more dissipation is present. That can be noticed by comparing the hysteresis of the SPT1P (1 pin) and SPT2P (2 pins) with respect to the STA (8 pins), by considering the great difference between the

actuators having the same motor EC 90: in fact, the two SEAs are comparable because the only difference is given by the different compliant element. Nevertheless, the full scale of the two SEAS having EC 90 motor is the same, the maximum applied torque and the input current of the chirp amplitude too, then, it can be said that the number of connections of the compliant element with the system is relevant. The material of which the compliant element is made up is not influent on the hysteresis. In Figure 65 hysteresis are shown.

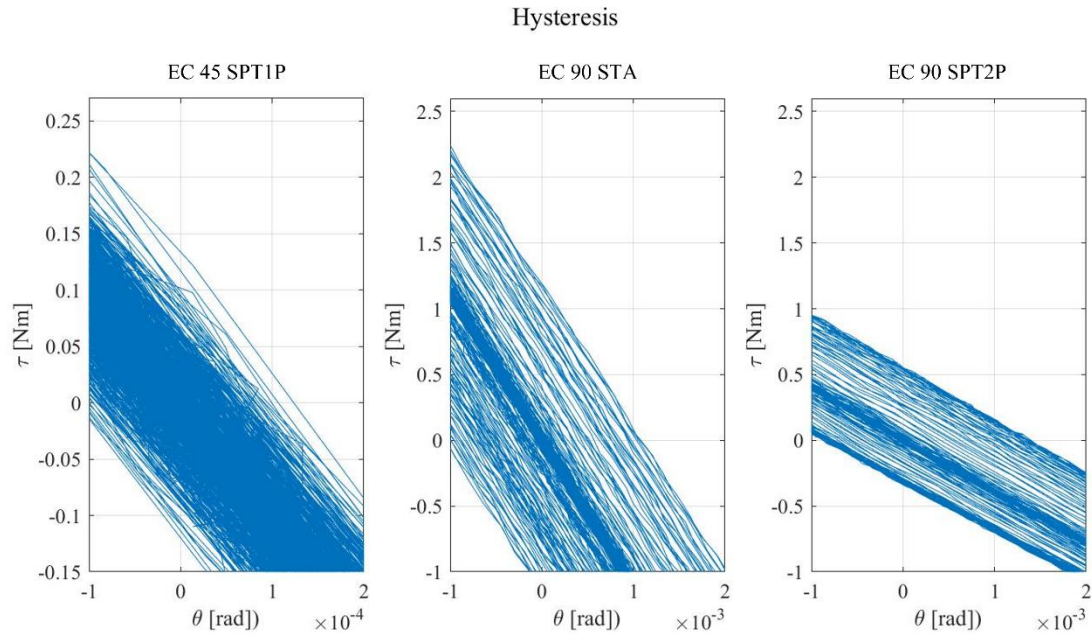


Figure 65: Hysteresis analysis of three different actuators.

4.1.2.1. Torsional stiffness evaluation of the compliant element for different EC45 SPT1P SEAs (FSJ45A joints)

Four different actuators composed of EC 45 motor and SPT1P custom made compliant element have been tested. The negative aspect of the spiral geometry of the spring is that the strain in the material greatly varies in different points of the geometry, this means that there are parts of the element that are not very exploited and that the shape lends itself to being optimized: for this reason, several tests for different actuator made up of the same element (EC 45, SPT1P and CSD-17-2A-100), have been tested. The optimization did not achieve appreciable results. To have a more precise results of the torsional stiffness of each spring, instead of a chirp input signal, a ramp input signal (current amplitude of $\pm 4A$) is given. A linear model is used to acquire the effective torsional stiffness of the complaint element under test. The main results are reported in Table 36, Table 37, Table 38, and Table 39, while the graphical interpretation is shown in Figure 66. The results obtained are:

- $K_{FSJ45A01} = 901,52 \frac{Nm}{rad}$
- $K_{FSJ45A02} = 838,02 \frac{Nm}{rad}$
- $K_{FSJ45A03} = 950,05 \frac{Nm}{rad}$
- $K_{FSJ45A04} = 987,14 \frac{Nm}{rad}$

Stiffness evaluation

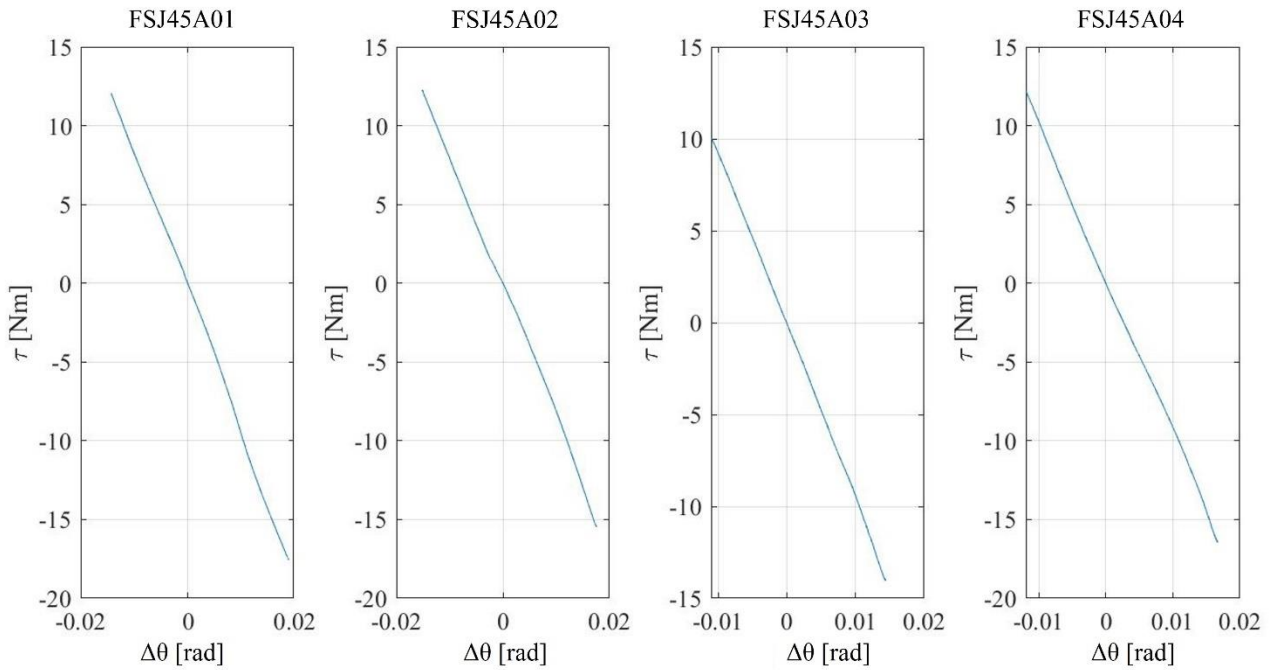


Figure 66: Torsional stiffness comparison between four actuators made up with same components: EC45, harmonic drive, custom mae compliant element with same geometry and same material (SPTIP).

FSJ45A01 - Linear regression model: $T \sim 1+\Delta\theta$ Encoder					
Estimated coefficients					
	Estimate	SE	tStat	pValue	
Intercept	-0,40625	0,0017993	-225,79	0	
$\Delta\theta$ Encoder	-901,52	0,16749	-5382,4	0	
Observations and errors data					
Number of observations	Error degrees of freedom	RMSE	R-Squared	Adjusted R-Squared	F-statistics vs. constant model
44001	43999	0,361	0,998	0,998	2,9e+07

Table 36: Linear regression model EC45 motor with SPTIP (FSJ45A01) compliant element. Focus on the torsional stiffness of the compliant element under test.

FSJ45A02 - Linear regression model: $T \sim 1+\Delta\theta$ Encoder					
Estimated coefficients					
	Estimate	SE	tStat	pValue	
Intercept	-0,2449	0,0019412	-126,16	0	
$\Delta\theta$ Encoder	-838,02	0,17256	-4856,4	0	
Observations and errors data					
Number of observations	Error degrees of freedom	RMSE	R-Squared	Adjusted R-Squared	F-statistics vs. constant model
44001	43999	0,383	0,998	0,998	2,36e+07

Table 37: Linear regression model EC45 motor with SPTIP (FSJ45A02) compliant element. Focus on the torsional stiffness of the compliant element under test.

FSJ45A03 - Linear regression model: $T \sim 1+\Delta\theta$ Encoder					
Estimated coefficients					
	Estimate	SE	tStat	pValue	
Intercept	-0,13787	0,00078613	-175,38	0	
$\Delta\theta$ Encoder	-950,05	0,087895	-10809	0	
Observations and errors data					
Number of observations	Error degrees of freedom	RMSE	R-Squared	Adjusted R-Squared	F-statistics vs. constant model
44001	43999	0,16	1	1	1,17e+08

Table 38: Linear regression model EC45 motor with SPT1P (FSJ45A03) compliant element. Focus on the torsional stiffness of the compliant element under test.

FSJ45A04 - Linear regression model: $T \sim 1+\Delta\theta$ Encoder					
Estimated coefficients					
	Estimate	SE	tStat	pValue	
Intercept	0,241	0,0013324	180,88	0	
$\Delta\theta$ Encoder	-987,14	0,12905	-7649,2	0	
Observations and errors data					
Number of observations	Error degrees of freedom	RMSE	R-Squared	Adjusted R-Squared	F-statistics vs. constant model
44001	43999	0,261	0,999	0,999	5,85e+07

Table 39: Linear regression model EC45 motor with SPT1P (FSJ45A04) compliant element. Focus on the torsional stiffness of the compliant element under test.

4.1.2.2. Torque and displacement comparison between Speedgoat and Simulink data

As explained in the chapter 3.7.2.2, the Simulink model for the offline SEA evaluation, has been used. In the Figure 67, the comparison between simulated data from the Simulink model and the experimental data retrieved by Speedgoat, is shown. The comparison has been done between the real and the simulated displacement over the real and simulated torque. It can be noticed that the simulation model narrowly behaves as the real one, unless not-idealities unmodelled.

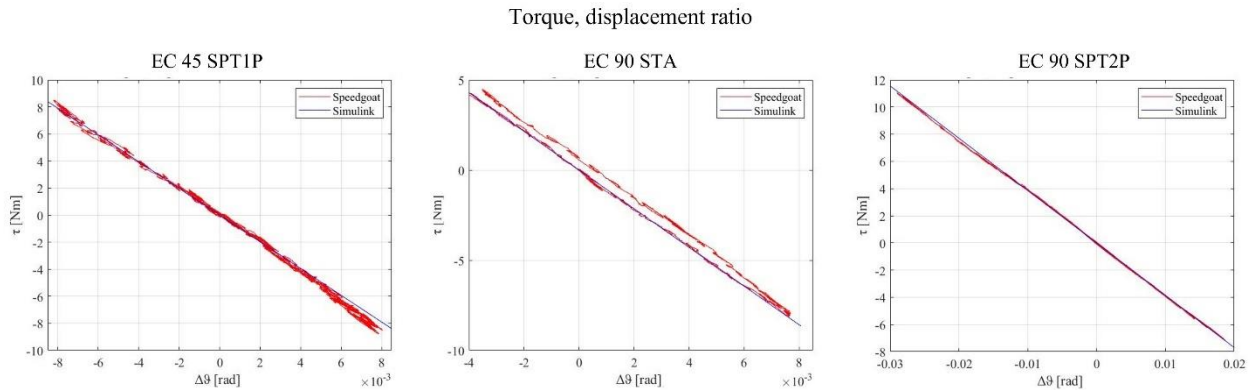


Figure 67: Torque and displacement comparison between Simulink and Speedgoat results for an infinite inertial load Simulink and test bench setup.

4.1.3. Speedgoat and Simulink data comparison: finite inertial load

The actuators EC 45 SPT1P, EC 90 STA and EC 90 SPT2P have been tested under finite inertial load. Thanks to the offline model, explained in chapter 3.7.2.3, the comparison between real and simulated data has been computed. The correct behaviour of the offline Simulink model is shown in Figure 68, where data comparison between current, angular velocity, displacement and torque are reported. The is given as example of the model behaviour. *Measured and Simulated data* are related to torsionmeter: commercial and the one modelled in Simulink-Simscape environment.

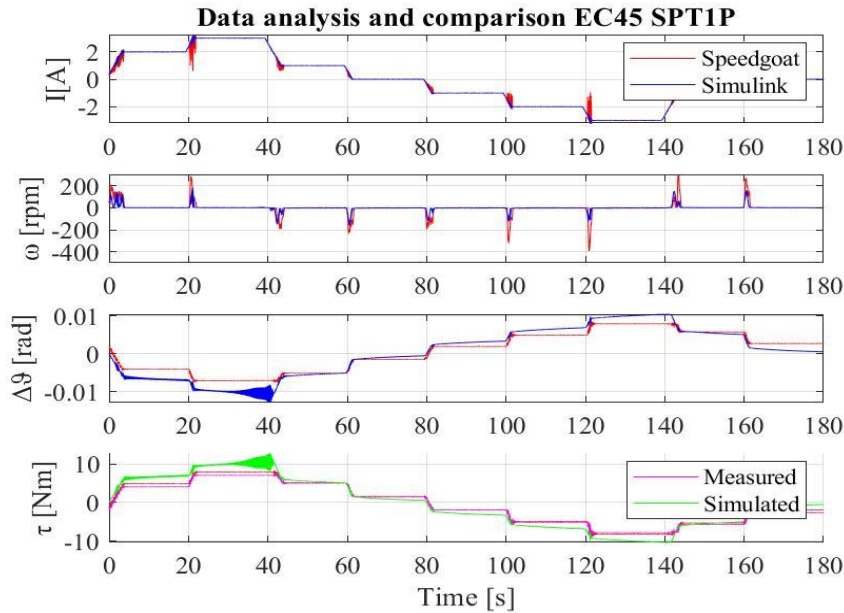


Figure 68: Current, speed, displacement, and torque comparison between Simulink and Speedgoat results for a finite inertial load Simulink and test bench setup.

In Figure 69, Figure 70, and Figure 71, the absolute errors between experimental and simulation data, are reported for each joint under test. To understand the entity of the errors reported in the following figures, a comparison with the full scale would be necessary. The models will therefore be refined to minimize errors.

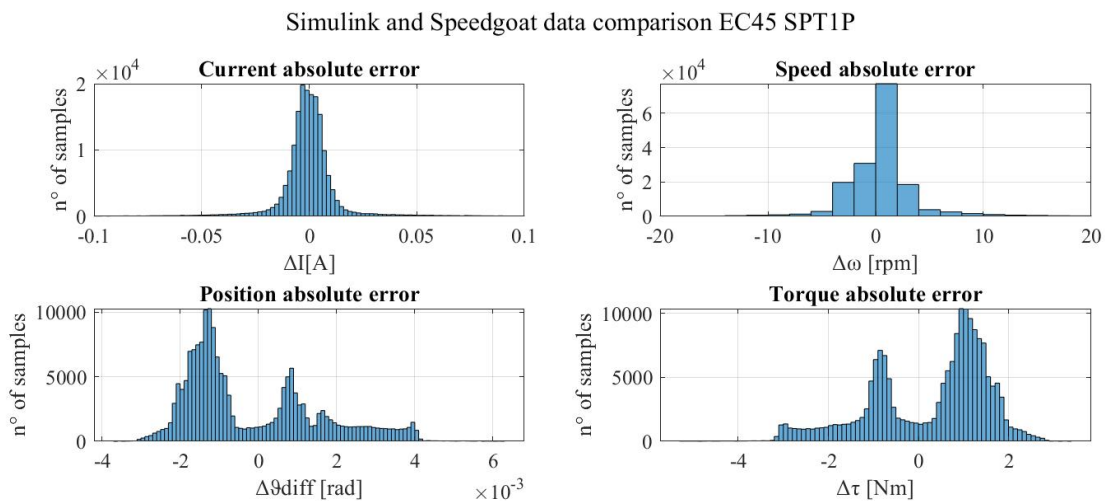


Figure 69: Absolute error of current, speed, displacement and torque comparison between Simulink and Speedgoat data for EC45 motor SPT1P compliant element

Simulink and Speedgoat data comparison EC90 STA

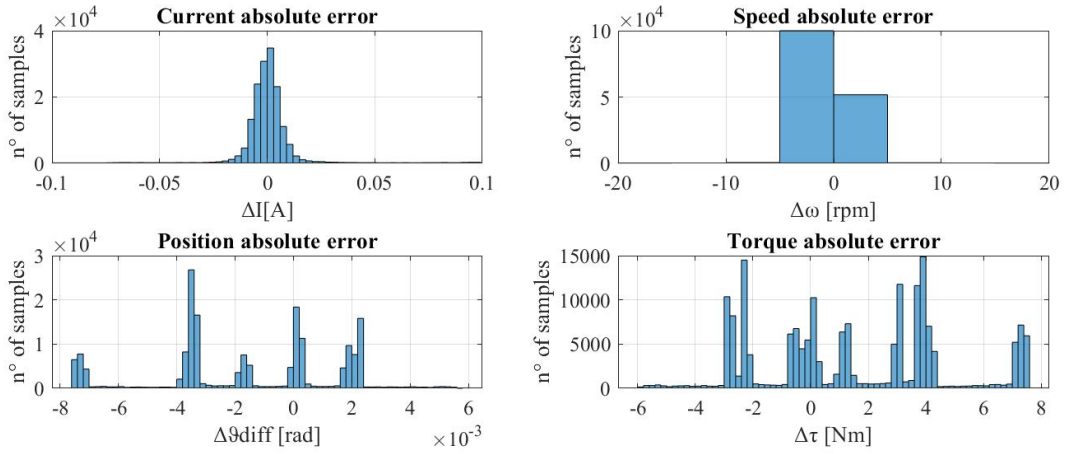


Figure 70: Absolute error of current, speed, displacement and torque comparison between Simulink and Speedgoat data for EC90 motor STA compliant element

Simulink and Speedgoat data comparison EC90 SPT2P

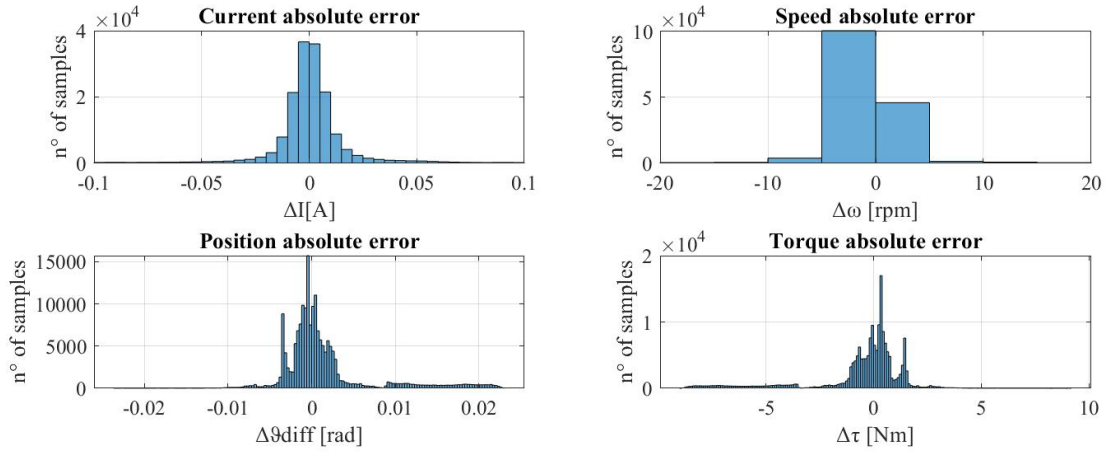


Figure 71: Absolute error of current, speed, displacement and torque comparison between Simulink and Speedgoat data for EC90 motor SPT2P compliant element

4.2. Control Strategy for 1 Degree of Freedom (DoF)

This section analyses the results of the position control developed on the single degree of freedom system. The strategy used for the tuning of the PID parameters is reported and a brief discussion is provided about the results obtained.

4.2.1. Position control

The position control has been implemented directly at slow shaft, based only on the information reported by the Aksim. This type of control can be useful in the case of a very slack SEA: in these conditions there are large variations in the output position, with the same motor position. On the other hand, for high stiffnesses also an upstream position control, as is the case for the position control implemented using EPOS, may be acceptable.

The following subsections show the graphs relating to the results obtained, both for the choice of the optimal parameters of the PID, and for the verification that the parameters are correct, when the reference position is followed.

4.2.1.1. Fixed Input Trajectory and PID Evaluation

As explained in section 3.8, to find the most suitable PID parameters, an experimental recursive approach has been adopted. The input trajectory is always constant: it is a sinusoidal wave with 30° of amplitude and a 10 s of period.

Proportional Term P Tuning

For the tuning of the proportional coefficient P, given a reference trajectory to follow, θ^{des} , several values of P coefficient have been tried, in have been chosen P=0.2, P=0.3 P=0.5 and P=0.6. The integral and derivative coefficients have remained constant and equal to I=0.3 and D=0.1. As shown in Figure 72, given a reference position to be tracked, the best value was P=0.5, also according with the RMSE values shown in Table 40.

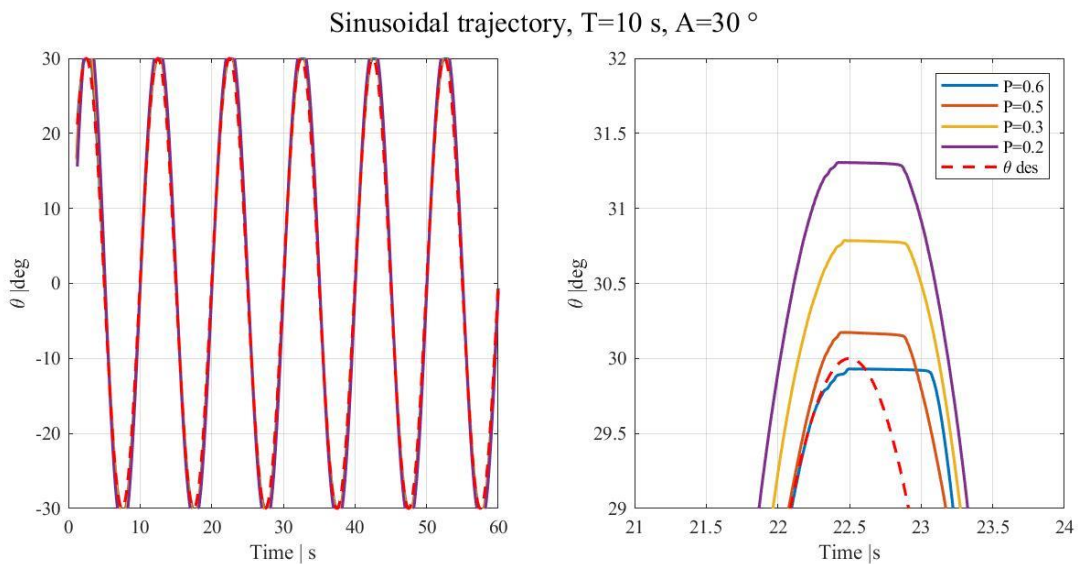


Figure 72: Analysis of the desired trajectory variation: sine wave with constant amplitude $A = 30^\circ$ and period $T = 10s$ as the proportional parameter P varies. (a) entire signal, (b) focus on a peak to see the differences

SINUSOIDAL INPUT DESIRED TRAJECTORY T=10 s, A= 30 deg				
I=0.3		D=0.1		
P	0.6	0.5	0.3	0.2
RMSE deg	0.0632	0.0717	0.0859	0.0951
max A deg	30.1327	31.3455	32.3442	33.0425
min A deg	-30.1303	-30.1713	-31.1642	-32.5452
mean delay s	-0.0097	-0.0364	-0.0374	-0.0382

Table 40: Summary and comparative table of the analysis of the data obtained during the tuning of the proportional term P, keeping constant the values of the integrative coefficient I and derivative D. Reference trajectory: sine wave with constant amplitude $A = 30^\circ$ and period $T = 10s$

Integrative Term I Tuning

For the tuning of the integrative coefficient I, given a reference trajectory to follow, θ^{des} , several values of I coefficient have been tried, have been chosen I=0.2, I=0.3 I=0.5 and I=0.8. The proportional and derivative

coefficients have remained constant and equal to $P=0.5$ and $D=0.1$. The P coefficient has been set to the optimal value defined with the P tuning. As shown in Figure 73, given a reference position to be tracked, the best value was $I=0.2$, also according with the RMSE values shown in Table 41.

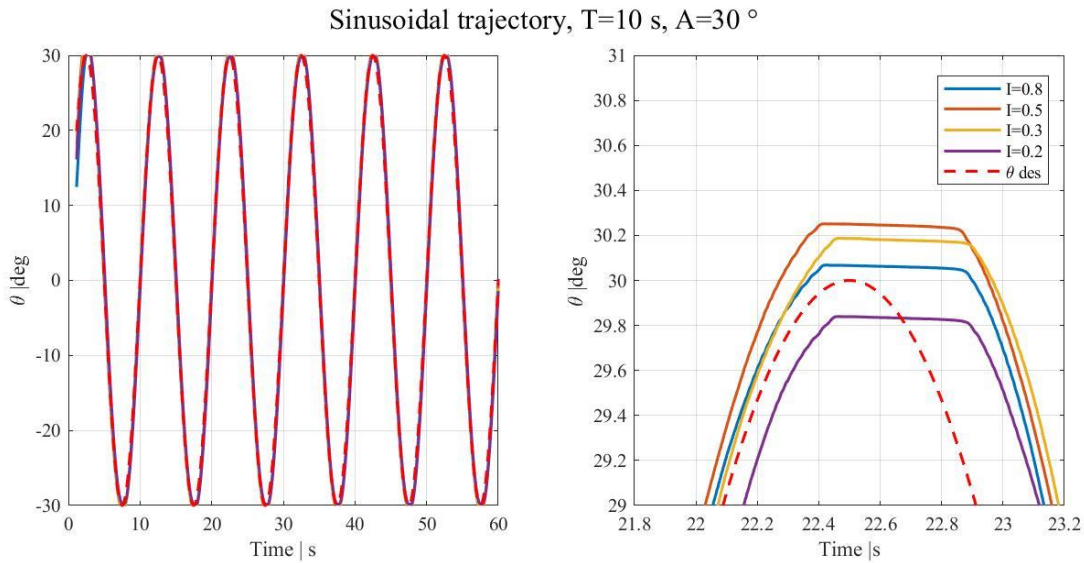


Figure 73: Analysis of the desired trajectory variation: sine wave with constant amplitude $A = 30^\circ$ and period $T = 10s$ as the integrative parameter I varies. (a) entire signal, (b) focus on a peak to see the differences

SINUSOIDAL INPUT DESIRED TRAJECTORY $T=10$ s, $A= 30$ deg				
P=0.5		D=0.1		
I	0.8	0.5	0.3	0.2
RMSE deg	0.0631	0.0637	0.0715	0.0748
max A deg	30.5685	32.1870	31.3297	30.6041
min A deg	-30.0903	-30.2178	-30.2668	-29.8493
mean delay s	-0.0613	-0.0449	-0.0366	-0.0387

Table 41: Summary and comparative table of the analysis of the data obtained during the tuning of the integrative term I keeping constant the values of the proportional coefficient P and derivative D . Reference trajectory: sine wave with constant amplitude $A = 30^\circ$ and period $T = 10s$

Derivative Term D Tuning

For the tuning of the derivative coefficient D , given a reference trajectory to follow, θ^{des} , several values of D coefficient have been tried, have been chosen $D=0.3$, $D=0.5$ and $D=0.7$. The proportional and integrative coefficients have remained constant and equal to $P=0.5$ and $I=0.2$. The P and the I coefficients have been set to the optimal value defined with the P and I tuning. As shown in Figure 74, given a reference position to be tracked, the best value was $D=0.3$, also according with the RMSE values shown in Table 42.

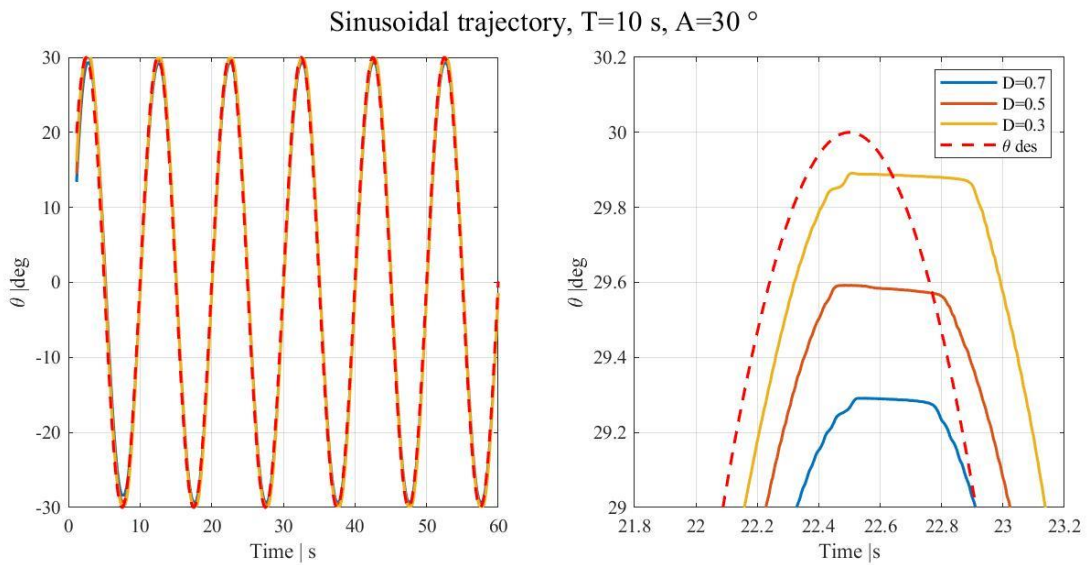


Figure 74: Analysis of the desired trajectory variation: sine wave with constant amplitude $A = 30^\circ$ and period $T = 10$ s as the derivative parameter D varies. (a) entire signal, (b) focus on a peak to see the differences

SINUSOIDAL INPUT DESIRED TRAJECTORY $T=10$ s, $A= 30$ deg				
P=0.5		I=0.2		
D	0.7	0.5	0.3	0.1
RMSE deg	0.0792	0.0776	0.0746	0.0748
max A deg	29.2913	30.1339	30.6370	30.6041
min A deg	-29.2963	-29.6385	-29.8472	-29.8493
mean delay s	-0.0700	-0.0542	-0.0389	-0.0387

Table 42: Summary and comparative table of the analysis of the data obtained during the tuning of the derivative term D keeping constant the values of the proportional coefficient P and integrative I . Reference trajectory: sine wave with constant amplitude $A = 30^\circ$

4.2.1.2. Variable Input Trajectory PID Evaluation and fixed PID coefficient

After finding the best coefficients of the PID, different trajectories were tried. Several sinusoids of constant amplitude, but different frequency, a step response and a ramp were tested.

Sinusoidal wave

The sinusoidal trajectories desired and to be tracked in position, were deliberately chosen so that they had two different frequencies: it is important to verify that the chosen parameters are suitable for both high and low frequencies. Furthermore, a further analysis on the integrative coefficient was developed. The results, reported in Figure 75, Figure 76, Table 43 and Table 44, show that the first choice of $I = 0.2$ was in fact the optimal one. The Table 43 and Table 44 show the results of the various variable frequency sinusoids tested. Different periods of 10s, 8s, 6s, 4s and 2s were analysed. The Figure 75 and Figure 76 instead show the extreme results, at lower and higher frequency.

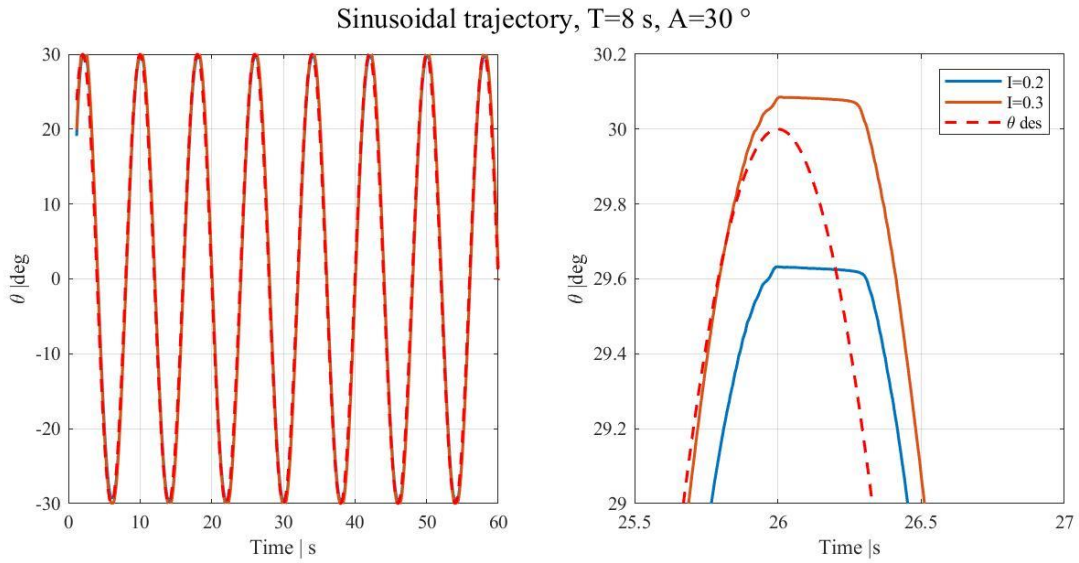


Figure 75: Analysis of the desired low frequency trajectory variation: sine wave with constant amplitude $A = 30^\circ$ and period $T = 8s$ as the proportional parameter $I = 0.2$ or $I = 0.3$ varies. (a) entire signal, (b) focus on a peak to see the differences

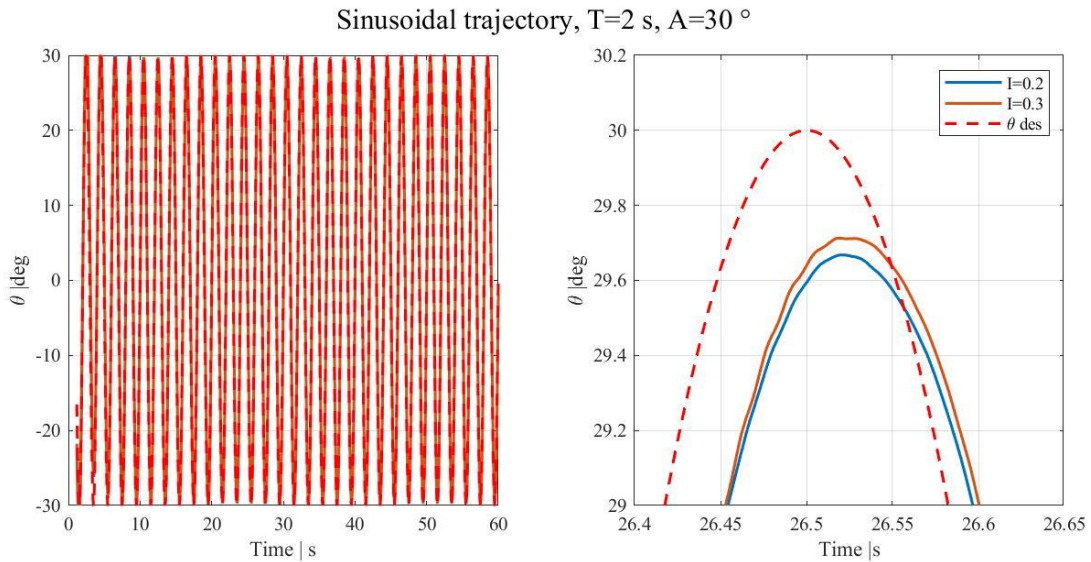


Figure 76: Analysis of the variation of the desired trajectory at high frequency: sine wave with constant amplitude $A = 30^\circ$ and period $T = 2s$ as the proportional parameter $I = 0.2$ or $I = 0.3$ varies. (a) entire signal, (b) focus on a peak to see the differences

SINUSOIDAL INPUT DESIRED TRAJECTORY T=variable, A= 30 deg					
	P=0.5	I=0.2	D=0.3	N=400	
period s	10	8	6	4	2
RMSE deg	0.0745	0.0782	0.0805	0.0814	0.0894
max A deg	30.6496	30.2894	29.6107	30.9362	32.9557
min A deg	-29.8500	29.6560	-29.4340	-29.2902	-32.6608
mean delay s	-0.0399	-0.1249	-0.0930	-0.1418	-0.1741

Table 43: Summary and comparative table of the data analysed and collected with the definitive parameters of the PID. Specific analysis of the integrative term $I = 0.2$

SINUSOIDAL INPUT DESIRED TRAJECTORY T=variable, A= 30 deg					
	P=0.5	I=0.3	D=0.3	N=400	
period s	10	8	6	4	2
RMSE deg	0.0716	0.0769	0.0822	0.0841	0.0910

max A deg	31.3893	31.2061	29.8038	30.4487	34.6268
min A deg	-30.2601	-30.0953	-29.8546	-29.4764	-31.2863
mean delay s	-0.0380	-0.1264	-0.883	-0.1348	-0.1757

Table 44: Summary and comparative table of the data analysed and collected with the definitive parameters of the PID. Specific analysis of the integrative term $I = 0.3$

Step

The most difficult trajectory to follow and reproduce is the step response: it is, in fact, difficult to follow a sudden change of position in an instant of infinitesimal time. The step is, in fact, a response that does not reproduce physiological movements and that will not be used as a control trajectory for an upper limb exoskeleton in contact with the patient. In any case, to verify the correct tuning of the parameters, a step response has been validated. As can be seen in Figure 77, the integrative term plays an important role: in fact, the coefficient I tends to keep the steady position constant, varying the trajectory gradually (almost jerky) until a negligible tracking error is reached. On the other hand, an overshoot response is not permissible in an upper limb exoskeleton interacting with the patient. this is another reason why the step responses are not supplied as input, but it is preferred to modulate the response either with a ramp, or by adding, in series to the step, a slew rate, to make the signal smoother. Different step responses were tested: with sudden steps of 10° , 20° , 30° and 40° . The results are shown in Table 45.

STEP INPUT TRAJECTORY				
P=0.5 I=0.3 D=0.3 N=400				
amplitude deg	10	20	30	40
overshoot %	9.0414	13.5338	15.8330	16.8272
RMSE deg	0.0553	0.0660	0.0904	0.0990
max A deg	10.9041	22.7068	34.7499	46.7309
rise time 90%	2.0426	1.9430	1.9090	1.8933
mean delay s	-0.0206	-0.0198	-0.0659	-0.0724

Table 45: Summary and comparative table of the data analysed and collected for a step trajectory with the definitive parameters of the PID.

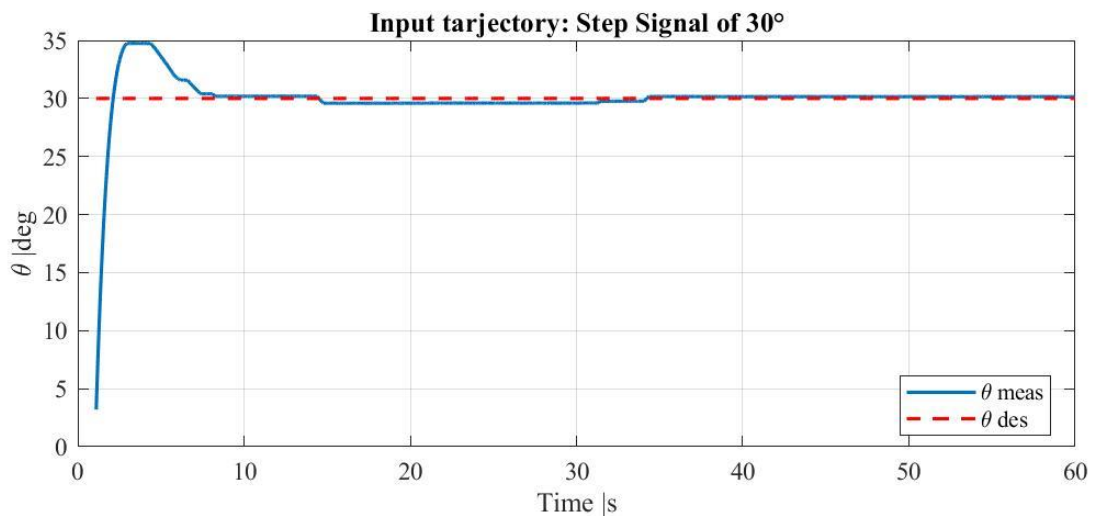


Figure 77: Reference position: 30° step with the optimal PID values found.

Ramp

To overcome the problems provided by a stepped trajectory, the position control was tested by providing a ramp as an input. Ramps with different slopes have been tested, with slopes of 1° , 10° and 20° , the results of which are reported in Table 46.

RAMP INPUT TRAJECTORY			
P=0.5 I=0.3 D=0.3 N=400			
amplitude deg	1	10	20
RMSE deg	0.0342	0.0236	0.0353

Table 46: Summary and comparative table of the data analysed and collected for a ramp trajectory with the definitive parameters of the PID.

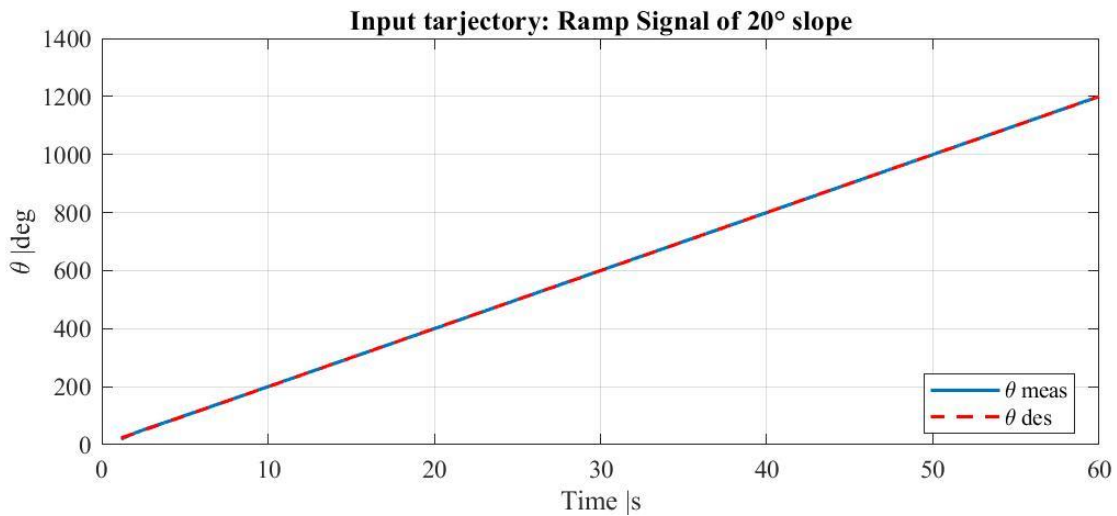


Figure 78: Reference position: 20° ramp with the optimal PID values found.

4.2.1.3. PID final optimal parameters tuned for position control

After the analysis described in chapter 3.8 whose results are reported in chapter 4.2, the optimal parameters of the position control on a single degree of freedom are reported in the Table 47.

P	I	D
0.5	0.3	0.3

Table 47: Optimal PID parameters for closed-loop position control

Table 48 shows the main contributions that the coefficients P I and D give to the system: it is in fact necessary to find the right trade-off between the parameters so that the system is accurate and not unstable. Furthermore, in the case of a purely proportional regulator the steady-state error is different from zero; for the PI and PID regulators the steady-state error is zero, the PID regulator goes to steady-state faster but with a greater overshoot.

Increasing PID parameters				
	Rise Time	Overshoot	Settling Time	Steady State Error
P	decrease	increase	irrelevant	decrease
I	decrease	increase	increase	decrease
D	irrelevant	decrease	decrease	irrelevant

Table 48: Relationship between PID parameters

4.3. Control Strategies for 2 Degrees of Freedom

This chapter analyses the main results obtained from the admittance and impedance control carried out on a two-degree-of-freedom system.

4.3.1. Admittance control: Joint Space

As explained in chapter 3.9.1, admittance control was developed in the space of the joints. Two systems were analysed, one purely elastic and one viscoelastic, the main results of which are reported in these sub-chapters. For a better graphical interpretation, the plots are represented in degrees, but inside the system and in the Simulink environment, the data were instead analysed in radians.

4.3.1.1. Purely elastic admittance filter

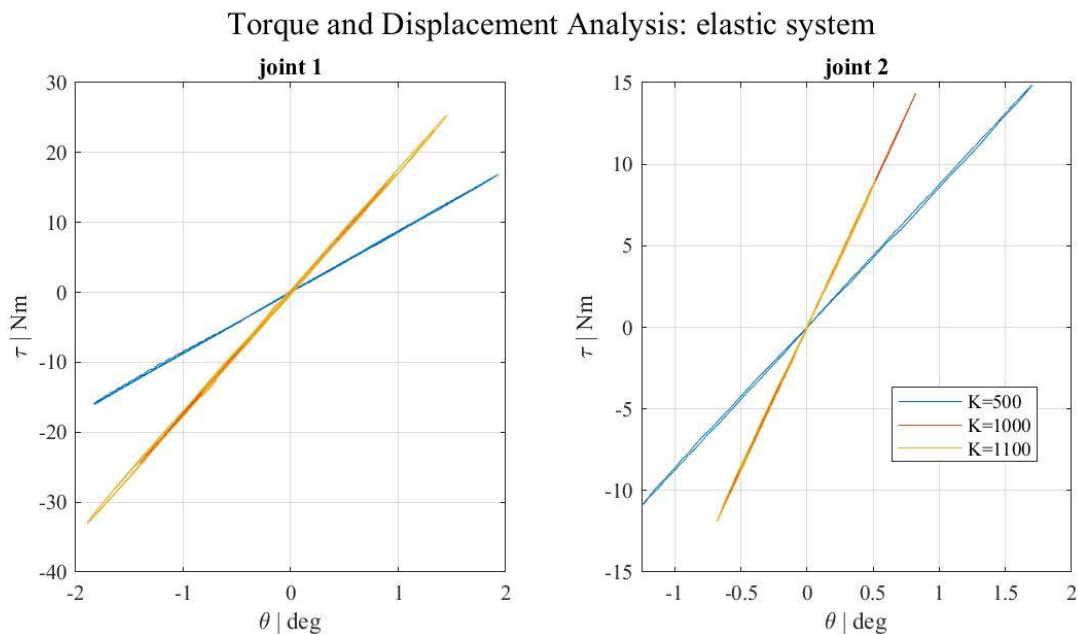


Figure 79: Elastic admittance experimental comparison between different combination of elastic coefficients

ELASTIC ADMITTANCE K Nm/rad					
desired K		measured K		error %	
along joint 1	along joint 2	along joint 1	along joint 2	along joint 1	along joint 2
1100,00	1100,00	1099,60	1099,90	0,03	0,01
1000,00	1000,00	998,90	999,00	0,11	0,10
500,00	500,00	498,70	499,30	0,26	0,14

Table 49: Torsional stiffnesses of the virtual dynamic spring imposed by the admittance filter. Absolute percentage error between imposed (desired) values and experimentally obtained values.

The admittance in the joint space was developed by testing different spring stiffnesses, to obtain a compliant dynamic for both scapular joint actuators. In a purely elastic system, the spring acts as a coefficient acting on the position of the system. Thanks to the elastic return force intertwined with the behaviour of the spring (Hooke's law), the reference position is always followed. Experimentally it has been obtained that the measured spring coefficient is approximately equal to the desired one, except for tiny percentage errors, as shown in

Table 49. Consider a purely elastic system in which the spring constant is strong, equal to $K=1000$ Nm/rad. In this case the transfer function of the admittance filter will be:

$$\frac{\theta^{dyn}}{\tau^{aksim}} = \frac{1}{1000}$$

Equation 50: Pure elastic admittance filter with loose spring constant, $K=1000$ Nm/rad

Referring to the control diagram shown in Figure 80, the Figure 81 shows the system performance after applying the admittance filter.

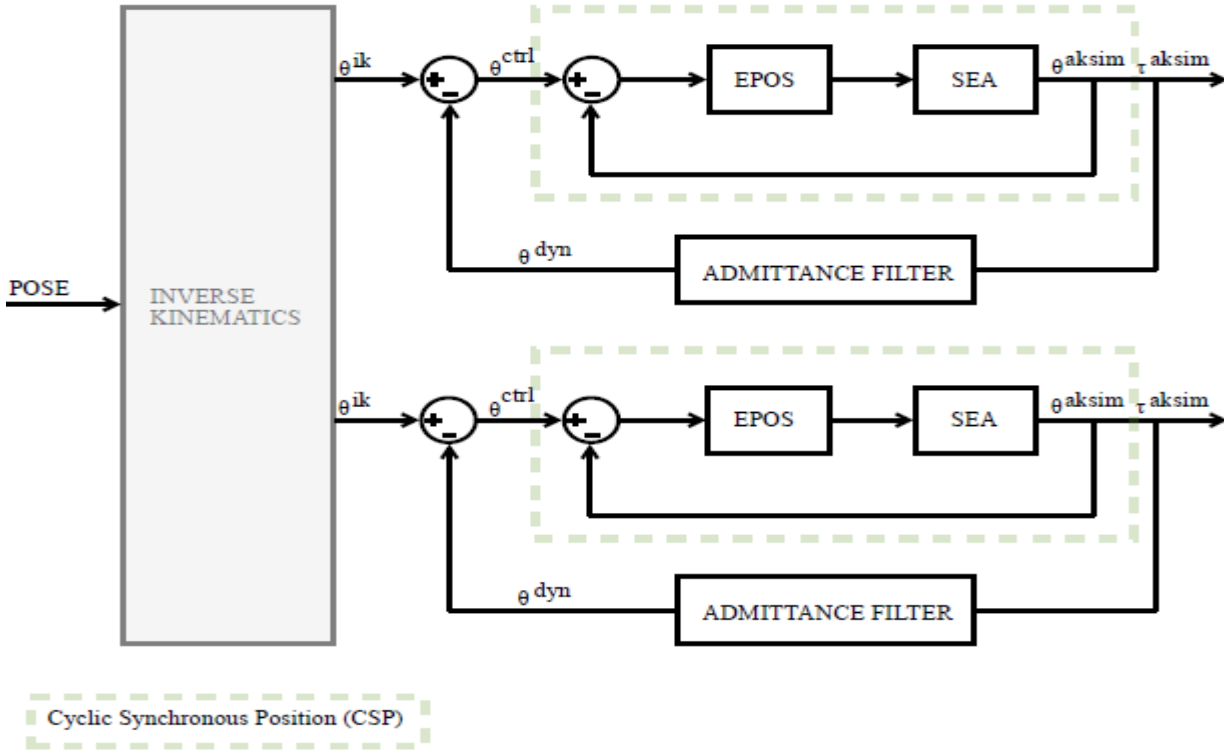


Figure 80: Admittance Control in Joint space

It can be seen how the virtual dynamics of the system change. By exerting a pair from outside τ_i , the θ_i^{ctrl} is unanimously different from the reference position θ_i^{ik} . To analyze the direct correlation between the input torque τ_i , and the output position of the filter in a purely elastic admittance, it can be noted that the θ_i^{dyn} is different from zero. The θ_i^{dyn} is equal to zero only when τ_i is null, so when the system is not perturbed. Recalling that $\theta^{ctrl} = \theta^{ik} - \theta^{dyn}$, then the θ_i^{dyn} has the inverse sign of θ_i^{ctrl} , as expected.

Joint space Admittance Analysis

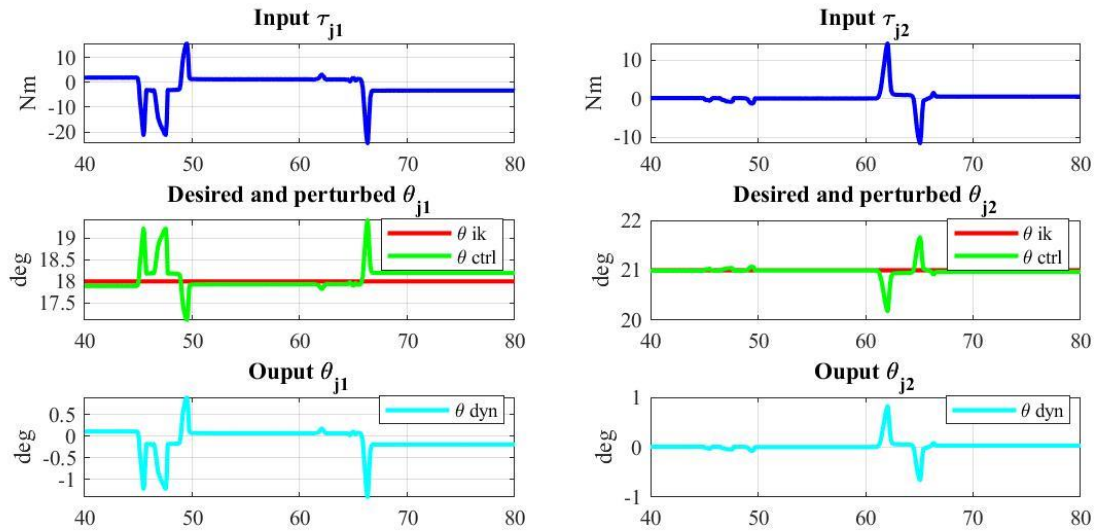


Figure 81: Pure elastic admittance filter analysis for each joint with a torsional stiffness of the spring constant and equal to $K=1000$ Nm/rad. Admittance filter behaviour, output dynamic position with respect to an external torque perturbation as input.

The Figure 82 shows the intensity with which the admittance filter acts. It can be noted that, as the external torque exerted and read by the Aksim τ_i^{aksim} encoders increase, the dynamic position θ_i^{dyn} at the output of the filter is increasingly distant from the reference position θ_i^{ik} . Working in the joint space, a greater displacement of the joint 1 corresponds to a perturbation of the first joint, while a greater displacement of the joint 2 corresponds to a perturbation of the second joint. A purely elastic behaviour tends to introduce oscillations, especially when a high torsional stiffness is applied. To overcome this unwanted behaviour, it is necessary to introduce a viscous behaviour, to obtain a viscoelastic system.

Joint space Admittance Analysis

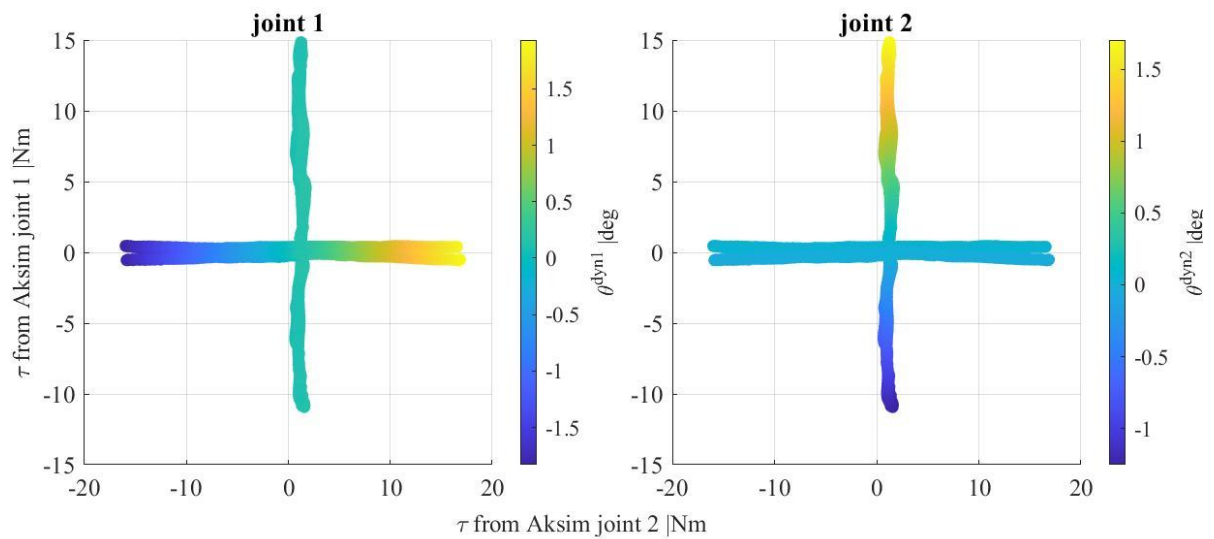


Figure 82: Intensity with which the virtual dynamics of the system is modified by varying the external torque exerted in a purely elastic system with strong spring constant.

4.3.1.2. Viscoelastic system

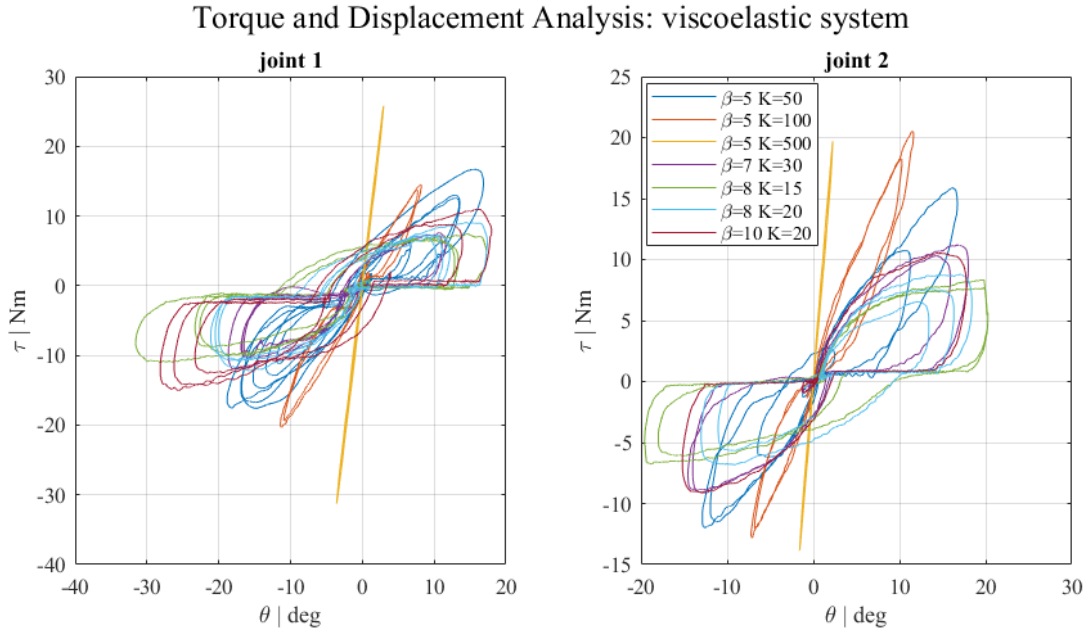


Figure 83: Viscoelastic admittance experimental comparison between different combination of viscous and elastic coefficients

In a viscoelastic system, it is possible to modify the virtual dynamics of the system by acting both on the reference trajectory, therefore on the position, and on the speed, adding a viscous coefficient. The Figure 83 shows the behaviour of a viscoelastic system as the coefficients vary. It can be noted that, with the same viscous coefficient, the higher the coefficient of the spring, the more the behaviour of the virtual dynamics will be modified to essentially act on the reference position. In a system in which the elastic coefficient is predominant with respect to the viscous coefficient, the trajectory defined at the input is certainly followed, but the system will be subjected to non-attenuated oscillations. On the other hand, in a system in which the viscous coefficient is much greater than the elastic one, the system will try to attenuate any oscillation, up to zero, but it will deviate from the reference system, therefore the relationship between the input torque and the output displacement will no longer be linear. Consider a viscoelastic system in which both the spring constant and the damping coefficient are loose, equal to $K=70 \text{ Nm/rad}$, $\beta=30 \text{ Nm/rad/s}$. In this case the transfer function of the admittance filter will be:

$$\frac{\theta^{dyn}}{\tau^{aksim}} = \frac{1}{30s + 70}$$

Equation 51: Pure elastic admittance filter with loose spring constant, $K=70 \text{ Nm/rad}$, $\beta=30 \text{ Nm/rad/s}$

Referring to the control diagram shown in Figure 50, the Figure 84 shows the system performance after applying the admittance filter. It can be seen how the virtual dynamics of the system change.

By exerting a torque from outside τ_i , the θ_i^{ctrl} is unanimously different from the reference position θ_i^{ik} . To analyse the direct correlation between the input torque τ_i , and the output position of the filter in a purely elastic admittance, it can be noted that the θ_i^{dyn} is different from zero. The θ_i^{dyn} is equal to zero only when τ_i , is null, so when the system is not perturbed. Recalling that $\theta^{ctrl} = \theta^{ik} - \theta^{dyn}$, then the θ_i^{dyn} has the inverse

sign of θ_i^{ctrl} , as expected. Thanks to the introduction of the viscous element which acts directly on the speed of the system, unwanted oscillations are attenuated, thus creating a more safe and user-friendly dynamics.

Joint space Admittance Analysis

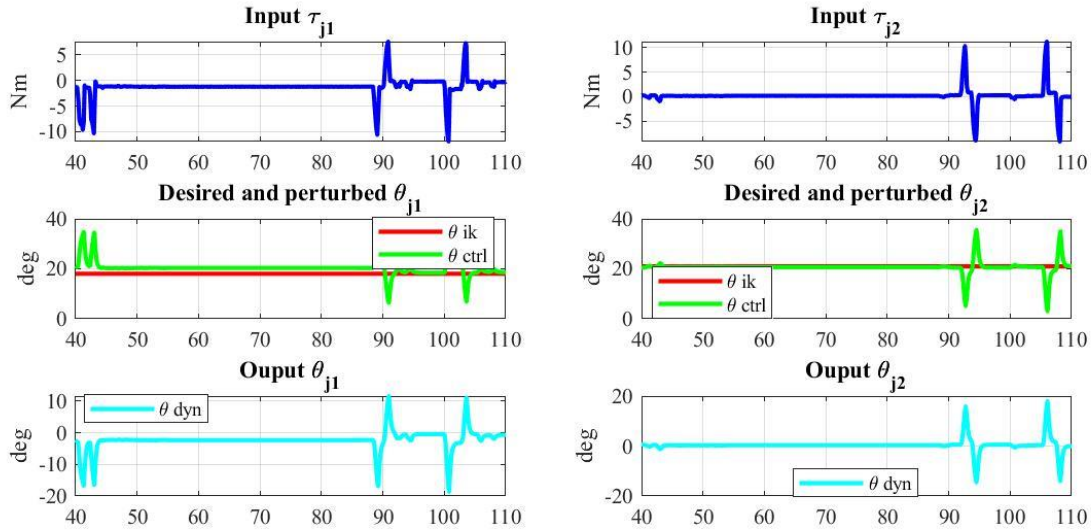


Figure 84: Viscoelastic admittance filter analysis for each joint with a loose spring constant $K=70$ Nm/rad, $\beta=30$ Nm/rad/s. Admittance filter behaviour, output dynamic position with respect to an external torque perturbation as input.

The Figure 85 shows the intensity with which the admittance filter acts. It can be noted that, as the external torque exerted and read by the Aksim τ_i^{aksim} encoders increase, the dynamic position θ_i^{dyn} at the output of the filter is increasingly distant from the reference position θ_i^{ik} . Working in the joint space, a greater displacement of the joint 1 corresponds to a perturbation of the first joint, while a greater displacement of the joint 2 corresponds to a perturbation of the second joint.

Joint space Admittance Analysis

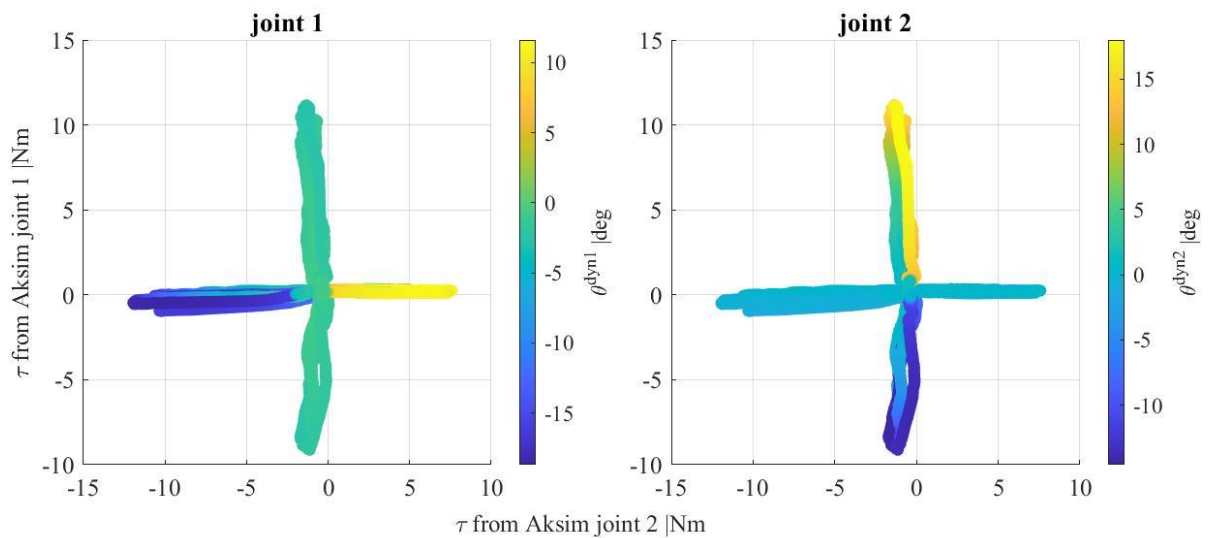


Figure 85: Intensity with which the virtual dynamics of the system is modified by varying the external torque exerted in a viscoelastic system.

4.3.2. Impedance control: Task Space

As explained in chapter 3.9.2 impedance control was developed in the task space, so in the cartesian space of the end effector. Three systems were analysed, one purely elastic, one purely viscous and one viscoelastic, the main results of which are reported in these sub-chapters.

4.3.2.1. Purely elastic system

A purely elastic impedance filter in the task space implies the presence of a linear spring in the Cartesian space. In this case the virtual dynamics of the system is modified only at the end-effector. As shown in Figure 86, the stiffness of the linear spring has a trend that respects the desired behaviour as the stiffness increases: the stiffer the spring, the less the mechanical impedance of the system affects. In fact, when the stiffness is loose, then the system tends to be transparent, thus making the impedance of the system predominate with respect to the imposed one. The main absolute errors are reported in Table 50.

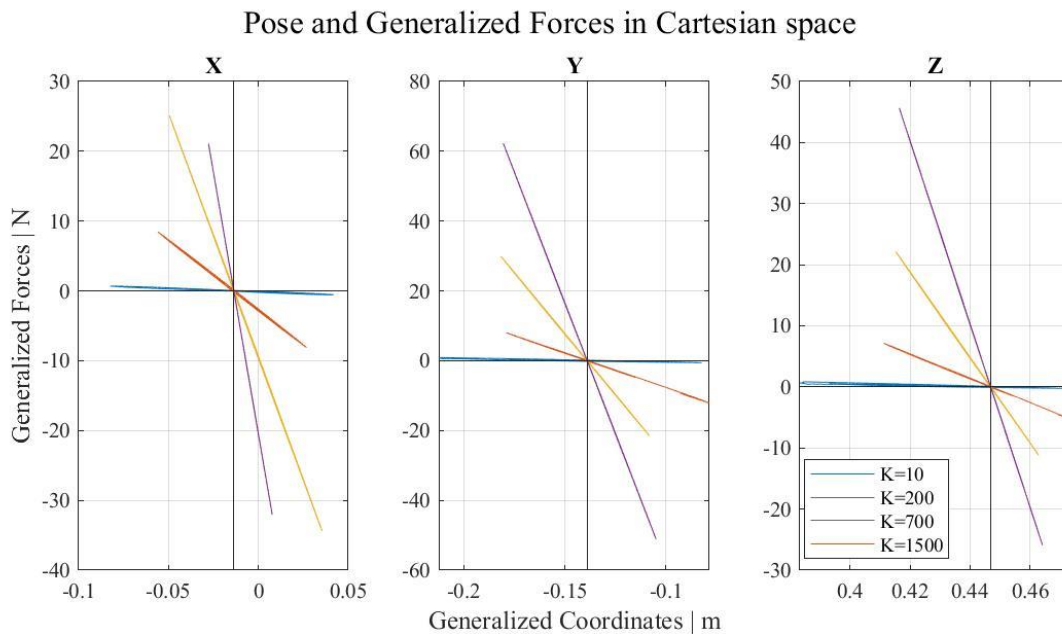


Figure 86: Coefficient of the elastic stiffness of the filter in impedance: measured value

ELASTIC IMPEDANCE FILTER K N/m								
desired K			measured K			error %		
along X	along Y	along Z	along X	along Y	along Z	along X	along Y	along Z
10,00	10,00	10,00	27,00	4,10	2,60	170,00	59,00	74,00
200,00	200,00	200,00	98,00	120,00	130,00	51,00	40,00	35,00
700,00	700,00	700,00	590,00	580,00	650,00	15,71	17,14	7,14
1500,00	1500,00	1500,00	1300,00	1400,00	1400,00	13,33	6,67	6,67

Table 50: Desired and measured elastic stiffness coefficients. Relative absolute error is reported.

Among all the purely elastic systems analysed, as shown in the legend of Figure 86, let's consider a purely elastic system in which the stiffness of the linear spring was rigid. In fact, the transfer function with which the impedance filter interacts with the virtual dynamic is:

$$\frac{Generalized\ Force^{des}}{Pose^{des}} = 1500$$

Equation 52: Transfer function of pure elastic impedance filter

Referring to the block diagram Figure 87, the analysis of the purely elastic impedance filter can be traced back to the study of the graphs shown in Figure 86.

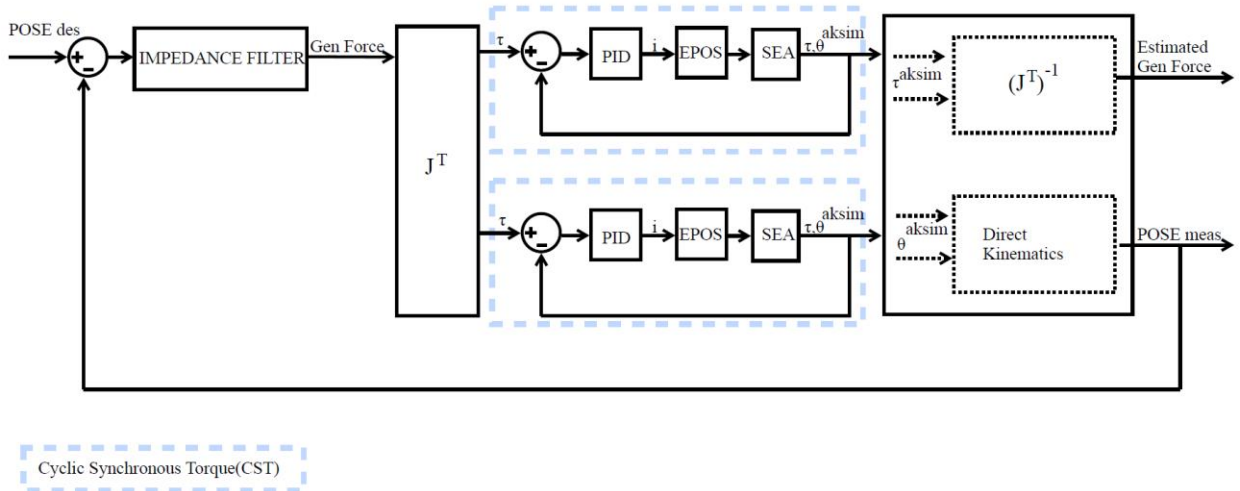


Figure 87: Impedance control scheme in task space

Let us first analyse the behaviour that occurs in each direction of the Cartesian space. Given a desired constant reference pose, when a perturbation is introduced, i.e., a deviation of the desired pose, a generalized force acting directly on the end effector is produced. In Figure 88 when there is a difference between the Pose des and the measured Pose, then a generalized force is produced, both along the X axis, both along the Y axis and along the Z axis. The force produced is a vector that has variable modulus, direction and intensity between the reference axes.

Task Space Impedance Analysis

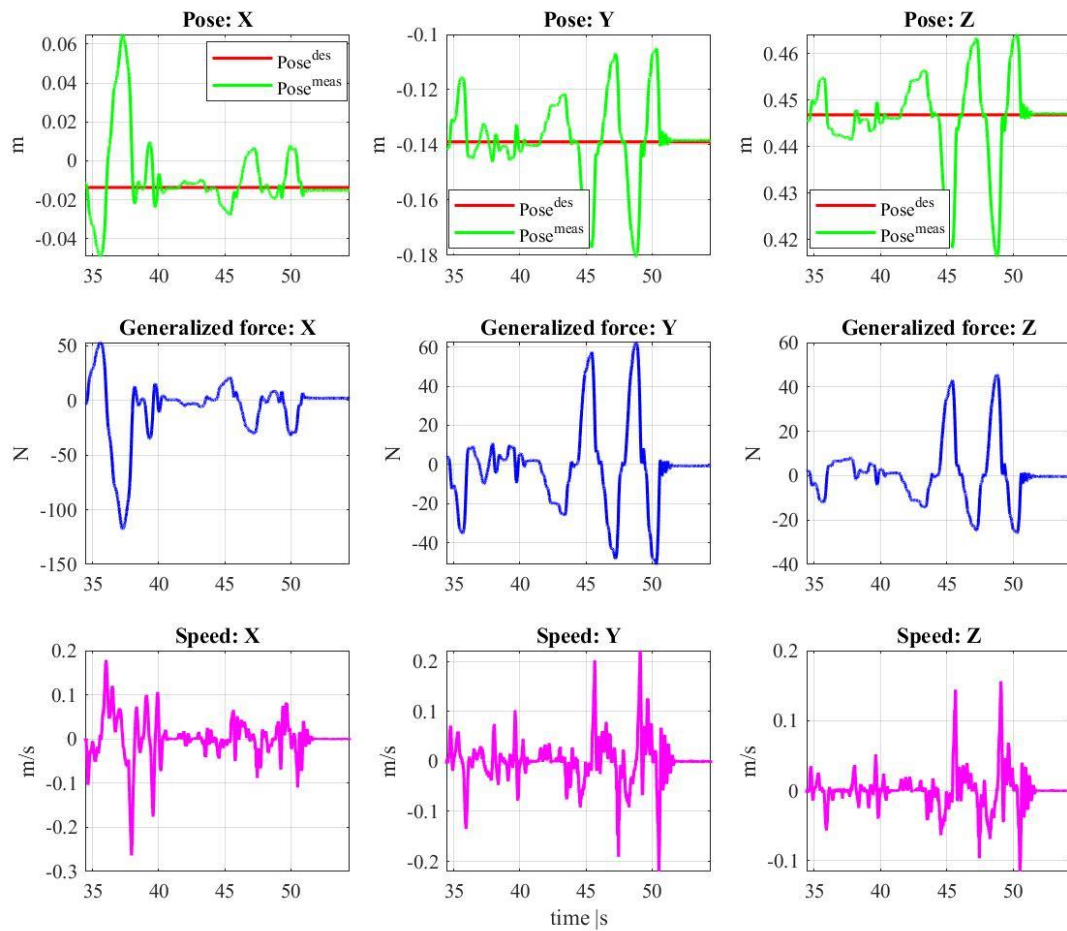


Figure 88: Input/output relationship of the impedance elastic filter. Focus on the perturbed pose and the obtained force.

On the other hand, analysing the system in its totality in the 3D Cartesian space, it is possible to note that, in a purely elastic system in which only the position is altered, the desired position is used as the equilibrium point of the system, in fact, as far as there is deviate from the reference position, the perturbation will never be too far from the defined trajectory. Furthermore, by analysing the desired forces and the estimated model-based forces, they act on the same level, except for non-idealities due to the torques generated by the force of gravity, as shown in Figure 89. In Figure 90, most significant graphs are shown in. The first plot analyses the intensity with which the recall force increases the more one deviates from the predefined trajectory: the force module is

therefore shown. In the second plot, on the other hand, the direction of the vector are shown: it can be seen that, in a purely elastic system, the direction of the forces points to the desired pose in the Cartesian space.

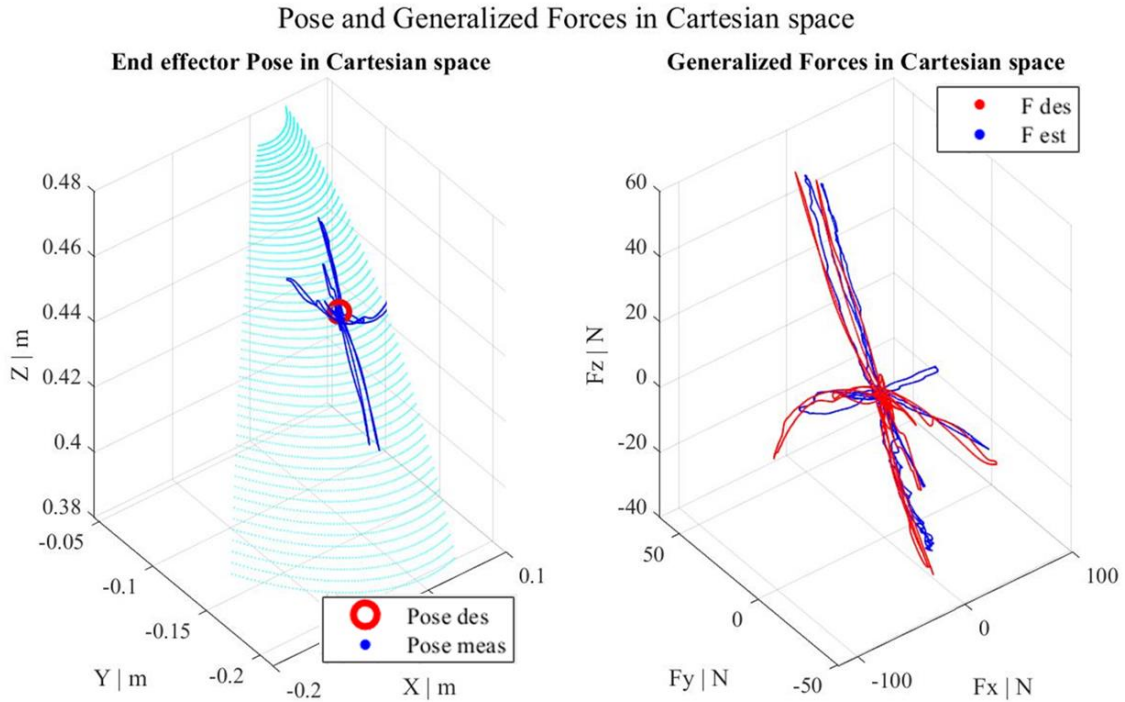


Figure 89: Pose and generalized forces in the cartesian space. Behaviour of a pure elastic impedance transfer function

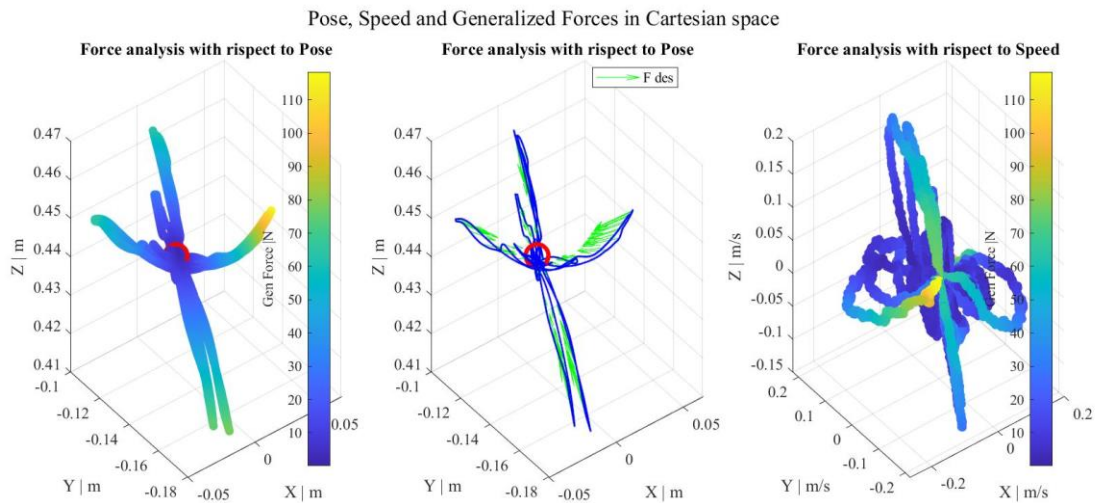


Figure 90: Force analysis with respect to pose and speed. Focus on the action of the elastic filter on position, but not on speed.

4.3.2.2. Purely viscous system

In a purely viscous system, only the speed is modulated; there is no influence on the position, so the trajectory is not tracked. As in the case of the purely elastic system, also for the purely viscous system the comparisons between the desired viscous coefficient of friction imposed and the measured one have been reported. With the same dynamics with which the analysis of the purely elastic system was made, even in a purely viscous system, the absolute error between the two quantities tends to zero as the coefficient increases. This is

justifiable by the fact that, when the system is not subjected to large coefficients that modify the dynamics of the system itself, the intrinsic impedance of the system overcomes that imposed by the filter.

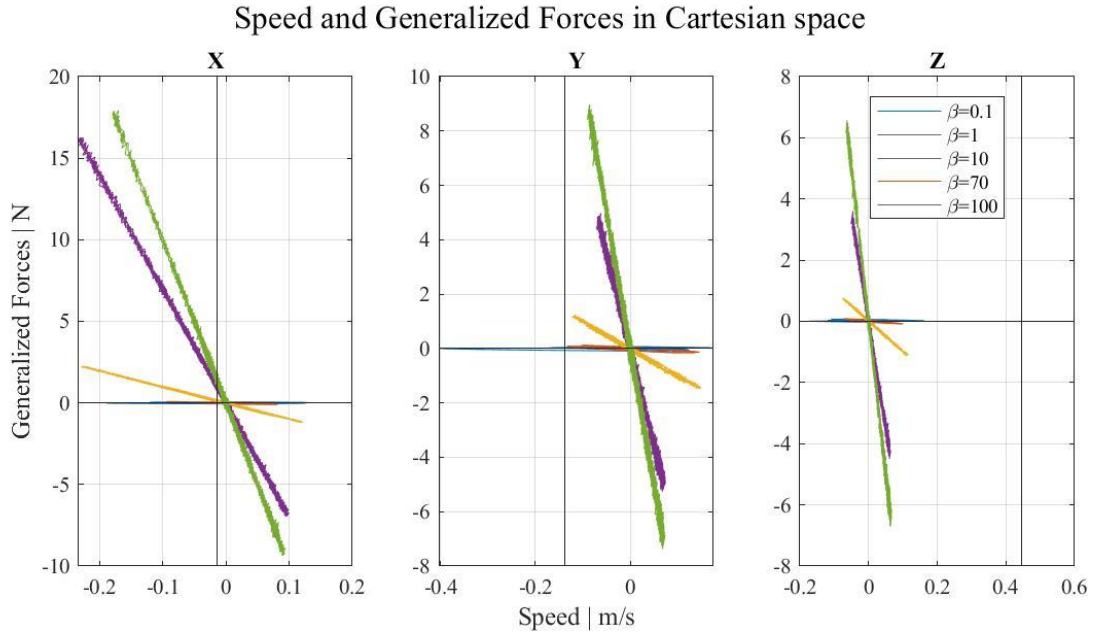


Figure 91: Viscous friction coefficients of a purely viscous system. Slope with respect to a force / speed graph.

VISCOUS IMPEDANCE FILTER β N/m/s								
desired β			measured β			error %		
10,00	10,00	10,00	74,00	19,00	24,00	640,00	90,00	140,00
70,00	70,00	70,00	130,00	92,00	170,00	85,71	31,43	142,86
100,00	100,00	100,00	150,00	110,00	120,00	50,00	10,00	20,00

Table 51: desired and measured viscous friction coefficients. Relative absolute error is reported.

Among all the purely viscous systems, as shown in the legend of Figure 91, we consider a purely viscous system in which the viscous coefficient of friction is high. In fact, the transfer function with which the impedance filter interacts with the virtual dynamics is:

$$\frac{\text{Generalized Force}^{des}}{\text{Pose}^{des}} = 70s$$

Equation 53: Transfer function of pure viscous impedance filter

First proceed with the analysis of the specific behaviour of each Cartesian axis. The input trajectory is always constant and the same used for each control method. Applied a perturbation, this causes a variation of position and speed; the latter is the cause of the force that is generated at the output of the impedance filter. Acting only on the speed of the system, but not having an equilibrium position of reference, once a perturbation is applied, the viscous coefficient acts only on the motion of the system. This can be deduced by analysing the measured pose that does not tend to a position of reference, even when there is no longer any perturbation in progress, on the contrary, once the perturbation is over, the system remains in the position in which it was brought, as shown in Figure 92.

Task Space Impedance Analysis

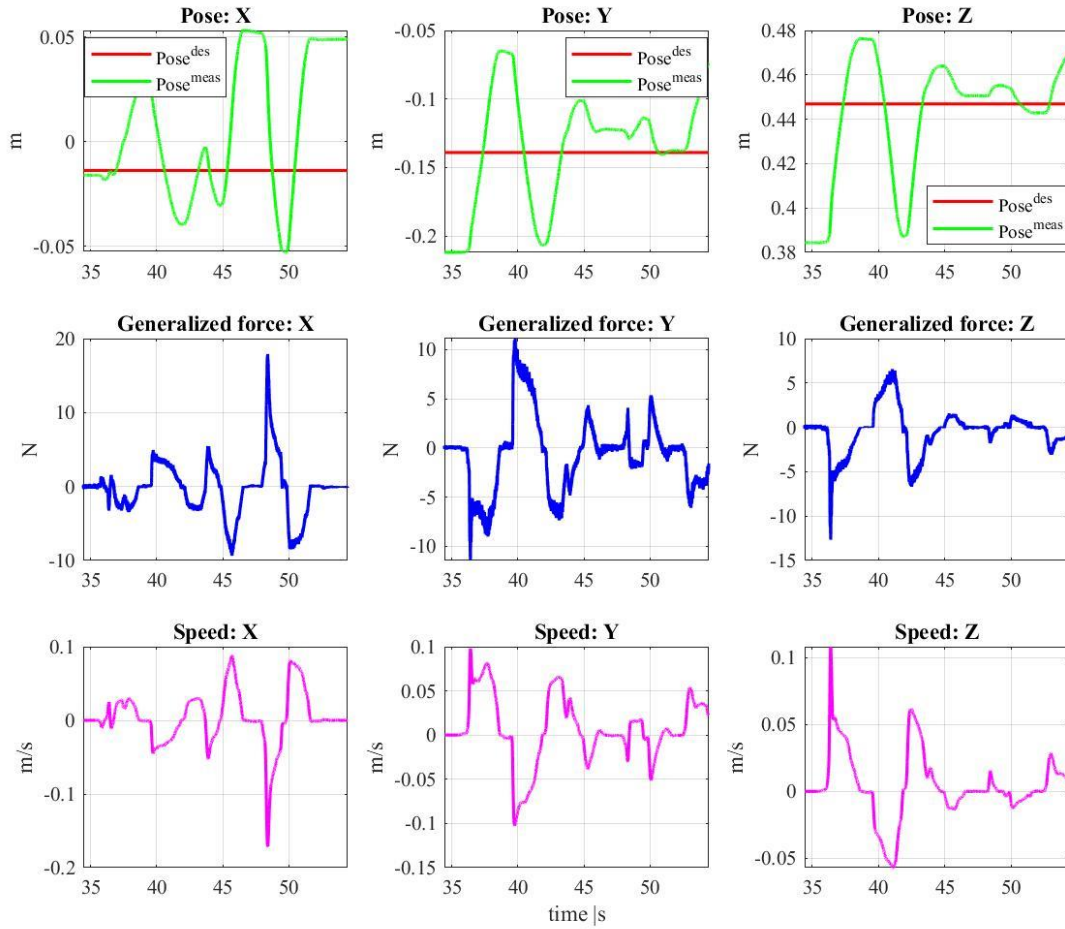


Figure 92: Input/output relationship of the impedance viscous filter. Focus on the perturbed pose, then the produced speed and the obtained force.

As far as the 3D analysis is concerned, then we refer to the fact that the perturbation occurs in a neighbourhood of the fixed reference trajectory. Furthermore, it appears that the desired and estimated forces are comparable. From the analysis of the force in module and in direction and towards Figure 94, the force is than to greater as the velocity is greater, while the direction of the force vector produced no longer points to the reference position, as the latter is not modulated by the filter. In the figures, in the points in which the trajectory of the perturbation changes direction, the speed is zero: in these specific points, in fact, the force is minimal.

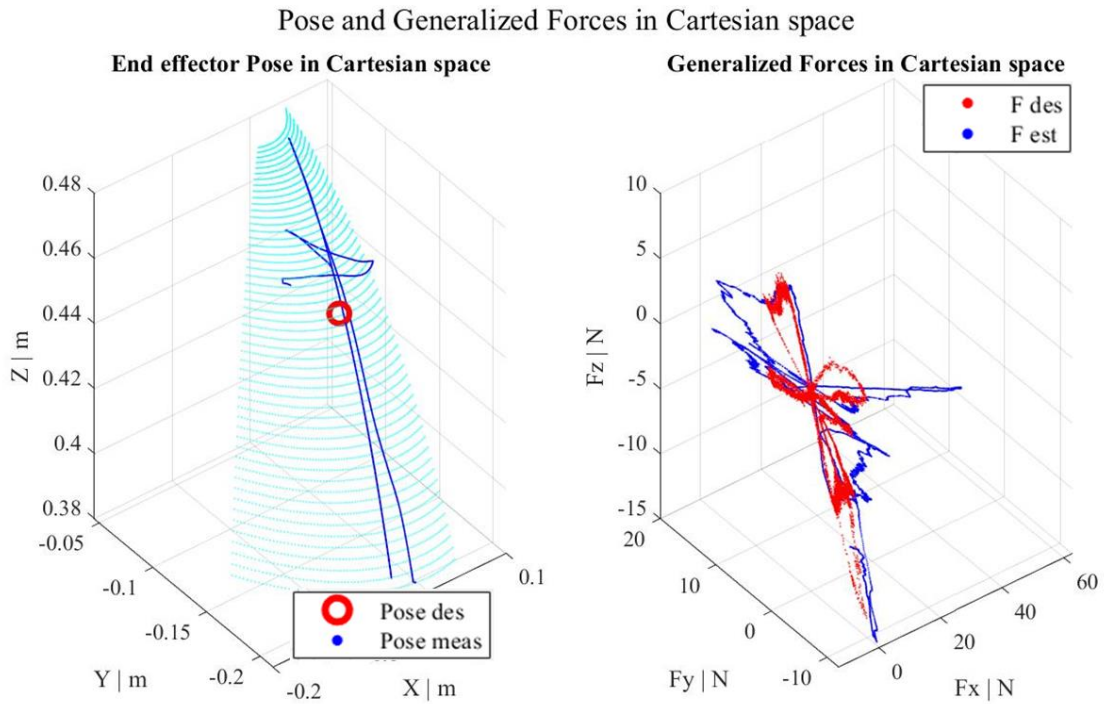


Figure 93: pose and generalized forces in the cartesian space. Behaviour of a pure viscous impedance transfer function

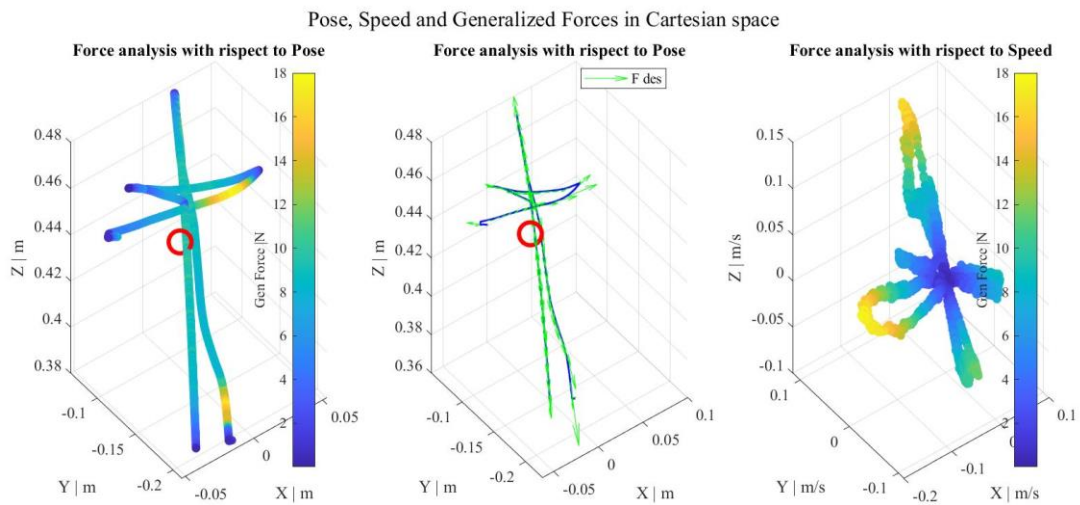


Figure 94: Force analysis with respect to pose and speed. Focus on the action of the viscous filter on speed, but not on pose

4.3.2.3. Viscoelastic system

A purely elastic system follows the reference trajectory but introduces oscillations. A purely viscous system introduces damping but does not follow a reference trajectory. It is therefore important to introduce a viscoelastic system to find the right compromise between elasticity and viscosity in the variation of the virtual dynamics of the system, to overcome the impedance of the system and thus be able to make the control compliant. In this regard, the absolute errors of many viscoelastic systems are analysed, both as a function of the linear stiffness of the spring and as a function of the viscous damping coefficient. It can be noted that, with the same viscous coefficient, the higher the coefficient of the spring, the more the behaviour of the virtual dynamics will be modified to essentially act on the reference position. in a system in which the elastic

coefficient is predominant with respect to the viscous coefficient, the trajectory defined at the input is certainly followed, but the system will be subjected to non-attenuated oscillations. On the other hand, in a system in which the viscous coefficient is much greater than the elastic one, the system will try to attenuate any oscillation, up to zero, but it will deviate from the reference system, therefore the relationship between the input torque and the output displacement will no longer be linear.

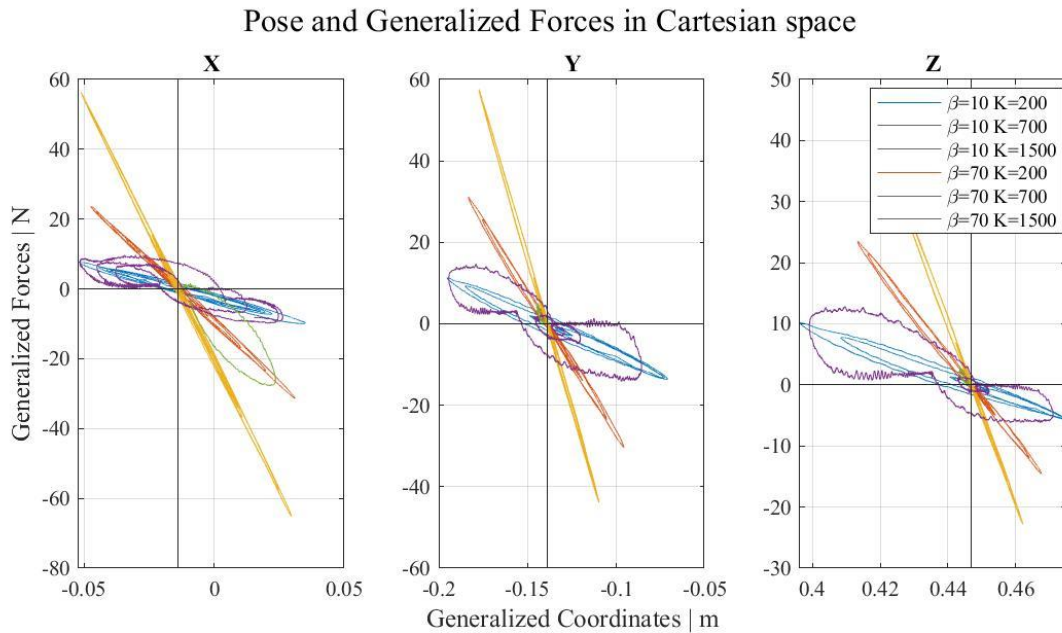


Figure 95: Linear stiffness coefficients of a viscoelastic system. Slope with respect to a force / pose graph.

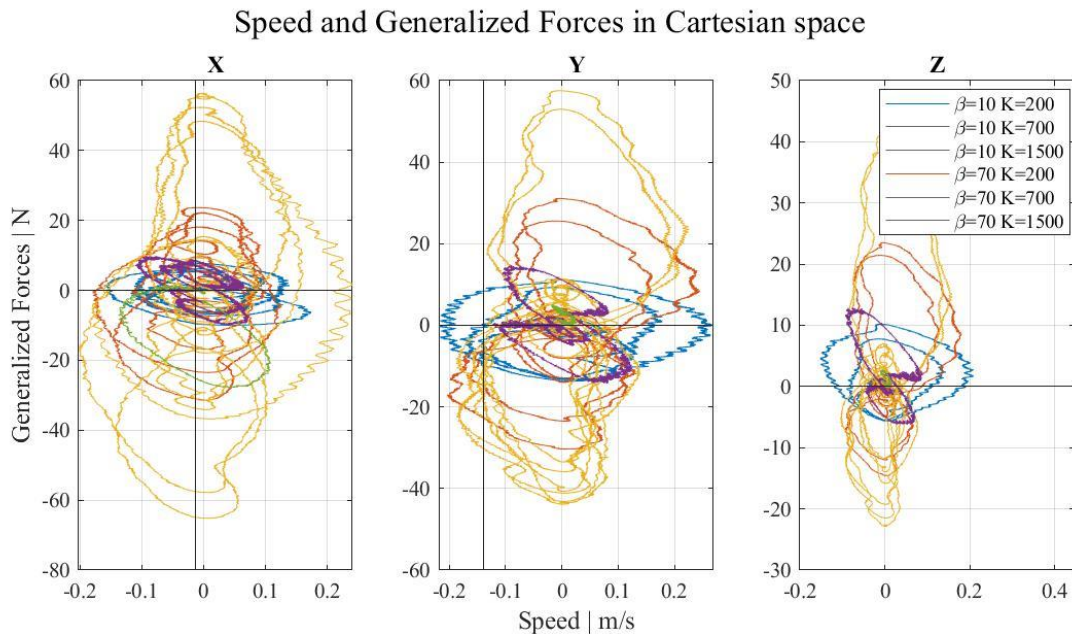


Figure 96: Viscous friction coefficients of a viscoelastic system. Slope with respect to a force / speed graph.

Among all the viscoelastic systems, as shown in the legend of Figure 96, has been considered a system in which the coefficient of static friction and that of the spring stiffness, have been previously analysed individually in the purely viscous and elastic systems. In fact, the transfer function with which the impedance filter interacts with the virtual dynamics is:

$$\frac{\text{Generalized Force}^{des}}{\text{Pose}^{des}} = 70s + 1500$$

Equation 54: Impedance transfer function for a viscoelastic filter

From the analysis of the Cartesian components, in this configuration the position is followed, while the speeds are reduced.

Task Space Impedance Analysis

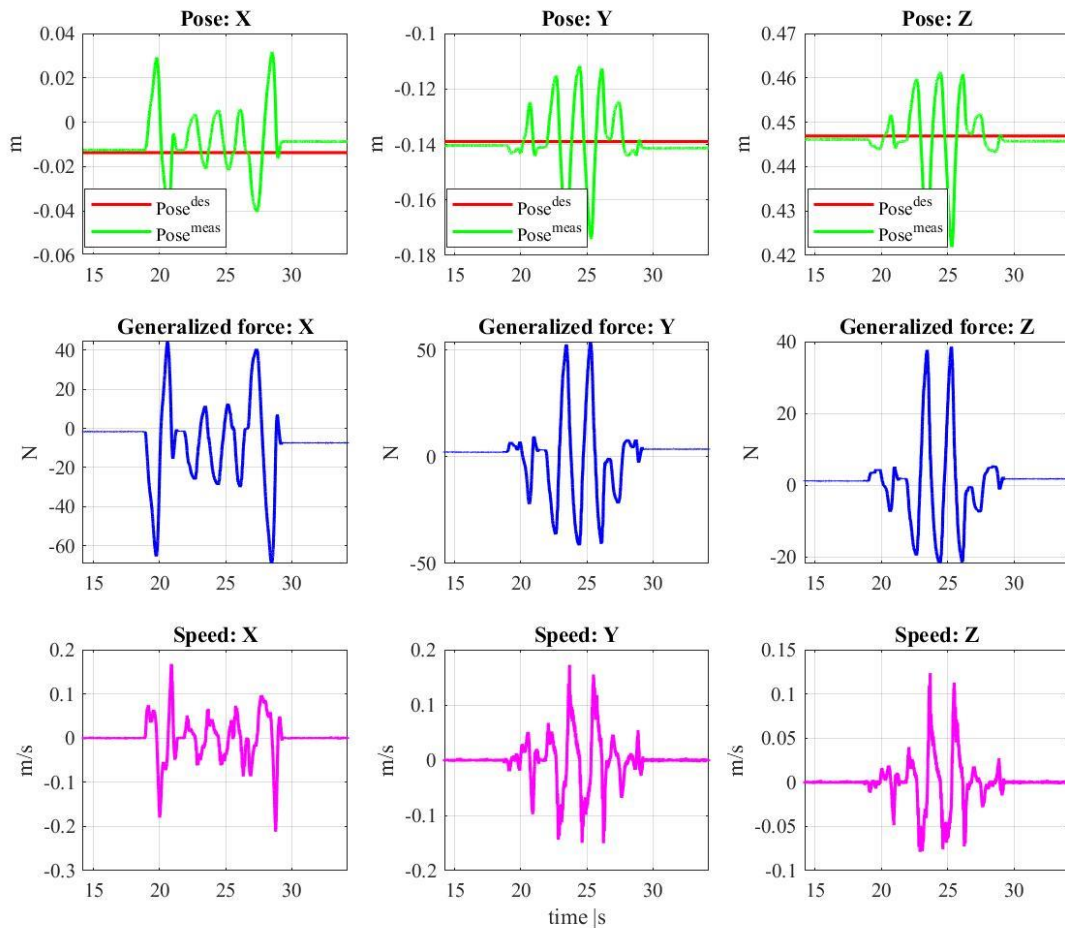


Figure 97: Input/output relationship of the impedance viscoelastic filter. Focus on the perturbed pose, then the produced speed and the obtained force.

On the other hand, analysing the behaviour on the end effector, the modulus of the force is greater as the distance from the reference position increases, but the direction is no longer strongly directed to the desired pose, but is attenuate, as shown in Figure 99.

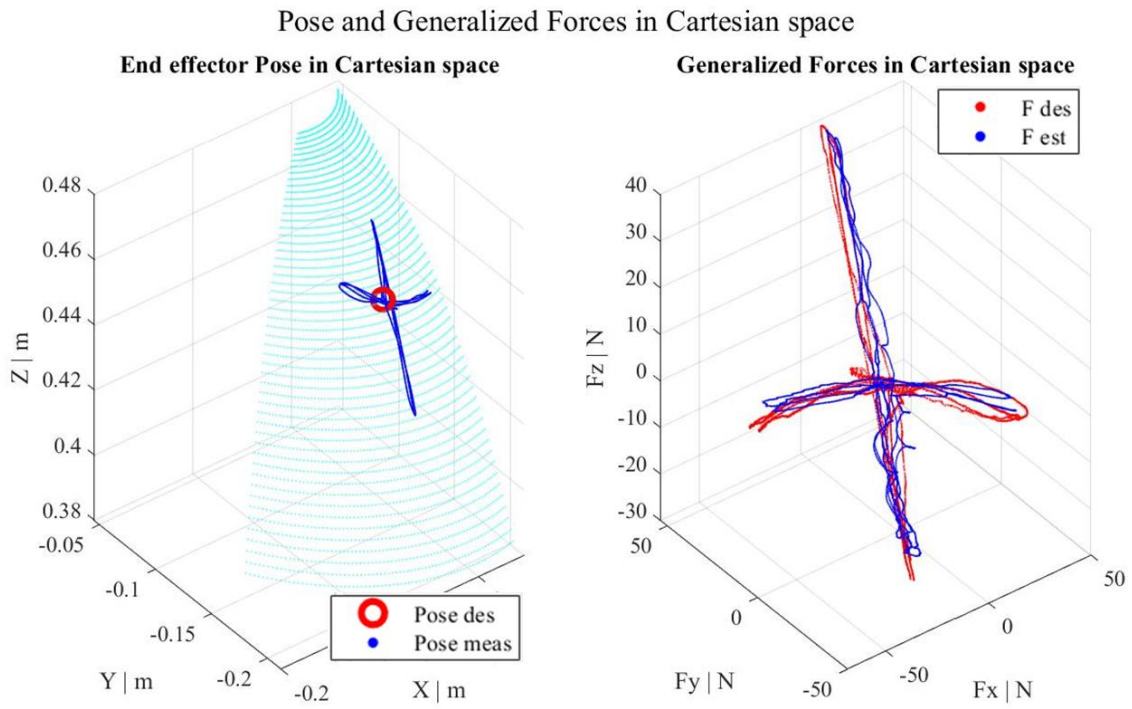


Figure 98: Pose and generalized forces in the cartesian space. Behaviour of a viscoelastic impedance transfer function

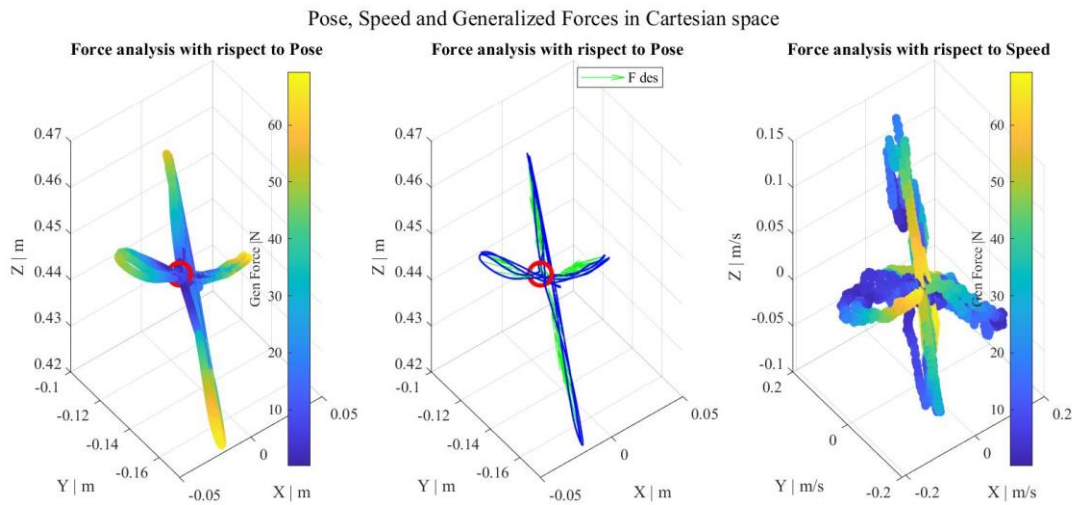


Figure 99: Force analysis with respect to pose and speed. Focus on the action of the viscoelastic filter on both pose and speed.

4.3.2.4. Transparency

In a transparent system, the system is not subjected to any resistance, neither return force (due to the elastic recall), nor attenuation (given by the viscosity), as shown in Figure 100. Whoever interacts with the system does not feel its weight and can move it freely without encountering external forces. The only feature that remains visible is the intrinsic impedance of the system. As shown in Figure 100, in a transparent system, the forces (green arrows) always and only point towards the direction of the perturbed trajectory.

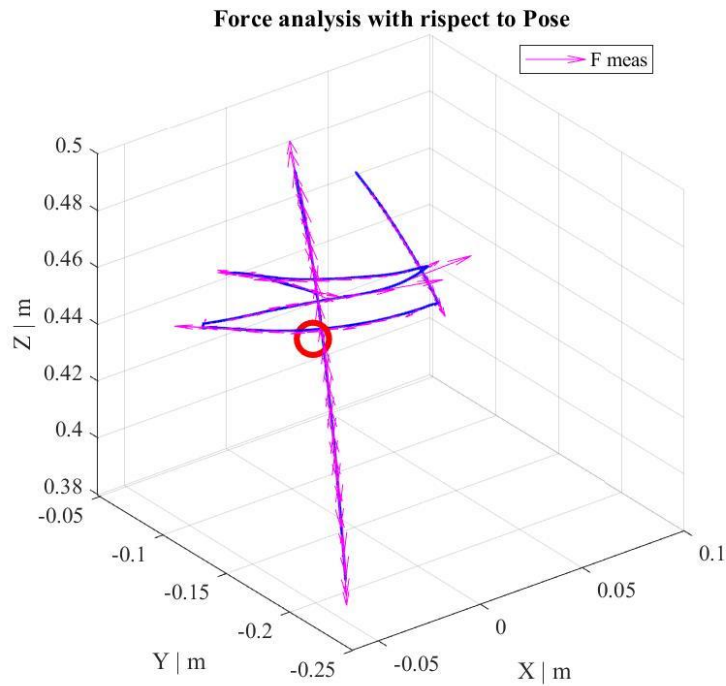


Figure 100: Force analysis in modulus and direction: transparent system

Thanks to the transparency control, it is possible to check what is the intrinsic impedance of the system. Having a couple control at the joints with zero input torque, the system suffers only from the intrinsic characteristics. By analysing the relationship between the model-based estimated forces and the position, velocity and acceleration caused by the system, an analysis on residual elasticity, viscosity and inertia was carried out, as reported in Figure 101. From this analysis no evident inertial or elastic contributions have been detected, but

viscous contributes, caused precisely by the mechanical friction inside the system, are decisive. Thanks to linear interpolation, the value of the viscous residual impedance was found, as shown in Table 52.

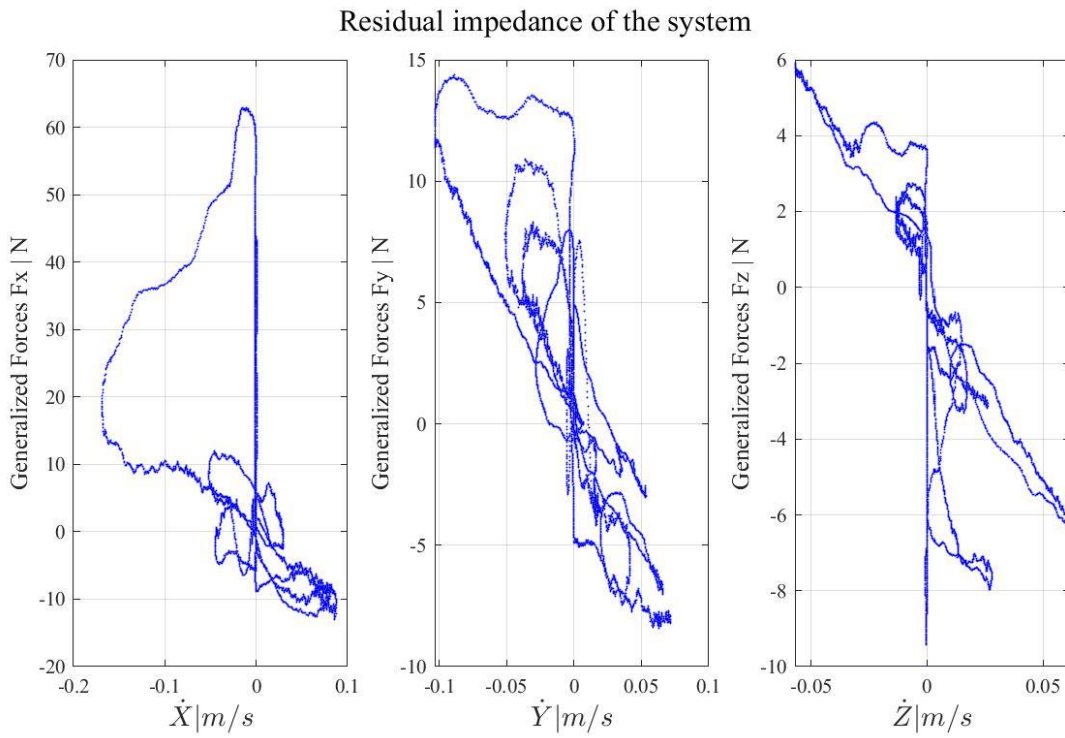


Figure 101: Residual impedance of the system

Residual Impedance		
β_x	β_y	β_z
150 N/(m/s)	110 N/(m/s)	130 N/(m/s)

Table 52: Residual impedance of the system: viscous component

4.3.2.5. Viscous, Elastic, Viscoelastic and Transparent impedance system

A comparison is now made between the three implemented systems: viscous, elastic, and viscoelastic. An additional comparison is made between those system and the transparent one. An example is shown in Figure 102, Figure 103 and Figure 104 where the trend difference of a viscous, elastic, viscoelastic and transparent control of an impedance control in the task space is shown. In general, from an analysis of the forces generated due to a perturbation of the pose, it can be seen how the return force of the impedance filter in the Cartesian space depends on the type of system being analysed, in particular it is possible to note how in an elastic system ($K = 1500 \text{ N / m}$) the force is completely directed towards the desired pose, in a viscous system ($\beta = 70 \text{ N / m / s}$) instead the force is directed along the perturbed trajectory, and how, to the combination of the two systems report a modulation both in the position and in the velocity creating a viscoelastic system that has the recall force to the equilibrium position, but still damped thanks to the viscous coefficient.

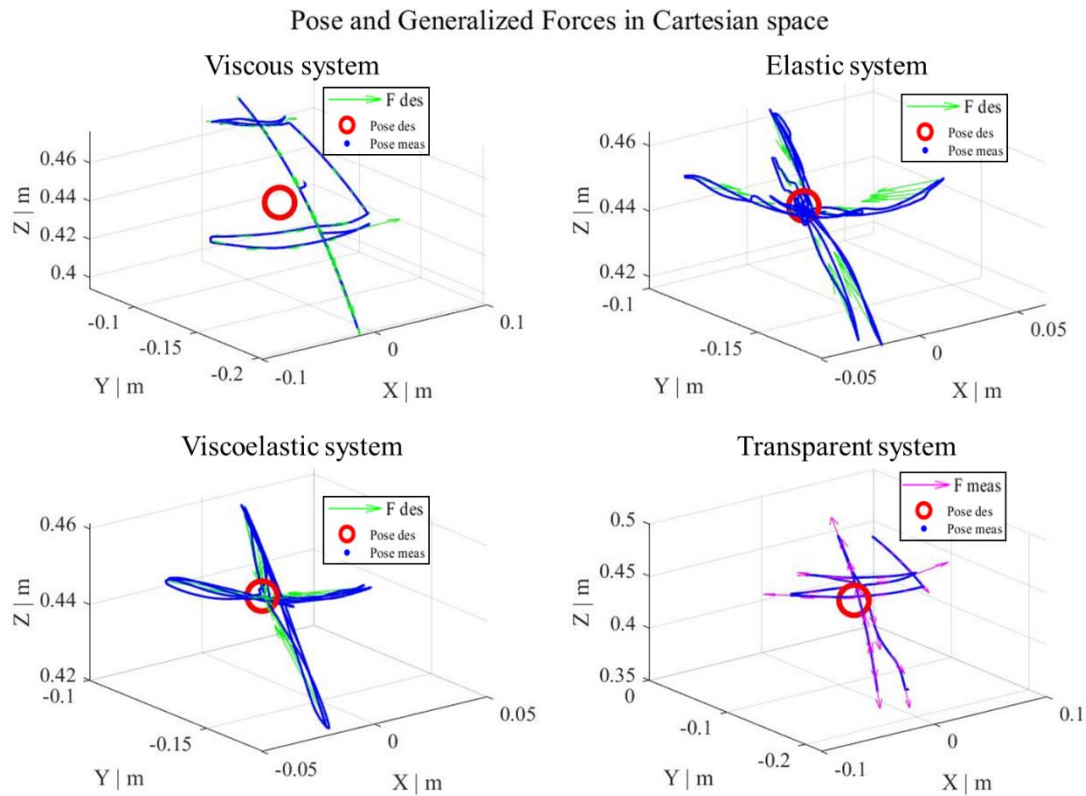


Figure 102: Comparison between viscous, elastic, and viscoelastic impedance control in task space

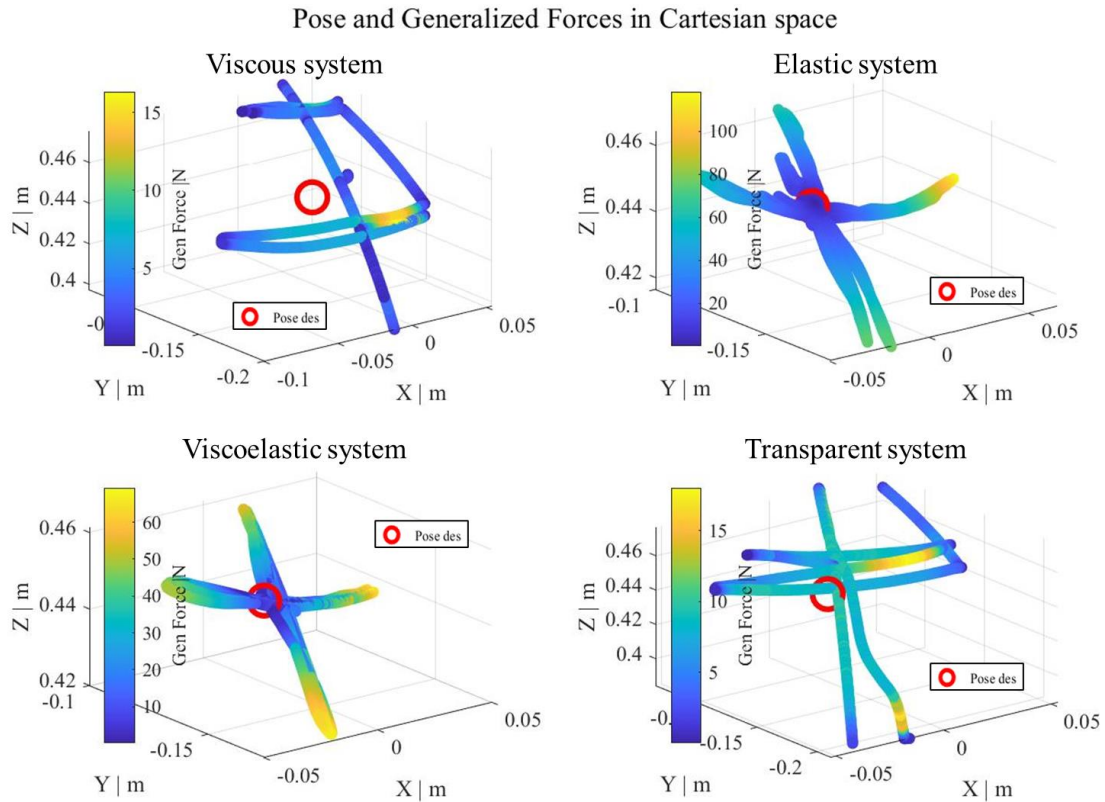


Figure 103: Comparison between viscous, elastic, viscoelastic and transparent system. Reference to relationship between pose and generalized force

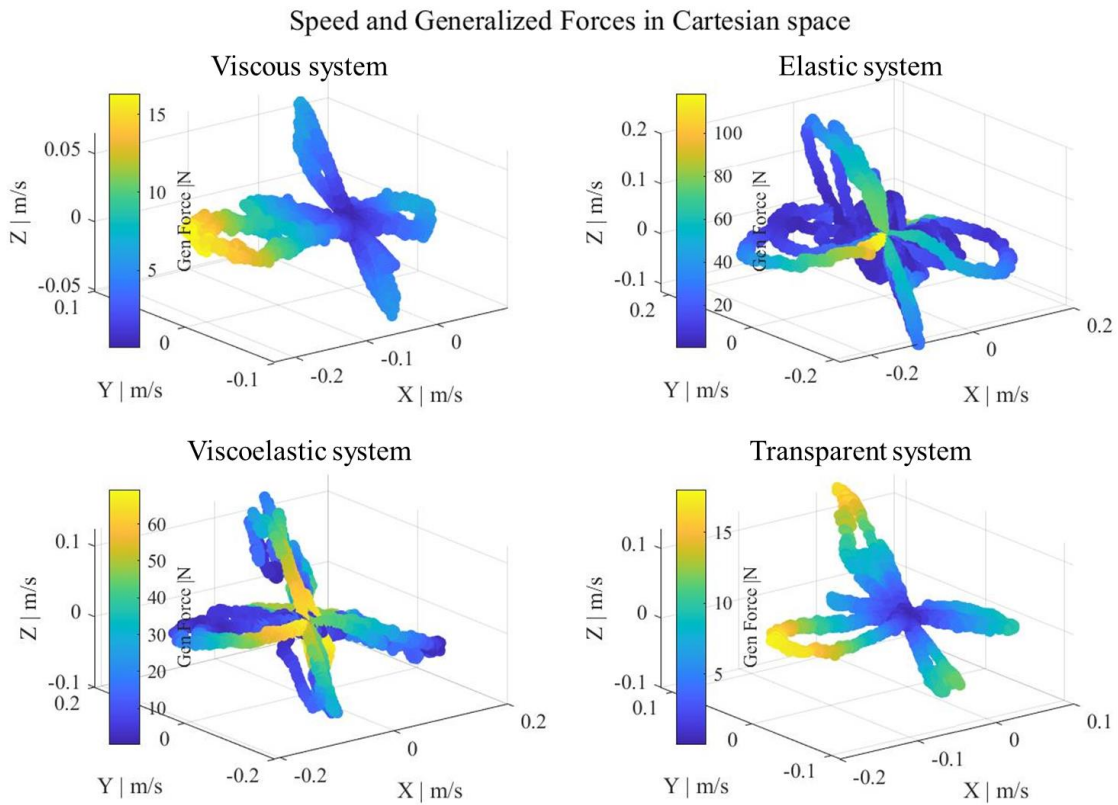


Figure 104: Comparison between viscous, elastic, viscoelastic and transparent system. Reference to relationship between speed and generalized force

Chapter 5: Conclusion

The main purpose of this thesis was to design and implement compliant control strategies for robotic rehabilitation. Specifically, the author investigated the implementation of such control strategies on a two degrees of freedom system, powered by Series Elastic Actuators, that will be used for the scapular motion of the Float EVO upper-limb exoskeleton.

To understand the functioning of the SEAs, frequency analysis has been performed: this analysis led to the conclusion that the SEAs are indeed reliable torque sensors. Having therefore evaluated, characterized, and studied the behaviour of the SEAs, it was possible to proceed with the implementation of different control strategies.

A first analysis was carried out on the single joint: a position control on slow shaft was performed. The position control has been implemented in a preparatory way: the compliant control strategies are based on a position control. Furthermore, the PID parameters have been tuned to understand the relationship between the parameters of the controller. It was concluded that it was necessary to use both a proportional, integrative, and derivative coefficient. The proportional coefficient was useful to modulate the signal amplitude, the derivative allowed to reach the steady state more quickly, while the integrative was necessary to minimize the tracking error. It was necessary to find the right trade off, considering that in biomedical robotic applications, it is not possible to have overshoot and steady state oscillations are not desired. After having performed the control in single joint position and having tested that the parameters of the proportional, derivative, and integrative coefficients found were the optimal ones, then the author proceeded with the analysis of the two degrees of freedom control.

The considered two-degrees-of-freedom system represents the scapular joint of Float EVO upper limb exoskeleton. A pure position control does not allow interaction with the device. A single position control is not sufficient to guarantee an appropriate and safe dynamic interaction between man and robot. The real-time adaptability between the robotic exoskeleton and the contact forces is needed to improve the interaction between two bodies. The need to implement compliant control strategies lies in making the human-robot interaction more user friendly and safer.

The rehabilitation process does not focus on a single control strategy, but rather on a combination of them. In this regard, the design of compliant control strategies allows to combine pure position or torque controls, applying a filter that modifies the virtual dynamics of the system. This filter can be based on the variation of a force, i.e. an admittance filter is applied, or on the variation of position, i.e. an impedance filter is imposed. Thanks to the alteration of the virtual dynamic, it is possible to obtain the behaviour of an exoskeleton from very rigid to very compliant.

The compliant control strategies were directly implemented on the scapular joint of Float EVO. The aim was to analyse the different behaviour of two apparently dual strategies: admittance control and impedance control. A further differentiation was carried out according to the type of implementation chosen: the admittance control was, in fact, developed at the level of the single joints. This implies that each joint is controlled

individually and that the combination of each sub-controls finally determines a specific behaviour in the Cartesian space. On the other hand, the impedance control was designed and implemented directly by manoeuvring the end effector, therefore a single control allows to modify the virtual dynamics of the system by acting directly on the end-effector in the Cartesian space.

In both control methods, a viscoelastic system was developed. From the analyses and experiments conducted, the author concluded that, both for an admittance control and for an impedance control, the viscoelastic system is preferable to a pure elastic or viscous control. To have optimal performance in a compliant control method, it is necessary to refer to both elastic and viscous characteristics of the viscoelastic system. In fact, thanks to the virtual behaviour imposed by the spring, the system, even if perturbed, always tends to a reference position. The speed with which the oscillations of the spring tend towards the reference are then attenuated by the viscosity imposed by the damper. If it were a purely elastic system, the system would tend to produce unwanted oscillations which would cause the exoskeleton to vibrate and therefore to injure the patient. On the other hand, a purely viscous behaviour does not follow a reference trajectory and could, therefore, lead the patient's arm to points in the space where the upper limb is subjected to excessive forces. Remember that the target patient is a post-stroke patient, it is possible that he is not aware of making potentially dangerous movements.

As future developments, a consideration arises from the fact that, in impedance control implemented in this thesis, it was not possible to make a direct comparison between the desired and measured forces, as no F/T sensor was mounted on the system. Thanks to F/T sensors, like ATI sensor, it is possible to implement a control using the tracking error of the closed control loop between the desired force and the measured one. In this thesis, only estimated model-based forces have been considered, these do not consider external forces such as torques generated by the force of gravity or energy losses caused by mechanical frictions.

The impedance in the task space was implemented on top of a torque control in the joint space. By making the system impedance zero, a pure zero torque control in the joint space was implemented. This last control strategy made it possible to analyse the transparency of the system: it was noted that the system has a high residual viscous impedance, while the elastic and inertial impedance are not relevant. In transparency mode, weight given by the exoskeleton (in this case, by the scapular joint) is bypassed.

Analysing admittance control, it was noticed that, thanks to the fact that the control was performed on a control position, it is not required gravity compensation, referring directly to the position to be tracked. The admittance control foresees that, once a trajectory is defined, it is followed, even if perturbed. On the other hand, in an impedance control, given a force / torque, this is exerted, at any point in the space independently from position. As future developments, to make these implementations more accurate and precise, it can be needed to introduce feedforward compensations, such as friction compensation (through the offline analysis of Lagrange equations on kinetic co-energy) and gravity (analysis of the Lagrange equations on potential energy). A further future development may be the use of external sensors that detect forces /torques acting (such as the use of an ATI F / T sensor) or the use of IMU inertial sensors for the detection of accelerations, to be able to implement

a filter, both in impedance and in admittance, which also considers the inertial component of the applied virtual system, without incurring the double derivation of the position that can be noisy.

To conclude, with this thesis the author wants to show how to develop and implement compliant control strategies on a scapular joint power by Series Elastic Actuators to find which is the optimal control and which makes the interaction between patient, exoskeleton and environment as safe and user friendly as possible.

Bibliography

- [1] H. S. Lo and S. Q. Xie, "Exoskeleton robots for upper-limb rehabilitation: State of the art and future prospects," *Medical engineering & physics*, vol. 34, no. 3, pp. 261-268, 2012.
- [2] T. Proietti, V. Crocher, A. Roby-Brami, and N. Jarrassé, "Upper-limb robotic exoskeletons for neurorehabilitation: a review on control strategies," *IEEE reviews in biomedical engineering*, vol. 9, pp. 4-14, 2016.
- [3] W.-W. H. Organization. "Rehabilitation." <https://www.who.int/news-room/fact-sheets/detail/rehabilitation> (accessed.
- [4] M. d. Salute, "Ictus." [Online]. Available: [Ictus \(salute.gov.it\)](http://ictus.salute.gov.it).
- [5] N. uk, "Stroke." [Online]. Available: <https://www.nhs.uk/conditions/stroke/>
- [6] N. E. Mayo *et al.*, "Disablement following stroke," *Disability and rehabilitation*, vol. 21, no. 5-6, pp. 258-268, 1999.
- [7] NINDS, "Post-stroke rehabilitation." [Online]. Available: <https://www.ninds.nih.gov/Disorders/Patient-Caregiver-Education/Fact-Sheets/Post-Stroke-Rehabilitation-Fact-Sheet>.
- [8] N. I. o. Health, "Post Stroke rehabilitation." [Online]. Available: <https://www.stroke.nih.gov/materials/rehabilitation.htm>.
- [9] R. W. Teasell and L. Kalra, "What's new in stroke rehabilitation: back to basics," *Stroke*, vol. 36, no. 2, pp. 215-217, 2005.
- [10] H. Feys *et al.*, "Early and repetitive stimulation of the arm can substantially improve the long-term outcome after stroke: a 5-year follow-up study of a randomized trial," *Stroke*, vol. 35, no. 4, pp. 924-929, 2004.
- [11] R. Bertani, C. Melegari, C. Maria, A. Bramanti, P. Bramanti, and R. S. Calabrò, "Effects of robot-assisted upper limb rehabilitation in stroke patients: a systematic review with meta-analysis," *Neurological Sciences*, vol. 38, no. 9, pp. 1561-1569, 2017.
- [12] U. gov, "Post-Stroke-Rehabilitation-Fact-Sheet". [Online]. Available: <https://www.ninds.nih.gov/Disorders/Patient-Caregiver-Education/Fact-Sheets/Post-Stroke-Rehabilitation-Fact-Sheet>
- [13] M. News, "Treatment of stroke's survivor." [Online]. Available: <https://www.medicalnewstoday.com/articles/7624#treatment>
- [14] D. Aoyagi, W. E. Ichinose, S. J. Harkema, D. J. Reinkensmeyer, and J. E. Bobrow, "A robot and control algorithm that can synchronously assist in naturalistic motion during body-weight-supported gait training following neurologic injury," *IEEE Transactions on neural systems and rehabilitation engineering*, vol. 15, no. 3, pp. 387-400, 2007.
- [15] P. Maciejasz, J. Eschweiler, K. Gerlach-Hahn, A. Jansen-Troy, and S. Leonhardt, "A survey on robotic devices for upper limb rehabilitation," *Journal of neuroengineering and rehabilitation*, vol. 11, no. 1, pp. 1-29, 2014.
- [16] R. J. Varghese, D. Freer, F. Deligianni, J. Liu, G.-Z. Yang, and R. Tong, "Wearable robotics for upper-limb rehabilitation and assistance: A review of the state-of-the-art challenges and future research," in *Wearable technology in medicine and health care*: Elsevier, 2018, p. 340.
- [17] J. Patton, S. L. Small, and W. Zev Rymer, "Functional restoration for the stroke survivor: informing the efforts of engineers," *Topics in stroke rehabilitation*, vol. 15, no. 6, pp. 521-541, 2008.
- [18] M. A. Gull, S. Bai, and T. Bak, "A review on design of upper limb exoskeletons," *Robotics*, vol. 9, no. 1, p. 16, 2020.
- [19] R. Gopura, K. Kiguchi, and D. Bandara, "A brief review on upper extremity robotic exoskeleton systems," in *2011 6th international Conference on Industrial and Information Systems*, 2011: IEEE, pp. 346-351.

- [20] R. Gopura, D. Bandara, K. Kiguchi, and G. K. Mann, "Developments in hardware systems of active upper-limb exoskeleton robots: A review," *Robotics and Autonomous Systems*, vol. 75, pp. 203-220, 2016.
- [21] M. Dictionary. <https://medical-dictionary.thefreedictionary.com/orthosis> (accessed).
- [22] C. Carignan, J. Tang, S. Roderick, and M. Naylor, "A configuration-space approach to controlling a rehabilitation arm exoskeleton," in *2007 IEEE 10th International Conference on Rehabilitation Robotics*, 2007: IEEE, pp. 179-187.
- [23] J. Gunasekara, R. Gopura, T. Jayawardane, and S. Lalitharathne, "Control methodologies for upper limb exoskeleton robots," in *2012 IEEE/SICE International Symposium on System Integration (SII)*, 2012: IEEE, pp. 19-24.
- [24] R. Gopura and K. Kiguchi, "Mechanical designs of active upper-limb exoskeleton robots: State-of-the-art and design difficulties," in *2009 IEEE International Conference on Rehabilitation Robotics*, 2009: IEEE, pp. 178-187.
- [25] Y. Shen, P. W. Ferguson, and J. Rosen, "Upper limb exoskeleton systems—overview," in *Wearable Robotics*: Elsevier, 2020, pp. 1-22.
- [26] J. Lobo-Prat, P. N. Kooren, A. H. Stienen, J. L. Herder, B. F. Koopman, and P. H. Veltink, "Non-invasive control interfaces for intention detection in active movement-assistive devices," *Journal of neuroengineering and rehabilitation*, vol. 11, no. 1, pp. 1-22, 2014.
- [27] J. C. Perry, J. M. Powell, and J. Rosen, "Isotropy of an upper limb exoskeleton and the kinematics and dynamics of the human arm," *Applied Bionics and Biomechanics*, vol. 6, no. 2, pp. 175-191, 2009.
- [28] C. Lee, S. Kwak, J. Kwak, and S. Oh, "Generalization of series elastic actuator configurations and dynamic behavior comparison," in *Actuators*, 2017, vol. 6, no. 3: Multidisciplinary Digital Publishing Institute, p. 26.
- [29] H. Vallery, J. Veneman, E. Van Asseldonk, R. Ekkelenkamp, M. Buss, and H. Van Der Kooij, "Compliant actuation of rehabilitation robots," *IEEE Robotics & Automation Magazine*, vol. 15, no. 3, pp. 60-69, 2008.
- [30] M. R. Islam, C. Spiewak, M. H. Rahman, and R. Fareh, "A brief review on robotic exoskeletons for upper extremity rehabilitation to find the gap between research prototype and commercial type," *Adv Robot Autom*, vol. 6, no. 3, p. 2, 2017.
- [31] J. Klein *et al.*, "Biomimetic orthosis for the neurorehabilitation of the elbow and shoulder (BONES)," in *2008 2nd IEEE RAS & EMBS international conference on biomedical robotics and biomechanics*, 2008: IEEE, pp. 535-541.
- [32] M. Guidali, A. Duschau-Wicke, S. Broggi, V. Klamroth-Marganska, T. Nef, and R. Riener, "A robotic system to train activities of daily living in a virtual environment," *Medical & biological engineering & computing*, vol. 49, no. 10, pp. 1213-1223, 2011.
- [33] S. Bai, X. Li, and J. Angeles, "A review of spherical motion generation using either spherical parallel manipulators or spherical motors," *Mechanism and Machine Theory*, vol. 140, pp. 377-388, 2019.
- [34] H.-C. Hsieh, D.-F. Chen, L. Chien, and C.-C. Lan, "Design of a parallel actuated exoskeleton for adaptive and safe robotic shoulder rehabilitation," *IEEE/ASME Transactions on Mechatronics*, vol. 22, no. 5, pp. 2034-2045, 2017.
- [35] E. Ruffaldi, M. Barsotti, D. Leonardis, G. Bassani, A. Frisoli, and M. Bergamasco, "Evaluating virtual embodiment with the alex exoskeleton," in *International Conference on Human Haptic Sensing and Touch Enabled Computer Applications*, 2014: Springer, pp. 133-140.
- [36] F. Stroppa, C. Loconsole, S. Marcheschi, and A. Frisoli, "A robot-assisted neuro-rehabilitation system for post-stroke patients' motor skill evaluation with ALEx exoskeleton," in *Converging Clinical and Engineering Research on Neurorehabilitation II*: Springer, 2017, pp. 501-505.
- [37] K. W. Robotics, "ALEx." [Online]. Available: <http://www.wearable-robotics.com/kinetek/products/alex/>.
- [38] Hocoma, "ArmeoPower." [Online]. Available: <https://www.hocoma.com/solutions/armeo-power/>.
- [39] R. S. Calabrò *et al.*, "Who may benefit from armeo power treatment? A neurophysiological approach to predict neurorehabilitation outcomes," *PM&R*, vol. 8, no. 10, pp. 971-978, 2016.

- [40] B. Kim and A. D. Deshpande, "An upper-body rehabilitation exoskeleton Harmony with an anatomical shoulder mechanism: Design, modeling, control, and performance evaluation," *The International Journal of Robotics Research*, vol. 36, no. 4, pp. 414-435, 2017.
- [41] A. C. de Oliveira *et al.*, "Exploring the capabilities of harmony for upper-limb stroke therapy," in *2019 IEEE 16th International Conference on Rehabilitation Robotics (ICORR)*, 2019: IEEE, pp. 637-643.
- [42] H. Bionics, "Harmony SHR." [Online]. Available: <https://www.harmonicbionics.com/harmony-shr/overview>.
- [43] A. L. Junior, R. M. de Andrade, and A. Bento Filho, "Series elastic actuator: Design analysis and comparison," *Recent Advances in Robotic Systems*, p. 203, 2016.
- [44] G. Carpino, D. Accoto, F. Sergi, N. Luigi Tagliamonte, and E. Guglielmelli, "A novel compact torsional spring for series elastic actuators for assistive wearable robots," *Journal of Mechanical Design*, vol. 134, no. 12, p. 121002, 2012.
- [45] S. Lee, T. Lemley, and G. Keohane, "A comparison study of the commutation methods for the three-phase permanent magnet brushless dc motor," in *Electrical Manufacturing Technical Conference 2009: Electrical Manufacturing and Coil Winding Expo, EMCWA 2009*, 2009, pp. 49-55.
- [46] D. W. Robinson, "Design and analysis of series elasticity in closed-loop actuator force control," Massachusetts Institute of Technology, 2000.
- [47] H. t. mechatronics, "Brushless DC motor." [Online]. Available: <https://howtomechatronics.com/how-it-works/how-brushless-motor-and-esc-work/>.
- [48] R. Krishnan, *Electric motor drives: modeling, analysis, and control*. Pearson, 2001.
- [49] Petrella, "Azionamenti Elettrici del motore." [Online]. Available: [http://www.diegm.uniud.it/petrella/Azionamenti%20Elettrici%20\(PN\)/Complementary%20stuff%20chapter%202.pdf](http://www.diegm.uniud.it/petrella/Azionamenti%20Elettrici%20(PN)/Complementary%20stuff%20chapter%202.pdf).
- [50] E. Kaliappan, "Modelling, analysis and simulation of permanent magnet brushless DC motors for sensorless operation," *International Journal of Power and Energy Conversion*, vol. 6, no. 3, pp. 234-251, 2015.
- [51] P. Yedamale, "Brushless DC (BLDC) motor fundamentals," *Microchip Technology Inc*, vol. 20, no. 1, pp. 3-15, 2003.
- [52] R. Petrella, "Il motore sincro a magneti permanenti: Struttura e principio di funzionamento." [Online]. Available: [http://www.diegm.uniud.it/petrella/Azionamenti%20Elettrici%20\(PN\)/Complementary%20stuff%20chapter%205%20\(d\)%20-%20Azionamenti%20con%20MSMP.pdf](http://www.diegm.uniud.it/petrella/Azionamenti%20Elettrici%20(PN)/Complementary%20stuff%20chapter%205%20(d)%20-%20Azionamenti%20con%20MSMP.pdf).
- [53] ResearchGate, "Exploded view of the different parts of a harmonic drive ". [Online]. Available: https://www.researchgate.net/figure/Exploded-view-of-the-different-parts-of-a-harmonic-drive-top-and-a-detailed_fig12_334030874.
- [54] P. L. García, S. Crispel, E. Saerens, T. Verstraten, and D. Lefeber, "Compact gearboxes for modern robotics: A review," *Frontiers in Robotics and AI*, vol. 7, p. 103, 2020.
- [55] B. Siciliano, L. Sciavicco, L. Villani, and G. Oriolo, *Robotics: modelling, planning and control*. Springer Science & Business Media, 2010.
- [56] B. Bona, *Dynamic modelling of mechatronic systems*. Celid, 2013.
- [57] S. Scherzinger, A. Roennau, and R. Dillmann, "Virtual Forward Dynamics Models for Cartesian Robot Control," *arXiv preprint arXiv:2009.11888*, 2020.
- [58] C. C. de Wit, B. Siciliano, and G. Bastin, *Theory of robot control*. Springer Science & Business Media, 2012.
- [59] e. funda, "Comparison of P, PI, PD and PID controller in control system engineering." [Online]. Available: <https://www.youtube.com/watch?v=OYPXiC7QJUM>.
- [60] N. Instruments, "PID." [Online]. Available: <https://www.ni.com/it-it/innovations/white-papers/06/pid-theory-explained.html>.
- [61] MATLAB, "Understanding PID Control, Part 1: What Is PID Control?." [Online]. Available: <https://www.youtube.com/watch?v=wkfEZmsQqiA&t=304s>.
- [62] MATLAB, "Understanding PID Control, Part 2: Expanding Beyond a Simple Integral." [Online]. Available: <https://www.youtube.com/watch?v=NVLXCwc8HzM>.

- [63] MATLAB, "Understanding PID Control, Part 3: Expanding Beyond a Simple Derivative." [Online]. Available: <https://www.youtube.com/watch?v=7dUVdrs1e18>.
- [64] MATLAB, "Understanding PID Control, Part 4: A PID Tuning Guide." [Online]. Available: <https://www.youtube.com/watch?v=sFOEsA0lrjs>.
- [65] MATLAB, "Understanding PID Control, Part 6: Manual and Automatic Tuning Methods." [Online]. Available: <https://www.youtube.com/watch?v=qj8vTO1eHo&t=9s>.
- [66] MATLAB, "Understanding PID Control, Part 7: Important PID Concepts." [Online]. Available: <https://www.youtube.com/watch?v=tbgV6caAVcs>.
- [67] W. Yu, *PID control with intelligent compensation for exoskeleton robots*. Academic Press, 2018.
- [68] W. Yu and J. Rosen, "A novel linear PID controller for an upper limb exoskeleton," in *49th IEEE Conference on Decision and Control (CDC)*, 2010: IEEE, pp. 3548-3553.
- [69] W. Yu, J. Rosen, and X. Li, "PID admittance control for an upper limb exoskeleton," in *Proceedings of the 2011 American control conference*, 2011: IEEE, pp. 1124-1129.
- [70] N. Hogan, "Impedance control: An approach to manipulation: Part I—Theory," 1985.
- [71] N. Hogan, "Impedance control: An approach to manipulation: Part II—Implementation," 1985.
- [72] D. Yamada, J. Huang, and T. Yabuta, "Comparison between admittance and impedance control of a multi-finger-arm robot using the guaranteed manipulability method," *Precision Instrument and Mechanology*, vol. 2, no. 1, pp. 85-93, 2013.
- [73] J. Sun, Y. Shen, and J. Rosen, "Sensor Reduction, Estimation, and Control of an Upper-Limb Exoskeleton," *IEEE Robotics and Automation Letters*, vol. 6, no. 2, pp. 1012-1019, 2021.
- [74] Y. Shen, J. Sun, J. Ma, and J. Rosen, "Admittance control scheme comparison of EXO-UL8: A dual-arm exoskeleton robotic system," in *2019 IEEE 16th International Conference on Rehabilitation Robotics (ICORR)*, 2019: IEEE, pp. 611-617.
- [75] A. Q. Keemink, H. van der Kooij, and A. H. Stienen, "Admittance control for physical human-robot interaction," *The International Journal of Robotics Research*, vol. 37, no. 11, pp. 1421-1444, 2018.
- [76] C. Ott, R. Mukherjee, and Y. Nakamura, "Unified impedance and admittance control," in *2010 IEEE international conference on robotics and automation*, 2010: IEEE, pp. 554-561.
- [77] C. Ott and Y. Nakamura, "Admittance Control using a Base Force/Torque Sensor," *IFAC Proceedings Volumes*, vol. 42, no. 16, pp. 467-472, 2009.
- [78] H. Zhong, X. Li, L. Gao, and H. Dong, "Development of Admittance Control Method with Parameter Self-optimization for Hydraulic Series Elastic Actuator," *International Journal of Control, Automation and Systems*, pp. 1-16, 2021.
- [79] H. F. Al-Shuka, S. Leonhardt, W.-H. Zhu, R. Song, C. Ding, and Y. Li, "Active impedance control of bioinspired motion robotic manipulators: An overview," *Applied bionics and biomechanics*, vol. 2018, 2018.
- [80] F. Almeida, A. Lopes, and P. Abreu, "Force-impedance control: a new control strategy of robotic manipulators," *Recent advances in Mechatronics*, vol. 1, pp. 126-137, 1999.
- [81] D. A. Lawrence, "Impedance control stability properties in common implementations," in *Proceedings. 1988 IEEE International Conference on Robotics and Automation*, 1988: IEEE, pp. 1185-1190.
- [82] H.-C. Lin, J. Smith, K. K. Babarahmati, N. Dehio, and M. Mistry, "A projected inverse dynamics approach for multi-arm cartesian impedance control," in *2018 IEEE International Conference on Robotics and Automation (ICRA)*, 2018: IEEE, pp. 5421-5428.
- [83] C. Natale, B. Siciliano, and L. Villani, "Spatial impedance control of redundant manipulators," in *Proceedings 1999 IEEE International Conference on Robotics and Automation (Cat. No. 99CH36288C)*, 1999, vol. 3: IEEE, pp. 1788-1793.
- [84] V. Noppeney, T. Boaventura, and A. Siqueira, "Task-space impedance control of a parallel Delta robot using dual quaternions and a neural network," *Journal of the Brazilian Society of Mechanical Sciences and Engineering*, vol. 43, no. 9, pp. 1-11, 2021.
- [85] J. Pratt, B. Krupp, and C. Morse, "Series elastic actuators for high fidelity force control," *Industrial Robot: An International Journal*, vol. 29, no. 3, pp. 234-241, 2002, doi: 10.1108/01439910210425522.

- [86] C. Silawatchananai and M. Parnichkun, "Force control of an upper limb exoskeleton for virtual reality using impedance control," in *2011 IEEE International Conference on Robotics and Biomimetics*, 2011: IEEE, pp. 2342-2347.
- [87] L. Piggott, S. Wagner, and M. Ziat, "Haptic neurorehabilitation and virtual reality for upper limb paralysis: a review," *Critical Reviews™ in Biomedical Engineering*, vol. 44, no. 1-2, 2016.
- [88] K. H. Lee, S. G. Baek, H. J. Lee, H. R. Choi, H. Moon, and J. C. Koo, "Improving transparency in physical human-robot interaction using an impedance compensator," in *2017 IEEE/RSJ International Conference on Intelligent Robots and Systems (IROS)*, 2017: IEEE, pp. 3591-3596.
- [89] Y. Zimmermann, A. Forino, R. Riener, and M. Hutter, "ANYexo: a versatile and dynamic upper-limb rehabilitation robot," *IEEE Robotics and Automation Letters*, vol. 4, no. 4, pp. 3649-3656, 2019.
- [90] K. H. Lee, S. G. Baek, H. J. Lee, H. R. Choi, H. Moon, and J. C. Koo, "Enhanced transparency for physical human-robot interaction using human hand impedance compensation," *IEEE/ASME Transactions on Mechatronics*, vol. 23, no. 6, pp. 2662-2670, 2018.
- [91] Speedgoat. [Online]. Available: <https://www.speedgoat.com/products-services/real-time-target-machines/performance>.
- [92] Wikipedia, "Root-mean-square error." [Online]. Available: https://en.wikipedia.org/wiki/Root-mean-square_deviation.
- [93] Wikipedia, "Standard Deviation." [Online]. Available: https://en.wikipedia.org/wiki/Standard_deviation.
- [94] Wikipedia, "Fast Fourier Transform." [Online]. Available: https://en.wikipedia.org/wiki/Fast_Fourier_transform.
- [95] M. Control, "How to address overshoot in servo control." [Online]. Available: <https://www.motioncontroltips.com/how-to-address-overshoot-in-servo-control/>.
- [96] Maxon, "EC 90 flat Ø90 mm, brushless, 90 Watt." [Online]. Available: https://www.maxongroup.com/medias/sys_master/8825435389982.pdf.
- [97] Maxon, "EC 45 flat Ø42.8 mm, brushless, 70 Watt." [Online]. Available: https://www.maxongroup.com/medias/sys_master/root/8833813184542/19-EN-264.pdf.
- [98] Maxon, "ESCON 70/10 Manuale di riferimento." [Online]. Available: https://www.maxongroup.com/medias/sys_master/root/8834398912542/422969-ESCON-70-10-Manuale-di-riferimento-It.pdf.
- [99] MMaxon, "ESCON 70/10 Hardware Reference." [Online]. Available: https://www.maxongroup.com/medias/sys_master/8818448400414.pdf.
- [100] Maxon, "EPOS4 Firmware Specification." [Online]. Available: https://www.maxongroup.com/medias/sys_master/root/8834324856862/EPOS4-Firmware-Specification-En.pdf.
- [101] Maxon, "EPOS4 Module/Compact 50/15 Hardware Reference." [Online]. Available: https://www.maxongroup.com/medias/sys_master/8825356681246.pdf.
- [102] H. Drive, "Engineering Data, CSD-2A Component Sets." [Online]. Available: https://harmonicdrive.de/fileadmin/user_upload/2014_11_ED_1019659_CSD-2A.pdf.
- [103] RLS, "AksIM-2 off-axis rotary absolute encoder." [Online]. Available: https://www.rls.si/media/wysiwyg/RLS/datasheet/MBD01_02.pdf.

Un ringraziamento particolare è rivolto al professor Chiaberge che mi ha dato la possibilità di entrare in contatto con una realtà meravigliosa quale l'Istituto Italiano di Tecnologia a Genova: in IIT, in particolare nel dipartimento di Rehab Technologies dove ho avuto la fortuna di svolgere la mia tesi, si respira un'aria di scienza che fa venir fame di conoscenza e voglia di mettersi in gioco.

Un grazie infinto lo porgo proprio a voi, Stefano, Federico ed Anna, grazie che mi avete sempre dato supporto, spiegando passo dopo passo ciò che non mi era chiaro, accompagnandomi verso la risoluzione senza darmi la risposta diretta. Grazie perché in questi mesi ho imparato, probabilmente a rilento, ma ho imparato veramente tanto: questa esperienza mi ha fatto crescere, sotto tantissimi punti di vista, in primis, personale. Grazie ENORME anche alla pazienza ai “meccanici”, a Luca che ormai è diventato un task da lavagna a casa e a Gian, il mago di Creo. Grazie anche al mio compagno di banco Angelo, che più volte mi ha distratta per farmi vedere come stesse crescendo bene Rosina.

Incredibile che sia giunta l'ora dei ringraziamenti, probabilmente sarà una sezione più lunga dello stato dell'arte, ma senza ogni persona che andrò a ringraziare, sicuramente non sarei qui.

Il grazie più grande di tutti va a mamma, che per anni, anni ed anni mi ha ascoltato ripetere materie a lei totalmente sconosciute ("ma Lalli per me questo è arabo!"), con un'attenzione infinita: vorrei firmare una petizione per dare una laurea in ingegneria anche a mamma. Rimanendo sui ringraziamenti famigliari, non posso che non ringraziare i miei più grandi fan e supporters, i miei fratelli, i "pesi", ormai commari, insomma, non so più che appellativo utilizzare per chiamarvi, di certo, Giuli e Fede, Fede e Giuli, meglio di voi non c'è nessuno. Grazie a Giuli che mi insegna ogni giorno che la distanza è solo fisica, che se vuoi esserci si sei anche a km di distanza, e grazie Fede, orecchio sempre pronto ad ascoltare ed occhio attento, ingegnere di famiglia che sa come spiegare le cose attraverso gli schemi: grazie bubi, ora non so più parlare, ma per spiegare le cose chiedo "posso farti un disegnetto?", rigorosamente a matita, su un post-it.

Un grazie enormemente gigante va a Ceci, amica dalla pancia delle mamme, alter-ego artistico e indissolubile compagna di vita. A te che in ogni momento ha dimostrato fierezza e gioia, ricaricando le mie quasi inesauribili pile.

Grazie a Leo, a te che, incredibilmente, hai supportato e sopportato tutti i miei alti e bassi. A te che sei stato sostegno e che hai avuto la pazienza di capire le mie scelte. Alla tua felpa rossa ed ovviamente solo a quella. Al caffè e al buongiorno. A te che ormai sai che cosa sia un segnale, che ogni tanto comprendi gli overshoots, ma solo se poi raggiungiamo uno steady-state. Grazie a te che, nonostante i nostri "nonostante" mi hai accompagnato fino a qui, mano nella mano. Grazie perché mi hai sempre spinto verso la direzione migliore per me, anche quando questo ci portava ad essere ancora più distanti. Grazie perché mi dimostri cosa vuol dire volere il bene dell'altro. Arriverà.

Grazie a Chiara, Chiara, lo sai bene, senza di te non mi sarei MAI laureata. Se non fosse stato per i 4 esami in un settimana di studio, per le 48 ore senza dormire in montagna, se non fosse stato per lo sfasamento che abbiamo come seno e coseno di fase up&down (riferimento categorico anche alla canzone!), beh, non sarei qui. Grazie perché programmini, schemini e full immersion sarebbero stati una noia mortale, invece con te sono stati un divertimento unico.

Grazie a Sausamu, il mio siciliano del cuore, a te che mi insegni cosa vuol dire perseverare, divertirsi ed essere un vero adulto. A te che sei una spalla incredibile, che mi ascolti parlare per ore senza mai distrarti un attimo e che mi sostieni, sempre facendo il tifo.

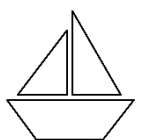
Grazie ad Angelo, Teo, Benni, Becca, Cino, Laretta e Lucone (anche se tutti sappiamo quale sia il tuo vero soprannome): grazie a voi, gruppo biomedico! Per i festeggiamenti degli esami (che passava solo Angelo) a suon di paste al pomodoro, per gli aperitivi e le serate, per i pomeriggi intensi di studio (sempre grazie ad Angelo) e per le feste con Laretta che finisce nel letto. Grazie perché con voi la triennale è volata, soprattutto per Benni perché di solito il tempo passa più in fretta quando ci si addormenta. Grazie perché mi sono letteralmente divertita. Un grazie particolare lo rivolgo a Teo ed Angelo, amici che mi hanno supportato anche al di fuori dell'università: Teo grazie per l'emozione, il coinvolgimento e il trasporto, a partire dal Capodanno di Courmayeur a finire a quando ti ho detto che mi sarei laureata; Angelino milanese, svizzero, abruzzese, con te tante parole non servono, sai che quando vuoi nonna Lalli è pronta che le polpette al sugo!

Grazie a PisaBella, che con il tuo sorriso porti il sole, che hai condiviso con me i momenti peggiori, per poi imparare insieme come rialzarci e ripartire più forti i prima. Un girasole immenso a te, a noi e a loro.

Un grazie alla tigre di Bianca, che non si ricorda di avermi regalato, ma che è sempre nello zainetto con me, ogni volta che faccio un esame.

Grazie Genova, GiuliCoinqui, Gabri, Pietrino, Rick, Annina, Giubbru, Indya, Fede, il Berna, il Vaso, AleSacchins, Marino e Dario: grazie a voi, colleghi in IIT, ma soprattutto amici fuori. Grazie per i tuffi al mare, i tramonti e i Milano-Torino. Grazie per le 5 del mattino e per gli indissolubili discorsi di confronto, conforto e sostegno che mi avete fatto tutti, incitandomi a non demordere e sgridandomi quando inutilmente mi buttavo giù. Grazie per ogni singolo momento, per avermi fatto notare quanto sia piemontese con "solo più", per i passaggi in motorino, le scale della Annunziata, gli strappi in macchina, maledetta primavera e gli specchietti rotti: Genova è bella, la tesi è stata una meraviglia, ma con voi ogni cosa ha acquisito un colore ed un sapore che difficilmente scorderò.

Insomma, grazie a tutti, tutti quanti! Fede Bianco, compagna di SanSi e Capo, Nahuel, il mio chef del cuore e delle papille gustative, Franci, Ubi, ai mastini ed i fantini, ad Anna, Pid, Marc, Greta, Albo, Lucri e tutti gli amici lodigiani. Grazie Geppo a ai tuoi gli sguardi ricchi di parole e grazie Cristina per ogni momento in cui mi sono sentita a casa. Grazie Bea per le colazione insieme e le chiacchiere mattutine e grazie Giovi per i tuoi favoli chocoPops. Ed inoltre grazie a Sarina, la mia ormai mezza americana, grazie per aver sempre creduto in me, grazie Lavi per tutte le colazione super sabaude, per i nostri viaggi in giro per il mondo e per avermi camminato accanto durante gli anni del Poli. Insomma, grazie a chiunque, che sicuramente non ho citato, ma non dimenticato (giusto per rimanere nei limiti delle ormai troppe pagine), grazie per avermi permesso, con i mezzi ed i metodi più disparati, di arrivare fino a questo immenso traguardo. Vi ringrazio e, davvero, vi voglio infinitamente bene.



Infine, un grazie a papà, alla foto in elicottero e allo sguardo silente. Grazie perché ora, non sarei qui, grazie perché mi hai insegnato, tacitamente, che, quello che si crede in prima battuta un fallimento, in realtà, è una grande conquista. A te, un grazie che arrivi fin lassù.

